Norwegian University of Life Sciences
Faculty of Veterinary Medicine and Bioscience
Department of Chemistry, Biotechnology
and Food Science

Philosophiae Doctor (PhD)
Thesis 2021:53

Biogas digestate as substrate and vector for the introduction of N_2O-respiring bacteria to agricultural soil

Digestat fra biogassproduksjon som substrat og vektor for introduksjon av N_2O-respirerende bakterier til landbuksjord

Kjell Rune Jonassen

Biogas digestate as substrate and vector for the introduction of N_2O-respiring bacteria to agricultural soil.

Digestat fra biogassproduksjon som substrat og vektor for introduksjon av N_2O-respirerende bakterier til landbuksjord.

Philosophiae Doctor (PhD) Thesis

Kjell Rune Jonassen

Norwegian University of Life Sciences
Faculty of Veterinary Medicine and Bioscience
Department of Chemistry, Biotechnology and Food Science.

Ås (2021)

Thesis number 2021:53
ISSN 1894-6402
ISBN 978-82-575-1824-0

PhD supervisors

Prof. Lars Bakken (main supervisor)
Faculty of Chemistry, Biotechnology and Food Science
Norwegian University of Life Sciences
1432 Ås, Norway
lars.bakken@nmbu.no

Prof. Åsa Frostegård (co-supervisor)
Faculty of Chemistry, Biotechnology and Food Science
Norwegian University of Life Sciences
1432 Ås, Norway
asa.frostegard@nmbu.no

Prof. Svein-Jarle Horn (co-supervisor)
Faculty of Chemistry, Biotechnology and Food Science
Norwegian University of Life Sciences
1432 Ås, Norway
svein.horn@nmbu.no

Dr. Rune Holmstad (co-supervisor)
Vestfjorden Avløpsselskap
Bjerkåsholmen 125
3470 Slemmestad, Norway
ruho@veas.nu

Thesis evaluation committee

Prof. Mark van Loosdrecht (Opponent 1)
Department of Biotechnology
Delft University of Technology
2629 HZ Delft, The Netherlands
m.c.m.vanloosdrecht@tudelft.nl

Prof. Anna Schnürer (Opponent 2)
Department of Molecular Sciences,
Swedish University of Agricultural Sciences,
750 07 Uppsala, Sweden.
anna.schnurer@slu.se

Assoc. Prof. Bjørge Westereng (Coordinator)
Faculty of Chemistry, Biotechnology and Food Science
Norwegian University of Life Sciences
1432 Ås, Norway
bjorge.westereng@nmbu.no

Table of contents

I. Acknowledgements

This work was carried out in the period from 09.2016 to 05.2021 in the MEP/Nitrogen group at the Department of Chemistry, Biotechnology and Food Science at the Norwegian University of Life Sciences (NMBU). The work was funded by the Norwegian Research Council under the public phd-program (project number: 260868), VEAS WWTP and NMBU.

I'm grateful for the inspiring and motivating supervision from my main supervisor, Lars Bakken, and the team of co-supervisors: Åsa Frostegård, Svein-Jarle Horn and Rune Holmstad. Thanks goes to Silas Vick for boosting this project with creative ideas and valuable assistance in designing/running experiments, and to Elisabeth G. Hiis and Lars Molstad for assistance whenever needed (night and day) with the automated gas incubation system. And - all past and present members of the NMBU Nitrogen group, the collaborators to Paper I and Paper II (and for the opportunity to be involved in side-projects, even those that turned out to be a waste of time)! Lastly, the great colleagues at VEAS - in particular Jan-Erik Eriksen and Pål Berg (decd.) for teaching me the tricks of the trade over early morning coffees.

A very special thank you goes to my patient friends, family and loved ones which probably have experienced an over-worked and somewhat distant friend, son, brother, uncle and boyfriend the last couple of years.

Kjell Rune Jonassen.

II. Summary

Anthropogenic nitrous oxide (N_2O) emissions are largely driven by the input of N-based fertilizers in agriculture. N_2O emissions from agricultural soils in Europe are estimated to 0.51 Tg annually (**Fig. I**), which sums to 48 % of total European N_2O emissions and 35 % of the climate forcing from European agriculture. Yet, N_2O emission mitigation from agriculture is still hampered by a lack of implemented abatement options.

Whilst several biogeochemical reactions may release N_2O (**Fig. I**) the enzyme nitrous oxide reductase (Nos) is the only known enzyme to reduce nitrous oxide. Nos is expressed in denitrifying and non-denitrifying prokaryotes and catalyzes the reduction of N_2O to N_2. The complete denitrification pathway is the stepwise reduction $NO_3^- \rightarrow NO_2^- \rightarrow NO \rightarrow N_2O \rightarrow N_2$, catalyzed by the enzymes Nar/Nap, Nir, Nor, and Nos that are encoded by the genes *nar*/*nap*, *nirK/nirS*, *nor,* and *nosZ*, respectively (**Fig. I**). A significant proportion of the denitrifying community in soils have truncated denitrification pathways, i.e. lacking one to three of the genes encoding the enzymes in the stepwise reduction of NO_3^- to N_2. The consequence of such modularity is that organisms lacking *nosZ* are net N_2O emitters, while organisms with *nosZ* only are net sinks for N_2O. However, organisms equipped with a complete denitrification pathway can also be strong sinks or sources of N_2O depending on their regulatory biology.

N_2O emissions from soils make up a substantial fraction of the climate forcing from food production and mitigation beyond that achieved by “good management practices” are needed if we are to limit global warming by 2 °C, as set in the Paris Agreement. One approach for reducing N_2O emissions is to modify the soil microbiome, increasing the proportion of N_2O-respiring bacteria (NRB) resulting in reduced N_2O emissions. This would, however, be costly and impractical as a standalone operation.

As an element towards a low-carbon circular economy, the volume of organic wastes channeled through AD is expected to increase in the coming decades. This presents a unique possibility for mitigation of N_2O emissions as the residues of biogas production, digestates, destined as bio-fertilizers in agriculture, could be enriched with N_2O-respiring bacteria before soil fertilization. Thus, providing a cost-efficient N_2O mitigation measure (**Fig. I**). Here we demonstrate the use of biogas digestates from anaerobic digestion (AD) as a widely available, low-cost vector for NRB to agricultural soils. .

A primary task was to search for suitable organisms that 1) could grow to high cell densities in digestate and 2) would act as net N_2O sinks in soil. To achieve this, enrichment culturing under anaerobic conditions with N_2O as the sole electron acceptor was used. The enrichment cultures were monitored both by measuring the gas kinetics and by inspecting the composition of the microbiota by genomics and proteomics. Based on genomic information and targeted isolation, we obtained axenic cultures of the organisms that became dominant in the enrichment cultures.

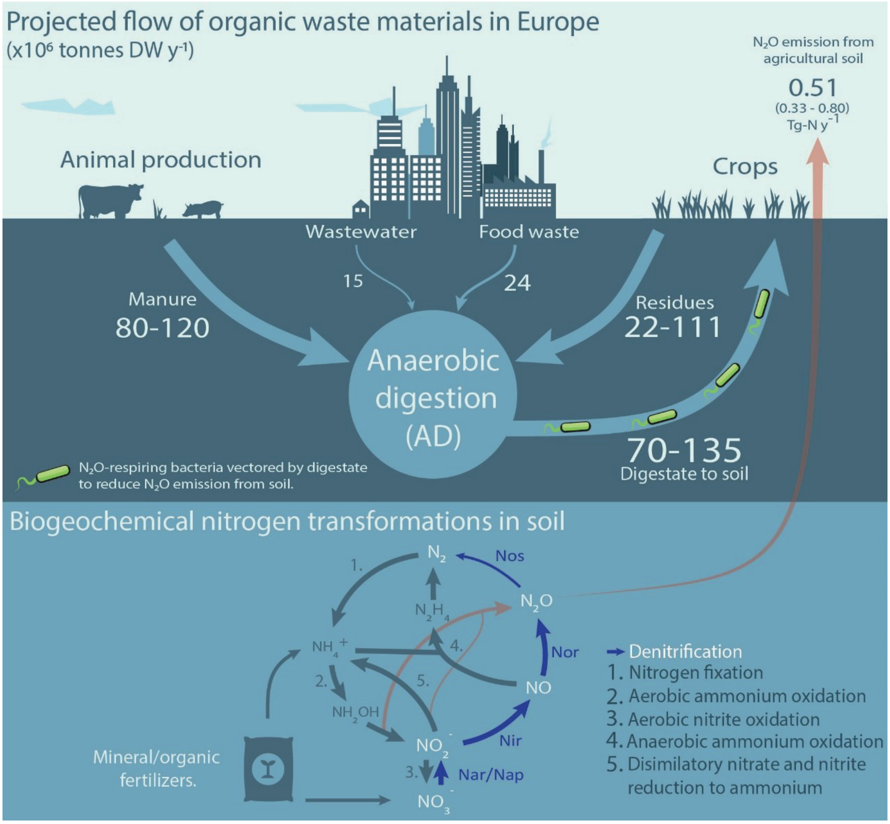

Figure I: Possible biomass streams in a future circular economy with a central role for anaerobic digestion. Solid arrows (top section) show streams of biomass available for anaerobic digestion (AD). The arrow from AD to agricultural soil indicates a credible pathway for digestate enriched with N_2O-respiring bacteria; fertilization with such enriched digestates strengthens the N_2O sink capacity of the soil, hence reduces N_2O emissions. The lower half of the picture shows the biogeochemical nitrogen transformations underlying these N_2O emissions (0.51 Tg y^{-1}), which are fed by fertilizers.

As a first approach, we enriched indigenous N_2O-respiring bacteria in anaerobically digested sewage sludge (digestate) by anoxic incubation with N_2O. The gas kinetics predicted that N_2O-respiring organisms grew to high cell densities, which was confirmed by metagenomic and metaproteomic (omics-) analyses of the enriched digestate. The omics demonstrated dominance of organisms equipped with the *nosZ* clade II (coding for N_2O-reductase), but also with the genes for the preceding steps of the denitrification pathway. Three digestate-derived N_2O-reducing bacteria were isolated, of which one (*Azonexus* sp.) matched the recovered Metagenome-Assembled Genome (MAG) of the dominant N_2O reducer with an average nucleotide identity (ANI) of 98.2%. This MAG also demonstrated a high complement of Nos in the enrichment as quantified by metaproteomics. Gas kinetics and meta-omics indicated that the anaerobic consortium of the digestate remained active during anaerobic incubation with N_2O and that N_2O-respiring bacteria grew by harvesting fermentation intermediates. The latter was supported by screening carbon catabolism profiles of the isolated organisms. The isolated *Azonexus* sp. demonstrated regulatory traits that would predict the organism to be a strong N_2O sink, and it reduced immediate N_2O emissions from digestate-amended soils. However, the *Azonexus* sp. was probably not an ideal N_2O-respiring inoculant in soil because it was equipped with a full-fledged denitrification pathway and because its capacity to utilize soil carbon was limited. The importance of an active methanogenic community throughout the enrichments, providing fermentation intermediates as a carbon source for the N_2O-respiring organisms, would predict a selective advantage for organisms with a streamlined (narrow) catabolic capacity, which was the case for the *Azonexus* sp.. It was evident that we needed to refine our search, to find organisms with a broader catabolic repertoire.

A new procedure to obtain more ideal isolates was designed, involving a deliberate enrichment of N_2O-respiring organisms with the characteristics of strong growth both in digestate and soil. We thought this could be achieved by "dual enrichment culturing", i.e. a sequence of enrichment cultures where a fraction of a batch enrichment was passaged to the next batch, alternating between sterile soil and sterile digestate as substrate. Our point of departure was to model this approach, using a simple logistic model for the competition for a common substrate, between three distinctive groups; 1: Organisms with a competitive advantage in digestate (digestate specialists), 2: Organisms with a competitive advantage in soil (soil specialists), and 3: organisms capable of sustaining growth in both environments (generalists). The modelling revealed that generalists could indeed become dominant within a limited number of batch cultures, depending on their competitive edge *vis a vis* the specialists. Based on this we realized a dual enrichment experiment, using the microbiota of wastewater digestate and soil as initial inocula, sterile digestate and sterile soil as substrate, and monitored the gas kinetics and the community composition (by 16S rDNA amplicon sequencing) throughout seven consecutive enrichment cultures. The gas kinetics corroborated the model's prediction of a gradual enrichment of organisms that grew both in soil and digestate, and the generalists that became dominant were identified as a limited number of Operational Taxonomic Units (OTUs, based on 16S rDNA sequencing). OTUs that became dominant circumscribed isolates obtained from the enrichment cultures. These OTUs also portrayed the targeted generalist as predicted by the modelling. Most isolates obtained had traits of strong N_2O sinks, of which a dominating *Cloacibacterium* sp., carrying Nos (Clade II) as the sole N-reductase, significantly reduced N_2O emissions in digestate amended soils of both neutral and acidic pH. A full-fledged denitrifying *Pseudomonas sp.* was able to persist in the soil for at least one month whereby significant N_2O emissions reduction was obtained upon a fertilization event. Genome analysis of the isolated organisms shed some light as to why these organisms had a competitive advantage in both soil and digestate.

Although the ideal isolate is yet to be found, we've opened an avenue to a concept that, within the expected expansion of AD, could be scaled to secure a substantial reduction in N_2O emissions.

III. Sammendrag

Menneskeskapte utslipp av drivhusgassen lystgass (N_2O) skyldes i stor grad tilførsel av nitrogenholdig gjødsel til landbruksjord. N_2O-utslipp fra landbruksjord i Europa er estimert til 0,51 Tg årlig (**Fig. I**), som utgjør om lag 48% av de totale utslippene av N_2O, som igjen representerer 35 % av det totale klimagassfotavtrykket fra europeisk landbruk. Begrensning av disse utslippene har vært utfordrende grunnet mangel på implementerte metoder og teknologier som effektivt reduserer lystgassutslippet fra landbruksjord.

Flere biogeokjemiske reaksjoner kan frigjøre N_2O (**Fig. I**), men enzymet lystgassreduktase (Nos) er det eneste kjente enzymet som reduserer N_2O til N_2. Nos uttrykkes av denitrifiserende prokaryoter og katalyserer reduksjonen av N_2O til N_2. Denitrifiserende prokaryoter katalyserer den trinnvise reduksjon av $NO_3^- \rightarrow NO_2^- \rightarrow NO \rightarrow N_2O \rightarrow N_2$, som katalyseres av enzymene Nar/Nap, Nir, Nor og Nos som er kodet av genene *nar*/*nap*, *nir*, *nor* og *nosZ* (**Fig. I**). Men, en betydelig andel av det denitrifiserende mikrobesamfunnet i jord er trunkert, dvs. en andel av denitrifikantene mangler ett til tre av genene som koder enzymene involvert i reduksjonen av NO_3^- til N_2. En organisme som kun mangler *nosZ* vil produsere N_2O. I motsatt tilfelle vil en organisme som kun er utstyrt med *nosZ* bare evne å redusere N_2O. Organismer utstyrt med et komplett sett av gener for en fullstendig denitrifikasjon kan være både sterke og svake N_2O-reduktanter. Dette bestemmes av deres regulatoriske biologi.

N_2O-utslipp fra jord utgjør en betydelig mengde av det totale klimafotavtrykket fra matproduksjon og en reduksjon av dette utslippet er nødvendig om vi skal nå de målene som er satt i Parisavtalen og begrense global oppvarming til 2 °C. En mulighet for å redusere N_2O-utslipp er å modifisere jordmikrobiomet ved å øke andelen N_2O-respirerende bakterier (NRB) – noe som vil redusere utslippene av N_2O. Men, som ett frittstående tiltak vil en storskala modifisering av mikrobiologien i jordsmonnet være svært ressurskrevende.

Som et ledd i overgangen til en lav-karbon sirkulærøkonomi forventes anaerob utråtning (AD) å øke i omfang og rekkevidde de neste årene. Denne utviklingen skaper en unik mulighet for å redusere N_2O-utslipp dersom digestater, restproduktet fra AD, som brukes som organisk gjødsel i landbruket, kan anrikes med N_2O-reduserende bakterier før disse digestatene benyttes som gjødsel (**Fig. I**). Her demonstrerer vi at lett tilgjengelige digestater kan benyttes som vekstsubstrat og en vektor for å overføre NRB til jord. En slik modifikasjon være et svært kostnadseffektivt N_2O-reduserende tiltak.

Det primære målet i denne avhandlingen var å lete etter egnede organismer som 1) kan gro til høy celletetthet i digestater, og 2) redusere N_2O-utslipp fra jord. For å oppnå dette ble anrikninger av slike organismer ved bruk av N_2O som eneste elektronakseptor gjennomført. Anrikningskulturene ble monitorert ved å måle gasskinetikk og ved overvåking av samfunnsprofiler og bakteriell populasjonsdynamikk ved bruk av DNA- og proteomanalyser. Med basis i den genetiske informasjonen var målet å isolere dominerende organismer fra anrikningskulturene.

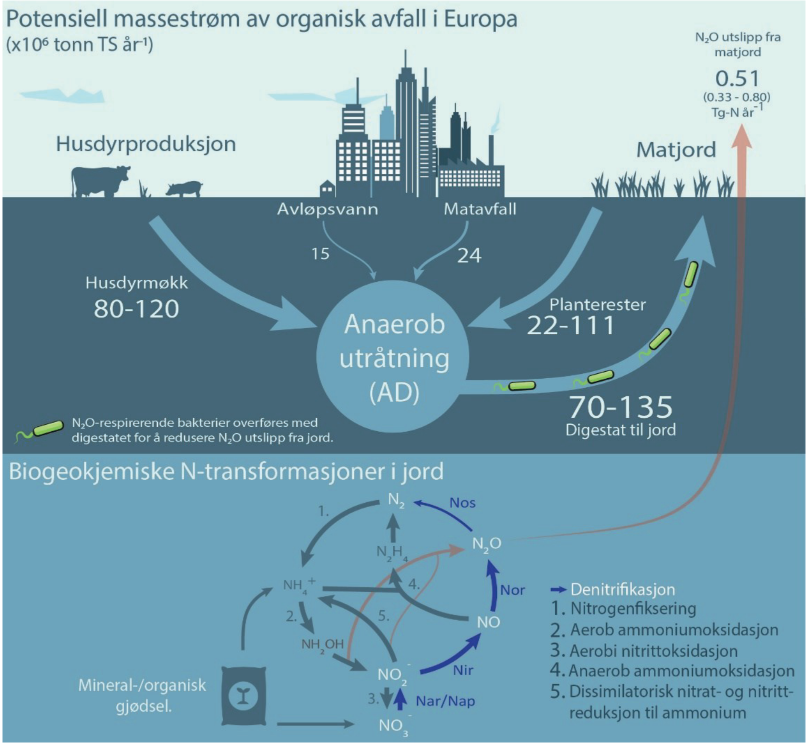

Figur I: **Mulige organiske avfallsstrømmer i Europa med en sentral rolle for anaerob utråtning (AD).** Øverste seksjon viser strømmer av organisk avfall som teoretisk er tilgjengelig for behandling via AD i dag. Pilen fra anaerob utråtning til matjord indikerer en mulig vei for storskala introduksjon av N_2O-respirerende bakterier som overføres med digestat til landbruksjord. Den nedre halvdelen av bildet viser de biogeokjemiske nitrogentransformasjonene som ligger til grunn for deler av disse N_2O-utslippene (0,51 Tg år^{-1}).

Som en første tilnærming anriket vi N_2O-reduserende bakterier som er naturlig tilstedeværende i digestat i anoksiske inkubasjoner hvor N_2O ble tilsatt som eneste elektronakseptor. Gasskinetikk predikerte at NRB vokste til høye celletettheter under inkubasjonen, som ble bekreftet av metagenom- og metaproteomanalyser av det anrikede digestatet. Meta-omikk analysene viste at organismer utstyrt med *nosZ* Type II (genet for N_2O-reduktase), men også med de øvrige genene for et komplett denitrifiseringsspor, dominerte anrikningen. Tre N_2O-reduserende bakterier ble isolert hvorav det ene isolatet, en *Azonexus* sp., samsvarte med et gjenvunnet *Dechloromonas*-beslektet metagenom som dominerte anrikningen med en aminosyreidentitet på 98,2% delt med det dominerende metagenomet. Metaproteomikk viste at dette metagenomet utrykte brorparten av Nos under anrikningen. Gasskinetikk og meta-omikk avslørte videre at det metanogene konsortiet i digestatet forblir aktivt også under den anaerobe inkubasjonen med N_2O, og at dominerende bakterier med en anaerob respiratorisk metabolisme sannsynligvis vokste ved å høste fermenteringsmellomprodukter fra det metanogene samfunnet. Det sistnevnte ble støttet ved karbonkatabolismeprofiler for de isolerte organismene. Den isolerte *Azonexus* sp. demonstrerte regulatoriske egenskaper som ville forutsi at organismen var en sterk N_2O-reduktant, og den reduserte N_2O-utslipp fra jord gjødslet med *Azonexus* anriket digestat. Likevel så var anrikningsvinneren sannsynligvis ikke en ideell N_2O-reduserende inokulant i jord fordi dens evne til å overleve i jord-miljøet sannsynligvis var begrenset. Betydningen av et aktivt metanogent bakteriesamfunn, som produsenter av karbonkilder for NRB igjennom anrikningene, gav sannsynligvis en selektiv fordel for organismer med en strømlinjeformet (smal) katabolsk kapasitet, som var tilfelle for *Azonexus* sp.. Det var tydelig at vi trengte å videreforedle anrikningsprosedyrene våre for å anrike kompetente organismer en bredere metabolsk fleksibilitet.

En ny tilnærming for å oppnå mer ideelle isolater som evner å vokse i både jord og i digestat ble designet med utgangspunkt i å selektivt anrike organismer med disse egenskapene. Vi antok at slike organismer kunne anrikes ved en «dobbelt-anrikning»-prosedyre der miljøet ble vekslet mellom jord og digestat. Mao: En sekvens av batch-anrikningskulturer hvor en overfører en fraksjon av anrikningen til en ny batch og vekslet mellom jord og digestat som vekstsubstrat. Med dette utgangspunktet ble logistisk vekst, kun med konkurranse om tilgjengelig karbon, modellert for tre ulike bakteriegrupper; 1) Organismer med konkurransefortrinn i digestat (digestat-spesialister), 2) Organismer med konkurransefortrinn i jord (jordspesialister), og 3) organismer som er i stand til å opprettholde vekst/aktivitet i begge miljøer (generalister). Modelleringen avslørte at generalister teoretisk sett kunne anrikes ved å passere fraksjoner av disse anrikningene mellom digestat og jord, avhengig av generalistenes konkurransefortrinn relativt til spesialistene.

Basert på denne modelleringen realiserte vi et nytt anrikningseksperiment med bruk av digestat og jord som initielt inokulum og sterilt digestat og jord som vekstsubstrat og lot populasjonene konkurrere om tilgjengelig karbon med tilsats av N_2O. Monitorering av gasskinetikk og populasjonsdynamikk (ved 16S amplikonsekvensering) igjennom syv sammenhengende anrikninger viste en populasjonsutvikling slik predikert fra modelleringen: Gasskinetikken støttet modellprediksjonen om en gradvis ankrikning av organismer som vokste i jord og digestat, og 16S-analysen vist at et fåtall operasjonelle taksonomiske enheter (OTUer) dominerte anrikningen. Isolatene fra disse anrikningskulturene var omsluttet av en dominerende gruppe OTUer som portretterte vekstegenskaper igjennom hele anrikningsserien som representerte de ønskede generalistvinnerne. Ett av isolatene, en *Cloacibacterium* sp., hvis genom kun kodet for genet for Nos, dominerte anrikningene, og denne reduserte også N_2O-utslipp i jord med lav pH. Et annet isolat, en *Pseudomonas* sp., demonstrert en mer langvarig N_2O reduserende aktivitet i jord da aktiviteten var fremtredende selv 30 dager etter gjødsling.

Genomanalyse av isolerte organismer kastet noe lys kring hvorfor disse organismer kunne ha et konkurransefortrinn i anrikningene. Selv om det ideelle isolatet ennå ikke er funnet, har vi åpnet en vei for et konsept som, i kontekst av den forventede utviklingen av AD, kan skaleres for å sikre betydelig reduksjon i N_2O-utslipp.

IV. List of papers

Paper I

Jonassen KR, Hagen LH, Vick SHW, Arntzen M, Eijsink VG, Frostegård Å, Molstad LM, Pope P, Bakken LR (2021) N_2O-respiring bacteria in biogas digestates for reduced agricultural emissions (Manuscript submitted to ISMEJ).

Manuscript preprint, supplementary methods and materials, and supplementary data available at https://www.biorxiv.org/

Paper II

Jonassen KR, Ormaasen I, Duffner C, Hvidsten TR, Frostegård Å, Bakken LR, Vick SHW (2021) A novel dual enrichment strategy provides soil- and digestate- competent N_2O-respiring bacteria for mitigating climate forcing in agriculture (Manuscript).

Manuscript preprint, supplementary materials, and supplementary data available at https://www.biorxiv.org/

V. Abbreviations

16S rRNA	16S ribosomal ribonucleic acid
AD	Anaerobic digestion
AOA	Ammonia oxidizing archaea
AOB	Ammonia oxidizing bacteria
CF	Climate forcing
DP	Denitrifying prokaryote
DRP	Denitrification regulatory phenotype
DW	Dry weight (% of wet weight)
DNRA	Dissimilatory nitrate/nitrite reduction to ammonium
GHG	Greenhouse gas
MAG	Metagenome assembled genome
Nar	Membrane bound nitrate reductase
Nap	Periplasmic nitrate reductase
Nir	Nitrite reductase
NOB	Nitrite oxidizing bacteria
Nor	Nitric oxide reductase
Nos	Nitrous oxide reductase
NRB	Nitrous oxide respiring bacteria
Pmf	Proton motive force
WWT/-P	Waste-water treatment /-plant

1. Introduction

1.1 Nitrous oxide emissions from agricultural soil

Nitrous oxide (N_2O) is a long-lived atmospheric GHG with a radiative forcing 310 times that of CO_2 (Forster et al., 2007). The main global driver of anthropogenic N_2O emissions is the input of reactive nitrogen species in agriculture (Davidson 2009). Industrial production of reactive nitrogen species (fertilizer-N) has played an essential role in feeding the worlds growing population through improving crop yields ever since the invention of the Haber-Bosh process, concomitantly resulting in an inadvertently increased global N-pollution where abiotic and biogeochemical N-transformations (**Chapter 1.2**) have propelled the atmospheric N_2O concentration over the last century (**Fig. 1**). In Europe, the N_2O emissions from agricultural soils are estimated to 0.51 Tg annually (Tian et al., 2020), which sums to 48 % of total European N_2O emissions, 3.5 % of Europe's total GHG emissions, and 35 % of the climate forcing from European agriculture (Eurostat, 2018).

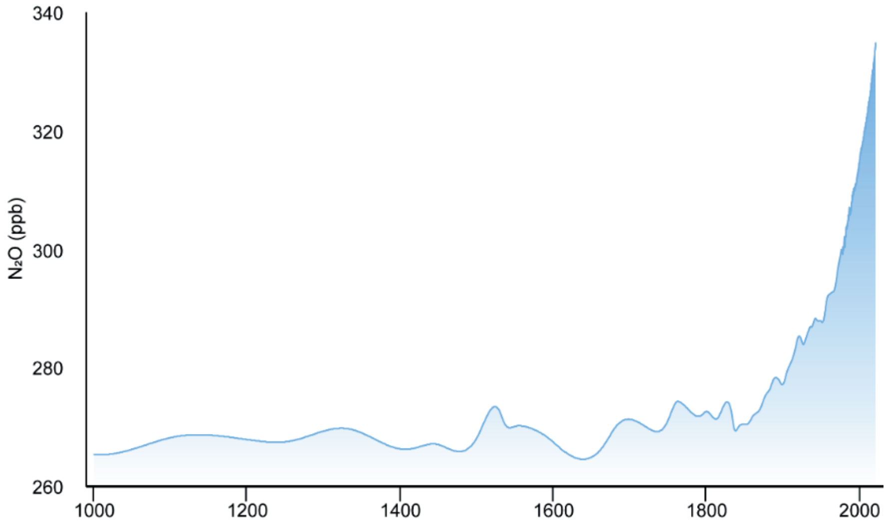

Figure 1: Atmospheric concentration of N_2O (ppb). The years 1000 to 1973: concentration in atmosphere determined by analysis of ice core samples. 1974 – present: monthly means of measurements of the NOAA/ESRL halocarbons program. Source: www.n2olevels.org

The last century's rise in atmospheric concentration of N_2O (334.7 ppm, December 2020) has caused concern among authorities and academic institutions for decades. However, mitigating N_2O release from agricultural sources is still hampered by the lack of implemented abatement options (Winiwarter et al., 2018), which is also underlined by the IPCC's call for more applied technologies targeting non-CO_2 (CH_4 and N_2O) GHG emissions (IPCC, 2018). Applying fertilizer according to crop needs (*best agronomic practice*) does reduce N_2O emissions to a certain extent (Zhang et al., 2015), but, besides such practices, there exists no widely accepted mitigation strategy for reducing N_2O emissions in agriculture (**Chapter 1.3**).

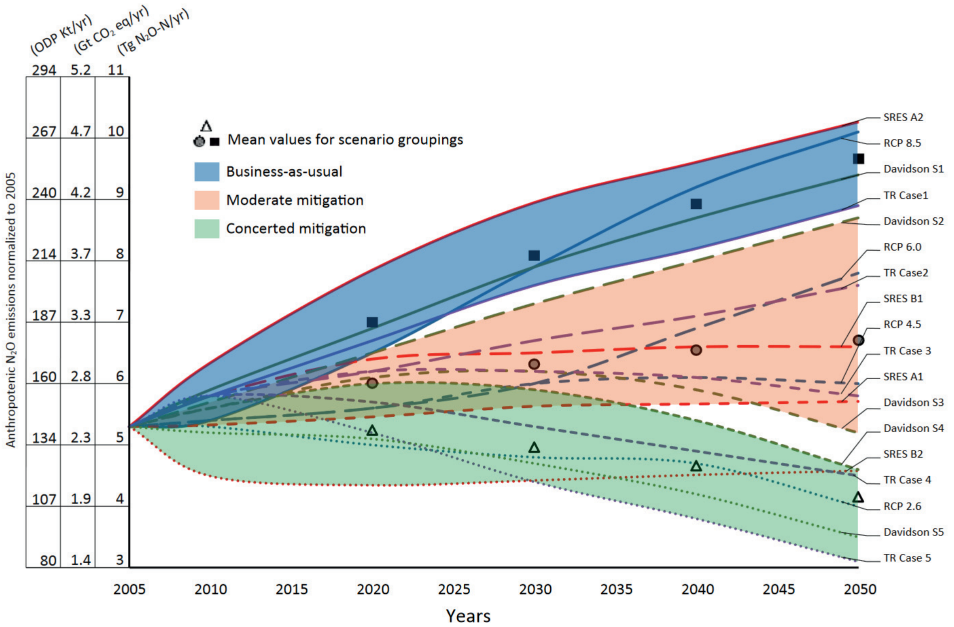

Figure 2: Projections of global anthropogenic N_2O emissions under several scenarios; business as usual (blue), moderate mitigation (orange), and intensive mitigation (green), plotted against ozone depletion potential (ODP) and CO_2 equivalents relative to net anthropogenic N_2O emissions. Projections based on published scenarios (SRES, RCP and UNEP (TR)) and Davidsons (2012) (S) projections. Projections were based on population growth rates, per capita consumption of calories (carbohydrates and protein) and relative distribution and redistribution of calories from animal and/to plant-based calory uptake, reduction in food waste and nutrient loss, land-use change, and other scenarios (Figure reprinted from Sutton et al., 2013 (reprints allowed for educational and nonprofit use)).

Sutton et al. (2013) illustratively portray the need for targeted efforts in dealing with N_2O emissions and predict an almost doubling of anthropogenic derived N_2O emissions by the year 2050 (normalized to the year 2005) if action is not taken (*business as usual* scenarios) (**Fig. 2**). The study also underlines the potential in several mitigation measures, such as improved manure management, improved fertilizer N recovery efficiency (% of added N recovered as plant N in a growing season (Cassman et al., 2002), and global dietary changes (= less meat consumption), which play important roles in scenarios projected to lead to stabilized and reduced atmospheric emissions (moderate and concerted scenarios). The more recent quantification of global nitrous oxide sources by Tian et al. (2020) estimates N_2O emissions from agriculture to 7.3 Tg N_2O-N y^{-1}, which would place recent years emissions in the business as usual scenarios of **Fig. 2**.

1.2 Biogeochemical N-transformations

Nitrogen is an essential element for all living organisms and is supplied to agricultural soil by the addition of organic or synthetic fertilizers, or by biological nitrogen fixation (**Fig. 3**). The latter process may significantly add to the input of reactive N to soil in some agricultural ecosystems (Herridge et al., 2008). The nitrogen recovery efficiency varies between crops. E.g. ~50 % for cereal production (Ladha et al., 2005; 2016) and 30 % for sugar cane production (Otto et al., 2016). Surplus N, that is not harvested as plant biomass, is immobilized in soil organic matter, lost to the atmosphere as NO, N_2O and N_2 by microbial transformations in the agricultural soil (**Fig. 3**), or lost from the agroecosystem by diffusive processes (ammonium volatilization, nitrate leaching). The reactive nitrogen lost by diffusive processes causes groundwater contamination, eutrophication of surface water and terrestrial ecosystems, and ultimately increased emissions of NO, N_2O, and N_2 via microbial nitrogen transformations in these systems.

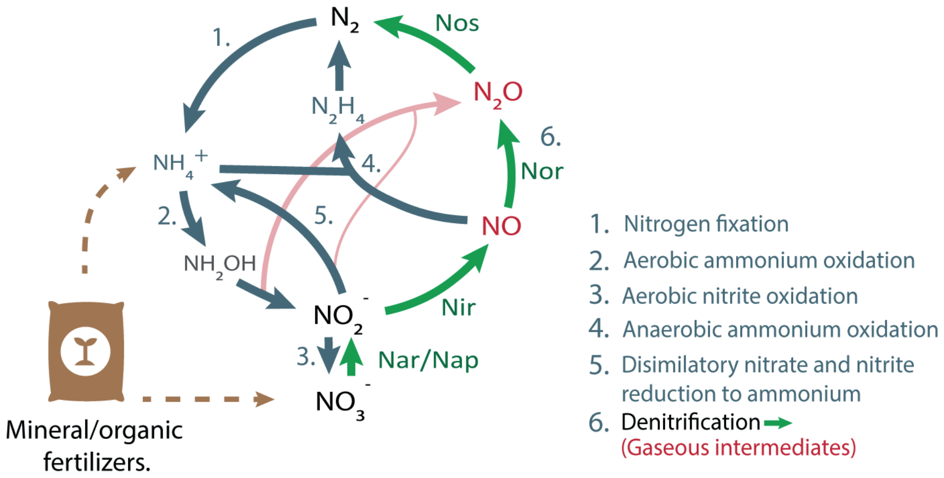

Figure 3: Microbial N-transformations. The input of fertilizer N enhances these reactions in agricultural soil, and indirectly also in natural ecosystems via a diffusive flow of reactive nitrogen from the agroecosystems.

N_2O is a by-product of several biogeochemical nitrogen transformations (**Fig. 3**).). Nitrification, the oxidation of ammonia to nitrite and nitrate, is catalyzed by ammonium-oxidizing and nitrite-oxidating bacteria (AOBs and NOBs), ammonia-oxidizing archaea (AOA), and comammox bacteria (2 and 3, **Fig. 3**). N_2O is released as a byproduct of the oxidation of ammonium via hydroxylamine in the above processes (Stein, 2019; 2020) or indirectly due to abiotic decomposition of hydroxylamine (Bremner et al., 1980; Heil et al 2015). The fraction of oxidized N released as N_2O by AOA is believed to be lower relative to AOB, as demonstrated for model bacterial and archaeal ammonia oxidizers by Hink et al. (2017). The proposed pathway of nitrifier-denitrification, where AOBs under low oxygen tension may channel electrons towards nitrite reductase (Nir) and nitric oxide reductase (Nor) enzyme equivalents (**Fig. 4**) (reviewed by Wrage et al., 2001), has been reported to account for a significant fraction of total N_2O emissions from soil (Shaw et al., 2006; Kool et al., 2011). However, the significance of nitrifier-denitrification is debated as quantitative isotope-based methods fail to omit other co-occurring processes (e.g. heterotrophic denitrification), and evidence to support a respiratory role of the coupled processes is not convincing (Hink et al., 2017). Literature is scarce when it comes to the environmental impact of the recently discovered organisms that catalyze complete nitrification, a process coined *comammox* (Daims et al., 2015; van Kessel et al., 2015), where single organisms perform complete oxidation of ammonium to nitrate (2 and 3, **Fig. 3**). Comammox bacteria are distributed in several natural systems (Gao et al., 2016a; Orellana et al., 2018), and their activity in some soils indicate a significant, but small, contribution to ammonia oxidation (Wang et al., 2020). Pure culture experiments with strains of *Nitrosospira inopinata* have demonstrated low yields of N_2O, comparable to that of ammonia-oxidizing archaea (Kits et al., 2019). Whilst DNRA (5, **Fig. 3**) generally is considered as a process that conserves nitrogen in soils, the release of N_2O has been observed from such organisms. It has been proposed that some DNRA organisms release N_2O as a mechanism to detoxify NO_2^- in high-pH environments (Stevens and Laughlin, 1998), but the mechanisms behind DNRA N_2O emissions are understudied, and therefore unclear. However, several DNRA organisms carry genes catalyzing reactions generating gaseous intermediates of denitrification (Mania et al., 2014). Pure culture studies have revealed that DNRA organisms of the metabolically flexible *Bacillus viereti* and, the less versatile, *Wollinella succinogenes,* both encoding Nor and Nos, may be potent N_2O sinks, but also sources under very high nitrate conditions (Mania et al., 2016). *Anaerobic ammonia oxidation* (Anammox) (4, **Fig. 3**) bacteria oxidize ammonium with nitrite (via NO) to hydrazine and then N_2 (Kartal et al 2010) but are generally not believed to emit N_2O under physiologically relevant conditions (Kartal et al., 2007). Lastly, chemo-denitrification, significant in soils with low pH (< 5), occurs when NO_2^- chemically reacts with organic compounds to produce N_2O and N_2 (Chalk and Smith, 1983).

Setting itself apart from the other processes of the biogeochemical N transformations - *denitrification* (presented in **Chapter 1.2.1**) is the only known metabolic pathway where N_2O is an intermediate, thus being produced and consumed (6, **Fig. 3**). Full-fledged denitrification pathways are generally only found in bacteria (with some known exceptions: e.g. the anaerobic ciliate endosymbiont *Candidatus Azoamicus ciliaticola* (Graf et al., 2021)). Truncated pathways are, in addition to bacteria, common traits of some fungi (Shoun et al., 1992; Keuschnig et al., 2020). However, a fungal N_2O reductase is yet to be found (Maeda et al 2015), making fungal denitrification a N_2O-generating process. In soil, denitrifying prokaryotes (DPs) make up 10 – 20 % of the soil community (Lycus et al., 2017).

1.2.1 Denitrification

DPs are facultative aerobes that sustain their anaerobic respiration by the stepwise reduction of $NO_3^- \rightarrow NO_2^- \rightarrow NO \rightarrow N_2O \rightarrow N_2$, catalyzed by the enzymes Nar/Nap, NirK/S, Nor and Nos (clade I or II), that is encoded by the genes *nar*/*nap*, *nir*, *nor* and *nosZ*, respectively (**Fig. 3, Fig.4**), when oxygen availability is limited (Zumft, 1997; Shapleigh, 2013). Nitrous oxide reductase (Nos), catalyzing the reduction of N_2O to N_2, is the only known enzyme that reduces nitrous oxide. The defining characteristic of a DP is, however, not straightforward, as a significant proportion of the denitrifying community in soils have truncated denitrification pathways (Jones et al., 2008), i.e. lacking one to three of the enzymes in the stepwise reduction of NO_3^- to N_2. Several definitions exist; from the stringent definition of any organisms that, as a minimum, reduce 80 % of NO_3^- to N_2 (Mahne and Tiedje, 1995), to the *senso stricto* definition of expressing a functional NirK or NirS, the first enzyme transforming soluble NO_2^- to gaseous NO (Zumft, 1997), to the less stringent definition of carrying at least one of the four enzymes (Shapleigh, 2013). In this thesis, the term DP is defined by the *senso stricto* definition, i.e. an organism that, as a minimum, supports growth through respiration of NO_2^- to NO. The term *nitrous oxide respiring bacteria* (short: NRB) is used collectively for organisms that as minimum supports growth by respiring N_2O (i.e. expresses functional Nos). The modular organization of the denitrification enzyme machinery has environmental implications (see **Chapter 1.3.1**), as truncated DPs lacking Nos will be net N_2O emitters, whilst NRBs carrying Nos as the sole nitrogen reductase will be net sinks.

In denitrifying respiration, the nitrogen oxides NO_3^-, NO_2^-, NO and N_2O are terminal electron acceptors in the electron transfer chain. Reduced electron carriers (NADH, FADH2), generated through glycolysis and in the TCA cycle, deliver electrons to the terminal N-oxidases via the respiratory chain to Nar, Nor, Nir and Nos. This generates a proton motive force (pmf) by transport of protons over the cell membrane, generating a proton gradient that drives ATP production by ATP synthase (**Fig. 4A**). In complete anaerobic respiration of NO_3^- the sequential reduction to N_2 involves the transfer of 10 e^- per molecule of N_2 formed. Nar is membrane-bound, with its catalytic site facing the cytoplasm, and contributes directly to the generation of pmf, whilst the other enzymes (Nir, Nor and Nos) are located in the periplasmic space, anchored or associated to the cell membrane, and contribute indirectly to pmf generation by receiving electrons via the cytochrome bc1 complex, cytochrome c1, pseudoazurin or quinols embedded and/or associated with the cell membrane (Spiro, 2012; Torres et al., 2016; Mania et al., 2020). The periplasmic nitrate reductase, Nap, is located in the periplasm and does not directly contribute to pmf as it reduces NO_3^- with H^+ being released and then consumed again (**Fig. 4A**). Nap's physiological role has been explained as a mechanism for disposal of excess electrons, under both oxic and anoxic conditions (Ellington et al., 2006).

Genes for catalytic subunits of the nitrogen reductases of denitrification are organized in operons together with accessory/peripheral genes, of which gene products support assembly and maturation of the reductase complexes or other functions (e.g. ion and electron transport) (Vaccaro et al., 2016). Organisms with genes coding for both nitrate reductases (Nap and Nar) are moderately common amongst DPs. Organisms carrying genes coding both the nitrite reductases (cytochrome cd1 containing NirS and copper-containing NirK) have not been identified. Two nitrous oxide reductase enzymes have been identified: Nos Clade I is characterized by a Tat-dependent signal peptide (indicating that folding takes place in the periplasm), the absence of a haem domain, and the presence of the peripheral genes n*osR* and *nosX* in the nos operon (Torres et al., 2016). NosR plausibly functions as an alternative electron donor to Nos Clade I (**Fig. 4A**) (Zhang et al., 2019).

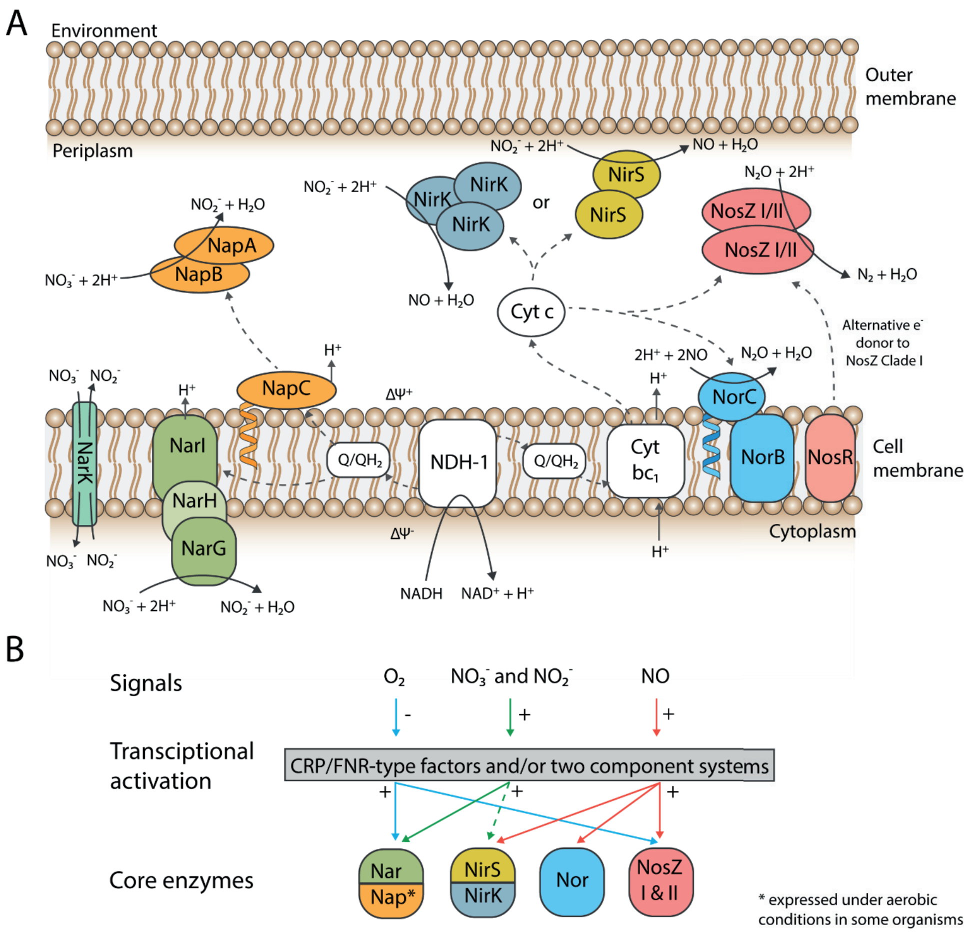

Figure 4: **A:** Simplified representation of the electron transport chain and associated reactions catalyzed by the denitrification reductases (Nar, Nap, NirK, NirS, Nor and Nos (Clade I or II) for a gram-negative DP. Enzymes are placed according to their cellular localization. NADH Dehydrogenase I (NDH-1) catalyzes the transfer of electrons from NADH generated in glycolysis or the TCA cycle, reducing quinone to quinol (Q/QH$_2$). Electron flow is indicated by dashed arrows. Reactions catalyzed are indicated with solid arrows. NosR has been shown to function as an alternative electron donor

to Nos Clade I (Zhang et al., 2019). Figure adapted from Torres et al. (2016) and Mania et al. (2020). **B:** Simplified sketch of regulatory roles of oxygen and, nitrate/nitrite and nitric oxide sensors. While the regulatory roles of O_2, NO_3^-/NO_2^- and NO are common to most denitrifying organisms, the regulatory networks differ between organisms (Spiro, 2012; 2016). (Panel B: Courtesy of Linda Bergaust).

Nos Clade II is generally sec-dependent (folding of the enzyme takes place in the cytoplasm) with some exceptions (Jones et al., 2013), may have a haem c domain, and organisms carrying this form of Nos lack the genes *nosR* and *nosX* in the Nos operon (Torres et al., 2016). Nos Clade II seems to be widespread amongst DPs and is found in high prevalence among non-denitrifying N_2O-respiring organisms (NRBs) (Jones et al., 2013). The ecological consequence/difference of nosZ Clade I and clade II organisms is not completely understood; Organisms with nosZ Clade II have been suggested to have higher growth yields and lower half-saturation constant (K_s) for N_2O compared to that of Clade I organisms (Yoon et al., 2016), which would indicate that these organisms play potential key roles as N_2O sinks in soil. This has been contested by Conthe et al. (2018), however, who found that Clade I organisms had higher overall catalytic efficiency (μ_{max}/K_s).

The flux through denitrification is controlled by transcriptional regulators that respond to O_2, NO_2^-/NO_3^- and NO (**Fig. 4B**) (Spiro, 2012). NO is a toxic intermediate, and it is commonly thought that tight regulation (coordination) of NO_2^- - and NO-reduction is essential to avoid cytotoxic NO concentrations. This would explain why most denitrifying organisms can keep NO-concentrations low during denitrification. In the model bacterium *Paracoccus denitrificans*, such NO homeostasis at nM concentrations is a result of high Vmax and low km for NO-reductase (Hassan et al., 2016). In contrast, *Agrobacterium tumefaciens* can produce cytotoxic NO concentrations under certain conditions (rapid transition from oxic to anoxic conditions), as demonstrated by Bergaust et al. (2008), and modeled by Kampschreur et al. (2012), which indicated that the cause is a positive feedback loop via NO-inhibition of NO-reductase. It is important to be aware, however, that such “NO-suicide” is an experimental artifact of culturing the organisms alone in gas-tight vials. Under natural conditions, NO will diffuse away or be reduced by surrounding organisms.

O_2 affects oxygen sensing transcriptional regulators that belong to FNR or CRP superfamilies. There are several orthologues of these regulators (FnrP in *Pseudomonas denitrificans*, ANR in *Pseudomonas aeruginosa*, and FnrN in *Rhizobium leguminosarum*) but all are assumed to work similarly: The DNA binding properties are modulated by oxygen, in which presence oxidizes $[4Fe\text{-}4S]^{2+}$ clusters to $[2Fe\text{-}2S]^{2+}$ that promote dimerization of the proteins leading to lowering of DNA affinity, which in turn affect the transcription of the Nar and Nos operons (**Fig. 4B**). Nitrate regulates the Nar-operon via nitrate sensors (NarR in *Paracoccus denitrificans*, NarXL two-component system in *Pseudomonas aeruginosa* and *stutzeri*), whilst NO stimulates transcription of nir, nor and nos operons via activation of NNR-type regulators (Spiro, 2012; 2017). Once Nir has expressed the reduction of NO_2^- to of NO triggers a positive feedback via the NO-sensor NNR, facilitating the expression of a full-fledged denitrifying proteome (Hassan et al., 2014). The consequence of this positive feedback loop (Nir producing NO which triggers more transcription of *nir*) has been studied intensively in the model bacterium *Paracoccus denitrificans*. It appears that in this organism, the initiation of *nir*-transcription occurs with low probability, but once initiated, the process escalates via the positive feedback loop. This was suggested as an explanation for the *bet-hedging* in this organism: only a fraction of the cells synthesize Nir (and engage in denitrification) in response to oxygen depletion (Lycus et al., 2018), while all cells synthesize Nos. The phenomenon is important because organisms with such *bet-hedging* are strong sinks for N_2O in the environment (the majority of cells reduce N_2O but do not produce N_2O).

1.3 Drivers of agricultural N_2O emissions

The soil environment is a mosaic of aerobic and anaerobic zones (Sexstone et al., 1985; Parkin, 1987; Schlüter et al., 2019), and several of the nitrogen redox processes (**Fig. 3**) occur simultaneously across microsites of the same soil (Abbasi and Adams, 2000). Advances in stable isotope labeling (Baggs, 2008), often in combination with inhibitors such as acetylene (which inhibits nitrification at around 100 ppm, and reduction of N_2O via Nos at 10 vol %), have made it possible to distinguish between N_2O derived from nitrification, denitrification and other sources (Klemedtsson et al., 1988; Stevens and Laughlin, 1998). Selective inhibition of AOB by N-octyne has also enabled the quantification of AOA's contribution to nitrification and N_2O production (Giguere et al., 2015).

The major contributing processes to N_2O emissions from soils and sediments are biological, where nitrification and denitrification accounts for approximately 70 % of the N_2O emitted to the atmosphere (Syakila and Kroeze 2011, Braker and Conrad, 2011). Of the two processes, denitrification is considered the most significant source of N_2O from most soils (Khalil et al., 2004, Ostrom et al., 2010). However, in some soils with particular physiochemical characteristics, e.g. soil with low carbon content where autotrophic nitrification probably plays a dominating role due to very low carbon availability leading to low activity of heterotrophic denitrifying organisms (Liu et al., 2016), or soils with low water content/water-filled pore space (WFPS) (Brümmer et al., 2008) were nitrification also dominates. In wetted soils with WFPS > 80 % denitrification dominates (Braker and Conrad, 2011).

The propensity of a soil community to emit N_2O depends on a plethora of factors in both the temporal and spatial scale (Butterbach-Bahl et al., 2013) and relies on interactions between soil physiochemical factors and biological processes (e.g. pH (Mørkved et al., 2007; Qu et al., 2014), soil porosity (Del Grosso et al., 2000), water saturation (Linn and Doran, 1984), carbon availability (Senbayram et al., 2012; Liu et al., 2016) and ammonium and nitrate concentrations) (discussed in **Chapter 1.3.1)**, and abiotically catalyzed reactions like chemo denitrification.

1.3.1 Mitigating agricultural N_2O emissions

The simplest mitigation measure would be to reduce the N input to soil, but abridged use of N-based fertilizers are associated with agronomic and economic consequences (lower yield, thus lower profit) (Venterea et al., 2012). Mitigation practices that take in to account agronomic practices and the demand for agricultural products are termed "best management practices" and include matching N supply with N demand, avoiding excess use of N-fertilizers, and precision fertilizer application, amongst others (van Groeningen et al., 2010; Zhang et al., 2015), and have the potential to significantly reduce N_2O emissions (~20 %) (Winiwarter et al., 2018). However, as the demand for agricultural fertilizers is expected to increase (estimated by Tenkorang and Lowenberg-DeBoer, 2009; 188 million tonnes by 2015, to 223 million tonnes by 2030), additional efforts targeting the N_2O emissions from agriculture is needed.

There is a negative correlation between soil acidity and N_2O emissions (Wang et al., 2018; Hénault et al 2019). Soil acidification is a consequence of intensified agriculture and longer-term application of N-based fertilizers as co-leaching of base-ions together with nitrate elevates pH in soil (Tian and Niu, 2015). pH is a major controller of N_2O emissions due to a negative effect of low pH on the maturation of Nos, which takes place in the periplasm (Liu et al., 2014), where pH equals that of the external environment, in contrast to the cytoplasm where pH is strongly regulated by cell metabolism (Wilks and Slonczewski, 2007). About ~40 % of the world's arable soils are acidic (Kunhikrishnan et al., 2016), and a feasible mitigating strategy for N_2O could be large-scale modification of soils' inherent pH through liming with calcareous minerals which has been shown to mitigate N_2O derived from denitrification and chemo denitrification in low pH soils (Wang et al., 2018, Hénault et al., 2019). However, the reduced N_2O emissions come at a possible expense as the increased emissions of carbonate-CO_2 (Nadeem et al., 2020; Wang et al., 2021) makes the net reduced GHG effect more uncertain.

The use of nitrification inhibitors (e.g. dicyandiamide (DCD), 3,4-dimethylepyrazole (DMPP) N-(n-butyl) thio phosphoric triamide (NBPT) and nitrapyrin), has been around for several years and has been demonstrated to improve fertilizer use efficiency. The inhibitors work by decreasing nitrification rates in soils (as ammonium is rapidly nitrified to nitrate in most soils which leads to losses from leaching and denitrification), thus N is retained as ammonium. In the meta-study of Abalos et al. (2014) crop yields were evaluated across several studies where the inhibitors NBPT, DMPP, and DCD were applied. While the effects on crop yields were variable, dependent on environmental and crop management factors, the use of inhibitors did reduce N_2O emissions. Thus, nitrification inhibitors were generally regarded as positive in reducing N2O asscociated climate forcing (CF) for a wide range of cropping systems, as also pointed out by others (Misselbrook et al., 2014; Ruser and Schulz, 2015). However, an often-overlooked side-effect is the increased ammonia volatilization from soils with pH≥7. This effect can be a major drawback as it may lead to indirect emissions of N_2O

elsewhere which may outweigh the effect on N_2O emission from the agricultural soils treated with inhibitors (Lam et al., 2017).

N_2O produced, be it of abiotic origin of by activity of nitrifying and denitrifying organisms, may be reduced to N_2 by any organism expressing a functional nitrous oxide reductase (Nos) under anoxic conditions (**Fig. 3 and 4**). Graf et al. (2014) screened the sequenced genomes of denitrifying bacteria and found that ~1/3 of the sequenced genomes with *nosZ* lacked genes for nitrite reductase (*nirK* or *nirS*). This modularity of the denitrifying enzyme machinery has, as mentioned in **Chapter 1.2.1**, environmental implications as some bacteria will be net N_2O emitters (if they lack the *nosZ* gene, coding for Nos), or net N_2O sinks (e.g. only carrying *nosZ*). This suggests that increasing the fraction of such N_2O-respiring bacteria (NRB) in soil could mitigate N_2O emissions, which was verified by the introduction of N_2O-respiring bacteria to soils by Domeignoz-Horta et al. (2016). They observed a significant decrease in N_2O emissions by inoculating soils with ~10^8 NRB-cells g^{-1} soil. A closer inspection of their data reveals that the NRB-inoculation could only reduce N_2O emission significantly in soils with pH > 6.5; in all soils with pH < 6.5, the effect of inoculation was not statistically significant. While this proves that the abundance of NRB in soil <u>can</u> affect N_2O-emission, attempts to find the expected correlation between N_2O emissions and the *nir/nosZ* gene abundance ratio of soils have given inconsistent results (Rocca et al., 2015). The presence of a gene in the microbiota evidently is no evidence for the expression of an active enzyme. It is worth noticing that NRBs are not the only sinks for N_2O in the environment. Organisms with a full-fledged denitrification pathway can both produce and reduce N_2O and may be either net sources or sinks for N_2O in the environment. This depends on their denitrification regulatory phenotype (DRP, Bergaust et al., 2011), which is shaped by the regulatory network controlling the stepwise reactions of denitrification, both at the transcriptional (Spiro, 2012; Lycus et al., 2018) and metabolic (Mania et al., 2020) level.

Whilst increasing the abundance of NRB by inoculation of soils has proven successful in reducing N_2O emissions, an upscaling would possibly be prohibitively expensive as a stand-alone operation (additional details in **Chapter 1.4.2**). Gao et al. (2016b; 2017) ingeniously prepared granulated organic fertilizers soaked in N_2O-respiring strains (grown *ex situ*) of *Azospirillum* and *Herbaspirillum*, and soil fertilization with these granules reduced N_2O emissions significantly, thus demonstrating the applicability of substances vectoring such organisms to soil. The potential impact of improving natural and engineered systems capacities for GHG mitigation through larger-scale microbiome manipulation has recently received broader scientific attention (Cavicchioli et al., 2019, D'hondt et al., 2021) (see **Chapter 1.4.3**).

N_2O-emission is also an irritating "joker" in the game of reducing the climate forcing of food production. For instance, N_2O may topple other agronomic attempts to reduce anthropogenic climate forcing such as carbon sequestration in agricultural soils that reduce anthropogenic CO_2 emissions is negated, as the net effect may be to increase climate forcing because they may enhance N_2O emissions (Li et al., 2005; Reay et al., 2012; Liu et al., 2017).

Likewise, the climate effect of cultivation of crops for biofuels, replacing fossil fuel, is nil because the N_2O-emission negates the cooling effect of reducing CO_2 (Reay et al., 2012).

1.4 Anaerobic digestion (AD) as a platform for GHG mitigation

1.4.1 Anaerobic digestion in the circular economy

The European Union, currently producing ~50 % of the global production of biomethane (Scarlat et al., 2018), has successfully implemented governmental policies to facilitate AD as a core technology in the management of urban organic wastes (EU1, EU2). Towards 2050 AD is expected to continue to be a key operation within the future circular economy in Europe (EU3). There are good reasons for this strategy: Of the three dominating organic waste management technologies anaerobic digestion, composting and incineration (Bartl, 2015), anaerobic digestion is the most sustainable by providing a residue (digestate) with high fertilizer value (retaining all the organic N), combined with the production of CH_4 which can replace fossil fuels. AD also scores better on overall environmental impact (Baldasano and Soriano, 2000). Although the mentioned organic waste management options all produce a slurry or solid residue and convert chemical energy to other forms, the energy yield from incineration or composting have medium to low value (heat) compared to methane (van Gool, 1987), and ashes from incineration have few useable applications to date. The CH_4 produced from anaerobic digestion may be used for more than heating and its applications include vehicle fuels, integration with existing gas networks, or generating electricity with combined heat and power units.

The authorities' explicit motive for promoting AD both for urban and agricultural wastes is to produce methane that replaces fossil fuels. However, there is evidence that AD can do more to reduce CF. In the meta-study by Miranda et al. (2015), the authors estimate the potential for reducing the livestock sector's CF by anaerobic digestion (AD), and recognize a quadruple effect: 1) eliminating CH_4 emission from storage that would occur without AD; 2) replacing fossil fuels; 3) producing digestate that replaces mineral fertilizers and 4) lowering the N_2O emissions from soil fertilized with digestate in place of soil fertilized with raw manure. The replacement of fossil fuels by the methane produced accounted for only 11% of the reduced climate forcing (per produced unit of food). The elimination of CH_4 emissions from storage accounts for more (43 %), while the reduction of greenhouse gas (GHG) emission after field application (primarily reduced N_2O emissions) accounts for 6.3 %. The latter is based on the assumption of a 33 % reduction in the N_2O emissions, but this estimate is very uncertain as there was large variation between studies, which was also underscored by Herrero et al. (2016).

AD is a biological process where complex organic material is broken down under anaerobic conditions to methane and carbon dioxide. The process can be divided into four main steps: 1: hydrolysis of larger biopolymers to their monomeric constituents, 2: acidogenesis and fermentative production of volatile fatty acids, 3: acetogenesis, where volatile fatty acids are reduced syntrophically to acetate, H_2, and CO_2 by hydrogen yielding fermentative organisms and 4: methanogenesis where acetoclastic archaea dismutate acetate to methane and CO_2, and hydrogenotrophic archaea utilizes hydrogen, carbon monoxide or formate to reduce CO_2 to methane. Hydrogen partial pressure is of significance, and the activity of hydrogenotrophic methanogenic archaea modulates the activity of fermentative organisms or/and syntrophic relationships within the microbial community, via their consumption of hydrogen (Schink, 1997). The organisms catalyzing steps 1-4 in AD are referred to as the "*methanogenic community*" in the following chapters.

The residue, digestate, from anaerobic digestion is a heterogeneous slurry of particulates consisting of non-degraded carbon and inorganic residues, microbial cells, and soluble intermediates from the hydrolysis, acidogenesis, and acetogenesis steps of AD. Composition and characteristics will vary based on the AD substrate and process configuration. Most digestates are good fertilizers due to their content of mineralized N (Gutser et al., 2005), more or less available P, mineral content (potassium and calcium) (Ehmann et al., 2018), substantial amounts of organic carbon which improves soil structure (Beni et al., 2012), provides substrates to the soil biota (Alburquerque et al., 2012) and increase soil organic C (Béghin-Tanneau et al., 2019). However, the present economic value of digestates is modest (Riding et al., 2015, personal communications with VEAS WWTP), partly due to high transport costs and logistics (timing of fertilization does not match with production) (Peng and Pivato, 2019). For digestates from WWT, an additional obstacle is market acceptance (e.g., the risk for food safety). Despite the qualities of digestates as organic fertilizers, valorization is needed (Peng and Pivato, 2019)

1.4.2 AD as a platform for large scale modification of soil microbiota

Increasing the fraction of bacteria carrying a strong capacity for N_2O reduction in soil has proven successful in mitigating N_2O emissions (**Chapter 1.3**). In principle, this could be achieved by agronomic practices that enhance the growth of organisms with a strong capacity for N_2O reduction, but to date, there is no clear path on how to achieve this. Alternatively, it could be achieved by heavy inoculation of soils with bacteria with a strong capacity for N_2O reduction, ideally, NRBs that only express Nos. Such heavy inoculation would be prohibitively expensive as a stand-alone operation, but, as hypothesized in this thesis, not if integrated with the established material pipeline of organic wastes via AD to soil (**Fig. 5**): if the digestates were engineered to contain N_2O-respiring bacteria, they would become an effective instrument for massive inoculation of soils, hence reducing the N_2O emissions.

Such an approach could introduce a much-needed valorization of organic wastes via AD (Peng and Pivato, 2019), as digestates in most cases are destined to be returned to soil as organic fertilizers and soil enhancement products. This option will become increasingly relevant since AD is expected to increase in extent and range in the coming decades as a consequence of the transition from fossil fuels to green sources of energy, as discussed above (**Chapter 1.4.1**). Ideally, the N_2O respiring organisms should be grown in the digestate, utilizing the available carbon sources, rather than adding bacteria to an organic fertilizer after first cultivating them in nutrient broth (as done by Gao et al., 2016b and 2017), see **Chapter 1.3.1** and **1.4.3**). This could open an avenue of effective enhancement of the N_2O reduction capacity of agricultural soils, hence reducing N_2O emissions.

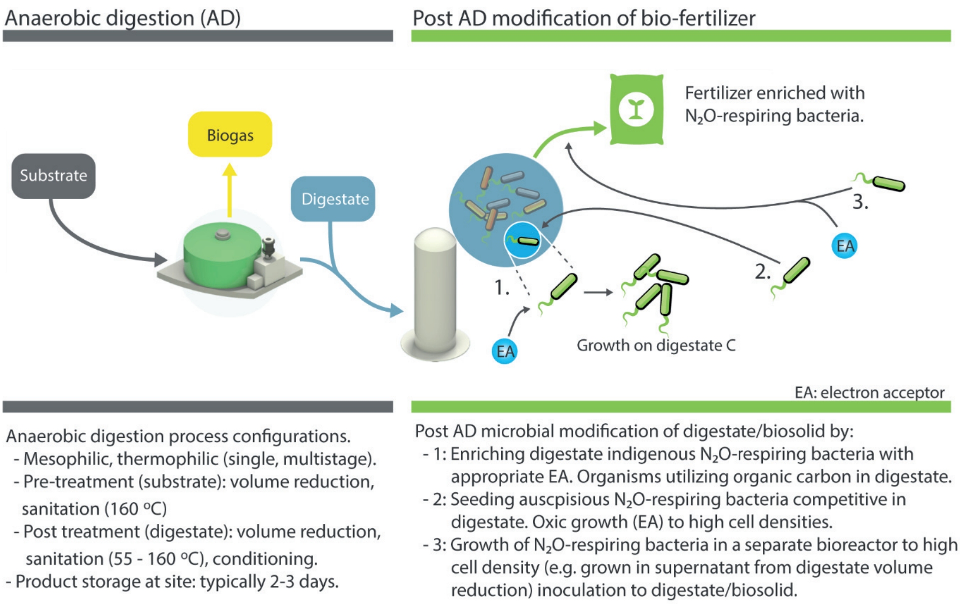

Figure 5: **Implementation of large-scale introduction of N_2O-respiring bacteria vectored by digestates provided by the growing industry of anaerobic digestion (AD) to soil**. Left: industrial AD configurations are typically, but not limited to, mesophilic/thermophilic single or multistage configurations. Sanitation techniques for pathogen reduction are common for several substrates, imposed by government regulations (Iranpour et al 2004), and can be performed after (digestate) or before (substrate) AD, generally by heat treatments of either substrate or digestate. Liquids can be removed from the digestates before transportation and mulching into soil. Right: Post AD modification of the bio-fertilizer/digestate by the introduction and/or growth of N_2O-respiring organisms at site. Implementation can in principle be done in several ways (not limited to the examples given): 1: Enriching digestate indigenous N_2O-respiring bacteria directly in the digestate using an electron acceptor that would select for such organisms (e.g. N_2O). 2: Seeding auspicious exogenous N_2O-respiring organisms in digestate and continue growth by e.g. aerating the digestate. 3: Heavy inoculation of digestate/biosolid with N_2O-respiring bacteria grown in separate bioreactors.

For most digestates country-specific legislation dictates the need for processing after AD (depending on the type of AD substrate) which governs possible end-use applications (see Iranpour et al. (2004) for details). Processing digestates to accommodate such regulations often involves heat treatments to reduce pathogens (sanitation). Of particular interest is Thermal Hydrolysis Processes (THP), where the material is heated to 160 °C followed by a sudden release of pressure (flash evaporation). THP before AD improves methane yields by making recalcitrant substrates bioavailable and improves the dewaterability of the produced digestate (Svensson et al., 2018). Alternatively, THP can be used to sterilize the digestates post AD (Svennevik et al., 2019), with multiple benefits for its use as a vector for N_2O-respiring organisms: 1) N_2O-respiring bacteria could be grown aerobically in the digestate material, due to the absence of competing aerobic organisms. 2) Recalcitrant carbon is solubilized, which could supply growing organisms with carbon. 3) Effective sterilization eliminates the risk of methane emissions from the digestate resident methanogenic community in anoxic micro-niches in the amended soil. 4) Inoculation with adequate organisms in such sterilized digestates might introduce robustness towards re-contamination of fecal coliforms in the digestates, as demonstrated by Svennevik et al. (2020).

1.4.3 Survival of inoculants in soils

Inoculating soils with bacteria to introduce or promote certain microbially mediated functions is not a new concept, and numerous studies have been conducted to explore this option and identify obstacles. A full review of this vast literature would be beyond the scope of this thesis, but some key points for the success or failure of soil-based inoculants will be discussed.

Strain selection is a key element of successful bioaugmentation. Still, the choice of inoculant has generally been oriented towards the selection of catabolically competent microorganisms, and considerations concerning the ecology of establishment and survival are seldom given the same level of thought (Dejonghe et al., 2001; Thompson et al., 2005; Verbruggen et al., 2013; Kaminsky et al., 2019). Survival and establishment of an inoculant in the residing soil community seem to increase if the environment resembles the environment from which the inoculant was obtained, as demonstrated by Belotte et al. (2003) who showed that soil isolates grew better in the soil from where they were isolated, as opposed to nearby soils. Concerning agricultural soils, this result would also advocate the need for examination of the community composition and dynamics of the native soil community as a basis for selection of promising N_2O-respiring candidates, as, presumably, environment-native strains would have a competitive edge in their own “backyard”. Dejonghue et al. (2001) suggested auspicious strains for successful soil inoculation are likely to be organisms with catabolic profiles that match the dominating substrate flux in the soil(s).

Microbial inoculants are generally grown in rich media *ex situ* before downstream formulation, storage (e.g. as dried powder), and transportation to end-users (Kaminsky et al., 2019), and should, ideally, persist in the target environment for as long as possible to maximize benefit and minimize costs (Verbryggen et al., 2013). As most natural environments are generally oligotrophic by nature, these ideal inoculant requirements are in conflict as one seeks the combination of two broad fitness traits: feature of an r-strategist (fast growth, high K_m and V_{max}) when produced, and features of a K-strategist (competitive in "crowded" populations, low K_m and V_{max}) after introduction to the environment. Fitness in microbial ecology is a (relative) measure of the ability of a microorganism to establish itself as a member of the microbiota of an environment, and several strategies that are employed by bacteria to increase fitness in the environment have been elucidated in the scientific literature. This has resulted in an array of specialized databases optimized for searching for indications of such traits in sequenced genomes, e.g. antagonistic effects such as the production of secondary metabolites, such as antibiotics (De Pascale et al., 2011), and various predatory lifestyles (Pérez et al., 2016) that are associated with the prevalence of certain genes (Pasternak et al., 2013). Or metabolic flexibility and ability to maximize utilization of the resources available in an environment whereby certain extracellular secreted carbohydrate-active enzymes and carbohydrate-binding modules associated with binding to cellulose (Kezuka et al., 2006), starch/glycogen (Koay et al., 2010; Chaen et al., 2012), peptidoglycans and chitin (Onaga and Taira, 2008) could indicate capacities of metabolizing more recalcitrant carbon sources. The gene products might also reflect environmental adaptations, as shown for organisms adapted to low pH environments and the increased occurrence of certain specific extracellular secreted peptidases (Nguyen et al., 2019), or by an increased tolerance to rapid changes in environmental conditions, e.g. glycogen metabolism has been shown to improve short term *E. coli* fitness (Sekar et al., 2020).

A key challenge of any microbial inoculant is to establish itself amongst the residing population. The likelihood of a successful invasion of an inoculant seems to be negatively correlated with the diversity of the residing community (van Elsas et al., 2012), as a broad spectrum of ecological niches would be pre-occupied by the native community members. This is referred to as the diversity-invasion effect, and reflects the key challenges of an invading organism; growth and establishment by utilizing resources not utilized by the resident community, or forceful "overtake" of a resident niche through competition or antagonism (van Elsas et al., 2012). Interestingly, even if the introduced strains fail in their invasion attempt, they may mediate changes (legacy effects) in the residing soil microbial community composition. Mallon et al. (2018) demonstrated this by inoculating soil communities with *E. coli* (**Fig. 6**) and observed a niche differentiation and a sustained clearing of the invaders overlapping niches for some time after *E. coli* was outcompeted (failed invasion) and hypothesized that the legacy effect of this "clearing" of niches might make a second invasion more successful.

Repeated inoculation has been demonstrated to produce successful results for polychlorinated biphenyls (PCB) degradation in soil, where a single inoculation event did not reduce soil PCB levels, but repeated inoculation resulted in a significant reduction (Gilbert and Crowley, 1998). However, the soil microbial community was not monitored in this study. Anthropogenic mediated bacterial invasions (compost addition to soil, bio-fertilizers, biocontrol, and remediation) are generally characterized by introducing large numbers of invading bacteria. Since digestates as organic fertilizers will be repeatedly introduced to soil, the use of these as vectors would imply repeated inoculation, hence a reasonable chance of establishment of invaders as sustained members of the soil microbiota.

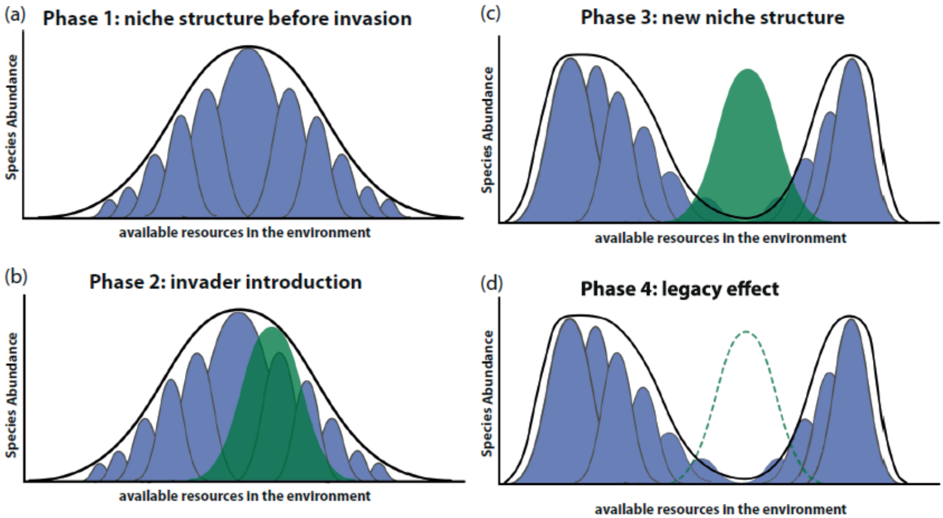

Figure 6: Conceptual model based on invasion experiments with *E. coli* to soil summarizing results of Mallon et al (2018). a) Before the invasion the community composition and niche structure are structured according to available resources in the environment. Available niches are covered by taxa with a certain total abundance in the community. b) Massive inoculation of an invading organism with overlapping niches to parts of the resident microbial community. c) As a function of sheer numbers, the invader outcompetes competitors by competition for substrates. This also alters the community composition and niche structure of the resident community, which leads to d) a legacy effect as the invader gradually diminishes. This "clearing" of niches might make the next invasion attempt more successful (Reprinted with permission from Mallon et al., 2018).

Another factor influencing the successful introduction of bacteria to a harsh new environment is the physical and chemo-physical characteristics of the vectors. Bioencapsulation by gelation, emulsion, and crosslinking have increased the survival of bio inoculants (reviewed by Schoebitz et al., 2013). Growth and incorporation in the vector material (e.g. digestate) may affect survival in soil if the inoculants are harbored within the material. The carrier may, itself, change the soil characteristics (e.g. pH, organic matter content, cation exchange capacity), which could influence microbial survival (Gómez-Brandón et al., 2016). But also, the chemo-physical characteristics within the organic macroparticulates may enhance survival by providing micro niches for microbes with more favorable conditions than in the bulk soil. Gao et al. (2016b and 2017) inoculated organic fertilizer pellets with N_2O-respiring bacteria (grown *ex situ*) and achieved strong N_2O emissions reductions even from acidic soil. The reason for this could be that the pellets remained intact for a long time with an inner pH much higher than that of the surrounding soil. This would secure longer-term survival and more efficient synthesis of functional Nos than if the bacteria were exposed to the lower pH of the soil itself. Residing within such particulates might also introduce shielding in micropores that prevents grazing from protozoa and fungal predators. In this context, biochar could be an interesting carrier material, providing a refuge from predators (Quilliam et al., 2013).

Industrial production of live inocula may lead to domestication, as unwanted (or lack of) selection pressures could render organisms less fit for the natural environment than its parental wild type. In the review of Kaminsky et al. (2019) they bring up this problem specifically as a vital point towards explaining the lack of efficacy and reproducibility of bio inoculants and identified the step of mass production to be of particular relevance. Plausible domestication involves streamlining of genomes towards rapid growth on simple nutrients at high concentrations while losing the ability to withstand stress and starvation (Steensels et al., 2019). E.g. wild type *E. coli* isolates have been shown to change phenotype (metabolism, morphotype, and fitness) after only 2-3 days in subcultures (Eydallin et al., 2014). *Pseudomonas fluorescens* grown in complex media and media with a single carbon source in experiments targeting the laboratory evolution demonstrated that populations grown on complex media showed broader fitness by means of carbon utilization (Barrett et al., 2005). It seems plausible that phenomena of laboratory evolution might be reduced if the inoculant could be grown in the substrate from which it was isolated.

The various challenges with soil inoculation have implications for our chances to reduce N_2O emission by using digestates as vectors for NRB, as explored in this thesis. Fertilization with digestates, or any other organic fertilizer, induce transient peaks of N_2O emission because the digestate contains ammonium and easily available organic material which fuel nitrification and heterotrophic activity respectively (Johansen et al., 2013; Baral et al., 2017; Verdi et al., 2019; Dietrich et al., 2020). Akiyama et al. (2004) measured N_2O emissions over time after fertilization with urea and various organic fertilizers in large-scale soil incubations. The results indicated that denitrification was the dominant N_2O source in soil fertilized with organic fertilizers, and most of the fertilizer-induced N_2O that was emitted occurred within a relatively short timeframe (7 to 30 days). This transient peak in N_2O emission after fertilization with organic fertilizers could plausibly be reduced by NRB in the fertilizers, even with NRB that are unable to survive for a long time in soils. This would be a significant achievement since the transient N_2O emission after fertilizer applications accounts for a large share of the annual emissions from agricultural soils (Molodovskaya et al., 2012). A more ambitious goal would be to reduce the emissions throughout the rest of the year, which would require long-term survival of the NRB.

2. Basis and research goals

N_2O emissions from fertilized soils represent a large proportion of the total climate forcing of agriculture (**Chapter 1.1**). Excessive input of reactive N fuels the biogeochemical nitrogen cycle, leading to N_2O emissions because of, amongst other causes, truncated denitrification pathways (**Chapter 1.2-3**). Bioaugmentation of agricultural soils by the introduction of N_2O-respring bacteria is a promising abatement option, however large-scale modification of soils microbiome would be excessively expensive as a standalone operation and the desired outcome of introducing biological inoculants, biased by production methods of inoculums, makes the effects unreliable for many applications (**Chapter 1.4.3**).

Authorities push to implement AD as the primary treatment of organic wastes, and digestates, the residue of biogas production, are expected to become a major organic fertilizer for agricultural soils (**Chapter 1.4.1**). This could open an avenue for large-scale inoculation of more reliable microbial inoculants if the industrialized pipelines of organic waste management, backboned by AD, could accommodate production of inoculants at site (**Chapter 1.4.2**) grown and vectored in/by digestate to soil.

The overall aim of this work was to assess if the material pipelines through AD can be exploited as an industrial platform for the production of organic fertilizers that effectively enhance the soils' capacity to reduce N_2O by vectoring N_2O-respiring bacteria/inoculants to soil. Development and application of new and existing strategies on how to enrich, isolate, and assess the N_2O-reducing capacity of the isolates in axenic cultures as well as their efficiency as inoculants in agricultural soil, were means to this goal.

The study was initiated by a detailed demonstration of the applicability of such a concept by selectively enriching N_2O-respiring bacteria in live digestate originating from a municipal WWTP (**Paper I**) (WWTP details in **Appendix A**). Lessons learned in the proof of concept were applied to obtain more ideal isolates competent in soil and digestate environments (**Paper II**). Detailed monitoring of both gas kinetics (see **Chapter 3.1**) and microbial population dynamics (using metagenomics and proteomics and 16S rDNA amplicon sequencing) of the enrichment cultures, isolation and full genome sequencing of N_2O-respiring bacteria, and assessment of the obtained isolates' effect on soil N_2O emissions reduction (see **Chapter 3.2**) after growth in, and vectored to soil by, digestate.

3. Methods

Methods used are thoroughly described in the enclosed materials and methods chapters of **Paper I** and **Paper II**. Additional information on a few experimental methods is given below.

3.1 Robotized incubation system and gas analysis system

Gas chromatography was the main pillar of the work conducted in this thesis and was used as an instrument to monitor the kinetics of O_2, CO_2, N_2O, N_2, and CH_4 in enrichment cultures, and to assess the denitrifying phenotype of isolates, and their response to the transition from oxic conditions to anoxia. NO was detected by chemiluminescence: the sampled gas flows with an air-stream and is mixed with ozone (O_3), which reacts with NO, producing light (chemiluminescence), which is detected by a PM tube, described in detail by Molstad et al. (2007; 2016) (**Fig. 7**).

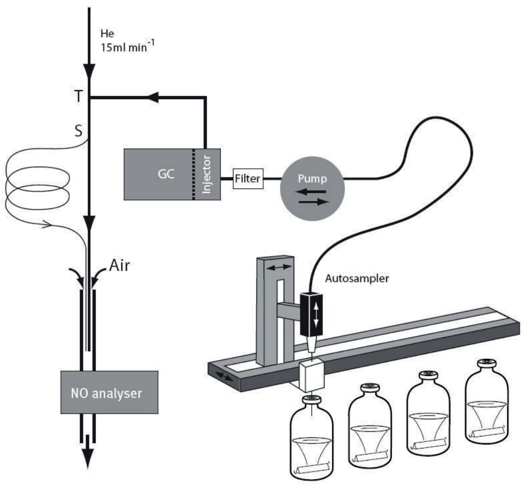

Figure 7: Sketch of the automated incubation and gas analysis system (Molstad et al., 2007; 2016).

Gas chromatography (GC) is a separation technique used to isolate volatile/gaseous components of a mixture depending on differences in the mode of partitioning between a flowing mobile phase (gas) and a stationary phase (separation column). Systems are normally set up with different mobile phases/carrier gasses that are compatible with the detectors of the system. The separation columns are temperature controlled, most have a "capillary" diameter and helical shape, and of varying length. The detector(s) are located at the end of the column and provides a quantitative (concentration and/or mass) measurement of the components in the mixture as they elute one by one with the carrier gas. Common types of detectors are mass spectrometer (MS), flame ionization (FID), thermal conductivity (TCD), electron capture (ECD and plasma emission detectors (PED).

The GC system used in this thesis is equipped with ECD, TCD, and FID detectors (a modified system that was equipped with a plasma emissions detector (PED) for detection of H_2 was used in one experiment), and the system allows for time incremental sampling and monitoring of N_2, O_2, CH_4, CO_2, N_2O and NO, at constant temperature in stirred or unstirred 120 mL cultures vials (**Fig. 7**). All vials were He-flushed through repeated vacuum and filling cycles to remove traces of N_2 and O_2 before the addition of relevant gases and electron acceptors before gas analysis and monitoring. The gas volume sampled and analyzed by the system is replaced with a corresponding volume of Helium after sampling. Mass loss due to sampling, and leakage of N_2 and O_2 through tubing and membranes is accounted for when calculating the rates of gas transformations for each time increment between two gas samplings. The data were used to assess N-mass balance (complemented by liquid measurements of NO_3^- and NO_2^-), and to estimate electron flow rates to the various terminal acceptors (O_2, NO_2^-, NO, N_2O) throughout the culture's/community's depletion of O_2 and N_yO_x. A spreadsheet with full transparency related to kinetics calculations and physical properties concerning gas solubilities is deposited online (Bakken 2021).

3.2 Assessing soils' propensity for N_2O-emission by incubation

Soils amended with digestate were monitored as microcosms in the robotized gas incubation and measurement system (**Chapter 3.1**). As a consequence of these vials being closed, the excess N_2O produced in the soil incubations, which otherwise would be released to the atmosphere, will be trapped inside the closed glass vials and ultimately reduced when the capacity of N_2O reduction surpasses that of production. This means that conventional emission ratios (N_2O/N_2O+N_2) would fall short. I_{N_2O} was used by Liu et al. (2014) as a proxy for the relative propensity of soils to emit N_2O from denitrification in microcosm experiments in closed vials, and its predictive capacity verified by Russenes et al. (2016), and therefore used in this work.

The N_2O production index (I_{N_2O}) was calculated for individual vials by equation 1:

$$I_{N_2O} = \frac{\int_0^T \mathrm{N_2O{-}N(t)dt}}{\int_0^T [\mathrm{N_2O{-}N(t) + N_2{-}N(t) + NO(t)]dt}}, \qquad (1)$$

where $\int_0^T N_2O - N(t)dt$ is the area under the curve for measured N_2O-N (µmol N vial^{-1} h) and $\int_0^T [N_2O - N(t) + N_2 - N(t) + NO(t)]dt$ is the area under the curve for measured N_2-N + N_2O-N + NO (µ mol N vial^{-1} h) (estimated using the trapezoidal rule), both for the time period 0-T (h).

4. Main results

Proof of concept: digestate enriched with NRB reduces soil N_2O emissions.

Our starting point was enriching digestate from biogas production for indigenous N_2O-respiring organisms in anoxic incubations with N_2O, aiming to isolate organisms capable of fast growth to high cell densities in digestate and with a high capacity for N_2O reduction. The digestate originated from anaerobic digesters at a municipal wastewater treatment plant (WWTP) that are fed by precipitated organic material from the sewage water and biofilm debris from the WWTP stationary nitrification and denitrification filters (**Appendix A**). Community dynamics throughout the enrichments in digestate were assessed by metagenomics, and activity was assessed by gas kinetics and metaproteomic analyses (omics samples: start, mid-point, end enrichment). Targeted isolation of N_2O-respiring organisms from the enriched material provided isolates that were genome sequenced, compared with the assembled metagenomes, and further vectored to soil by aerobic growth in sterilized digestate, to assess their effects as N_2O-reducing inoculants in soil. Individual strains were also subjected to experiments in axenic cultures in liquid growth medium to assess their denitrifying regulatory phenotype (DRP, Bergaust et al. 2011) and carbon catabolism profiles.

Initially, the digestates contained populations of organisms capable of respring O_2, NO_3^- and N_2O. The capacity for O_2- and NO_3^- - respiration exceeded that for N_2O-reduction, implying that NRBs were outnumbered by other respiring organisms in the digestate pre-enrichment (**Fig. S3**, **Paper I**). In the enrichments with N_2O, the N_2-N production kinetics indicated that the majority of N_2O-respiring cells present in the digestate initially were unable to grow when supplied with N_2O, and their activity died out during the first 50 hours of incubation. A marginal subpopulation of N_2O-respiring organisms did, however, grow to reach dominance (**Figure 1, Paper I**). The kinetics was very reproducible as repeated enrichments revealed almost identical gas kinetics during the first 100 hours of incubation (**Fig. S2**, **Paper I**).

Assembly and binning of the sequenced material from the DNA extracted from samples taken during the enrichment culturing yielded 278 meta-genome assembled genomes (MAGs), of which 149 were deemed of sufficient quality for downstream analysis (scaffolds for proteomics). Six of the MAGs contained the gene *nosZ* (encoding nitrous oxide reductase, Nos) of which a *Dechlormonas* affiliated MAG (MAG 260), initially not detected in the metagenome, reached dominance by means of abundance end-enrichment (**Fig. 9**). This MAG contained *nosZ* type II (coding for N_2O-reductase), but it also contained the genes for the preceding steps of the denitrification pathway.

Proteins were extracted from the same samples as those used for metagenomics, and analyzed with the 149 MAGs as a scaffold, to reveal which proteins were expressed by each

MAG. This analysis revealed that the dominating N_2O-respiring MAGs of the enrichment that carried *nosZ*, but that were also equipped with genes for the entire denitrification pathway, only expressed Nos in the enrichment, as no other denitrification-reductases were detected. MAG260 expressed a disproportional large complement of Nos at the end of the enrichment culturing (**Fig 4A**, **Paper I**).

Three digestate derived N_2O-respiring bacteria were obtained through isolation from the enriched material, and genome sequencing revealed that they were all full-fledged denitrifiers (i.e. carrying all genes necessary for complete reduction of NO_3^- to N_2) (**Fig. 4C**, **Paper I**). One of these isolates, *Azonexus* sp. AN, was circumscribed by MAG260 with 98.2 % average nucleotide identity (ANI) (**Fig. 8**, **Fig. 2 Paper I**). The two other isolates, *Pseudomons* sp. PS, and *Azospira* sp. AS were not recovered in the metagenome.

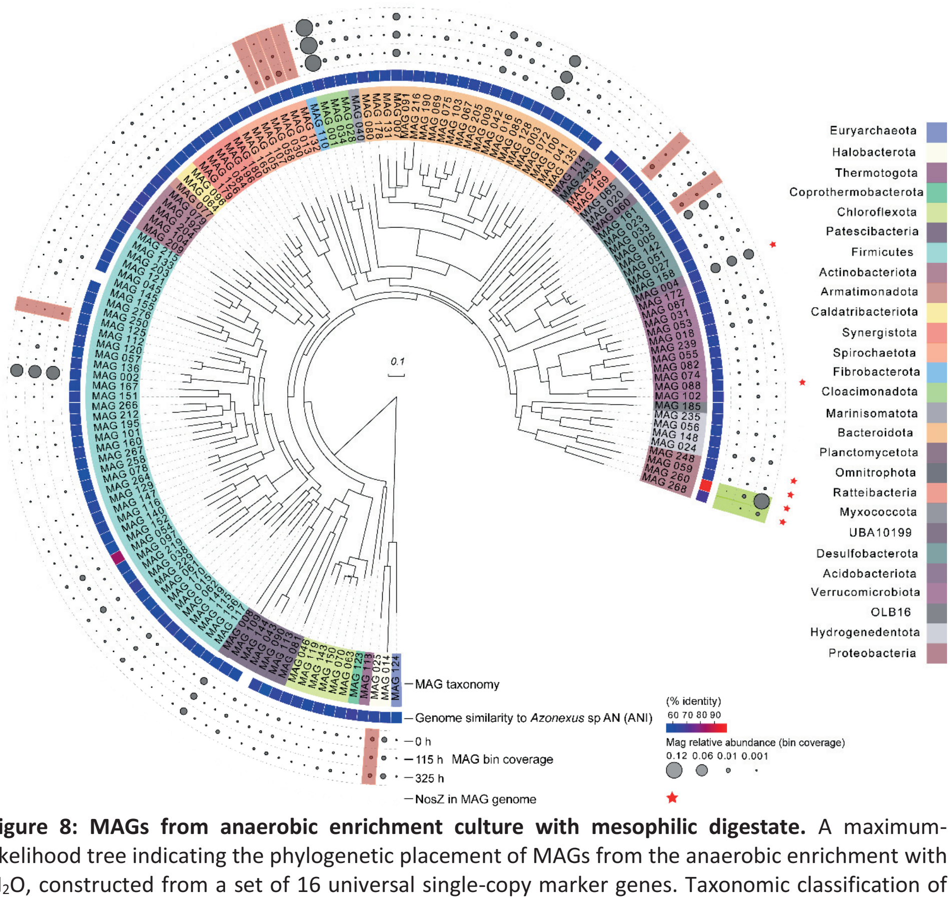

Figure 8: MAGs from anaerobic enrichment culture with mesophilic digestate. A maximum-likelihood tree indicating the phylogenetic placement of MAGs from the anaerobic enrichment with N_2O, constructed from a set of 16 universal single-copy marker genes. Taxonomic classification of the MAGs was inferred using the Genome Taxonomy Database (GTDB) and is displayed at the phylum level by label and branch coloring. Branch label decorations indicate (from innermost ring to outermost); MAG similarity (average nucleotide identity) to the genome of the isolate *Azonexus* sp. AN, the relative abundance of the MAG in the community as calculated from sequence coverage, with MAGs showing an increasing abundance with time highlighted in green and those showing a

decreasing abundance highlighted in red and the presence or absence of the *nosZ* gene in the MAG indicated with a star (Figure by Silas Vick/Live Hagen).

Gas kinetics indicated that the methanogenic consortium of the digestate remained largely intact and active during anaerobic incubation with N_2O, except for a direct and reversible inhibition of methanogenesis (**Fig. S3**, **Paper I**). This was corroborated by the metagenome and metaproteome analyses, which were used to construct a metabolic map for a selection of MAGs having central functions in the methanogenic community (**Fig. 9**).

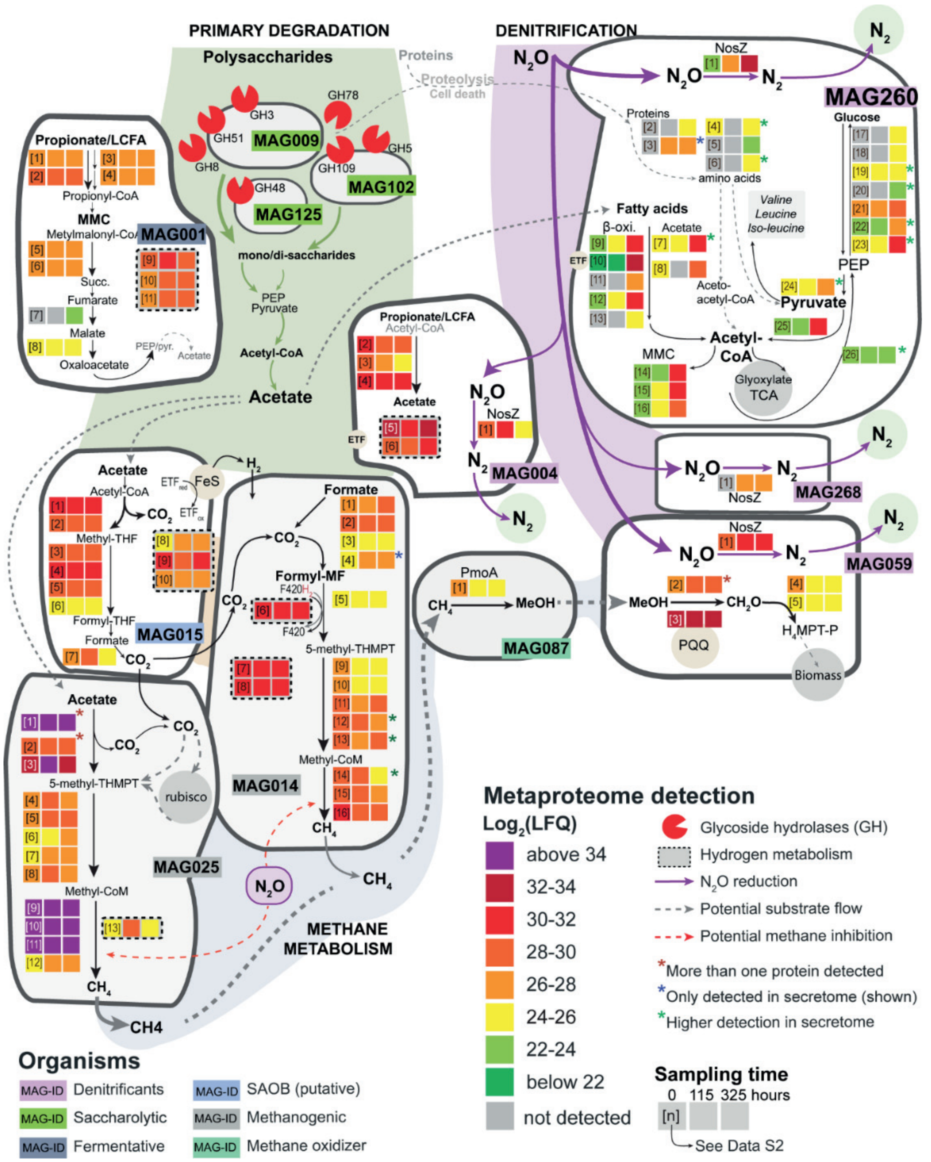

Figure 9: Metaproteome-centric metabolic map of the substrate flow in the microbial consortium. For metabolic reconstruction of the substrate flow, including primary degradation of carbon sources

and N_2O reduction, we scanned the detected proteins affiliated to each MAG for enzymes involved in specific metabolic pathways. Detected protein levels (log_2(LFQ)) for the three sampling time points (after 0, 115, and 325 hours) are indicated by colored squares (**Fig. S12** of **Paper I,** by Live H. Hagen).

The detected methane monooxygenase in MAG087, together with methanol dehydrogenase proteins of MAG059 and constitutive expression of methyl coenzyme-M in the acetoclastic and hydrogenotrophic methanogen related MAGs 025 and 014, respectively, could suggest a possible N_2O driven methanotrophy, but the gas kinetics results suggested that such a pathway could only have played a marginal role in our enrichments (**Fig. S4CD**, **Paper I**). We concluded that the presence of methyl coenzyme-M in the methanogenic MAGs was sustained by brief periods of methanogenesis in response to transient depletion of N_2O occurring throughout (shown in **Fig. 1A**, **Paper I**). The tentative metabolic network (**Fig. 9**) further suggested that the growing population of NRBs grew by harvesting fermentation intermediates from the methanogenic community. This was further corroborated by a screening of carbon catabolism profiles of the isolated organisms (**Fig. 10**) were two of the three isolates (the dominating AN, and AS) had catabolic repertoires limited to small VFAs (e.g. acetate, butyrate), intermediates in the TCA cycle and/or β-oxidation/methyl malonyl-CoA pathways of fatty acid degradation (e.g. malate, fumarate, succinate) and a single amino acid (glutamate). For *Azonexus* sp. AN this was consistent with the detected proteins of the pathways shown in **Fig. 9** for MAG260. The isolate PS demonstrated the largest metabolic repertoire of the isolates in this assay. The carbon metabolism profiles were further corroborated by attempts to grow the three isolates aerobically in autoclaved digestate: while PS grew well and reached high cell densities without any provision of additional carbon sources, AN and AS showed early retardation of growth unless provided with an extra dose of carbon (mix of glutamate, acetate, pyruvate, and ethanol) (**Figs. S25-S26**, **Paper I**). A high degree of specialization and metabolic streamlining may explain the observed dominance of AN during enrichment culturing.

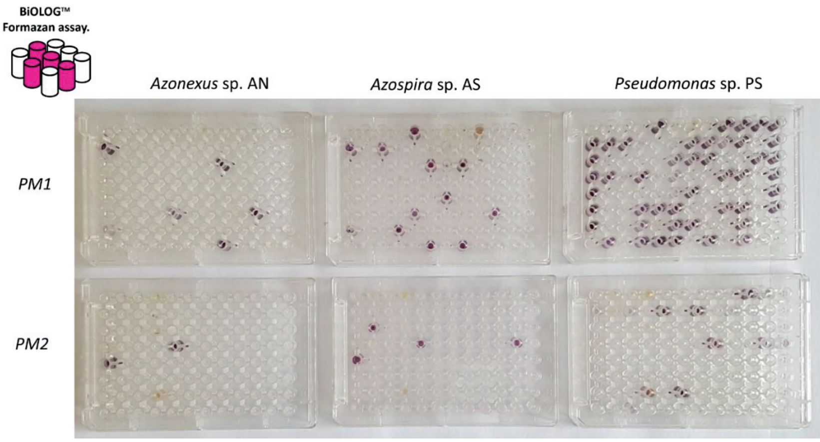

Figure 10: Image of BiOLOG™ colorimetric formazan assay PM1 and PM2 culture plates. Each well contains a single carbon source and was inoculated with organisms washed in a non-carbon growth medium containing tetrazolium supplied by BiOLOG. NAD(P)H dependent cellular oxireductases may

reduce tetrazolium to insoluble formazan (purple) which indicates actively respiring cells. Shown for *Azonexus* sp. AN (circumscribed by MAG260), *Azospira* sp. AS and *Pseudomonas* sp. PS (Carbon content of wells are summarized **Table S3**, **Paper I**).

Azonexus sp. AN carried Nap (periplasmic nitrate reductase), Nir, Nor, and Nos clade II (**Fig. 4C**, **Paper I**), which would predict it to be a strong N_2O sink at the metabolic level as Nos outcompetes Nap for electrons (Mania et al., 2020). However, as the expression of functional genes cannot be predicted from its genome alone (Rocca et al., 2015) we conducted several batch culture experiments, which were monitored for all relevant electron acceptors (O_2, NO_3^-, NO_2^-, NO, and N_2O) as the cultures depleted the oxygen and switched to anaerobic respiration. The batch cultures were provided with NO_3^- or NO_2^- in the liquid, and O_2 with or without N_2O in the headspace. The experiments were designed to unravel the isolates' denitrification regulatory phenotype (DRP), to evaluate their capacity to act as sinks (or sources) for N_2O in the environment. One example is shown *Azonexus* sp. AN in **Fig. 11** (additional explanation is given in **Fig. S15**, **Paper I**). **Fig. 11** also illustrates the importance of calculating the electron flow rate throughout the transition from aerobic to anaerobic conditions in the incubations: The severe depression in electron flow after depletion of O_2 and N_2O, and the subsequent exponential increase is a strong indication of *bet-hedging*.

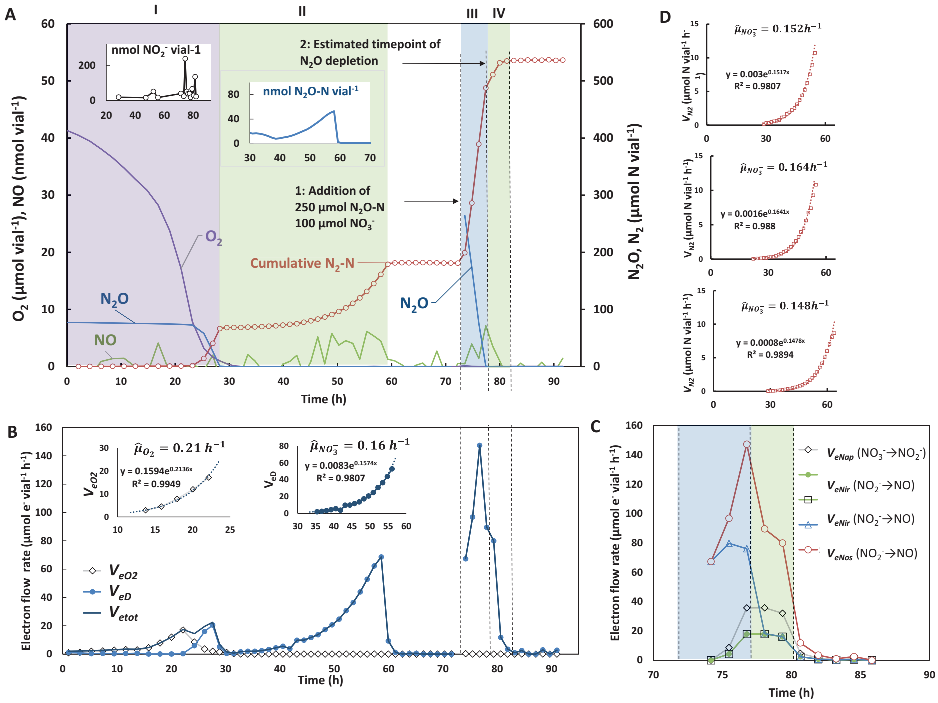

Figure 11: Denitrification phenotype of *Azonexus sp*. (AN) when provided with N_2O and NO_3^-. The panels A-C show kinetics of gases and NO_2^-, calculated electron flow rates and estimation of growth parameters for *Azonexus* sp. AN grown in gas-tight 120 mL vials, initially supplemented with 1 mL O_2,

1 mL N_2O, and 2mM NO_3^- in 50 mL Sistrom's succinate medium. The vials were incubated at constant temperature and stirring (20 °C, 700 rpm), and given a dose of 250 µmol N_2O-N, and 100 µmol NO_3^- after 72 hours. Panels A-C show results for a single vial (replicate vials gave very similar results, except for a time frameshift with respect to NO_3^- reduction). Panel A: measured O_2, NO and N_2O, and cumulative N_2 throughout the incubation. Inserted panels show measured NO_2^- (nmol vial^{-1}) and N_2O (nmol N vial^{-1}). The panel highlights four periods: I, reduction of initial O_2 and N_2O; II, reduction of initial NO_3^-; III, reduction of the injected 250 µmol N_2O-N; IV, subsequent reduction of the remaining NO_3^- (100 µmol NO_3^- was injected together with N_2O at the beginning of period III). Panel B: Electron flow rates: $\boldsymbol{V_{eO2}}$ is the electron flow rate to terminal oxidases (electron acceptor = O_2), $\boldsymbol{V_{eD}}$ is the electron flow rate to denitrification reductases (electron acceptors= NO_3^-, NO_2^-, NO, and N_2O), $\boldsymbol{V_{etot}}$ = $\boldsymbol{V_{eO2}}$ + $\boldsymbol{V_{eD}}$. The inserted panels show exponential regression of $\boldsymbol{V_{eO2}}$ and $\boldsymbol{V_{eD}}$ against time, thus estimating the aerobic and anaerobic growth rates ($\hat{\mu}_{O2}$ =0.21 h^{-1}, $\hat{\mu}_{NO3}$ =0.16 h^{-1}). Panel C: Electron flow rates to individual N-reductases (and the sum of all) during periods III and IV (Panel A), illustrating the preferential electron flow to Nos ($N_2O \rightarrow N_2$). Panel D shows a few results of a separate experiment; three replicate vials supplemented with 2 mM NO_3^- and 1 mL O_2. The panels show exponential regression of N_2 production rates for individual vials. The kinetics of O_2-reduction (not shown) and N_2-production were used to estimate the fraction of cells expressing Nap (F_{den}), using the model of Hassan et al (2016). The F_{den} estimates for the individual vials were 0.14, 0.12, and 0.03, which would indicate *bet-hedging* with respect to Nap (Additional details in **Fig. S15** of **Paper I**).

As predicted from its genotype (encoding genes for Nap, NirS, Nor, and Nos) *Azonexus* sp. AN reduced NO_3^- quantitatively to N_2, with a very low transient accumulation of N_2O and NO when provided NO_3^-. We expected Nos to outcompete Nap for electrons, which was verified as all electrons were directed towards N_2O reductase in incubations supplemented with NO_3^- and N_2O, until the external supplied N_2O was reduced (**Fig. 11C**). The depression of electron flow after depletion of the first dose of N_2O (**Fig. 11A**), and the exponential increase thereafter suggested that AN is *bet-hedging* (Lycus et al., 2018); as this indicated that the majority of cells expressed Nos when transitioning to anaerobic conditions, but only a minor fraction expressed Nap. This was corroborated by the calculated $\boldsymbol{F_{den}}$ values (=fraction of cells expressing Nap) varying from 0.02 – 0.14 (calculated from data in **Fig. 11D**, additional $\boldsymbol{F_{den}}$ values shown in **Fig. S15**, **Paper I**), and by proteome analysis at various time points throughout the cultures' depletion of externally provided NO_3^- and O_2. The proteomics results demonstrated a significantly higher ratio of detected LFQ(Nos)/LFQ(Nap) (~25X) at the transition between oxic and anoxic conditions, before the ratio gradually decreased (LFQ(Nos)/LFQ(Nap) ~5X) as nitrate-reduction rates increased throughout the incubation (**Fig S17**, **Paper I**).

The DRP of AN would thus predict it being a strong N_2O sink in the environment. And while it did eliminate the immediate N_2O emissions from digestate-amended soils fertilized with NO_3^- (**Fig. 5**, **Paper I**), it's metabolic streamlining towards harvesting fermentation intermediates (**Figs. 10** and **11**) would render the enrichment winner as not an ideal N_2O-respiring soil inoculant as life in soil would, probably, require a broader catabolic repertoire.

The other isolates' DRPs, and their effect as N_2O-respiring inoculants in soil, are described in detail in **Paper I**. In short; *Pseudomonas* sp. PS appeared to be the most robust candidate as a sink for N_2O in soil for two reasons; 1) it could utilize a wide range of carbon substrates, and 2) its N_2O sink strength is independent of the type of nitrogen oxyanion present (NO_2^- or NO_3^-) (**Figs. S22** to**S24**, **Paper I**).

In summary, this first enrichment culturing was successful in providing isolates that could be effective instruments to reduce N_2O emissions from soils if vectored by digestates. The experiments also revealed that the N_2O-respiring bacteria grew by harvesting the intermediates of the methanogenic consortium, which remained metabolically intact during the incubations with N_2O, except for the inhibition of methanogenesis by N_2O, whose metabolic role in the consortium was replaced by the N_2O-respiring bacteria. This could explain why two of the three isolates had a “streamlined” catabolic repertoire limited to the exploitation of intermediates produced by the methanogenic consortium. Such organisms are unlikely to survive for a long time in soil, hence deemed to be suboptimal for achieving long-lasting effects on N_2O emission from soil. Although the third isolate (*Pseudomonas* sp. PS) was more promising by having a broader catabolic repertoire, we concluded that the ideal organism was yet to be found. Another hypothetical shortcoming is the risk for selecting organisms that are notoriously unable to survive in soil, for other reasons than a limited catabolic repertoire. It was evident that we needed to further refine our search organisms with broader metabolic flexibility which might secure a competitive edge *vis-à-vis* the indigenous organisms in soil (Bay et al., 2021).

Selecting more ideal N_2O-respiring organisms

A new approach to obtain more ideal isolates by a more rigorous and directed selection for N_2O-respiring organisms with characteristics of growth in digestate and N_2O respiration in soils was developed. The experiment was designed based on modelled growth of a simplified community consisting organisms organized in three groups; 1: organisms with a competitive advantage in digestate (digestate specialists, **D**), 2: organisms with a competitive advantage in soil (soil specialists, **S**), and 3: organisms capable of sustaining growth in both environments (generalists, **G**). By assuming logistic growth and first-order death rates of these three groups (with theoretically assigned growth and death rates), and assuming that growth would only be limited by competition for a common pool of organic carbon, the model (**Fig. 12A**, **Figs. S1** to **S6**, **Paper II**) predicted that competitive *generalists* (**G**) would reach dominance after a limited number of repeated passages between soil and digestate, and showed that the selective pressure could be controlled by the duration of each batch enrichment and the fraction of enriched material transferred from one enrichment to the next.

Using this strategy we designed the dual enrichment experiment where enrichments of N_2O-respiring bacteria originating from live digestate (D-line) (sampled from the same WWTP as in **Paper I**), or a live soil and digestate mixture (SD-line), were passaged through six enrichment cycles in sterilized materials, alternating between autoclaved digestate and ϒ-sterilized soil, while providing N_2O throughout by repeated injections (**Fig. 12B**). Sterile substrates were used after the initial enrichment in live materials to avoid repeated reoccurrence and dominance of substrate indigenous specialists. At the conclusion of each enrichment, samples were taken for DNA extraction that were subjected to 16S rDNA amplicon sequencing and OTU clustering. The enrichments were continued beyond (30 – 80 h) the community's depletion of easily available carbon sources, indicated by stagnating and declining rates of N_2O-reduction (N_2-production) (**Fig. 2, Paper II**). This would allow for competition for scarce resources amongst the species of the enrichment culture.

A: Theoretical framework

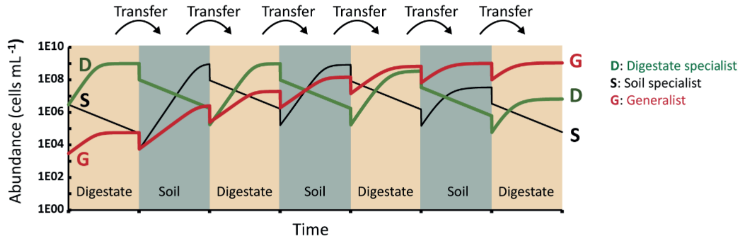

B: Enrichment setup

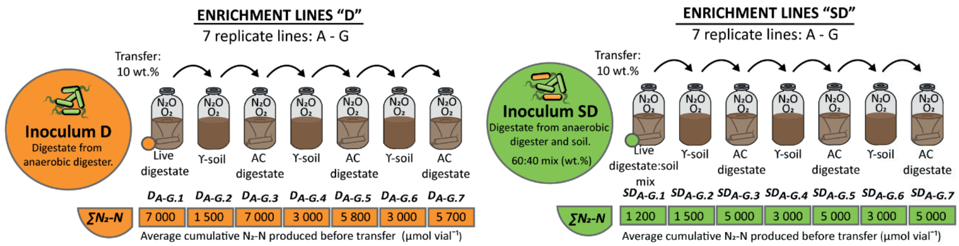

Figure 12: **Panel A**: Simulation of the competition between three populations through a series of enrichment cultures. The three populations (S=soil specialists, D= digestate specialists, and G=generalists) were simulated with the parameter values shown in **Table S1** of **Paper II**, 100 hours incubation time for each batch and transfer of 10% of the culture volume to the next enrichment batch. **Panel B**: Experimental setup for dual enrichment of soil and digestate competent N_2O-respiring bacteria with seven independent replicates for each line. Each enrichment cycle was initiated with 3 mL N_2O and 3 mL O_2 in the headspace. Additional N_2O was added throughout. The enrichments were concluded when the cultures had reduced N_2O equivalent to the N_2-N shown beneath the enrichment vials.

The top 500 most abundant OTUs (across all samples) were clustered in groups based on their abundance development throughout the enrichments, and visualized as a heatmap based on abundance, allowing us to identify clades (groups) of dominant OTUs with generalist properties, OTUs portraying the predicted traits of substrate specialists and OTUs lost by death or dilution by means of abundance (**Fig. 13A**).

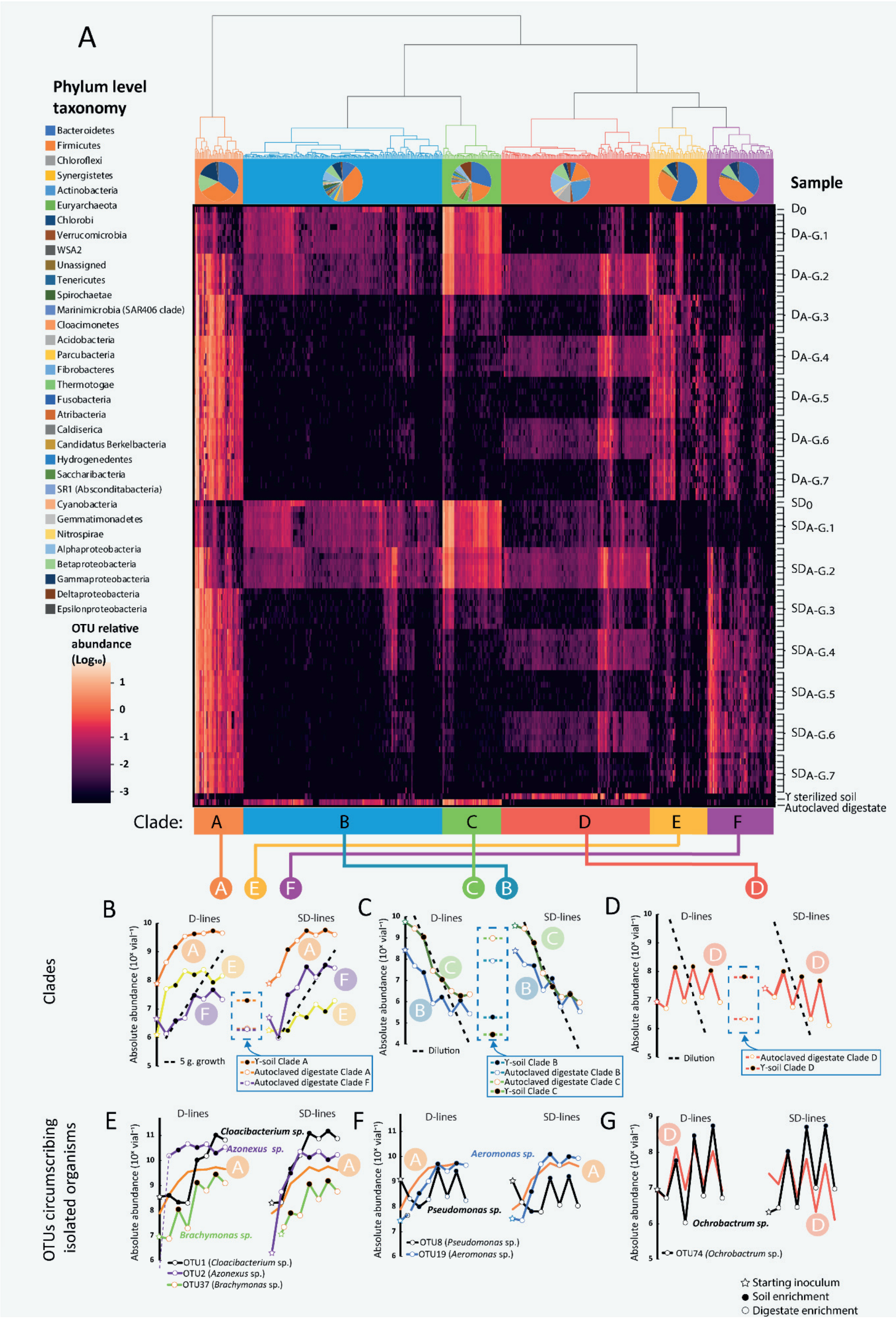

Figure 13: Abundance of clustered OTU's throughout the dual enrichment culturing. Panel A: Heatmapping and hierarchical clustering of the 500 most abundant OTUs from all biological replicates of the dual enrichment culturing. D and SD denote two different staring inoculums, D_0 and

SD_0 denote the starting materials. Background samples were sterile soil and autoclaved digestate, used as growth mediums in the enrichments, was included. **Panels B-D** show the average absolute abundances (copies vial^{-1}= ddPCR 16S copies · relative abundance) for the OTU's within each clade throughout each enrichment; filled symbol = enrichment in soil, open symbol = enrichment in digestate, star = starting inoculum. The first point represents the live starting material before enrichment with N_2O. The dashed lines in panels **C** and **D** represent the predicted decline by dilution, given a 10 % transfer rate, i.e. neither growth nor death. The dashed line in panel **B** represents a growth rate of 5 generations per enrichment. The OTU-abundancies in sterile materials are shown within dashed frames. **Panels E-G** shows the absolute abundance of the OTU's which circumscribe the isolates, together with the averages of their resident clades (Figure from **Paper II**).

The absolute abundance of OTUs circumscribed by Clade A, E, and F (from **Fig. 12A**) are shown in **Fig. 13B**. These clades consisted of organisms capable of growth in both environments. Clade D seemed to consist of organisms that were soil specialists (**Fig. 13D**), as indicated by an abundance pattern where the groups reappeared in soil only. Clade B and C consisted of OTUs that did not grow, and their diminishing abundance matched that predicted by the dilution (1:10 dilution for each transfer) (**Fig. 13C**). Targeted isolation of N_2O-respiring bacteria from the final enrichments resulted in 7 isolates, of which 6 were full genome sequenced. Six of our isolates where circumscribed by OTUs clustered in Clade A, which demonstrated generalist traits by growing in both materials (**Fig. 13EF**). One isolate was circumscribed by an OTU clustered in Clade D that which was more of a soil specialist by growing in soil only (**Fig. 13G**). Interestingly, as the first enrichments of the D lines ($D_{A\text{-}G.1}$) was a replica of the enrichment of **Paper I**, one obtained isolate, an *Azonexus* sp., matched the isolated *Azonexus* sp. AN that dominated the enrichments in live digestate of **Paper I** (98.2 % 16S identity. **Tab. S9**, **Paper II**) also dominated by means of abundance in the $D_{A\text{-}G.1}$ lines. The gas kinetics of this first D line enrichment, and the OTU circumscribing this *Azonexus* sp. isolate demonstrated striking similarity with the enrichment of **Paper I**.

The genomes of the isolated organisms were screened for various genes, including genes indicating a predatory lifestyle and a capacity to utilize polymers, potentially shedding light on their observed capacity to grow in the enrichment cultures, and as axenic cultures in autoclaved digestate. Only two of the strains (*Cloacibacterium sp.* CB-01 and CB03) had genes indicating a predatory lifestyle, which could hypothetically explain why the OTU circumscribing these strains achieved dominance throughout the enrichment. Further, we found a correlation between the isolates' capacity to grow in autoclaved digestate and the number of genes coding for proteases and carbohydrate-active enzymes (CAZymes) containing signal peptides (**Fig. S32H**, **Paper II**). This suggests that genome analysis could become a useful tool in screening isolates, although further phenotype characterization is clearly needed.

Both the D and SD enrichment lines were dominated by an OTU circumscribing the two obtained isolates of *Cloacibacterium* spp. (CB-01 and CB-03). These isolates had a truncated denitrifying genotype where CB-01 encoded genes for Nos and Nor, and CB-03 encoded genes for Nos, Nor, and NasC (assimilatory NO_3^- reductase). The reduction of N_2O to N_2 (CB-01), and NO_3^- to NO_2^- (CB-03) was verified in separate DRP experiments (**Fig. 4EF**, **Paper II**). We assessed that CB-01 would be the most favorable isolate of the two since CB-03 would also convert NO_3^- to NO_2^-, and CB-03 was therefore omitted from any testing of N_2O-respiring capabilities in soil. Interestingly, CB-01 performed as a strong sink for N_2O in both high and low pH soils. As the *Cloacibacterium* sp. did not demonstrate functional transcription of Nos at low pH when growing as an axenic culture in culture media (**Fig. S31**, **Paper II**), the ability to form biofilms that would allow shielding of the pervasive effect of low pH, or, as CB-01 was non-motile, due to pH buffering effects within micropores of the digestate particulates/flocs, could allow for maturation of a functional Nos in low pH soil. Longer-term effects in soil were more modest for the *Cloacibacterium* sp. (**Fig. S35-36**, **Paper II**): 30 days after amending soils with *Cloacibacterium* sp. CB-01, we mimicked a fertilization event by adding NO_3^- and imposing anoxic conditions by letting the amended soil respire a small dose of O_2. The *Cloacibacterium*/digestate amended soil marginally reduced N_2O emission relative to the controls. Another isolate, a *Psedudomonas* sp., carrying all the necessary genes for a full-fledged denitrification pathway that demonstrated a denitrification phenotype that would predict it being a strong N_2O sink (**Fig. 4A**, **Paper II**), demonstrated both short- (**Fig. 5**, **Paper II**) and longer-term (30 days) effects on N_2O emission after soil amendment in soil with pH 6.6 (**Fig. S35-36**, **Paper II**). However, the *Pseudomonas* sp. did not augment the soil's capacity for N_2O reduction in low pH soil (nor did the other isolates).

5. Concluding remarks

The work presented in **Paper I** and **II** demonstrate the applicability of digestates as growth substrates and vectors for transferring NRBs to soil. Such an approach could allow for large-scale cultivation of N_2O-respiring bacteria for soil application at modest costs. The technique is attractive because it is scalable; if a major part of waste materials in European agroecosystems could be treated by AD, the resulting digestates would suffice to treat a large share of total European farmland (**Fig. 1** of **Paper I**).

An important finding of **Paper I** was that relying on live digestate as inoculum for enriching NRBs selected for organisms adapted to harvesting intermediates of the methanogenic community, and, also, that the longevity of the N_2O reducing effect in the digestate amended soil was likely modest (**Fig. S30**, **Paper I**). The most abundant *nosZ* carrying MAG, MAG260, which circumscribed the isolated *Azonexus* sp. AN, was equipped all the genes for a full-fledged denitrification pathway and also expressed over 90 % of the total detected Nos in the digestate at the final sampling point. Whereas the only reconstructed MAG that contained solely *nosZ* among the denitrification enzymes, MAG004, did not increase in relative abundance (but persisted throughout the incubation), and contributed 0.2 % of the total Nos protein pool. While it may be expected that under conditions with N_2O as the sole electron acceptor an organism carrying only the *nosZ* gene as the sole denitrifying enzyme might have a competitive edge over full-fledged denitrifiers due to a potentially more streamlined respiratory proteome; exogenous N_2O did not select for digestate-indigenous non-denitrifying bacteria with only *nosZ*, and Nos was also the only denitrification enzyme detected by proteomics in the enrichment. The latter supports the current understanding of denitrification regulation whereby *nosZ* is the only denitrification gene transcribed in response to a signal other than nitrogen-oxides (Spiro, 2016).

Our eco-physiological genome analysis of the isolates obtained in **Paper II** revealed that several of the soil and digestate competent isolates had the genetic potential to utilize complex carbon sources and encoded several traits that might enhance survival under such a competitive situation. It was, however, evident from the longer-term soil incubations that most of our soil and digestate competent isolates did not have traits that would allow them longer-term establishment in the soil microbial community – with the possible exception of one isolate. Longer-term survival might be achieved by growing NRB in dewatered digestates, preferably pelleted in some way, to provide NRB with a “safe haven” against predation and inhibition by the indigenous soil microbiota, and with a locally high pH to allow unconstrained synthesis of functional Nos even in acid soils, as indicated by the N_2O-respiring activity of *Cloacibacterium* sp. CB-01 when amended with digestate to acidic soil. Repeated inoculations might also give inoculants permanent residence within the residing community in soil due to the clearing of niches by heavy inoculation of NRBs, which might make a second invasion more successful (Mallon et al., 2018), which should be explored in future experiments. However, the characteristics of transient peak emissions of N_2O from soil after fertilization with organic fertilizers suggest that a significant fraction of the N_2O emitted occurs within a reasonable short timeframe after fertilization (**Chapter 1.4.3**). It is therefore conceivable that even short-lived NRBs could significantly reduce N_2O emissions from such agroecosystems. While not all members of the identified generalist OTUs were obtained as pure cultures, additional isolation efforts might also have uncovered more organisms with good qualities for soil amendment (if culturable). None the less, two very promising soil and digestate competent N_2O-respiring inoculum candidates were obtained from the dual enrichment experiment: A *Cloacibacterium* sp. carrying only *nosZ* that was capable of reducing N_2O at low and high(er) pH in soil, possibly aided by the formation of biofilms or localization within digestate particles, that offered a shielding towards the low pH environment, and a full-fledged denitrifying *Pseudomonas* sp. that maintained its activity in digestate amended soil for at least one month. Both were seemingly capable of utilizing a much larger repertoire of the carbon available in the digestate compared to the enrichment winner of **Paper I**.

The digestate used in this work was sampled from a municipal WWTP (**Appendix A**) and harbored NRBs that survived AD and which probably originated from the AD substrate. The NRBs were initially outnumbered by respiring bacteria that were net producers of N_2O (**Fig. S5**, **Paper I**). This may, in part, explain the large variation in N_2O emissions from digestate amended soils reported in the literature (Herrero et al., 2016; Baral et al., 2017), as the proportion of organisms capable of reducing N_2O in the digestate may vary greatly due to differences in substrate and operational parameters of AD.

In a broader perspective, the use of digestates as vectors for NRBs to soil can, as a principle, be taken as a blueprint for future applications that aim to engineer the soil microbiome, be it for enhancing plant growth, bioremediation, or any other desirable microbially mediated function vectored by digestates to soil.

6. Application and future perspectives

Anaerobic digestion is applied on a wide range of substrates and the work presented has demonstrated that simple modifications to the existing material pipeline of digestate to soils could provide a low-cost N_2O mitigation measure by letting N_2O-respiring bacteria utilize available carbon in the waste material before it's used as organic fertilizers in agriculture. The work has provided tools and methodologies to obtain auspicious organisms with the desired traits of growth in digestate and soil, and with a strong capacity for N_2O reduction, but also unraveled pitfalls and shortcomings that need to be addressed in future research.

The ideal N_2O reducing inoculant should have properties of strong N_2O reduction, capacity to grow in digestate and soil, and possibly a truncated denitrifying phenotype to avoid depleting soil NO_3^-. It seems clear that the ideal NRB(s) for this purpose is yet to be found. Still, the enrichment technique developed in **Paper II** resulted in isolates with better performance in soil compared to enrichments and isolation of organisms in digestate only (**Paper I**), and further improvements of this technique could allow for the selection of more competitive strains. The technique could be modified by using different growth substrates to obtain auspicious isolates specifically to "match" certain soil types. E.g. an interesting option would be to include a selection of strains that can synthesize functional Nos at low pH because such organisms do exist (Lycus et al., 2017). We also suspected that some of the obtained isolates were shielded by digestate particles or formed biofilms that offered a similar shielding from the pervasive effects of pH on Nos maturation. So, another interesting option would be to grow NRB in dewatered and pelleted digestate materials, and further explore possible shielding effects of the vector, as incorporation of inoculants in similar organic fertilizer products has been showed to significantly reduce N_2O emissions also from acidic soils (Gao et al., 2016b; 2017).

So far, the method has only been tested in microcosms, measuring the N_2O/N_2 product ratio during denitrification. Although this provides reasonable predictions as to the propensity of soils to emit N_2O under field conditions (Russenes et al., 2016), there is an obvious need for testing the approach in field plot experiments, which are in the making.

References

Abalos D, Jeffery S, Sanz-Cobena A, Guardia G, Vallejo A (2014) Meta-analysis of the effect of urease and nitrification inhibitors on crop productivity and nitrogen use efficiency. Agriculture, Ecosystems & Environment, 189, 136-144.

Abbasi MK, Adams WA (2000) Gaseous N emission during simultaneous nitrification–denitrification associated with mineral N fertilization to a grassland soil under field conditions. Soil Biology and Biochemistry, 32(8-9), 1251-1259.

Akiyama H, McTaggart IP, Ball BC, Scott A (2004) N2O, NO, and NH3 emissions from soil after the application of organic fertilizers, urea and water. Water, Air, and Soil Pollution, 156(1), 113-129.

Alburquerque JA, De La Fuente C, Campoy CM, Carrasco L, Nájera I, Baixauli C, Caravaca F, Roldán A, Cegarra AJ, Bernal MP (2012) Agricultural use of digestate for horticultural crop production and improvement of soil properties, Eur. J. Agron., 43 (2012), pp. 119-128.

Baggs EM (2008) A review of stable isotope techniques for N2O source partitioning in soils: recent progress, remaining challenges and future considerations. Rapid Communications in Mass Spectrometry: An International Journal Devoted to the Rapid Dissemination of Up-to-the-Minute Research in Mass Spectrometry, 22(11), 1664-1672.

Bakken LR (2021) Spreadsheet for gas kinetics in batch cultures. Researchgate DOI: 10.13140/RG.2.2.19802.36809

Baldasano JM, Soriano C (2000) Emission of greenhouse gases from anaerobic digestion processes: comparison with other municipal solid waste treatments. Water science and technology, 41(3), 275-282.

Baral KR, Labouriau R, Olesen JE, Petersen SO (2017) Nitrous oxide emissions and nitrogen use efficiency of manure and digestates applied to spring barley. Agric Ecosyst Environ 2017; 239: 188–198.

Barrett RD, MacLean RC, Bell G (2005) Experimental evolution of Pseudomonas fluorescens in simple and complex environments. The American Naturalist, 166(4), 470-480.

Bartl A (2015) Withdrawal of the circular economy package: a wasted opportunity or a new challenge? Waste Manag. 44, 1-2.

Bay SK, Dong X, Bradley JA, Leung PM, Grinter R, Jirapanjawat T, Arbdt SK, Cook PLM, LaRowe DE, Nauer PA, Chiri E, Greening C (2021) Trace gas oxidizers are widespread and active members of soil microbial communities. Nature Microbiology, 6(2), 246-256.

Béghin-Tanneau R, Guérin F, Guiresse M, Kleiber D, Scheiner JD (2019) Carbon sequestration in soil amended with anaerobic digested matter. Soil and Tillage Research, 192, 87-94.

Belotte D, Curien JB, Maclean RC, Bell G (2003) An experimental test of local adaptation in soil bacteria. Evolution, 57(1), 27-36.

Beni C, Servadio P, Marconi S, Neri U, Aromolo R, Diana G (2012). Anaerobic digestate administration: effect on soil physical and mechanical behavior. Commun. Soil Sci. Plant Anal., 43, pp. 821-834.

Bergaust L, Shapleigh J, Frostegård Å, Bakken LR (2008) Transcription and activities of NOx reductases in Agrobacterium tumefaciens: the influence of nitrite, nitrate and oxygen availability. Environmental Microbiology 10:3070-3081

Bergaust L, Bakken L, Frostegård Å (2011) Denitrification regulatory phenotype, a new term for the characterization of denitrifying bacteria. Biochemical Society transactions. 39. 207-12.

Braker G, Conrad R (2011) Diversity, structure, and size of N2O-producing microbial communities in soils—what matters for their functioning?. Advances in applied microbiology, 75, 33-70.

Bremner JM, Blackmer AM, Waring SA (1980) Formation of nitrous oxide and dinitrogen by chemical decomposition of hydroxylamine in soils. Soil Biology and Biochemistry, 12(3), 263-269.

Brümmer C, Brüggemann N, Butterbach-Bahl K, Falk U, Szarzynski J, Vielhauer K, Wassmann R, Papen H (2008) Soil-atmosphere exchange of N2O and NO in near-natural savanna and agricultural land in Burkina Faso (W. Africa). Ecosystems, 11(4), 582-600.

Butterbach-Bahl K, Baggs EM, Dannenmann M, KieseR, Zechmeister-Boltenstern S (2013) Nitrous oxide emissions from soils: How well do we understand the processes and their controls? Philosophical Transactions of the Royal Society B: Biological Sciences, 368: 20130122.

Cassman KG, Dobermann A, Walters DT (2002) Agroecosystems, nitrogen-use efficiency, and nitrogen management. J. Hum. Environ. **31**, 132–140.

Cavicchioli R, Ripple WJ, Timmis KN, Azam F, Bakken LR, Baylis M, et al (2019). Scientists' warning to humanity: microorganisms and climate change. Nature Reviews Microbiology, 17(9), 569-586.

Chaen K, Noguchi J, Omori T, Kakuta Y, Kimura M (2012) Crystal structure of the rice branching enzyme I (BEI) in complex with maltopentaose. Biochemical and biophysical research communications, 424(3), 508-511.

Chalk PM & Smith CJ (1983) Chemodenitrification. In: Freney JR& Simpson JR (eds) Gaseous Loss of Nitrogen from Plant-SoilSystems, pp 65–89. Nijhoff/Junk, The Hague.

Conthe M, Wittorf L, Kuenen JG, Kleerebezem R, van Loosdrecht MC, Hallin S (2018) Life on N 2 O: deciphering the ecophysiology of N 2 O respiring bacterial communities in a continuous culture. The ISME journal, 12(4), 1142-1153.

Daims H, Lebedeva EV, Pjevac P, Han P, Herbold C, Albertsen M, Jehmlich N, Palatinszky M, Vierheilig J, Bulaev A, Kirkegaard RH, von Bergen M, Rattei T, Bendinger B, Nielsen PH, Wagner M (2015) Complete nitrification by Nitrospira bacteria. Nature, 528(7583), 504-509.

Davidson EA (2009) The contribution of manure and fertilizer nitrogen to atmospheric nitrous oxide since 1860. Nat. Geosci. **2**, 659–662.

De Pascale G, Nazi I, Harrison PH, Wright GD (2011) β-Lactone natural products and derivatives inactivate homoserine transacetylase, a target for antimicrobial agents. The Journal of antibiotics, 64(7), 483-487.

Dejonghe W, Boon N, Seghers D, Top EM, Verstraete W (2001) Bioaugmentation of soils by increasing microbial richness: missing links. Environmental Microbiology, 3(10), 649-657.

Del Grosso SJ, Parton WJ, Mosier AR, Ojima DS, Kulmala AE, Phongpan S (2000) General model for N_2O and N_2 gas emissions from soils due to denitrification. Clobal Biogeochemical Cycles 14:1045-1060.

D'Hondt K, Kostic T, McDowell R, Eudes F, Singh BK, Sarkar S, Makakis M, Schelkle B, Maguin E, Sessitsch A (2021) Microbiome innovations for a sustainable future. Nature Microbiology, 6(2), 138-142.

Dietrich M, Fongen M, Foereid B (2020) Greenhouse gas emissions from digestate in soil. International journal of recycling organic waste in agriculture, 9(1), 1-19.

Domeignoz-Horta LA, Putz M, Spor A, Bru D, Breuil MC, Hallin S (2016) Non-denitrifying nitrous oxide reducing bacteria – an effective N2O sink in soil. Soil Biol Biochem 103:376-379.

Ehmann A, Thumm U, Lewandowski I (2018) Fertilizing potential of separated biogas digestates in annual and perennial biomass production systems. Frontiers in Sustainable Food Systems, 2, 12.

Ellington MJK, Fosdike WLJ, Sawers RG, Richardson DJ, Ferguson SJ (2006) Regulation of the nap operon encoding the periplasmic nitrate reductase of Paracoccus pantotrophus: delineation of DNA sequences required for redox control. Archives of microbiology, 184(5), 298-304.

EU1: European Union (1997), COM(97) 599, Energy for the Future: Renewable Sources of Energy - White Paper for a Community Strategy and Action Plan, European commission.

EU2: European Union (2007): COM(2007) 1, An energy policy for Europe. Communication from the Commission to the European Council and the European Parliament, European Commission.

EU3: European Union (2012), COM(2011) 112, A roadmap for moving to a competitive Low Carbon Exonomy in 2050. Communication from the Commission to the European Parliament, the Council, the European Economic and Social Committee and the Committee of the regions.

Eurostat (2017) Agri-environmental indicator – greenhouse gas emissions. ISSN 2443-8219, https://ec.europa.eu/eurostat/statistics-explained/pdfscache/16817.pdf

Eydallin G, Ryall B, Maharjan R, Ferenci T (2014) The nature of laboratory domestication changes in freshly isolated E scherichia coli strains. Environmental Microbiology, 16(3), 813-828.

Forster P, Ramaswamy V, Artaxo P, Berntsen T, Betts R, Fahey DW, Haywood J., et al. Solomon S, Qin D, Manning M, Chen Z, Marquis M, Averyt KB, Tignor M, et al. (2007) Changes in atmospheric constituents and in radiative forcing, Climate Change 2007: the Physical Science Basis. Contribution of Working Group I to the Fourth Assessment Report of the Intergovernmental Panel on Climate Change, CambridgeCambridge University Press (pg. 129-234).

Gao JF, Fan XY, Pan KL, Li HY, Sun LX (2016) Diversity, abundance and activity of ammonia-oxidizing microorganisms in fine particulate matter. Scientific reports, 6(1), 1-12.

Gao N, Shen WS, Kakuta H, Tanaka N, Fujiwara T, Nishizawa T, Takaya N, Nagamine T, Isobe K, Otsuka S, Senoo K (2016) Inoculation with nitrous oxide (N_2O)-reducing denitrifier strains simultaneously mitigates N_2O emission from pasture soil and promotes growth of pasture plants. Soil Biology and Biochemistry 97:83–91.

Gao N, Shen W, Camargo E, Shiratori Y, Nishizawa T, Isobe K, He X, Senoo K (2017) Nitrous oxide (N_2O)-reducing denitrifier-inoculated organic fertilizer mitigates N_2O emissions from agricultural soils. Biology and Fertility of Soils 53:885–898.

Giguere AT, Taylor AE, Myrold DD, Bottomley PJ (2015) Nitrifcation Responses of Soil Ammonia-Oxidizing Archaea and Bacteria to Ammonium Concentrations. Soil Sci. Soc. Am. J. 79:1366–1374.

Gilbert ES, Crowley DE (1998) Repeated application of carvone-induced bacteria to enhance biodegradation of polychlorinated biphenyls in soil. Applied microbiology and biotechnology, 50(4), 489-494.

Gómez-Brandón, M., Juárez, M. F. D., Zangerle, M., & Insam, H. (2016). Effects of digestate on soil chemical and microbiological properties: A comparative study with compost and vermicompost. Journal of Hazardous Materials, 302, 267-274.

Graf DRH, Jones CM, Hallin S (2014) Intergenomic comparisons highlight modularity of the denitrification pathway and underpin the importance of community structure for N2O emissions. PLOS one 9:12 e114118.

Graf JS, Schorn S, Kitzinger K, Ahmerkamp S, Woehle C, Huettel B, Schubert CJ, Kuypers MMM, Milucka J (2021) Anaerobic endosymbiont generates energy for ciliate host by denitrification. Nature, 1-6.

Gutser R, Ebertseder T, Weber A, Schraml M, Schmidhalter U (2005) Short-term and residual availability of nitrogen after long-term application of organic fertilizers on arable land. J. Plant Nutr. Soil Sci., 168, pp. 439-446.

Hassan J, Bergaust LL, Wheat ID, Bakken LR (2014) Low probability of initiating nirS transcription explains observed gas kinetics and growth of bacteria switching from aerobic respiration to denitrification. PLoS Comput Biol, 10(11), e1003933.

Hassan J, Qu Z, Bergaust L, Bakken LR (2016) Transient accumulation of NO_2^- and N_2O during denitrification explained by assuming cell diversification by stochastic transcription of denitrification genes. PLoS Computational Biology 12:e1004621.

Heil J, Liu S, Vereecken H, Brueggemann N (2015) Abiotic nitrous oxide production from hydroxylamine in soils and their dependence on soil properties. Soil Biology and Biochemistry, 84, 107-115.

Hénault C, Bourennane H, Ayzac A et al (2019) Management of soil pH promotes nitrous oxide reduction and thus mitigates soil emissions of this greenhouse gas. Sci Rep **9,** 20182.

Herrero M. Henderson B, Havlik P, Thornton PK, Conant RT, Smith P, Wirsenius S, Hristov AN, gerber P, Gill M, Butterbach-Bahl K, Valin H, Garnett T, Stehfest E (2016) Greenhouse gas mitigation potential in the livestock sector. Nature Climate Change 6:452-461.

Herridge DF, Peoples MB, Boddey RM (2008) Global inputs of biological nitrogen fixation in agricultural systems. Plant and soil, 311(1), 1-18.

Hink L, Nicol GW, Prosser JI (2017) Archaea produce lower yields of N2O than bacteria during aerobic ammonia oxidation in soil. Environmental microbiology, 19(12), 4829-4837.

IPCC (2018) Global warming of 1.5 °C. An IPCC special report on the impacts of global warming of 1.5 °C above pre-industrial levels and related global greenhouse gas emission pathways, in the context of strengthening the global response to the threat of climate change. In Press.

Iranpour R, Cox H, Kearney R, Clark J, Pincince A, Daigger G (2004) Regulations for biosolids land application in US and European Union. J. Residuals Sci. Tech. **1**(4), 209–222.

Johansen A, Carter MS, Jensen ES, Hauggard-Nielsen, H, Ambus P (2013) Effects of digestate from anaerobically digested cattle slurry and plant materials on soil microbial community and emission of CO2 and N2O. Applied Soil Ecology, 63, 36-44.

Jones CM, Stres B, Rosenquist M, Hallin S (2008) Phylogenetic analysis of nitrite, nitric oxide, and nitrous oxide respiratory enzymes reveal a complex evolutionary history for denitrification. Mol. Biol. Evol.25:1955–1966.

Jones CM, Graf DR, Bru D, Philippot L, Hallin S (2013) The unaccounted yet abundant nitrous oxide-reducing microbial community: a potential nitrous oxide sink. The ISME journal, 7(2), 417-426.

Kaminsky LM, Trexler RV, Malik RJ, Hockett KL, Bell TH (2019) The inherent conflicts in developing soil microbial inoculants. Trends in biotechnology, 37(2), 140-151.

Kampschreur M, Kleerebezem R, Picioreanu, Bakken LR, Bergaust L, deVries S, Jetten M, van Loosdrecht MCM (2012) Metabolic modeling of denitrification in Agrobacterium tumefaciens: a tool to study inhibiting and activating compounds for the denitrification pathway. Frontiers in Microbiology, 3, 370.

Kartal B, Kuypers MM, Lavik G, Schalk J, Op den Camp HJ, Jetten MS, Strous M (2007). Anammox bacteria disguised as denitrifiers: nitrate reduction to dinitrogen gas via nitrite and ammonium. Environmental microbiology, 9(3), 635-642.

Kartal B, Tan NC, Van de Biezen E, Kampschreur MJ, van Loosdrecht MC, Jetten MS (2010) Effect of nitric oxide on anammox bacteria. Applied and environmental microbiology, 76(18), 6304-6306.

Keuschnig C, Gorfer M, Mania D, Frostegård Å, Bakken LR, Larose C (2020) NO and N2O transformations of diferse fungi in hyposica: evidence for anaerobic respiration only in Fusarium strains. Environmental Microbiology 22: 2182–2195.

Kezuka Y, Ohishi M, Itoh Y, Watanabe J, Mitsutomi M, Watanabe T, Nonaka, T. (2006). Structural studies of a two-domain chitinase from Streptomyces griseus HUT6037. Journal of molecular biology, 358(2), 472-484.

Khalil K, Mary B, Renault P (2004) Nitrous oxide production by nitrification and denitrification in soil aggregates as affected by O2 concentration. Soil Biology and Biochemistry, 36(4), 687-699.

Kits KD, Jung MY, Vierheilig J, Pjevac P, Sedlacek CJ, Liu S, Herbold C, Stein LY, Richter A, Wissel H, Brüggemann N, Wagner M, Daims H (2019) Low yield and abiotic origin of N2O formed by the complete nitrifier Nitrospira inopinata. Nature communications, 10(1), 1-12.

Klemedtsson L, Svensson BH, Rosswall T (1988) A method of selective inhibition to distinguish between nitrification and denitrification as sources of nitrous oxide in soil. Biology and Fertility of Soils, 6(2), 112-119.

Koay A, Woodcroft B, Petrie EJ, Yue H, Emanuelle S, Bieri M, Bailey MF, Hargreaves M, Park JT, Park KH, Ralph S, Neumann D, Stapleton D, Gooley, P. R. (2010). AMPK β subunits display isoform specific affinities for carbohydrates. FEBS letters, 584(15), 3499-3503.

Kool DM, Dolfing J, Wrage N, Van Groenigen JW (2011) Nitrifier denitrification as a distinct and significant source of nitrous oxide from soil. Soil Biology and Biochemistry, 43(1), 174-178.

Kunhikrishnan A, Thangarajan R, Bolan NS, Xu Y, Mandal S, Gleeson DB, Seshadri B, Zaman M, Barton L, Tang C, Luo J, Ding W, Kirkham MB, Naidu R (2016) Functional relationships of soil acidification, liming, and greenhouse gas flux. Advances in agronomy, 139, 1-71.

Ladha JK, Tirol-Padre A, Reddy CK, Cassman KG, Verma S, Powlson DS, van Kessel C, Richter DB,Chakraborty D, Pathak H (2016) Global nitrogen budgets in cereals: A 50-year assessment for maize, rice and wheat production systems. Scientific reports, 6(1), 1-9.

Ladha JK, Pathak HJ, Krupnik T, Six J, Van Kessel C (2005) Efficiency of fertilizer nitrogen in cereal production: retrospects and prospects. Adv. Agron. **87**, 85–156.

Lam SK, Suter H, Mosier AR, Chen D (2017) Using nitrification inhibitors to mitigate agricultural N2O emission: a double-edged sword?. Global Change Biology, 23(2), 485-489.

Li CS, Frolking S, Butterbach-Bahl K (2005) Carbon sequestration in arable soils is likely to increase nitrous oxide emissions, offsetting reductions in climate radiative forcing. Climatic Change, 72, 321–338.

Linn DM, Doran JW (1984) Effect of water-filled pore space on carbon dioxide and nitrous oxide production in tilled and non-tilled soils. Soil Sci. Soc. Am. J. 48:1267-1272.

Liu B, Frostegård Å, Bakken LR (2014) Impaired Reduction of N_2O to N_2 in acid soils Is due to a posttranscriptional interference with the expression of nosZ. mBio 5(3):e01383-14.

Liu R, Hu H, Suter H, Hayden HL, He J, Mele P, Chen D (2016) Nitrification is a primary driver of nitrous oxide production in laboratory microcosms from different land-use soils. Frontiers in microbiology, 7, 1373.

Liu S, Lin F, Wu S, Ji C, Sun Y, Jin Y, Li S, Li Z, Zou J (2017) A meta-analysis of fertilizer-induced soil NO and combined NO+ N2O emissions. *Global Change Biology*, *23*(6), 2520-2532.

Lycus P, Bøthun KL, Bergaust L, Shapleigh JP, Bakken LR, Frostegård Å (2017) Phenotypic and genotypic richness of denitrifiers revealed by a novel isolation strategy. The ISME journal, 11(10), 2219-2232.

Lycus P, Soriano-Laguna MJ, Kjos M, Richardson DJ, Gates AJ, Milligan DA., Frostegård Å, Bakken LR (2018) A bet-hedging strategy for denitrifying bacteria curtails their release of N2O. Proceedings of the National Academy of Sciences, 115(46), 11820-11825.

Maeda K, Spor A, Edel-Hermann V, Heraud C, Breuil M C, Bizouard F, Toyoda S, Yoshida N, Steinberg C, Philippot, L. (2015). N2O production, a widespread trait in fungi. Scientific reports, 5(1), 1-7.

Mahne I, Tiedje JM (1995) Criteria and methodology for identifying respiratory denitrifiers. Applied and Environmental Microbiology, 61(3), 1110-1115.

Mallon CA, Le Roux X, Van Doorn GS, Dini-Andreote F, Poly F, Salles JF (2018) The impact of failure: unsuccessful bacterial invasions steer the soil microbial community away from the invader's niche. The ISME journal, 12(3), 728-741.

Mania D, Heylen K, van Spanning RJ, Frostegård Å (2014) The nitrate-ammonifying and nosZ-carrying bacterium Bacillus vireti is a potent source and sink for nitric and nitrous oxide under high nitrate conditions. Environmental microbiology, 16(10), 3196-3210.

Mania D, Heylen K, vanSpanning RJM, Frostegård Å (2016) Regulation of nitrogen metabolism in the nitrate ammonifying soil bacterium Bacillus vireti and evidence for its ability to grow using N2O as electron acceptor. Environmental Microbiology 18: 2937–2950.

Mania D, Woliy K, Degefu T, Frostegård Å (2020). A common mechanism for efficient N2O reduction in diverse isolates of nodule-forming bradyrhizobia. Environmental microbiology, 22(1), 17-31.

Miranda ND, Tuomisto HL, McCulloch MD (2015) Meta-analysis of greenhouse gas emissions from anaerobic digestion processes in dairy farms. Environmental Science and Technology 49:5211-5219.

Misselbrook TH, Cardenas LM, Camp V, Thorman RE, Williams JR, Rollett AJ, Chambers BJ (2014) An assessment of nitrification inhibitors to reduce nitrous oxide emissions from UK agriculture. *Environmental Research Letters*, *9*(11), 115006.

Molodovskaya M, Singurindy O, Richards BK, Warland J, Johnson MS, Steenhuis TS (2012) Temporal variability of nitrous oxide from fertilized croplands: hot moment analysis. Soil Science Society of America Journal, 76(5), 1728-1740

Molstad L, Dörsch P, Bakken, LR (2007) Robotized incubation system for monitoring gases (O2, NO, N2O N2) in denitrifying cultures. Journal of microbiological methods, 71(3), 202-211.

Molstad L, Dörsch P, Bakken L (2016) Improved robotized incubation system for gas kinetics in batch cultures. Technical report.

Mørkved PT, Dörsch P, Bakken LR (2007) The N2O product ratio of nitrification and its dependence on long-term changes in soil pH. Soil Biology and Biochemistry, 39(8), 2048-2057.

Nadeem S, Bakken LR, Frostegård Å, Gaby JC, Dörsch P (2020) Contingent Effects of Liming on N2O-Emissions Driven by Autotrophic Nitrification. *Frontiers in Environmental Science*.

Nguyen TT, Myrold DD, Mueller RS (2019) Distributions of extracellular peptidases across prokaryotic genomes reflect phylogeny and habitat. Frontiers in microbiology, 10, 413.

Onaga S, Taira T (2008) A new type of plant chitinase containing LysM domains from a fern (Pteris ryukyuensis): Roles of LysM domains in chitin binding and antifungal activity, Glycobiology, Volume 18, Issue 5, Pages 414–423.

Orellana LH, Chee-Sanford JC, Sanford RA, Löffler FE, & Konstantinidis KT (2018) Year-round shotgun metagenomes reveal stable microbial communities in agricultural soils and novel ammonia oxidizers responding to fertilization. Applied and environmental microbiology, 84(2).

Ostrom NE, Sutka R, Ostrom PH, Grandy AS, Huizinga KM, Gandhi H, von Fischer JC, Robertson GP (2010) Isotopologue data reveal bacterial denitrification as the primary source of N2O during a high flux event following cultivation of a native temperate grassland. Soil Biology and Biochemistry, 42(3), 499-506.

Otto R, Castro SAQ, Mariano E, Castro SGQ, Franco HCJ, Trivelin PCO (2016) Nitrogen use efficiency for sugarcane-biofuel production: what is next?. Bioenergy Research, 9(4), 1272-1289.

Parkin TB (1987) Soil microsites as a source of denitrification variability. Soil Science Society of America Journal, 51(5), 1194-1199.

Pasternak Z, Pietrokovski S, Rotem O, Gophna U, Lurie-Weinberger MN, Jurkevitch E (2013) By their genes ye shall know them: genomic signatures of predatory bacteria. The ISME Journal, 7(4), 756-769.

Peng W, Pivato A (2019) Sustainable management of digestate from the organic fraction of municipal solid waste and food waste under the concepts of back to earth alternatives and circular economy. *Waste and biomass valorization*, *10*(2), 465-481.

Pérez J, Moraleda-Muñoz A, Marcos-Torres FJ, Muñoz-Dorado J (2016) Bacterial predation: 75 years and counting!. *Environmental microbiology*, *18*(3), 766-779.

Qu Z, Wang J, Almøy T, Bakken LR (2014) Excessive use of nitrogen in Chinese agriculture results in high N2O/(N2O+ N2) product ratio of denitrification, primarily due to acidification of the soils. Global change biology, 20(5), 1685-1698.

Quilliam RS, Glanville HC, Wade SC, Jones DL (2013) Life in the‘charosphere’e Does biochar in agricultural soil providea significant habitat for microorganisms? Soil Biol Biochem 65:287-293.

Reay DS, Davidson EA, Smith KA, Smith P, Melillo JM, Crutzen PJ (2012) Global agriculture and nitrous oxide emissions. Nature Climate Change 2:410-416.

Riding MJ, Herbert BMJ, Ricketts L, Dodd I, Ostle N, Semple KT (2015) Harmonizing conflicts between science, regulation, perception and environmental impact: The case of soil conditioners from bioenergy. Environ. Int. 75, 52-67.

Rocca JD, Hall EK, Lennon JT, Evans SE, Waldrop MP, Cotner JB., Nemergut DR, Graham EB,Wallenstein MD (2015) Relationships between protein-encoding gene abundance and corresponding process are commonly assumed yet rarely observed. The ISME journal, 9(8), 1693-1699.

Ruser R, Schulz R (2015) The effect of nitrification inhibitors on the nitrous oxide (N2O) release from agricultural soils—a review. Journal of Plant Nutrition and Soil Science, 178(2), 171-188.

Russenes AL, Korsæth A, Bakken LR, Dörsch P (2016) Spatial variation in soil pH controls off-season N_2O emission in an agricultural soil. Soil Biology and Biochemistry 99: 36-46.

Scarlat N, Dallemand JF, Fahl F (2018). Biogas: Developments and perspectives in Europe. Renewable Energy 129, p. 457 – 472.

Schink B (1997) Energetics of syntrophic cooperation in methanogenic degradation. Microbiology and molecular biology reviews, 61(2), 262-280.

Senbayram M, Chen R, Budai A, Bakken L, Dittert K (2012) N2O emission and the N2O/(N2O+ N2) product ratio of denitrification as controlled by available carbon substrates and nitrate concentrations. Agriculture, Ecosystems & Environment, 147, 4-12.

Shapleigh JP (2013) The prokaryotes: Prokaryotic Physiology and Biochemistry. In, Rosenberg E, De Long EF, Lory S, Stackebrandt E and Thompsons D (eds), The prokaryotes. Springer Berling Heidelbers, Berlin, Heidelberg, pp.405-425.

Shaw LJ, Nicol GW, Smith Z, Fear J, Prosser JI, Baggs EM (2006) Nitrosospira spp. can produce nitrous oxide via a nitrifier denitrification pathway. Environmental Microbiology, 8(2), 214-222.

Schoebitz M, Lopez MD, Roldan A (2013) Bioencapsulation of microbial inoculants for better soil–plant fertilization. A review. Agron. Sustain. Dev. 33:751–765

Shoun H, Kim DH, Uchiyama H, Sugiyama J (1992) Denitrification by fungi. FEMS Microbiology Letters, 94(3), 277-281.

Schlüter S, Zawallich J, Vogel H-J, Dörsch P (2019) Physical constraints for respiration in microbial hotspots in soil and their importance for denitrification. Biogeosciences. 16. 3665-3678. 10.5194/bg-16-3665-2019.

Sekar K, Linker SM, Nguyen J, Grünhagen A, Stocker R, Sauer U (2020) Bacterial glycogen provides short-term benefits in changing environments. Applied and environmental microbiology, 86(9).

Sexstone AJ, Revsbech NP, Parkin TB, Tiedje JM (1985) Direct measurement of oxygen profiles and denitrification rates in soil aggregates. Soil science society of America journal, 49(3), 645-651.

Spiro S (2012) Nitrous oxide production and consumption: regulation of gene expression by gas-sensitive transcription factors. Philosophical Transactions of the Royal Society B: Biological Sciences, 367(1593), 1213-1225.

Spiro S (2016) Regulation of denitrification. Metalloenzymes in denitrification: applications and environmental impacts. London: Royal Society of Chemistry, 312-30.

Steensels J, Gallone B, Voordeckers K, Verstrepen KJ (2019) Domestication of Industrial Microbe. Current Biology Review, R381–R393

Stein LY (2019) Insights into the physiology of ammonia-oxidizing microorganisms. Current Opinion in Chemical Biology 49:9-15.

Stein LY (2020) The Long-Term Relationship between Microbial Metabolism and Greenhouse Gases. Trends in Microbiology 28: 500- 511.

Stevens RJ, Laughlin RJ (1998) Measurement of nitrous oxide and di-nitrogen emissions from agricultural soils. Nutrient Cycling in Agroecosystems, 52(2), 131-139.

Sutton MA, Skiba UM, Davidson EA, Kanter D, van Grinsven HJM, Oenema O, Maas R, Pathak H (2013) Drawing Down N2O to Protect Climate and the Ozone Layer. A UNEP Synthesis Report (Nairobi: United Nations Environment Programme).

Syakila A, Kroeze C (2011). The global nitrous oxide budget revisited. Greenhouse gas measurement and management, 1(1), 17-26.

Svennevik OK, Solheim OE, Beck G, Sørland GH, Jonassen KR, Rus E, Westereng B, Horn SJ, Higgins MJ, Nilsen PJ (2019) Effects of post anaerobic digestion thermal hydrolysis on dewaterability and moisture distribution in digestates. Water Sci Technol, 80 (7): 1338–1346.

Svennevik OK, Jonassen KR, Svensson K, Hagen LH, Westereng B, Solheim OE, Nilsen PJ, Horn SJ, Bakken L (2020) Protecting Thermally Hydrolyzed Biosolids from Pathogenic Bacterial Growth by Addition of Compost. Waste Biomass Valor.

Svensson K, Kjørlaug O, Higgins MJ, Linjordet R, Horn SJ (2018) Post-anaerobic digestion thermal hydrolysis of sewage sludge and food waste: Effect on methane yields, dewaterability and solids reduction. Water research, 132, 158-166.

Thompson IP, Van Der Gast CJ, Ciric L, Singer AC (2005) Bioaugmentation for bioremediation: the challenge of strain selection. Environmental Microbiology, 7(7), 909-915.

Tian D, Niu S (2015) A global analysis of soil acidification caused by nitrogen addition. Environmental Research Letters, 10(2), 024019.

Tian H, Xu R, Canadell JG, Thompson RL, Winiwarter W, Suntharalingam P, ..., Yao Y (2020) A comprehensive quantification of global nitrous oxide sources and sinks. Nature, 586(7828), 248-256.

Torres MJ, Simon J, Rowley G, Bedmar EJ, Richardson DJ, Gates AJ, Delgado MJ (1016) Chapter Seven - Nitrous Oxide Metabolism in Nitrate-Reducing Bacteria: Physiology and Regulatory Mechanisms, Advances in Microbial Physiology, Academic Press, Volume 68.

Vaccaro BJ, Thorgersen MP, Lancaster WA, Price MN, Wetmore KM, Poole FL, Deutschbauer A, Arkin AP, Adams MW (2016) Determining roles of accessory genes in denitrification by mutant fitness analyses. Applied and Environmental Microbiology 82:51-61. DOI:10.1128/AEM.02602-15 van Elsas JD, Chiurazzi M, Mallon CA, Elhottovā D, Krištůfek V, Salles JF (2012) Microbial diversity determines the invasion of soil by a bacterial pathogen. Proceedings of the National Academy of Sciences, 109(4), 1159-1164.

van Gool W (1987) The values of energy carriers. Energy 12, 509-518.

van Groenigen JW, Velthof GL, Oenema O, Van Groenigen KJ, Van Kessel C (2010) Towards an agronomic assessment of N2O emissions: a case study for arable crops. *European journal of soil science*, *61*(6), 903-913.

van Kessel MA, Speth DR, Albertsen M, Nielsen PH, den Camp HJO, Kartal B, Jetten MSN, Lücker S (2015) Complete nitrification by a single microorganism. Nature, 528(7583), 555-559.

Venterea R, Halvorson AD, Kitchen N, Liebig MA, Cavigelli MA, Del Grosso SJ, Motavalli PP, Nelson KA, Spokas KA, Singh BP, Stewart CE, Ranaivoson A, Strock J, Collins H (2012) Challenges and opportunities for mitigating nitrous oxide emissions from fertilized cropping systems. Frontiers in Ecology and the Environment. 10. 562-570.

Verbruggen E, van der Heijden MG, Rillig MC, Kiers ET (2013) Mycorrhizal fungal establishment in agricultural soils: factors determining inoculation success. New Phytologist, 197(4), 1104-1109.

Verdi L, Kuikman PJ, Orlandini S, Mancini M, Napoli M, Marta AD (2019) Does the use of digestate to replace mineral fertilizers have less emissions of N2O and NH3?. Agricultural and Forest Meteorology, 269, 112-118.

Wang Y, Guo J, Vogt RD, Mulder J, Wang J, Zhang X (2018) Soil pH as the chief modifier for regional nitrous oxide emissions: new evidence and implications for global estimates and mitigation. Global change biology, 24(2), e617-e626.

Wang X, Wang S, Jiang Y, Zhou J, Han C, Zhu G (2020) Comammox bacterial abundance, activity, and contribution in agricultural rhizosphere soils. Science of The Total Environment, 727, 138563.

Wang Y, Yao Z, Zhan Y, Zheng X, Zhou M, Yan G, Wang L, Werner C, Butterbach-Bahl K (2021) Potential benefits of liming to acid soils on climate change mitigation and food security Global Change Biology, online.

Wilks JC, Slonczewski JL 2007. pH of the Cytoplasm and Periplasm of Escherichia coli: Rapid Measurement by Green Fluorescent Protein Fluorimetry. Appl Env Micr 189:5601-5607.

Winiwarter W, Höglund-Isaksson L, Klimont Z, Schöpp W, Amann M (2018) Technical opportunities to reduce global anthropogenic emissions of nitrous oxide. Environ Res Lett, 13:014011.

Wrage N, Velthof GL, Van Beusichem ML, Oenema O (2001) Role of nitrifier denitrification in the production of nitrous oxide. Soil biology and Biochemistry, 33(12-13), 1723-1732.

Yoon S, Nissen S, Park D, Sanford RA, Löffler FE (2016) Nitrous oxide reduction kinetics distinguish bacteria harboring clade I NosZ from those harboring clade II NosZ. *Applied and environmental microbiology*, *82*(13), 3793-3800.

Zhang X, Davidson EA, Mauzerall DL, Searchinger TD, Dumas P, Shen Y (2015) Managing nitrogen for sustainable development. Nature, 528(7580), 51-59.

Zhang L, Wüst A, Prasser B, Müller C, Einsle O (2019) Functional assembly of nitrous oxide reductase provides insights into copper site maturation. Proceedings of the National Academy of Sciences, 116(26), 12822-12827.

Zumft WG (1997) Cell biology and molecular basis of denitrification. Microbiology and molecular biology reviews, 61(4), 533-616.

Appendix A

This thesis was written as a part of the authors duties as a process engineer at the VEAS wastewater treatment plant. **Appendix A** gives a short description of the treatments plant and some information as to why N_2O reducing biofertilizers is within the company's interest towards integration in the developing circular bioeconomy.

A1 VEAS WWTP

VEAS (Vestfjorden Avløpsselskap) is Norway's largest wastewater treatment plant (WWTP) and serves 640 000 inhabitants in the greater Oslo region. Including commuting workers and discharge from industry, the total loading to the plant is equivalent to ~750 000 person equivalents. Average yearly effluent permits restricted to 70 % N-, 90 % P-, 80/85 % BOD/COD removal. The plant is designed for a maximum hydraulic loading of 11 m^3/s.

The wastewater is transported to VEAS by gravity through a ~40 km sewage tunnel (d=3 m), with several connection points to neighboring municipalities' grid of wastewater pipes and pumping stations. The effluent from the plant (~100 million m^3 $year^{-1}$) is discharged to the Oslo-fjord.

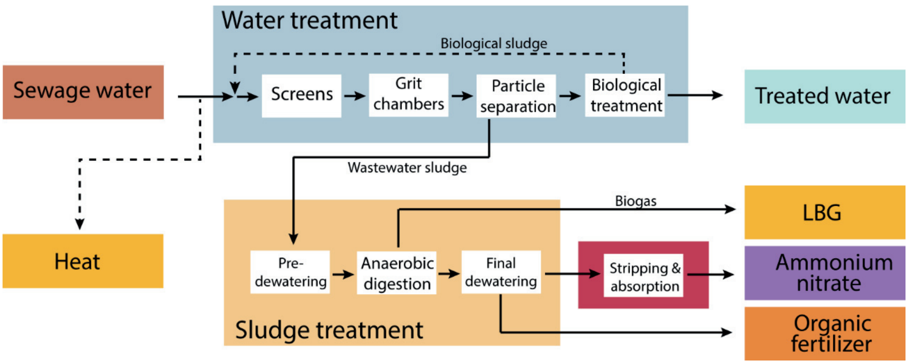

Figure A1: Simplified process scheme of the "VEAS-concept". The water treatment consists of mechanical treatment (screens and grit chambers), chemical treatment (grit chambers and particle separation) and biological treatment (nitrification and denitrification stationary filters). Biological sludge from the biological treatment is returned to the inlet. Wastewater sludge from the particle separation step is dewatered through rotary drum filters prior to anaerobic digestion. Slaked lime is added to the digestate before final dewatering in in heated chamber filter presses generating a filtrate and a biosolid. Heat, recovered from the influent, liquid biogas (LBG), ammonium nitrate and the digestate based biosolid (organic fertilizer) is traded on the open market.

The "VEAS-concept" (**Fig. A1**) is founded on effective particle separation and utilization of the wastewaters content of organic carbon for energy production, where effective air jet mixing of precipitation chemicals in the grit chambers upstream of particle separation in sedimentation basins (designed for high surface loads: 12 – 13 m/s), secures adequate removal of particulates before soluble species are metabolized sequentially in stationary nitrification- and denitrification reactors (biological treatment, **Fig. A1**) (Sagberg et al 1998). Expanded clay in the biological water treatment double functions as a biofilm carrier material and as a filtering aid, rendering final sedimentation or filtering obsolete. This configuration secures a modest foot print and very low water retention times (< 3 hours) at average inlet flow (3 m^3/s) .

The process configuration in the water treatment has it's draw backs: Firstly, loading of soluble organic carbon to the denitrification filters stimulates growth of heterotrophs competing for oxygen as the primary electron acceptor with the autotrophic nitrifying community (Knutsen 2017). This results in a situation where the nitrification rate currently is the bottle neck in the water treatment lines. Secondly, since the wastewater leaving the nitrification reactors is carbon exhausted an external carbon source (methanol) is added prior to the denitrification step. Lastly: retention of biomass and particulates in the filter medium (leca) requires intensive and frequent backflushing/washing of the filters. Water used for backwashing of the filters is is returned to the plant inlet and currently represents ~20 % of the total hydraulic load through the plant.

In the context of municipal wastewater treatment, further treatment of the inorganic/organic fraction separated from the wastewater is more traditional/conventional: Mesophilic (37°C) anaerobic digesters (ADs) are fed with a mixture of primary, secondary and biological sludge separated in the sedimentation basins (particle separation, **Fig. A1**), before being thickened to 7 % DW in rotary drum filters (Pre-dewatering, **Fig. A1**) (volatile solids of the substrate is ~80 %). An average hydraulic retention time (HRT) of 24 days through AD results in a specific methane yield of ~700 Nm^3/kg-VS with an average organic reduction of 63 %. Before final dewatering and heat-sanitation in chamber filter presses a slurry of slaked lime (10 % TS) is mixed in with the digestate. This elevates digestate pH from 7.8 to 12 and shifts the ammonium/ammonia equilibrium towards ammonia, which is utilized in the stripping/absorption plant, where ammonia is stripped of the filtrate water and reacted with nitric acid, to produce ammonium nitrate (**Fig. A1**).

A2 VEAS WWTP in the future circular economy

VEAS has been committed to the core principles of *circular economy* for several decades when; redistributing organic wastes for agricultural purposes, producing ammonium nitrate utilized in industrial production of mineral fertilizers, exploiting wastewater heat that is redistributed for house heating and providing cleaner fuels for transport (LBG) (**Fig. A1**). As the business model and structure of the company is ever changing to maximize the plants benefit to society (economical and environmental), VEAS is committed to investing in R&D with technology suppliers and academic institutions in order to develop new technologies and business models in such a scheme (**Fig. A2**).

Annually the plant produces ~40 000 tons organic fertilizer supplemented with slaked lime (45 % TS, 30 wt.% $Ca(OH)_2$), ~4000 tons of ammonium nitrate (15 wt. % N), ~64 GWh LBG, and recovers ~70 GWh of heat energy from the influent waste water. Energy and products yielded in the different processes (heat, liquid methane, and ammonium nitrate) is traded on the open marked generating revenue. However, the digestate based organic fertilizer, used as a supplement fertilizer in cereal farming, is still a product with a negative trade value, and product development has been at a stand-still since the mid 90's.

Figure A2: Integration of VEAS as an organic waste management industry with the surrounding society in practice. VEAS WWTP is the key enabler in this construction; collecting organic waste from a large population and returning refined products from the waste streams back to society in the form of energy (heat and bio-methane), bio-fertilizers (digestate) and N-based fertilizers (ammonium nitrate).

References:

Knutsen MF (2017) Robustness of nitrifying biofilter functionality: Role of competition between heterotrophic and nitrifying bacteria on ammonium removal efficiency and microbial community structure (Master's thesis, NTNU).

Sagberg P, Ryrfors P, Berg KG (1998) The mass balances of nitrogen and carbon in a compact nitrogen and phosphorus WWTP. In *Chemical Water and Wastewater Treatment V* (pp. 231-242). Springer, Berlin, Heidelberg.

Paper I

N_2O-respiring bacteria in biogas digestates for reduced agricultural emissions

Kjell Rune Jonassen[1,3], Live H. Hagen[1], Silas H.W. Vick[1], Magnus Ø. Arntzen[1], Vincent G.H. Eijsink[1], Åsa Frostegård[1], Pawel Lycus[1], Lars Molstad[4], Phillip B. Pope[1,2], Lars R. Bakken[1*]

[1)] Faculty of Chemistry, Biotechnology and Food Science, NMBU - Norwegian University of Life Sciences, 1432 Ås, Norway

[2)] Faculty of Biosciences, NMBU - Norwegian University of Life Sciences, Norway

[3)] VEAS WWTP, Bjerkåsholmen 125, 3470 Slemmestad, Norway.

[4)] Faculty of Science and Technology, Norwegian University of Life Sciences, Norway

* corresponding author

Abstract

Inoculating agricultural soils with N_2O-respiring bacteria (NRB) can reduce N_2O-emissions, but would be impractical as a standalone operation. Here we demonstrate that digestates obtained after biogas production are suitable substrates and vectors for NRB. We show that indigenous NRB in digestates grew to high abundance during anaerobic enrichment under N_2O. Gas-kinetics and meta-omic analyses showed that these NRB's, recovered as metagenome-assembled genomes (MAGs), grew by harvesting fermentation intermediates of the methanogenic consortium. Three NRB's were isolated, one of which matched the recovered MAG of a *Dechloromonas*, deemed by proteomics to be the dominant producer of N_2O-reductase in the enrichment. While the isolates harbored genes required for a full denitrification pathway and could thus both produce and sequester N_2O, their regulatory traits predicted that they act as N_2O sinks in soil, which was confirmed experimentally. The isolates were grown by aerobic respiration in digestates, and fertilization with these NRB-enriched digestates reduced N_2O emissions from soil. Our use of digestates for low-cost and large-scale inoculation with NRB in soil can be taken as a blueprint for future applications of this powerful instrument to engineer the soil microbiome, be it for enhancing plant growth, bioremediation, or any other desirable function.

Introduction

Nitrous oxide is an intermediate in the nitrogen cycle and a powerful greenhouse gas emitted in large volumes from agricultural soils, accounting for ~1/3 of total anthropogenic N_2O emissions (Tian et al 2020). Reduced emissions can be achieved by minimizing the consumption of fertilizer nitrogen through improved agronomic practice and reduction of meat consumption (Snyder et al 2014, Sutton et al, 2011), but such measures are unlikely to do more than stabilize the global consumption of fertilizer N (Erisman et al 2008). This calls for more inventive approaches to reduce N_2O emissions, targeting the microbiomes of soil (D'Hondt et al 2021), in particular the physiology and regulatory biology of the organisms involved in production and consumption of N_2O in soil (Bakken and Frostegård 2020).

N_2O turnover in soil involves several metabolic pathways, controlled by a plethora of fluctuating physical and chemical variables (Butterbach-Bahl et al 2013, Hu et al 2015).

Heterotrophic denitrification is the dominant N_2O source in most soils, while autotrophic ammonia oxidation may dominate in well drained calcareous soils (Song et al 2018 and references therein). Heterotrophic denitrifying organisms are both sources and sinks for N_2O because N_2O is a free intermediate in their stepwise reduction of nitrate to dinitrogen ($NO_3^- \rightarrow NO_2^- \rightarrow NO \rightarrow N_2O \rightarrow N_2$). Denitrification involves four enzymes collectively referred to as denitrification reductases: nitrate reductase (Nar/Nap), nitrite reductase (Nir), nitric oxide reductase (Nor) and nitrous oxide reductase (Nos), encoded by the genes *nar*/*nap*, *nir*, *nor* and *nosZ*, respectively. Oxygen is a strong repressor of denitrification, both at the transcriptional and the metabolic level (Zumft 1997, Qu et al 2016). Many organisms have truncated denitrification pathways, lacking from one to three of the four reductase genes (Shapleigh 2013, Lycus et al 2017), and truncated denitrifiers can thus act as either N_2O producers (organisms without *nosZ*) or N_2O reducers (organisms with *nosZ* only). The organisms with *nosZ* only, coined non-denitrifying N_2O-reducers (Sanford et al 2013), have attracted much interest as N_2O sinks in the environment (Hallin et al 2018). Of note, organisms with a full-fledged denitrification pathway may also be strong N_2O sinks depending on the relative activities and regulation of the various enzymes in the denitrification pathway (Lycus et al 2018; Mania et al 2020). Despite their promise, feasible ways to utilize N_2O-reducing organisms to reduce N_2O emissions have not yet emerged.

A soil with a strong N_2O-reducing capacity will emit less N_2O than one dominated by net N_2O producing organisms, as experimentally verified by Domeignoz-Horta et al (2016), who showed that soils emitted less N_2O if inoculated with large numbers (10^7 - 10^8 cells g^{-1} soil) of organisms expressing Nos as their sole denitrification reductase. As a standalone operation, the large-scale production and distribution of N_2O-respiring bacteria would be prohibitively expensive and impractical. However, the use of N_2O-respiring bacteria could become feasible if adapted to an existing fertilization pipeline, such as fertilization with the nitrogen- and phosphate-rich organic waste (digestate) generated by biogas production in anaerobic digesters. Anaerobic digestion (**AD**) is already a core technology for treating urban organic wastes, and is expected to treat an increasing proportion of the much larger volumes of waste produced by the agricultural sector (**Figure 1**), as an element of the roadmap towards a low-carbon circular economy (Scarlat et al 2018). This means that digestates from **AD** are likely to become a major organic fertilizer for agricultural soils, with a huge potential for reducing N_2O emissions if enriched with N_2O-respiring bacteria prior to application.

Here we provide the first proof of this promising concept. Firstly, we demonstrate selective enrichment and isolation of fast-growing digestate-adapted N_2O-respiring bacteria using a digestate from a wastewater treatment plant. Secondly, we demonstrate that the use of digestates enriched with such organisms as a soil amendment reduces the proportion of N leaving soil as N_2O, confirming the suitability of such digestates for this purpose. Analysis of the enrichment process with multi-omics and in-depth monitoring of gas kinetics provides valuable insights into Nos-synthesis by the various enriched taxa, and the metabolic pathways of the anaerobic consortium providing substrates for these enriched N_2O-respiring organisms.

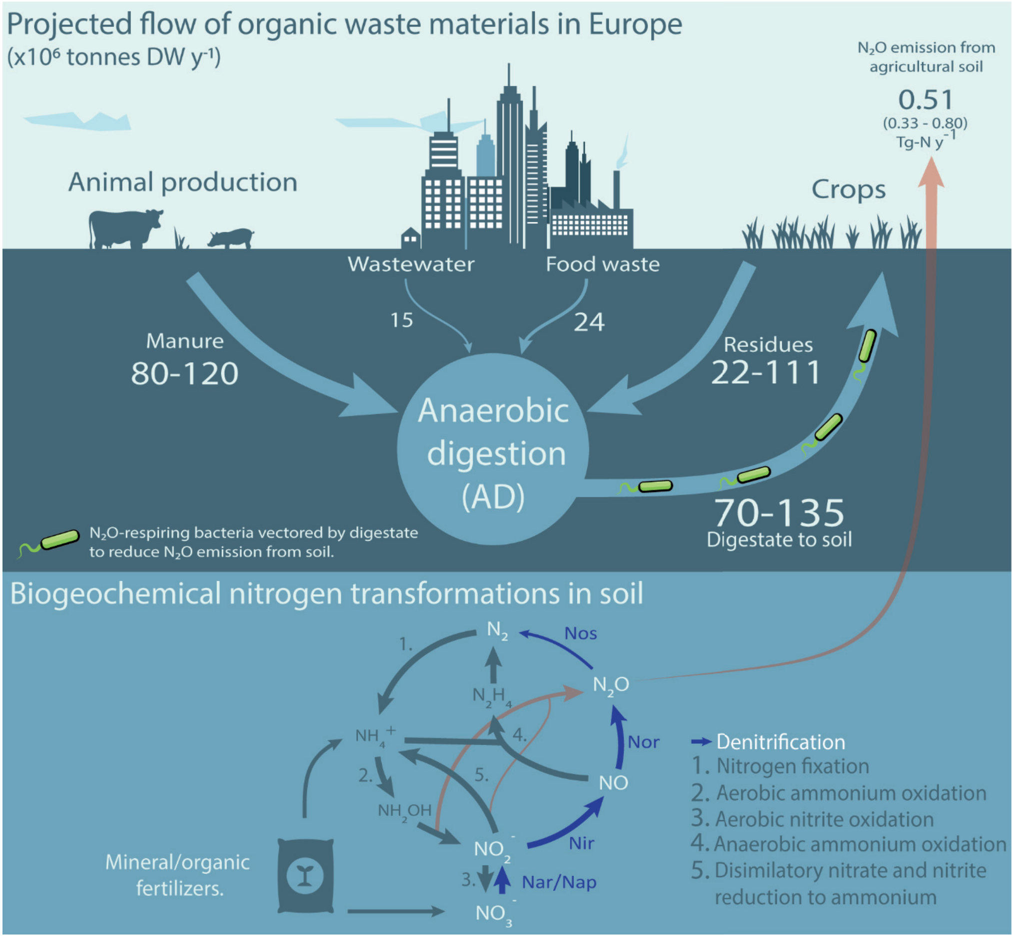

Figure 1. Possible biomass streams in a future circular economy with a central role for anaerobic digestion. Solid arrows (top section) show streams of biomass available for anaerobic digestion (AD). Numbers indicate known estimates of currently used or potentially available amounts in Europe, in million tonnes dry-weight (DW) per year (Foged et al 2011, Holm-Nielsen et al 2009, Stenmarck et al 2016, Meyer et al 2018). The arrow from anaerobic digestion to agricultural soil, indicates a credible pathway for digestate enriched with N_2O-reducing bacteria (assuming enrichment at **AD** site); fertilization with such enriched digestates strengthens the N_2O sink capacity of the soil, hence reducing N_2O emissions. N_2O emissions from agricultural soil in Europe are estimated at 0.51 tG per year (min 0.33 – max 0.80), representing some 48 % of total European N_2O emissions (Tian et al 2020), which account for approximately 3.5 % of the global warming effect from European greenhouse gas emissions and 35 % of the global warming effect from European agriculture (Eurostat 2018). The lower half of the picture shows the microbial nitrogen transformations underlying these N_2O emissions, which are fed by fertilizers. Today, **AD** is primarily used for treating urban organic wastes, which comprise only ~10 % of the biomass potentially available for **AD**. The amount of biomass treated by **AD** is expected to increase by an order of magnitude when adopted on a large scale in the agricultural sector. This would generate 70-135 Mt DW of digestate annually (assuming 50% degradation by AD), which is equivalent to 400-780 kg DW ha^{-1} y^{-1} if spread evenly on the total farmland of Europe (173 million ha).

Materials and methods

The digestates were taken from two anaerobic digesters, one mesophilic (37 °C) and one thermophilic (52 °C), which were running in parallel, producing biogas from sludge produced by a wastewater treatment. The sludge was a poly-aluminum chloride (PAX-XL61™, Kemira) and ferric chloride (PIX318™, Kemira) precipitated municipal wastewater sludge, with an organic matter content of 5.6% (w/w). Both digestors reduced the organic matter by approximately 60%, producing digestates containing ~2.1 % organic matter, 1.8-1.9 g NH_4^+-N L^{-1}, ~16 and 32 Meq VFA L^{-1} , pH=7.6-7.8 and 8.2; mesophilic and thermophilic, respectively (see Suppl Methods 1 for further details). The digestates were transported to the laboratory in 1 L insulated steel-vessels and used for incubation experiments 3-6 hours after sampling.

The robotized incubation system developed by Molstad et al (2007, 2016) was used in all experiments where gas kinetics was monitored. The system hosts 30 parallel stirred batches in 120 mL serum vials, crimp sealed with gas tight butyl rubber septa, which are monitored for headspace concentration of O_2, N_2, N_2O, NO, CO_2 and CH_4 by frequent sampling. After each sampling, the system returns an equal volume of He, and elaborated routines are used to account for the gas loss by sampling to calculate the production/consumption-rate of each gas for each time interval between two samplings. More details are given in Suppl Methods 2.

Enrichment culturing of N_2O-respiring bacteria (NRB) in digestate was done as stirred (300 rmp) batches of 50 mL digestate per vial. Prior to incubation, the headspace air was replaced with Helium by repeated evacuation and He-filling (Molstad et al 2007), and supplemented with N_2O, and N_2O in the headspace was sustained by repeated injections in response to depletion. Liquid samples (1 mL) were taken by syringe, for metagenomic and metaproteomic analyses, and for quantification of volatile fatty acids (VFA) and 16srDNA abundance. The samples were stored -80 °C before analyzed. The growth of NRB in the enrichments was modelled based on the N_2O reduction kinetics. The modelling and the analytic methods (quantification of VFA and 16srDNA abundance) are described in detail in Suppl Methods 3.

Metagenomics and metaprotomics: Sequencing of DNA (Illumina HiSec4000), and the methods for Metagenome-Assembled Gemome (MAG) binning, and the phylogenetic placement of the MAGs is described in detail in Suppl Methods 4. Proteins were extracted and digested to peptides, which were analyzed by nanoLC-MS/MS, and the acquired spectra were inspected, using the metagenome-assembled genomes (149 MAGs) as a scaffold (Suppl Methods 5).

Isolation of N_2O-respiring bacteria (NRB) (Suppl Methods 6). NRB present in the enrichment cultures were isolated by spreading diluted samples on agar plates with different media composition, then incubated in an anaerobic atmosphere with N_2O. Visible colonies were re-streaked and subsequently cultured under aerobic conditions, and 16s-sequenced. Three isolates, **AS** (*Azospira* sp), **AN** (Azonexus sp) and **SP** (*Pseudomonas* sp) (names based on their 16s sequence), were selected for genome sequencing, characterization of their denitrification phenotypes, and for testing their effect as N_2O sinks in soil.

Genome sequencing and phenotyping of isolates. Three isolates were genome sequenced and compared with MAG's of the enrichment culture (Suppl Methods 7). The isolates' ability to utilize various organic C substrates was tested on BiOLOG Phenotype MicroArray™ microtiter plates, and their characteristic regulation of denitrification was tested through a range of incubation experiments as in previous investigations (Bergaust et al 2010, Liu et al 2014, Lycus et al 2018, Mania et al 2020), by monitoring the kinetics of O_2, N_2, N_2O, NO and NO_2^- throughout the cultures' depletion of O_2 and transition from aerobic to anaerobic respiration in stirred batch cultures with He + O_2 (+/- N_2O) in the headspace (Suppl Methods 8). The kinetics of electron flow throughout the oxic and anoxic phase in these experiments were used to assess if the organisms were *bet hedging*, as demonstrated for *Paracoccus denitrificans* (Lycus et al 2018), i.e. that only a minority of cells express nitrate- and/or nitrite-reductase, while all express Nos, in response in response to oxygen depletion. Putative *bet hedging* was corroborated by measuring the abundance of nitrate-, nitrite- and nitrous oxide reductase (Suppl Methods 9).

N_2O mitigation experiments (Suppl Methods 9). To assess the capacity of the isolates to reduce the N_2O emission from soil, they were grown aerobically in sterilized digestate, which was then added to soil in microcosms, for measuring the NO-, N_2O- and N_2- kinetics of denitrification in the soil. For comparison, the experiments included soils amended with sterilized digestate, live digestate (no pretreatment), and digestate in which N_2O-reducing bacteria had been enriched by anaerobic incubation with N_2O (as for the initial enrichment culturing).

Data availability

The sequencing data for this study have been deposited in the European Nucleotide Archive (ENA) at EMBL-EBI under accession number PRJEB41283 (isolates AN, AS and PS) and PRJEB41816 (metagenome) (https://www.ebi.ac.uk/ena/browser/view/PRJEBxxxx). Functionally annotated MAGs and metagenomic assembly are available in FigShare (DOI: 10.6084/m9.figshare.13102451 and 10.6084/ m9.figshare.13102493). The proteomics data has been deposited to the ProteomeXchange Consortium (http://proteomecentral.proteomexchange.org) via the PRIDE partner repository (Vizcaino et al 2013) with the dataset identifier PXD022030* and PXD023233** for the metaproteome and proteome of *Azonexus* sp. AN, respectively.

* Reviewer access: Username: reviewer_pxd022030@ebi.ac.uk. Password: GdTR3biE

** Reviewers access: Username: reviewer_pxd023233@ebi.ac.uk Password: nMz62S8O

Results and Discussion

Enrichment of indigenous N_2O- respiring bacteria (NRB) in digestates

We hypothesized that suitable organisms could be found in anaerobic digesters fed with sewage sludge, since such sludge contains a diverse community of denitrifying bacteria stemming from prior nitrification/denitrification steps (Lu et al 2014). We further hypothesized that these bacteria could be selectively enriched in digestates by anaerobic incubation with N_2O. We decided to enrich at 20 ^{o}C, rather than at the temperatures of the anaerobic digesters (37 and 52 ^{0}C), to avoid selecting for organisms unable to grow within the normal temperature range of soils.

The digestates were incubated anaerobically as stirred batch cultures with N_2O in the headspace (He atmosphere), and the activity and apparent growth of N_2O reducers was assessed by monitoring the N_2O-reduction to N_2. **Figure 2A** shows the results for the first experiment, where culture vials were liquid samplws were taken at three time points (0, 115 and 325 h) for metagenomics, metaproteomics, and quantification of 16S rDNA and volatile fatty acids (VFAs). N_2O was periodically depleted (100-140 h) in this experiment, precluding detailed analysis of the growth kinetics throughout. This was avoided in the second enrichment, for which complete gas data are shown in **Figure 2BC**. Apart from the deviations caused by the temporary depletion of N_2O in the first experiment, both experiments showed very similar N_2 production rates (**Figures 2B and S1B**). The gas kinetics of the second enrichment are discussed in detail below.

Figure 2B shows declining rates of N_2-production (V_{N2}) during the first 50 h, followed by exponential increase. This was modelled as the activity of two groups of NRB, one growing exponentially from low initial abundance, and one which was more abundant initially, but whose activity declined gradually (further explained in **Figure S1**). The modelling, indicated that the cell density of the growing NRB increased exponentially (specific growth rate, $\mu = 0.1$ h^{-1}) from a very low initial density (~$2.5 \cdot 10^3$ cells mL^{-1}) to $1.6 \cdot 10^8$ cells mL^{-1} after 110 h, and continued to increase at a gradually declining rate to reach ~$3 \cdot 10^9$ cells mL^{-1} at the end of the incubation period (215 h). The modelled cell-specific electron flow rate (V_{e-}, **Figure 2C**) was sustained at around 5 fmol e^- $cell^{-1}$ h^{-1} during the exponential growth, and declined gradually thereafter, as the number of cells continued to increase, while the overall rate of N_2O-respiration remained more or less constant (V_{N2}, **Figure 2B**). Enrichment culturing as shown in **Figure 2BC** was repeated three times, demonstrating that the characteristic N_2 production kinetics was highly reproducible (**Figure S2**).

The provision of substrate for the N_2O-respiring bacteria can be understood by considering the enrichment culture as a continuation of the metabolism of the anaerobic digester (**AD**), albeit slowed down by the lower temperature (20 ^oC, versus 37 ^oC in the digester). In **AD**, organic polymers are degraded and converted to CO_2 and CH_4 through several steps, conducted by separate guilds of the methanogenic microbial consortium: 1) hydrolysis of polysaccharides to monomers by organisms with carbohydrate-active enzymes, 2) primary fermentation of the resulting monomers to volatile fatty acids (VFAs), 3) secondary fermentation of VFAs to acetate, H_2 and CO_2, and 4) methane production from acetate, CO_2, H_2, and methylated compounds. By providing N_2O to this (anaerobic) system, organisms that respire N_2O can tap into the existing flow of carbon, competing with the methanogenic consortium for intermediates, such as monomeric sugars, VFAs (such as acetate) and hydrogen (Stams et al 2003). Thus, the respiration and growth of the N_2O-respiring bacteria is sustained by a flow of carbon for which the primary source is the depolymerization of organic polymers. It is possible that the retardation of growth after ~100 h of enrichment was due to carbon becoming limiting. Thus, at this point, the population of N_2O-respiring organisms may have reached high enough cell densities to reap most of the intermediates produced by the consortium.

Parallel incubations of digestates without N_2O confirmed the presence of an active methanogenic consortium, sustaining a methane production rate of ~0.2 µmol CH_4 mL^{-1} h^{-1} throughout (**Figure S3**). Methane production was inhibited by N_2O, and partly restored in periods when N_2O was depleted (**Figure 2A, Figures S3**&**S4**). We also conducted parallel incubations with O_2 and NO_3^- as electron acceptors. These incubations showed that methanogenesis was completely inhibited by NO_3^-, and partly inhibited by O_2 (concentration in the liquid ranged from 20 to 90 µM O_2) (**Figures S3**). The rates of O_2 and NO_3^- reduction indicated that the digestate contained a much higher number of cells able to respire O_2 and NO_3^- than cells able to respire N_2O (**Figure S5A-C**). During the enrichment culturing with NO_3^-, almost all reduced nitrogen appeared in the form of N_2O during the first 50 h (**Figure S5E**), another piece of evidence that in the digestate (prior to enrichment culturing), the organisms reducing NO_3^- to N_2O outnumbered those able to reduce N_2O to N_2. The measured production of CH_4 and electron flows to electron acceptors deduced from measured gases (N_2, O_2 and CO_2) were used to assess the effect of the three electron acceptors (N_2O, NO_3^- and O_2) on C-mineralization. While oxygen appeared to have a marginal effect, NO_3^- and N_2O caused severe retardation of C-mineralization during the first 50 and 100 h, respectively (**Figure S5A-D). **This retarded mineralization is plausibly due to the inhibition of methanogenesis, causing a transient accumulation of H_2 and VFAs until the N_2O-reducing bacteria reach a cell density that allowed them to effectively reap these compounds. This was corroborated by measurements of H_2 and VFAs (**Figure S13**).

To track the origin of the enriched N_2O-respiring bacteria in the digestate, we considered the possibility that these are indigenous wastewater-sludge bacteria that survive the passage through the anaerobic digester, which had a retention time of 20-24 days. We assessed survival of N_2O-respiring bacteria by comparing the N_2O reduction potential of wastewater sludge and the digestate. The results indicated that ≤ 1/3 of the N_2O-respiring bacteria in the sludge survived the passage (**Figure S6**). We also did enrichment culturing with a digestate from a thermophilic digester (52 ^{o}C) operated in parallel with the mesophilic digester (provided with the same feed), and found that it too contained N_2O reducers that could be enriched, although the estimated initial numbers were orders of magnitude lower than in the mesophilic digestate **(Figure S7)**.

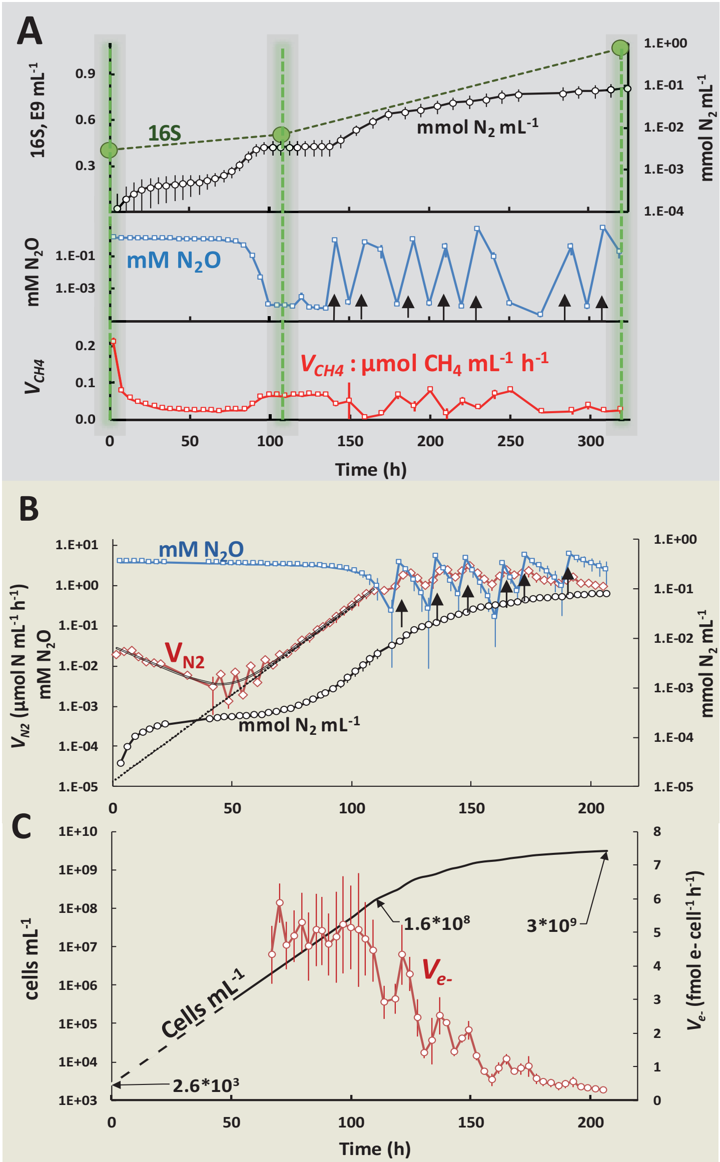

Figure 2: **Gas kinetics in anaerobic enrichment cultures with digestate.**

Panel A shows results for the enrichment culture (triplicate culture vials) sampled for metagenomics, metaproteomics, quantification of volatile fatty acids (VFAs) and 16S rDNA abundance (sampling times = 0, 115 and 325 hours, marked by vertical green lines). The top panel shows the amounts of N_2 produced (mmol N_2 L^{-1} digestate, log scale) and 16S rDNA copy numbers. The mid panel shows the concentration of N_2O in the digestate (log scale), which was replenished by repeated injections from t=140 h and onwards (indicated by black arrows). The bottom panel shows the rate of methane production. Standard deviations (n=3) are shown as vertical lines in all panels.

Panel B and C show the results of a repeated enrichment experiment where N_2O-depletion (as seen at t=100-140 h in panel A) was avoided, to allow more precise assessment and modelling of growth kinetics. Panel B: N_2O concentration in the digestate (mM N_2O), rate of N_2-production (V_{N2}) and N_2 produced (mmol N_2 mL^{-1} digestate), all log scaled. The curved black line shows the modelled V_{N2} assuming two populations, one growing exponentially (μ = 0.1 h^{-1}), and one whose activity was dying out gradually (rate = -0.03 h^{-1}). The dotted black line is the activity of the exponentially growing population extrapolated to time=0. Panel C shows the modelled density (cells mL^{-1}) of cells growing by N_2O respiration, extrapolated back to t=0 h (dashed line), and the cell specific respiratory activity (V_{e-}, fmol electrons $cell^{-1}$ h^{-1}), which declined gradually after 110 h. Standard deviations (n = 3) are shown as vertical lines. **Figure S1** provides additional data for the experiment depicted in Panel A, as well as a detailed description of the modelling procedures and their results.

MAG-centric metaproteomic analysis of the enrichment cultures

We analyzed the metagenome and metaproteome at three timepoints (0, 115 and 325 h, **Figure 2A**), to explore the effect of the anaerobic incubation with N_2O on the entire microbial consortium, and to identify the organisms growing by N_2O reduction. Metagenomic sequences were assembled and resultant contigs assigned to 278 metagenome-assembled genomes (MAGs), of which 149 were deemed to be of sufficient quality (completeness > 50% and contamination < 20%, Supplementary Data S1) for downstream analysis. The phylogenetic relationship and the relative abundance of the MAGs throughout the enrichment are summarized in **Figure 3**, which also shows selected features revealed by the combined metagenomic and metaproteomic analyses, including information about genes and detected proteins involved in N_2O reduction, other denitrification steps, methanogenesis, syntrophic acetate oxidation and methane oxidation.

Closer inspections of the abundance of individual MAGs, based on their coverage in the metagenome and metaproteome, showed that the majority of the MAGs had a near constant population density throughout the incubation, while two MAGs (260 and 268) increased substantially (**Figure 4**; further analyses in **Supplementary Section B, Figures S8-S11**). The stable abundance of the majority indicates that the methanogenic consortium remained intact despite the downshift in temperature (20 °C versus 37 °C) and the inhibition of methanogenesis by N_2O. Only 9 MAGs showed a consistent decline in abundance throughout the enrichment (**Table S1**). These MAGs could theoretically correspond to microbes whose metabolism is dependent on efficient H_2 scavenging by methanogens (Schink 1997), but we found no genomic evidence for this, and surmise that organisms circumscribed by the declining MAGs were unable to adapt to the temperature downshift from 37 °C to 20 °C.

Six MAGs, including the two that were clearly growing (MAG260 & MAG268) contained the *nosZ* gene and thus had the genetic potential to produce N_2O-reductase (Nos) (**Figure 4**). Nos proteins originating from five of these MAGs were detected in the metaproteome. Importantly, while all but one of these MAGs contained genes encoding the other denitrification reductases, none of these were detected in the metaproteome, suggesting that the organisms can regulate the expression of their denitrification machinery to suit available electron acceptors, in this case N_2O. Three of the MAGs with detectable Nos in the proteome (MAG004, MAG059, MAG248) appeared to be non-growing during the enrichment. The detected levels of their Nos proteins remained more or less constant, and their estimated abundance in the metagenome and -proteome did not increase (**Figure 4B**). It is conceivable that these three MAGs belong to the initial population of N_2O reducers whose N_2O-reduction activity was present initially but gradually decreased during the early phase of the enrichment (**Figure 2A**). The two growing MAGs (MAG260 and MAG268) showed increasing Nos levels and increasing abundance both in terms of coverage and metaproteomic detection (**Figure 4B**), in proportion with the N_2 produced (**Figure S11**). MAG260 reached the highest abundance of the two and accounted for 92% of the total detectable Nos pool at the final time point. MAG260 is taxonomically most closely affiliated with the genus *Dechloromonas* (GTDB, 97.9% amino acid similarity). Interestingly, Nap rather than Nar takes the role of nitrate reductase in MAG260 (**Figure 4**), which makes it a promising organism for N_2O mitigation since organisms with Nap only (lacking Nar) preferentially channel electrons to N_2O rather than to NO_3^- (Mania et al 2020). MAG260, MAG004 and MAG088 contain a clade II *nosZ*, characterized by a *sec*-dependent signal peptide, in contrast to the more common *tat*-dependent clade I *nosZ*. The physiological implications of clade I versus clade II *nosZ* remains unclear. Organisms with *nosZ* Clade II have high growth yield and high affinity (low k_s) for N_2O, compared to thise with *nosZ* Clade II (Yoon et al 2016), suggesting a key role of *nosZ* Clade II organisms for N_2O reduction in soil, but this was contested by Conthe et al (2018), who found that Clade I organisms had higher "catalytic efficiency" (V_{max}/k_s) than those with Clade II.

The apparent inhibition of methanogenesis by N_2O seen in the present study has been observed frequently (Andalib et al 2011) and is probably due to inhibition of coenzyme M methyltransferase (Kengen et al 1988), which is a membrane bound enzyme essential for methanogenesis and common to all methanogenic archaea (Fischer et al 1992). The gas kinetics demonstrate that the inhibition of was reversible, being partly restored whenever N_2O was depleted (**Figure 2**). In the enrichment culture where metagenomics and metaproteomics was monitored, several such incidents of N_2O depletion occurred (**Figure 2A**) and during these periods CH_4 accumulated to levels amounting to 10% of levels in control vials without N_2O (**Figure S4B**). These observations suggest that methanogens would be able to grow, albeit sporadically, during the enrichment, which is corroborated by the sustained detection of the complete methanogenesis pathway, including the crucial coenzyme M methyl-transferase, of *Methanothrix* (MAG025), *Methanoregulaceae* (MAG014) and *Methanobacterium* (MAG124) at high levels in the metaproteome. In fact, both MAG coverage data and 16S rDNA copy numbers assessed by ddPCR suggested that the majority of the original methanogenic consortium continued to grow (**Supplementary Section B**). A tentative map of the metabolic flow of the methanogenic consortium, including the reaping of intermediates (monosaccharides, fatty acids, acetate and H_2) by N_2O-respiring bacteria is shown in **Figure S12.** Since methane production was inhibited from the very beginning of the incubation, while it took ~100 hours for the N_2O-respiring bacteria to reach high enough numbers to become a significant sink for intermediates (**Figure 2**), one would expect transient accumulation of volatile fatty acids and H_2, which was corroborated by measurements of these metabolites (**Figure S13**).

Of note, we detected methane monooxygenase and methanol dehydrogenase proteins from MAG087 and MAG059, respectively, in the metaproteome. This opens up the tantalizing hypothesis of N_2O-driven methane oxidation, a process only recently suggested to occur (Valenzuela et al 2020; Cheng et al 2019). However, a close inspection of the N_2O- and CH_4-kinetics indicated that N_2O-driven methane oxidation played a minor role (**Figure S4CD**).

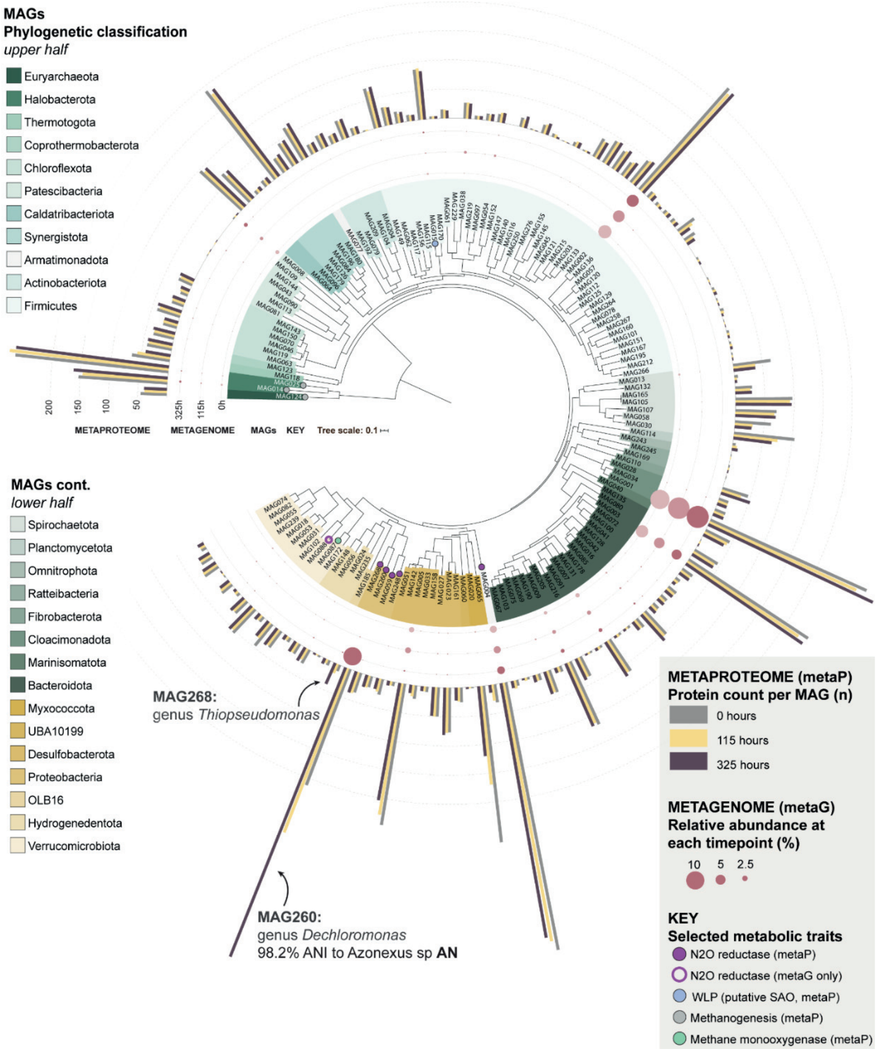

Figure 3: MAGs from the anaerobic enrichment culture with the mesophilic digestate. The figure shows a maximum likelihood tree indicating the phylogenetic placement of MAGs from the anaerobic enrichment. The tree was constructed from a concatenated set of protein sequences of single-copy genes. Taxonomic classification of the MAGs was inferred using the Genome Taxonomy Database (GTDB) and is displayed at the phylum level by label and branch coloring. Branch label decorations indicate the presence of genes involved in selected metabolic traits in the MAGs. The relative abundance of the MAG in the community as calculated from sequence coverage is indicated by bubbles at branch tips and bar charts indicate the number of detected proteins affiliated with each MAG at the three time points during incubation. Four of the 149 MAGs that met the completeness and contamination threshold for construction of the metaproteome database were lacking the universal single-copy marker genes and were omitted from the tree. Total protein counts per MAG were calculated by aggregating both secretome and cell-associated proteomes.

<u>Isolation of N_2O-respiring bacteria and their geno- and phenotyping</u>

Whilst this enrichment culture could be used directly as a soil amendment, this approach is likely to have several disadvantages. First, it would require the use of large volumes of N_2O

for enrichment, a process which would be costly and require significant infrastructure. An alternative approach would be to introduce an axenic or mixed culture of digestate-derived, and likely digestate-adapted, N_2O-respiring bacteria to sterilized/sanitized digestates. This approach has multiple benefits: 1) it would remove the need for N_2O enrichment on site as isolates could be grown aerobically in the digestate material, 2) one could chose organisms with favorable denitrification genotypes and regulatory phenotypes, 3) the sanitation would eliminate the methanogenic consortium hence reducing the risk of methane emissions from anoxic micro-niches in the amended soil, and 4) sanitation of digestates aligns with current practices that require such a pretreatment prior to use for fertilization. For these reasons an isolation effort was undertaken to obtain suitable digestate-adapted N_2O-respiring microorganisms from the N_2O-enrichment cultures. These efforts resulted in the recovery of three axenic N_2O-respiring bacterial cultures, which were subjected to subsequent genomic and phenotypic characterization.

The isolates were phylogenetically assigned to *Pseudomonas* sp. (**PS**), *Azospira* sp. **(AS)** and *Azonexus* sp. (**AN**) (working names in bold) based on full length 16S rDNA obtained from the sequenced genomes (accessions ERR4842639 - 40, **Table S2**, phylogenetic trees shown in **Figure S14**). All were equipped with genes for a complete denitrification pathway (**Figure 4C**). **AN** and **AS** carried *napAB*, encoding the periplasmic nitrate reductase (Nap) and *nosZ* clade II, whilst **PS** carried genes for the membrane bound nitrate reductase (Nar), encoded by *narG*, and *nosZ* clade I. All had *nirS* and *norBC*, coding for nitrite reductase (NirS) and and nitric oxide reductase (Nor), respeictivey. Pairwise comparison of average nucleotide identities (ANI) with MAGs from the enrichment metagenomes showed that the isolate **AN** matched the *Dechloromonas*-affiliated MAG260 with 98.2 % ANI, suggesting the isolate is circumscribed by MAG260 (Richter and Resselló-Móra 2009). Given the GTDB phylogeny of **AN** and MAG260 and the 16S rDNA gene homology of **AN** (95.2 % sequence identity to *Azonexus hydrophilus* DSM23864, **Fig S14C**), we conclude that **AN** likely represents a novel species within the *Azonexus* lineage. Unfortunately, the 16S rDNA gene was not recovered in MAG260, preventing direct comparison with related populations. No significant ANI matches in our MAG inventory were identified for the genomes of **PS** and **AS.**

The carbon catabolism profiles of the isolates were assayed using Biolog^{TM} PM1 and PM2 microplates, to screen the range of carbon sources utilized (**Supplementary Section E)**. **PS** utilized a wide spectrum of carbon sources (amino acids, nucleic acids, volatile fatty acids (VFA), alcohols, sugar alcohols, monosaccharides and amino sugars), but only one polymer (laminarin). **AN** and **AS** could only utilize small VFAs (*eg*. acetate, butyrate), intermediates in the TCA cycle and/or the β-oxidation/methyl malonyl-CoA pathways of fatty acid degradation (*eg*. malate, fumarate, succinate), and a single amino acid (glutamate). Thus, all three would be able to grow in a live digestate by reaping the VFA's produced by the methanogenic consortium. While the utilization of VFAs as C-substrates is one of several options for **PS**, **AN** and **AS** appear to depend on the provision of VFAs. This was confirmed by attempts to grow the three isolates in an autoclaved digestate: while **PS** grew well and reached high cell densities without any provision of extra carbon sources, **AN** and **AS** showed early retardation of growth unless provided with an extra dose of suitable carbon source (glutamate, acetate, pyruvate or ethanol) (**Figure S25 and S26**). A high degree of specialization and metabolic streamlining may thus explain the observed dominance of **AN** (MAG260) during enrichment culturing.

To evaluate the potentials of these isolates to act as sinks for N_2O, we characterized their denitrification phenotypes, by monitoring kinetics of oxygen depletion, subsequent denitrification and transient accumulation of denitrification intermediates (NO_2^-, NO, N_2O). The experiments were designed to assess properties associated with strong N_2O reduction such as 1) *bet hedging*, i.e. that all cells express N_2O reductase while only a fraction of the cells express nitrite- and/or nitrate-reductase, as demonstrated for *Paracoccus denitrificans* (Lycus et al 2018); 2) strong metabolic preference for N_2O-reduction over NO_3^- -reduction, as demonstrated for organisms with periplasmic nitrate reductase (Mania et al 2020). **Supplementary section F** provides the results of all the experiments and a synopsis of the findings. In short: *Azonexus* sp. (**AN**) had a clear preference for N_2O over NO_3^- reduction, but not over NO_2^- reduction, ascribed to *bet hedging* with respect to the expression of nitrate reductase (a few cells express Nap, while all cells express Nos), which was corroborated by proteomics: the Nos/Nap abundance ratio was ~25 during the initial phase of denitrification (**Figure S17**). *Azospira* sp. (**AS**) had a similar preference for N_2O over NO_3 reduction, albeit less pronounced than in **AN**, and no preference for N_2O over NO_2^-. *Pseudomonas* sp. (**PS**) showed a phenotype resembling that of *Paracoccus denitrificans* (Lycus et al 2018), with denitrification kinetics indicating that Nir is expressed in a minority of cells in response to O_2 depletion, while all cells appeared to express N_2O reductase. This regulation makes **PS** a more robust sink for N_2O than the two other isolates, since it kept N_2O extremely low even when provided with NO_2^-.

In summary, **PS** appeared to be the most robust candidate as a sink for N_2O in soil for two reasons; 1) it can utilize a wide range of carbon substrates, and 2) its N_2O sink strength is independent of the type of nitrogen oxyanion present (NO_2^- or NO_3^-). In contrast, **AN** and **AS** appear to be streamlined for harvesting intermediates produced by anaerobic consortia, hence their metabolic activity in soil could be limited. In addition, they could be sources rather than sinks for N_2O if provided with NO_2^-, which is likely to happen in soils, at least in soils of neutral pH, during hypoxic/anoxic spells (Lim et al 2018).

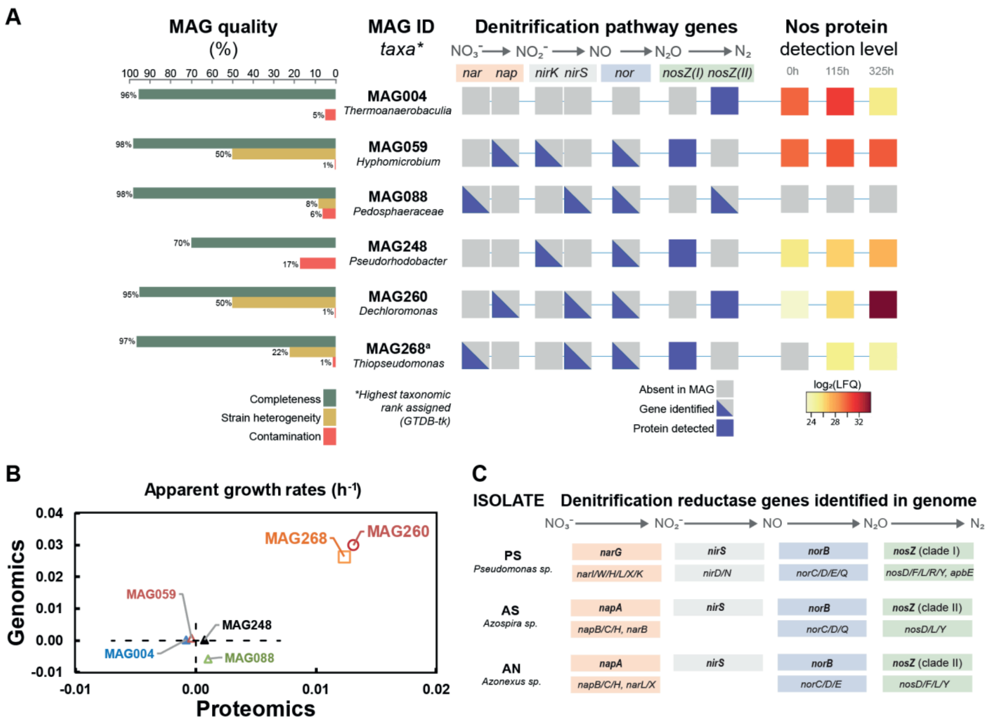

Figure 4: Overview of MAGs with *nosZ* and denitrification genes in isolated organisms. Panel A shows the quality (completeness, strain heterogeneity and contamination), taxonomic classification based on GTDB and NCBI, presence of denitrifying genes and proteins, and the detected levels of Nos (N_2O reductase, encoded by *nosZ*) throughout the enrichment culturing for the six MAGs containing the *nosZ* gene (**Supplementary Data S1** and **S2**). Nos was detected in the proteome of five MAGs, but the detection level increased significantly throughout for only MAG260 and 248, respectively. None of the MAGs produced detectable amounts of the other denitrification reductases. [a)] LFQ values for one of the two detected predicted Nos proteins for MAG268 is shown. Panel B shows the apparent growth rates of the MAGs, based on their coverage in the metagenome and metaproteome (regression of ln(N) against time; see **Figure S11** for more details). Panel C shows the taxonomic classification (16S rDNA), working names (abbreviations) and denitrification genotypes of three isolates from the enrichment culturing. The genes coding catalytic subunits of denitrification reductases are shown in bold, above the accessory genes (Vaccaro et al 2016) that were also identified. More information about accessory genes is presented in **Figure S14**. The isolate **AN** has 98.2 % ANI to MAG260.

Effects on N_2O emissions

To assess if fertilization with digestates containing N_2O-reducing bacteria could reduce N_2O emissions from denitrification in soil, we conducted a series of incubation experiments with soils fertilized with digestates with and without N_2O-reducing bacteria. The fertilized soils were incubated in closed culture vials containing He + 0.5 vol % O_2, and O_2, NO, N_2O and N_2 were monitored during oxygen depletion and anaerobic growth. The experiments included soils amended with digestates in which indigenous N_2O-reducing bacteria had been enriched by anaerobic incubation with N_2O (**Figure 2**), as well as autoclaved digestates in which the isolates from the current study had been grown by aerobic cultivation (see **Figures S25** & **S26** for cultivation details). The experiments included two types of control digestates: Live digestate (directly from the digester), and live digestate heated to 70 ^{o}C for 2 hours (to eliminate most of the indigenous consortium). In all cases, 3 mL of digestate was added to 10 g of soil. Since soil acidity has a pervasive effect on the synthesis of functional N_2O reductase (Liu et al 2014), we tested the digestates with two soils from a liming experiment (Nadeem et al 2020) with different pH (pH_{CaCl2} = 5.5 and 6.6).

The transient N_2O accumulation during denitrification was generally higher in the acid than in the near-neutral soil (**Figure 5**), which was expected since the synthesis of functional Nos is hampered by low pH (Bergaust et al 2010, Liu et al 2014). Based on the kinetics of both N_2 and N_2O (see **Figure S27 and S28**), we calculated the N_2O-index ($\boldsymbol{I_{N2O}}$) which is a measure of the molar amounts of N_2O relative to N_2+N_2O in the headspace for a specific period (0-T), see equation at top of **Figure 5**). Low values of $\boldsymbol{I_{N2O}}$ indicate efficient N_2O-reduction. In this case, we calculated $\boldsymbol{I_{N2O}}$ for the incubation period until 40% of the available NO_3^- had been recovered as N_2+N_2O (=$\boldsymbol{I_{N2O\ 40}}$) and for the incubation period until 100% was recovered ($\boldsymbol{I_{N2O\ 100}}$).

Extremely low $\boldsymbol{I_{N2O}}$ values were recorded for the treatments with digestate in which N_2O-reducing bacteria were enriched by anaerobic incubation with N_2O, even in the acid soil. This is in line with the current understanding of how pH affects N_2O-reduction: low pH slows down the synthesis of functional Nos, but once synthesized, it remains functional even at low pH (Bergaust et al 2010). Functional Nos had already been expressed during the enrichment and was evidently active after amendment to the soils.

$\boldsymbol{I_{N2O}}$ values were generally high for treatment with live digestate, which probably reflects that the digestate is dominated by N_2O-producing organisms (**Figure S5E**). This interpretation is corroborated by the observed effect of heat-treating the live digestate; this lowered $\boldsymbol{I_{N2O}}$ substantially.

The presence of the isolates in the digestates had clear but variable effects on $\boldsymbol{I_{N2O}}$. Compared to the heat treated digestate ("70 C dig" Fig 5), **AN** and **AS** increased the $\boldsymbol{I_{N2O}}$-values in the soil with pH=5.5, while in the soil with pH 6.6, their effect was marginal. The high $\boldsymbol{I_{N2O}}$ for **AN** and **AS** in the acid soil plausibly reflect that the isolates were grown aerobically in the digestate, hence synthesizing their denitrification enzymes after transfer to soil, which would be hampered by low pH. In contrast to AN and AS, **PS** resulted in very low $\boldsymbol{I_{N2O}}$ values in both soils, suggesting that this organism has an exceptional capacity to synthesize functional Nos at low pH.

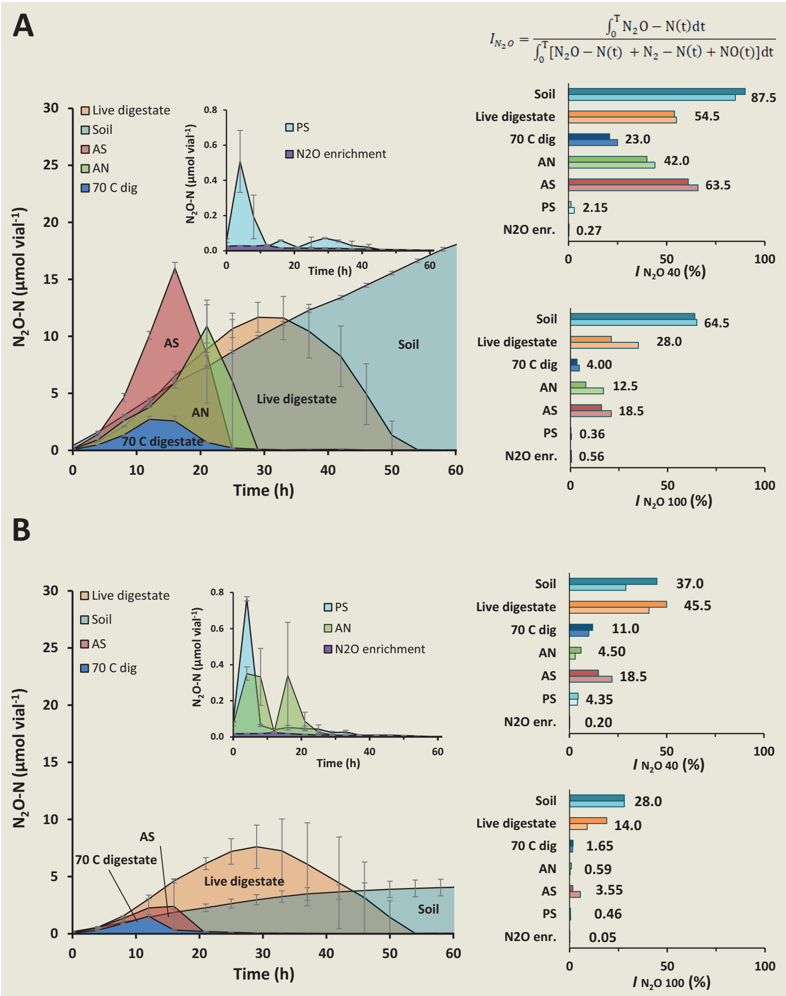

Figure 5: Soil incubations. N_2O kinetics during incubation of soils amended with six different digestates and a control sample (soil only). Panel A shows results for the pH 5.5 soil, while panel B the pH 6.6 soil. The digestates treatments are: "Live digestate", digestate directly from the anaerobic digester; "70 C dig", live digestate heat treated to 70 °C for two hours; AN, AS and PS: autoclaved digestate on which isolates AN, AS and PS had been grown aerobically (see Figure **S25&S26** for details on the cultivation); "N_2O enr"= digestate enriched with N_2O-respiring bacteria (as in **Fig 2**). The left panels show the N_2O levels observed during each treatment; the insets, with altered scaling, show N_2O levels for treatments that resulted in very low N_2O levels (the PS and N_2O enr. treatments). The bar graphs to the right show the N_2O indexes ($\boldsymbol{I_{N2O}}$**,** bar height = single culture vial values, numerical value = average of duplicate culture vials), which are calculated by dividing the area under the N_2O-curve by the sum of the areas under the N_2O and N_2-curve, expressed as % (see equation in the figure and Liu et al 2014; the N_2 curves are provided in **Figures S27&S28**). $\boldsymbol{I_{N2O}}$ have proven to be a robust proxy for potential N_2O emission from soil (Russenes et al 2016). Two $\boldsymbol{I_{N2O}}$ values are shown: one for the timespan until 40% of the NO_3^--N was recovered as N_2+N_2O+NO ($\mathbf{I_{N2O\ 40\%}}$), and one for 100% recovery ($\mathbf{I_{N2O\ 100\%}}$). More details (including N_2 and NO kinetics) are shown in **Figure S27 and S28.**

These results show that the emission of N_2O from soil fertilized with digestates can be manipulated by tailoring the digestate microbiome. Interestingly, measurements of methane in these soil incubations showed that the methanogenic consortia in digestates that had not been heat treated (i.e. the live digestate and the N_2O enrichment) remained metabolically intact in the soil, and started producing methane as soon as N_2O and nitrogen oxyanions had been depleted, while no methane was produced in the soils amended with autoclaved digestate, and that heated to 70 ^{o}C (**Figure S29**).

In an effort to determine the survival of the N_2O-scavenging capacity of a digestate enriched with N_2O reducers, we also tested its effect on soil N_2O emissions after a 70-hour aerobic storage period (in soil or as enrichment culture, at 20 °C). These experiments demonstrated a sustained beneficial effect on $\boldsymbol{I_{N2O}}$ after 70 hours of aerobic storage (**Figure S30**). This result indicates that the enrichment strategies discussed here are robust, although long-lasting storage experiments as well as field trials are needed.

Concluding remarks

This feasibility study identifies an avenue for large scale cultivation of N_2O reducers for soil application, which could be low cost if implemented as an add-on to biogas production systems. Further efforts should be directed towards selecting organisms that are both strong sinks for N_2O and able to survive and compete in soil, to secure long-lasting effects on N_2O emissions. A tantalizing added value would be provided by selecting organisms (or consortia of organisms) that are not only strong N_2O-sinks, but also promote plant growth and disease resistance (Gao et al 2016, 2017).

Gas kinetics, metagenomics and metaproteomics revealed that the methanogenic consortium of the digestate remains active during anaerobic incubation with N_2O, and that bacteria with an anaerobic respiratory metabolism grew by harvesting fermentation intermediates. The inhibition of methanogenesis by N_2O implies that the respiring organisms would have immediate access to the electron donors that would otherwise be used by the methanogens, i.e. acetate and $H_{2,}$ while they would have to compete with fermentative organisms for the “earlier” intermediates such as alcohols and VFA. The importance of fermentation intermediates as a carbon source for the N_2O-respiring bacteria would predict a selective advantage for organisms with a streamlined (narrow) catabolic capacity, i.e. limited to short fatty acids, and our results lend some support to this: the catabolic capacity of the organism that became dominant (MAG260, isolate **AN**) was indeed limited, as was also the case for isolate **AS**. Such organisms are probably not ideal N_2O-sinks in soil because their ability to survive in this environment would be limited. Organisms with a wider catabolic capacity, such as the isolated *Pseudomonas* sp. (**PS**), are stronger candidates for long term survival and N_2O-reducing activity in soil. The ideal organisms are probably yet to be found, however, and refinements of the enrichment culturing process are clearly needed.

The digestate used in this study contained N_2O-respiring bacteria, most likely survivors from the raw sludge, which however, were clearly outnumbered by bacteria that are net producers of N_2O. We surmise that the relative amounts of N_2O-producers and N_2O-reducers in digestates may vary, depending on the feeding material and configuration for the anaerobic digestion. This could explain the observed large variation of digestates on N_2O emission from soils (Baral et al 2017, Herrero et al 2016). The high abundance of both NO_3^- - and O_2-respiring organisms in digestates has practical implications for the attempts to grow isolated strains in digestates: they could be outnumbered by the indigenous NO_3^- - and O_2-respiring organisms (**Figure S5**). Hence, we foresee that future implementation of this strategy will require a brief heat treatment or other sanitizing procedure. A bonus of such sanitation is that it eliminates methane production by the digestate in soil.

We failed to enrich organisms lacking all other denitrification genes than *nosZ*; the only reconstructed genome with *nosZ* only (**MAG004**) did not grow at all. Failure to selectively enrich such organisms by anaerobic incubation with N_2O was also experienced by Conthe et al (2018). The organisms that did grow by respiring N_2O in our enrichment, were all equipped with genes for the full denitrification pathway, although the only denitrification enzyme expressed/detected during the enrichment was Nos. This agrees with the current understanding of the gene regulatory network of denitrification; *nosZ* is the only gene whose transcription does not depend on the presence of NO_3^-, NO_2^- or NO (Spiro 2016), which were all absent during the enrichment.

Two of the reconstructed MAGs had periplasmic nitrate reductase (*nap*), as was the case for two of the three isolates (AN and AS). This in itself would predict preference for N_2O- over NO_3^- reduction at a metabolic level (Mania et al 2020), but otherwise their potential for being N_2O sinks cannot be predicted by their genomes. The phenotyping of the isolates revealed conspicuous patterns of *bet hedging* as demonstrated for *Paracoccus denitricans* (Lycus et al 2018). The *bet hedging* in *P. denitrificans* is characterized by expression of Nir (and Nor) in a minority of the cells, while Nos is expressed in all cells, in response to oxygen depletion, hence the population as a whole is a strong sink for N_2O. The isolated *Pseudomonas* sp. (PS) displayed denitrification kinetics that closely resembles that of *P. denitrificans*. The two other isolates (**AN** and **AS**) showed indications of *bet hedging* as well, but of another sort: Nap appears to be expressed in a minority of the cells. This different regulatory phenotype had clear implications for the ability of organisms to function as N_2O-sinks: while all isolates were strong N_2O sinks when provided with NO_3^- only, **AN** and **AS** accumulated large amounts of N_2O if provided with NO_2^-.

The N_2O sink capacity of the organisms was tested by fertilizing soils with digestates with and without the organisms, and monitoring the gas kinetics in response to oxygen depletion, thus imitating the hot spots/hot moments of hypoxia/anoxia induced by digestates in soil (Kuzyakov and Blagodatskaya 2015). Since the isolates were raised by aerobic growth in autoclaved digestates, they would have to synthesize all denitrification enzymes in the soil, hence the synthesis of functional Nos was expected to be hampered by low pH (Liu et al 2014). The results for isolates **AS** and **AN** lend support to this (high $\boldsymbol{I_{N2O}}$ in the soil with pH=5.5). **AN** was also dominating in the digestate enrichment culture, and in this case the organism had a strong and pH-independent effect on N_2O emission, plausibly due synthesis of Nos prior to incorporation into the soils.

In summary, we have demonstrated that a digestate from biogas production can be transformed into an effective agent for mitigating N_2O emission from soil, simply by allowing the right bacteria to grow to high cell densities in the digestate prior to fertilization. The technique is attractive because it can be integrated in existing biogas production systems, and hence is scalable. If we manage to treat a major part of waste materials in agroecosystems by AD, the resulting digestates would suffice to treat a large share of total farmland, as illustrated by **Figure 1**. Estimation of the potential N_2O-mitigation effect is premature, but the documented feasibility and the scalability of the approach warrant further refinement as well as rigorous testing under field condition. Our approach suggests one avenue for a much needed valorization of organic wastes (Peng and Pivato 2019) via anaerobic digestion. Future developments of this approach could extend beyond the scope of climate change mitigation and include the enrichment of microbes for pesticide- and other organic pollutant degradation (Sun et al 2018), plant growth promotion (Backer et al 2018) and inoculation of other plant symbiotic bacteria (Poole et al 2018).

References

Andalib M, Nakhla E, McIntee, Zhu J (2011) Simultaneous denitrification and methanogenesis (SDM): Review of two decades of research. Desalination 279:1-14. DOI:10.1016/j.desal.2011.06.018

Bakken LR, Frostegård Å (2020) Emerging options for mitigating N2O emissions from food production by manipulating the soil microbiota. Current Opinion in Environmental Sustainability 47:89-94. https://doi.org/10.1016/j.cosust.2020.08.010

Backer R, Rokem JS, Ilangumaran G, Lamont J, Praslikova D, Ricci E, Subramnian S, Smith DL (2018) Plant growth-promoting rhizobacteria: context, mechanisms of action, and roadmap to commercialization of biostimulants for sustainable agriculture, Front. Plant Sci. 9:1473. doi: 10.3389/fpls.2018.01473

Baral KR, Labouriau R, Olesen J, Petersen SO (2017) Nitrous oxide emissions and nitrogen use efficiency of manure and digestates applied to spring barley. Agriculture Ecosystems & Environment 239:188-198. DOI:10.1016/j.agee.2017.01.012

Bergaust L, Mao Y, Bakken LR, Frostegård Å (2010) Denitrification response patterns during the transition to anoxic respiration and posttranscriptional effects of suboptimal pH on nitrogen oxide reductase in *Paracoccus denitrificans*. Applied and Environmental Microbiology 76:6387-6396. DOI:10.1128/AEM.00608-10

Butterbach-Bahl K, Baggs EM, Dannenmann M, Kiese R, Zechmeister-Boltenstern S (2013) Nitrous oxide emissions from soils: how well do we understand the processes and their controls? Philosophical Transactions of the Royal Society B 368:20130122. DOI:10.1098/rstb.2013.0122

Cheng C, Shen X, Xie, H, Hu Z, Pavlostathis SG, Zhang J (2019) Coupled methane and nitrous oxide biotransformation in freshwater wetland sediment microcosms. Science of the Total Environment 648:916-922. DOI:10.1016/j.scitotenv.2018.08.185

Conthe M, Wittorf L, Kuenen JG, Kleerebezem R, van Loosdrecht MCM, Hallin S (2018) Life on N_2O: deciphering the ecophysiology of N_2O respiring bacterial communities in a continuous culture. The ISME Journal 12:1142–1153. DOI:10.1038/s41396-018-0063-7

D'Hondt K, Kostic R, McDowell R, Eudes F Singh BK, Sarkar S, Markakis B, Schelkle B, Maguin E, Sessitsch A (2021) Microbiome innovations for a sustainable future. Nature Microbiology 6:138-142. doi.org/10.1038/s41564-020-00857-w

Domeignoz-Horta LA, Putz M, Spor A, Bru D, Breuil MC, Hallin S, Philippot L (2016) Non-denitrifying nitrous oxide reducing bacteria – an effective N_2O sink in soil. Soil Biology and Biochemistry 103:376-379. DOI:10.1016/j.soilbio.2016.09.010

Erisman JW, Sutton MA, Galloway J, Klimont Z, Winiwarter W (2008) How a century of ammonia synthesis changed the world. Nature Geoscience 1:636-639.

Eurostat (2017) Agri-environmental indicator – greenhouse gas emissions. ISSN 2443-8219, https://ec.europa.eu/eurostat/statistics-explained/pdfscache/16817.pdf

Fischer R, Gärtner P, Yeliseev A, Thauer RK (1992) N^5-Methyltetrahydromethanopterin: coenzyme M methyltransferase in methanogenic archaebacteria is a membrane protein. Archives of Microbiology 158:208-217. DOI:10.1007/BF00290817

Foged HL, Flotats X, Blasi AB, Palatsi J, Magri A, Schelde KM (2011) Inventory of manure processing activities in Europe. Technical report No. I concerning “Manure Processing Activities in Europe” to the European Commission, Directorate-General Environment. 138.

Gao N, Shen WS, Kakuta H, Tanaka N, Fujiwara T, Nishizawa T, Takaya N, Nagamine T, Isobe K, Otsuka S, Senoo K (2016) Inoculation with nitrous oxide (N_2O)-reducing denitrifier strains simultaneously mitigates N_2O emission from pasture soil and promotes growth of pasture plants. Soil Biology and Biochemistry 97:83–91. DOI:10.1016/j.soilbio.2016.03.004

Gao N, Shen W, Camargo E, Shiratori Y, Nishizawa T, Isobe K, He X, Senoo K (2017) Nitrous oxide (N_2O)-reducing denitrifier-inoculated organic fertilizer mitigates N_2O emissions from agricultural soils. Biology and Fertility of Soils 53:885–898. DOI:10.1007/s00374-017-1231-z

Hallin S, Philippot L, Löffler RA, Jones CM (2018) Genomics and ecology of novel N_2O-reducing microorganisms. Trends in Microbiology 26:43-55. DOI:10.1016/j.tim.2017.07.003

Herrero M. Henderson B, Havlik P, Thornton PK, Conant RT, Smith P, Wirsenius S, Hristov AN, Gerber P, Gill M, Butterbach-Bahl K, Valin H, Garnett T, Stehfest E (2016) Greenhouse gas mitigation potential in the livestock sector. Nature Climate Change 6:452-461. DOI:10.1038/nclimate2925

Holm-Nielsen JB, Al-Seadi T, Oleskowicz-Popiel P (2009) The future of anaerobic digestion and biogas utilization. Bioresource Technology 100:5478–5484. DOI:10.1016/j.biortech.2008.12.046

Hu HW, Chen D, He JZ (2015) Microbial regulation of terrestrial nitrous oxide formation: understanding the biological pathways for prediction of emission rates. FEMS Microbiology Reviews 39:729-749. DOI:10.1093/femsre/fuv021

Kengen SWM, Mosterd JJ, Nelissen, RLH (1988) Reductive activation of the methyl-tetrahydromethanotering: coenzyme M methyl transferase from *Methanobacterium thermoautotrophicum* strain ΔH. Archives of Microbiology 150:405-412. DOI:10.1007/BF00408315

Kuzyakov Y, Blagodatskaya E (2015) Microbial hotspots and hot moments in soil: Concept & review. Soil Biology and Biochemistry 83:184-199. DOI:10.1016/j.soilbio.2015.01.025

Liu B, Frostegård Å, Bakken LR (2014) Impaired Reduction of N_2O to N_2 in acid soils is due to a posttranscriptional interference with the expression of *nosZ.* mBio 5:e01383-14. DOI:10.1128/mBio.01383-14.

Lim YN, Frostegård Å, Bakken LR (2018) Nitrite kinetics during anoxia: The role of abiotic reactions versus microbial reduction. Soil Biology and Biochemistry 119:203–209. DOI:10.1016/j.soilbio.2018.01.006

Lu H, Chandran K, Stensel D (2014) Microbial ecology of denitrification in biological wastewater treatment. Water Research 64:237-254. DOI:10.1016/j.watres.2014.06.042

Lycus P, Bøthun KL, Bergaust L, Shapleigh JP, Bakken LR, Frostegård Å (2017) Phenotypic and genotypic richness of denitrifiers revealed by a novel isolation strategy. The ISME Journal 11:2219-2232. DOI:10.1038/ismej.2017.82

Lycus P, Soriana-Laguna, Kjos M, Richardson DJ, Gates AJ, Milligan DA, Frostegård Å, Bergaust L, Bakken LR (2018) A bet-hedging strategy for denitrifying bacteria curtails their release of N_2O. Proceedings of the National Academy of Sciences USA 115:11820-11825. DOI:10.1073/pnas.1805000115

Molstad L, Dörsch P, Bakken LR (2007) Robotized incubation system for monitoring gases (O_2, NO, N_2O, N_2) in denitrifying cultures. Journal of Microbiological Methods 71:202-211. DOI:10.1016/j.mimet.2007.08.011

Molstad L, Dörsch P, Bakken LR (2016) Improved robotized incubation system for gas kinetics in batch cultures. Researchgate. DOI:10.13140/RG.2.2.30688.07680

Mania D, Wolily K, Degefu T, Frostegård Å (2020) A common mechanism for efficient N_2O reduction in diverse isolates of nodule-forming bradyrhizobia. Environmental Microbiology 22:17-31. DOI:10.1111/1462-2920.14731

Meyer A, Ehimen E, Holm-Nielsen J (2018) Future European biogas: Animal manure, straw and grass potentials for a sustainable European biogas production. Biomass and Energy 111:154-164. DOI:10.1016/j.biombioe.2017.05.013

Nadeem S, Bakken LR, Frostegård Å, Gaby JC, Dörsch P (2020) Contingent effects of liming on N_2O-emissions driven by autotrophic nitrification. Frontiers in Environmental Science 8:598513. DOI:10.3389/fenvs.2020.598513

Peng W, Pivato A (2019) Sustainable Management of Digestate from the Organic Fraction of Municipal Solid Waste and Food Waste Under the Concepts of Back to Earth Alternatives and Circular Economy. Waste Biomass Valor (2019) 10:465–481. DOI 10.1007/s12649-017-0071-2

Poole P, Ramachandran V, Terpolilli J (2018) Rhizobia: from saprophytes to endosymbionts Nature Reviews Microbiology 16:291-303. doi:10.1038/nrmicro.2017.171

Qu Z, Bakken LR, Frostegård Å, Bergaust L (2016) Transcriptional and metabolic regulation of denitrification in *Paracoccus denitrificans* allows low but significant activity of nitrous oxide reductase under oxic conditions. Environmental Microbiology 18:2951-2963. DOI:10.1111/1462-2920.13128

Richter M, Rosselló-Móra R (2009) Shifting the genomic gold standard for the prokaryotic species definition. Proceedings of the National Academy of Sciences USA 106:19126-19131. DOI:10.1073/pnas.0906412106

Russenes AL, Korsæth A, Bakken LR, Dörsch P (2016) Spatial variation in soil pH controls off-season N_2O emission in an agricultural soil. Soil Biology and Biochemistry 99:36-46. DOI:10.1016/j.soilbio.2016.04.019

Sanford RA, Wagner DD, Wu Quingzhong, Chee-Sanford JC, Thomas SH, Cruz-Garzia C, Rodrigues G, Massol-Deya A, Krishnani KK, Ritalahti KM, Nissen S, Konstantinidis KT, Löffler FE (2013) Unexpected nondenitrifier nitrous oxide reductase gene diversity and abundance in soils. Proceedings of the National Academy of Sciences USA 109:19709-19714. DOI:10.1073/pnas.1211238109

Scarlat N, Dallemand JF, Fahl F (2018) Biogas: Developments and perspectives in Europe. Renewable Energy 129:457-472. DOI:10.1016/j.renene.2018.03.006

Shapleigh JP (2013) Denitrifying Prokaryotes. in: Rosenberg E, DeLong EF, Lory S, Stackebrandt E, Thompson F (editors). Prokaryotes - Prokaryotic Physiology and Biochemistry (Springer Berlin, Heidelberg, 405–425). DOI:10.1007/978-3-642-30141-4_71

Schink B (1997) Energetics of syntrophic cooperation in methanogenic degradation. Microbiology and Molecular Biology Reviews 61:262-280. DOI:1092-2172/97/$04.0010

Snyder CS, Davidson EA, Smith P, Venterea RT (2014) Agriculture: sustainable crop and animal production tohelp mitigate nitrous oxide emissions. Current Opinions in Environmental Sustainability 9-10:46-54.

Song X, Liu M, Ju X, Gao B, Su F, Chen X, Rees RM (2018) Nitrous oxide emissions increase exponentially when optimum nitrogen fertilizer rates are exceeded in the North China Plain. Environmental Science and Technology 52:12504−12513. DOI:10.1021/acs.est.8b03931

Sutton M, Erisman W, Leip A, vanGrinsven H, Winiwarter W (2011) Too much of a good thing. Nature 472: 159-161.

Spiro S (2016) Regulation of denitrification. (Chapter 13) in: Isabel M, José JGM, Sofia RP, Luisa BM (editors). RSC Metallobiology Series 9: Matalloenzymes in denitrification (Royal Society of Chemistry Cambridge, UK, 312-331). https://doi.org/10.1039/9781782623762-00312

Stams AJM, Elferink SJWHO, Westermann P (2003) Metabolic Interactions Between Methanogenic Consortia and Anaerobic Respiring Bacteria. in: Ahring BK (editors). Biomethanation I. Advances in Biochemical Engineering/Biotechnology, vol 81 (Springer Berlin, Heidelberg). DOI: 10.1007/3-540-45839-5_2

Stenmarck AA, Jensen C, Quested T, Moates G (2016) Estimates of European food waste levels, Report of the project FUSIONS (contract number: 311972) granted by the European Commission (FP7). DOI:10.13140/RG.2.1.4658.4721

Sun S, Sidhu V, Rong Y, Zheng Y (2018) Pesticide Pollution in Agricultural Soils and Sustainable Remediation Methods: a Review. Current Pollution Reports 4:240-250. doi.org/10.1007/s40726-018-0092-x

Tian H, et al (2020) A comprehensive quantification of global nitrous oxide sources and sinks. Nature 586:248-255. DOI:10.1038/s41586-020-2780-0

Valenzuela EI, Padilla-Loma C, Gómez-Hernández N, López-Lozano NE, Casas-Flores S, Cervantes FJ (2020) Humic substances mediate anaerobic methane oxidation linked to nitrous oxide reduction in wetland sediments. Frontiers in Microbiology 11:587. DOI:10.3389/fmicb.2020.00587

Vaccaro BJ, Thorgersen MP, Lancaster WA, Price MN, Wetmore KM, Poole FL, Deutschbauer A, Arkin AP, Adams MWW (2016) Determining roles of accessory genes in denitrification by mutant fitness analyses. Applied and Environmental Microbiology 82:51-61. DOI:10.1128/AEM.02602-15

Yoon S, Nissen S, Park D, Sanford RA. Löffler FE (2016) Nitrous oxide reduction kinetics distinguish bacteria harboring Clade I NosZ from those harboring Clade II NosZ. Applied and Environmental Microbiology 82:3793-3800. doi:10.1128/AEM.00409-16.

Zumft WG (1997) Cell biology and molecular basis of denitrification. Microbiology and Molecular Biology Reviews 61:533-616. DOI:1092-2172/97/$04.0010

Supplementary Methods

N_2O-respiring bacteria in biogas digestates for reduced agricultural emissions

Kjell Rune Jonassen, Live H Hagen, Silas HW Vick, Magnus Ø Arntzen, Vincent GH Eijsink, Åsa Frostegård, Pawel Lycus, Lars Molstad, Phillip B Pope, Lars R Bakken

Correspondence to: lars.bakken@nmbu.no

1. Digestates

The digestate material used in this study originated from mesophilic (37 ^oC) and thermophilic (52 ^oC) anaerobic digesters operated semi continuously and in parallel at a 750 000-person equivalent wastewater treatment plant (WWTP) (Oslo, Norway). The total individual reactor volume was 6 000 m^3 with a normal operation level of 5000 ± 300 m^3 of digestate. Mixing/stirring was maintained by intermittent recirculation of produced biogas (average 150 Nm^3/h) through lances releasing gas at the bottom of the reactor, and by continuous recirculation of digested sludge (216 – 432 m^3/h) from the bottom and back to the top. The substrate (raw sludge), top fed to the digesters, was a poly aluminum chloride (PAX-XL61™, Kemira) and ferric chloride (PIX318™, Kemira) precipitated municipal wastewater sludge, dewatered, by addition of 1.6 ± 0.5 kg ton^{-1} total solids cationic polyacrylamide based polymer flocculant (Zetag 7550®, Kemetyl) by decantation of free water through rotary drum filters, and buffered in a stirred holding tank (retention time ~24 hours) prior to anaerobic digestion. The total solids content (TS %) of the raw sludge was 7.1 ± 0.5 %, and loss of ignition (LOI, % of dry weight) was 79 ± 3 % (measured by the WWTP, given as yearly average). Yearly average operational parameters of the digesters were provided by the WWTP and are shown in Table 1.

Chemical and physical properties of the digestates, the slurry of anaerobically digested wastewater sludge, were analyzed in the NS-EN ISO/IEC 17025 accredited laboratory belonging to the WWTP. Total alkalinity, pH and total volatile fatty acid (VFA) concentration in the digestates were determined using a two-point titration procedure described in EN12176:1998. Total solids (TS %) and volatile solids (VS %) were determined according to EN15934 and EN15935, respectively. The sum of NH_3 and NH_4^+ was measured as described by Greenberg et al (1980), using a ThermoOrion Model 95-12 ammonia electrode. Instrument drifting and reproducibility were controlled by carrying out parallel measurements on reference materials.

Yearly average digestate characteristics were provided by the WWTP and are shown in Table 1 together with corresponding digestate and operational characteristics at the time of sampling for the digestate material used for enrichment culturing.

Table 1 Operational parameters for the mesophilic and the thermophilic anaerobic digesters and digestate characteristics at the time of sampling for enrichment culturing. Enrichment culturing was repeated several times with digestate from the mesophilic AD, each with freshly sampled digestate (Sampling 1-7).

	Digestate characteristics							**AD operational parameters**		
	pH	% dry weight [a]	LOI [b] (% of DW)	TAK [c] (meq L^{-1})	VFA [c] (meq L^{-1})	VFA/TAK	NH_3+NH_4^+ (mg-N L^{-1})	CH_4 prod. [d] rate (mmol L^{-1} h^{-1})	HRT [e] (d)	VS loading rate[f] (kgVS $m^{-3}d^{-1}$)
Mesophilic (WWTP average):	**7.6**	**3.84**	**54.2**	**185**	**16.1**	**0.087**	**1824**	**1.5**	**24.4**	**2.4**
Sample 1[g]	7.6	3.85	55.8	188	16.0	0.085	n.d.	1.48	17.2	3.3
Sample 2[g]	7.7	3.81	57.0	187	15.2	0.081	n.d.	1.55	22.0	2.4
Sample 3[g]	7.7	3.81	57.0	187	15.2	0.081	n.d.	1.55	22.0	2.4
Sample 4[g]	7.8	3.79	58.1	184	17.1	0.082	n.d.	1.21	28.2	1.9
Sample 5[g]	7.6	3.70	56.1	188	15.1	0.080	n.d.	1.25	30.8	1.9
Sample 6[g]	7.8	3.91	56.4	184	16.6	0.084	n.d.	1.36	21.1	2.1
Sample 7[g]	7.6	3.69	57.6	198	16.3	0.082	n.d	1.24	25.4	2.1
Thermophilic (WWTP average):	**8.1**	**3.79**	**54.7**	**207**	**31.2**	**0.150**	**1922**	**1.64**	**22.8**	**2.5**
Sample[h]	8.2	3.74	52.1	237	36.9	0.156	n.d.	1.61	17.3	3.3

[a] Dry weight % expressed as percentage of wet weight.
[b] Loss of ignition as percentage of dry weight.
[c] VFA = volatile fatty acids. TAK = total alkalinity.
[d] m^3 gas (1 bar, 0 ^{0}C), 45% CO_2, 55% CH_4.
[e] Hydraulic retention time (days)
[f] VS = volatile solids= fraction of organic material, determined by ignition (LOI)
[g] Sample 1 (date: 2017.04.26) was used for the enrichment analyzed by genomics and proteomics (Figure 2A), Sample 2 (date 2017.12.12): repeated experiment shown in Figure 2B&C, Sample 3 (date 2018.05.01): third repeat of the enrichment (Figure S2), Sample 4 (date 2020.05.02): oxic cultivation of isolates (Figure S25, S26), Samples 5 and 6 (dates:2020.05.05, 2020.05.15): digestate used for soil inoculation (Figures S27, S28, S29), Sample 7 (date2020.08.26): final enrichment where H_2 was monitored (Figure S13).
[h] Thermophilic digestate was only used in the first enrichment experiment (Figure S6 and S7)

Samples of digestates for enrichment culturing were taken from the mesophilic and thermophilic anaerobic digestors at sampling points located on the recirculation loop of the digesters. The digestates were transported to the laboratory in 1 L vacuum isolated steel vessels which were filled completely to minimize the exposure to O_2 and used in enrichment culturing within 3-6 hours after sampling. During the 3-6 hours between sampling and initiation of enrichment culturing, the temperature in the thermos fell to ~20 °C. For each enrichment culturing, we took new samples, and the operational parameters and digestate characteristics for each case are shown in Table 1. Raw wastewater sludge was used in some experiment, and this was taken downstream of the buffer tank (see above) and transported in 1 L steel vessels a described for digestates.

2 Incubation- and gas measurement system, calculation of concentrations and rates of transformations.

In all incubations described below, we used a temperature controlled robotized incubation system, as described by Molstad et al (2007, 2016). This system samples the headspace of 120 mL closed vials at intervals, and analyses O_2, N_2, N_2O, NO, CO_2 and CH_4 in a single gas sample, using a gas chromatograph (789A GC-System, Agilent Technologies) and a chemiluminescence NO analyzer (Model 200A, Teledyne Instruments). The sampled gas is replaced by an equal volume of He. Mass loss due to sampling, and leakage of N_2 and O_2 through tubing, valves and septa are accounted for when estimating the rates of production/consumption for each time increment between two samplings. The measured gas concentrations in the headspace can be converted to concentrations in the liquid, based on the solubility of the individual gases and the empirically determined transport coefficient for gas exchange between the headspace and the liquid (explained in detail by Molstad et al 2007). The concentration of N_2O is reported as mol N_2O L^{-1} in the liquid, rather than the concentration in the headspace, since the concentration in the liquid is what the organisms experience. The amounts of N_2 produced (and N_2O reduced) are expressed either as mol N_2 and N_2O, or as mol N (N_2-N and N_2O-N). The latter is a convention in denitrification research which simplifies nitrogen mass balance calculations. An example excel spreadsheet with dummy data, but otherwise identical to the ones used in this work, transparent with respect to all calculations regarding gas kinetics and solubility of gases, in addition to accompanying e-learning videos, is available (see Bakken 2020).

3. Enrichment culturing and samples for molecular analyzes and VFA quantification

Within 3-6 hours after sampling digestates from the WWTP (Table 1) triplicates of 50 mL mesophilic, thermophilic and a heat treated mesophilic digestate (heat treated at 55 °C for two hours in a temperature controlled water bath) were transferred to 120 mL glass vials with a 23 mm Teflon coated triangular magnet. The vials were crimp sealed with a butyl rubber septum, and headspace air was removed and replaced by helium by repeated evacuation and He-filling ("He-washing", see Molstad et al 2007). The procedure of filling and helium washing took ~1 hour. The vials were then placed on a magnetic stirring plate (stirring speed 300 rpm) in the thermostatic water-bath (20 ^{o}C) of the incubation robot and the He overpressure was released after temperature equilibration with the water bath (~10 minutes). Then 3 mL medical grade N_2O (Aga, Norway) was injected to the vials, and the gas kinetics was monitored by frequent sampling of the headspace. Additional N_2O was injected several times throughout the incubation, in response to depletion. Negative controls without injection of N_2O were included.

Samples for metagenomics and metaproteomics were taken at three time points during the enrichment culturing, using a syringe flushed with helium to minimize oxygen contamination. The samples were placed in an ultra-freezer (-80 °C) immediately after sampling. The first samples (1 mL vial^{-1}, sample name "0h" used throughout) were taken prior to the first injection of N_2O. Subsequent samples were taken after 115 h (0.2 mL vial^{-1}) sample name "115h" used throughout the text), and at the end of the incubation (t = 325 hours, 1 mL vial^{-1}) sample name "325h" used throughout the text).

This enrichment culturing experiment was repeated several times (each time using freshly sampled digestate, Table 1) to check reproducibility of the gas kinetics, while metagenomic and metaproteomic analyses were done only in the first experiment (Figure 2A). The repeated enrichment experiments were done to refine the analyses of the gas kinetics, and to explore inhibition of methanogenesis by N_2O. In addition, we incubated mesophilic digestates provided with either NO_3^- or O_2 (no N_2O) to assess the potential for NO_3^- and O_2- consumption, and the effects of these electron acceptors on methanogenesis. In the final enrichment culturing, we used an improved version of the incubation robot, equipped with an extra detector (Plasma Emission Detector, LDetek) for quantification of H_2, thus testing if the inhibition of methanogenesis by N_2O resulted in H_2 accumulation.

We also conducted N_2O enrichments with mesophilic digestates (fresh as well as heat treated) amended with raw sludge (1 mL in 50 mL digestate per vial) to assess the potential for N_2O reduction in raw sludge versus the digestate, hence implicitly assessing to which degree N_2O-reducing organisms in the raw sludge survive in the digester.

DNA extraction and quantification of 16S copy numbers

The samples taken from the enrichment culturing from mesophilic vials (after 0, 115 and 325 hours) and from heat treated mesophilic vials (0h and 325h) were thawed at room temperature and centrifuged at 10 000 × g for 3 minutes. DNA extraction from the resulting pellet was performed using PowerLyzer® PowerSoil® DNA Isolation kit (QIAGEN) following the manufacturer's protocol. Extracted DNA was stored at -20 °C prior to high throughput metagenome sequencing (see *Metagenomics* paragraph below) and quantification of the 16S gene copy number with quantitative digital droplet PCR (ddPCR). ddPCR was performed on technical triplicates of DNA preparations from each mesophilic sample. The ddPCR reaction mix was prepared according to the manufacturer's instructions. Each sample contained 10 µL QX200 ddPCR EvaGreen Supermix (Bio-Rad), 2 µL of DNA template, and 100 nM final concentration of the universal primer-pair PRK341F (5'-CCTACGGGRBGCASCAG-3') and PRK806R (5'-GGACTACYVGGGTATCT-3') (Eurofins Genomic) targeting the V3-V4 region of 16S rDNA (Yu et al 2005). Oil droplets where generated in a QX200 droplet generator from 20 µL reaction mix and 70 µL droplet generation oil for EvaGreen (Bio-Rad) and 40 µL of the oil droplet suspension was transferred to a well of a 96 well twin.tec plate (Eppendorf) that was heat sealed with aluminum foil (PX1™ PCR plate sealer (Bio-Rad)). The PCR reaction was conducted in a 2720 Thermal Cycler (Applied Biosystems) with 2 °C s^{-1} ramp rate, a lid temperature of 105 °C, and ran for 40 cycles, as recommended by the supplier, with temperature settings: 95 °C for 30 seconds (denaturation), 55 °C for 30 seconds (annealing) and 45 seconds at 72 °C (extension). The last cycle was followed by 5 minutes at 4 °C and 5 minutes at 90 °C (for signal stabilization). PCR products where analyzed in a QX200 droplet reader (Bio-Rad), and the data was analyzed using the Quantasoft™ Analysis Pro 1.0.596 software (Bio-Rad).

VFA quantification

Samples taken during enrichment culturing (sample: 0h, 115h and 325h) were stored frozen (-80°C) until analyzed for VFA. In addition, we analyzed VFA in freshly sampled, i.e. digestate that was frozen (-80 °C) immediately after sampling, from the anaerobic digester. The frozen samples were thawed in room temperature and centrifuged at 12 000 × g for 5 minutes.

Thereafter the supernatant was pH adjusted to ~2.5 using concentrated H_2SO_4 and centrifugated for 1 minute at 12 000 × g. The supernatant of individual samples was divided in three aliquots (technical triplicates). Quantification of VFAs (formate, acetate, propionate, iso-butyrate, valerate and iso-valerate) was done with high pressure liquid chromatography (HPLC) using a Dionex Ultimate 3000 system (Dionex, USA), operated at 40 °C with flowrate 0.3 mL min^{-1}, equipped with a UV detector (210 nm) and a Zorbax Eclipse Plus C18 column (Agilent, USA) (150 x 2.1 mm, 3.5 µm particles) and a guard column (12.5 x 2.1 mm; 5 µm particles) (Agilent, USA) for all samples. Standards covered the range (mM); 0.8–330, 0.5–220, 0.5–170, 0.7–135, 0.4–135, 0.4– 113 and 0.3-112 for formate, acetate, propionate, iso-butyrate, valerate and iso-valerate, respectively. The sample volume was 1 µL. Separation was achieved by applying a gradient of 2.5 µM H_2SO_4 and methanol as outlined in Table 2.

Table 2 Elution profile, VFA quantification.

Time (min)	Methanol (anhydrous) (%)	2.5 mM H_2SO_4 (%)
(0.0 – 2.5)	0	100
(2.5 – 25)	15	85
(25 – 35)	0	100

Modelling growth of N_2O reducing bacteria based on the measured N_2O kinetics

Growth of N_2O-respiring organisms in the enrichment cultures was estimated from the measured kinetics of N_2O reduction, using parameters for anaerobic growth of the model denitrifying bacterium *Paracoccus denitrificans* as determined in our laboratory (Bergaust et al 2010, 2012): Cell dry-weight = 310 (+/-50) fg $cell^{-1}$, growth yield, Y_{e-} = 1.9 · 10^{13} cells mol^{-1} electrons to N_2O (= 5.7 g cell dry-weight mol^{-1} e^-), growth rate = 0.1 h^{-1} (the cell specific rate of electron flow at this growth rate, V_{emax}, = 5.26 · 10^{-15} mol e^- h^{-1}). These parameters were determined in experiments with succinate as the sole C source and at 20 °C (i.e. the same temperature as in all enrichment cultivations). Details of the modelling are explained in the legend of **Figure S2**. It should be noted that the calculated cell numbers are expressed as "*Paracoccus* equivalents" i.e. cells with 310 · 10^{-15} g dry weight $cell^{-1}$. The estimated cell densities can be converted to cell dry weights mL^{-1} with reasonable confidence because different denitrifying organisms have fairly similar growth yields in terms of g dry weight mol^{-1} e^- to N_2O, namely 4-6 g cell dry weight mol^{-1} e^- (Hein et al 2017, Yoon et al 2016).

4 Metagenomics

Metagenomics

Isolated DNA from the mesophilic enrichment (samples 0h, 115h and 325h) was sequenced on an Illumina HiSeq4000 system, using TruSeq PCR-free library preparation. This also included DNA from the parallel enrichment with a pre-heated (55 °C for 2 hours) mesophilic digestate (Figure S6), to improve downstream analysis (i.e. binning) by increasing the differential coverage (Albertsen et al 2013). All reads were trimmed using Trimmomatic v0.36 (Bolger et al 2014) in pair end mode (Bolger et al 2014), before assembly with metaSPADes v3.10.1 (Nurk et al 2017). Both individual assemblies and co-assemblies of all samples from the enrichment were carried out, of which the co-assemblies were evaluated to give a better result according to metaQuast v4.5 (Mikheenko et al 2016). Metagenome assembled genomes (MAGs) was recovered from the co-assemblies (contigs > 500 bp) using MaxBin2 v2.2.1 (Yu-Wei et al 2016), and the quality of the MAGs was evaluated using CheckM v1.0.13 (Parks et al 2014). The binning effort resulted in 278 MAGs, of which 149 were considered to be of sufficient quality (completeness >50 %, contamination <20 %) for downstream analysis (**Supplementary Data S1**). Gene calling and functional annotation of the metagenomes were carried out using Prodigal v2.6.1 (Hyatt et al 2010) and InterProScan5 v5.32-71.0 (Jones et al 2014). Raw reads from each experimental sample were mapped to a concatenated fasta file of the 149 MAGs (Bowtie2 v2.3.4.1 (Langmead and Salzberg 2012) and Samtools v1.3.1) (Li et al 2009) and the relative abundance of each MAG was calculated using CoverM v0.3.2 (https://github.com/wwood/CoverM) requiring a minimum read identity of 95% and minimum read alignment of 75%.

Phylogenetic placement and taxonomic classification

A set of 16 universal single-copy ribosomal proteins (L2-L6, L14-L16, L18, L22, L24, S3, S8, S10, S17 and S18) was used to build a phylogenetic tree consisting of the 149 MAGs. The ribosomal proteins were identified within the functionally annotated MAGs. Four MAGs lacked all 16 protein sequences, and these were excluded from the phylogenetic tree but included in the taxonomic classification described below, which analyzes 100+ marker genes. Separate alignments were built for every ribosomal protein using MUSCLE v3.8.31 (Edgar 2004). The alignments were manually checked for misalignments and all conserved, single-copy ribosomal protein sequences that occurred more than once in a MAG were excluded GBlocks (Castresana 2000, Talavera and Castresana 2007) (parameters: -b2=50, -b3=20, -b4=2) was used to find conserved regions in each alignment, and the aligned regions for single proteins were then concatenated in an alignment of 2528 residues. Maximum likelihood phylogenies were built with RAxML-ng (Stamatakis 2014) using the PROTGAMMAWAG method, and the consensus tree was visualized using iTOL (Letunic and Bork 2019). A complete version of the tree is available in Newick format as Supplementary Data S3. The taxonomic classification of the MAGs was inferred using a set of 120 bacterial and 122 archaeal marker genes via the Genome Taxonomy Database GTDB v1.0.2 (Chaumeil et al 2019) using *classify_wf* with default parameters.

5.Quantitative metaproteomics

Samples were prepared by an initial centrifugation of mesophilic digestate samples in replicates (taken at 0, 115 and 325 hours) to separate the fiber fraction from the secretome. The secretome was filtered with a 0.22 µm sterile filter to remove cells and debris and treated with TCA (10 % final concentration) to precipitate the proteins. The fiber fraction was resuspended in dissociation buffer (1 % methanol, 1 % tert-butanol, 0.1 % Tween-80, pH 2) and, after gently mixed for 30 s at room temperature, released material (including cells) was separated from the plant material via a gentle spin (100 × *g*, 30 sec) and the supernatant retained in a fresh tube (Frank et al 2016). This procedure was repeated three times to increase the yield. Cell lysates were prepared by bead-beating in lysis buffer (50 mM tris-HCl, 200 mM NaCl, 1 mM DTT, 0.1% Trition X-100, pH 7.5), using glass beads (diameter ≤ 106 µm), followed by centrifugation (16.000 × *g*, 15 minutes) to spin down beads and cellular debris. The proteins in the collected lysate were precipitated using TCA as above.

The TCA precipitated proteins were resuspended in Laemmli sample buffer and subjected to SDS-PAGE (270V, 4 minutes). Each sample (secretome, cell lysate) was excised from the gels in four fractions = gel pieces). After washing the gel pieces with 25 mM ammonium biocarbonate, pH 7.8 in 50% acetonitrile, proteins were reduced by incubation in 10 mM DTT for 30 minutes at 56 °C, followed by carbamidomethylation by incubation with 55 mM iodoacetamide for 30 minutes at room temperature. Subsequently, the proteins were digested into peptides using 300 ng trypsin per sample and incubation at 37 °C, overnight. The peptides were desalted using C18 ZipTips (Merch Millipore, Darmstadt, Germany), according to the manufacturer's instructions, and analysed by nanoLC-MS/MS using a Dionex Ultimate 3000 UHPLC (Thermo Scientific) coupled to a Q-Exactive hybrid quadupole orbitrap mass spectrometer (Thermo Scientific, Bremen, Germany). Peptides were separated using an analytical column (Acclaim PepMap RSLC C18, 2 µm, 100 Å, 75 µm i.d. × 50 cm, nanoViper) with a 90-minutes gradient from 3.2 to 44 % [v/v] acetonitrile in 0.1 % [v/v] formic acid) at flow rate 300 nL/min. The Q-Exactive mass spectrometer was operated in data-dependent mode acquiring one full scan (400-1500 m/z) at R=70000 followed by (up to) 10 dependent MS/MS scans at R=35000.

The acquired MS/MS spectra were searched against the proteome of the 149 MAGs recovered from the abovementioned metagenomics data (785 999 protein sequences), using MaxQuant version 1.6.3.3 (Cox and Mann 2008). Common contaminants, such as human keratins, trypsin and bovine serum albumin were concatenated to the sample specific database as well as reversed sequences of all protein entries for estimation of false discovery rates. Proteins were quantified using the MaxLFQ algorithm in MaxQuant (Cox et al 2014). Protein N-terminal acetylation and oxidation of methionine were used as variable modifications, while carbamidomethylation of cysteine residues was used as a fixed modification. Tolerance levels for peptide identifications were 4.5 ppm and 20 ppm for MS and MS/MS, respectively, and two missed cleavages of trypsin were allowed. Additional quality filtering and downstream interpretation were performed in the software platform Perseus version 1.6.0.7 (Tyanova et al 2016). This included removal of contaminations, hits to reversed sequences and hits based on a single modified peptide. Furthermore, all identifications were filtered in order to achieve a protein false discovery rate (FDR) of 1% using the target-decoy strategy. For a protein group to be considered valid, we required the protein group to have at least one unique peptide and be detected in at least two of the three replicates for samples taken at 0 and 325 hours. For the sample taken after 115 hours, only duplicates were available, in this case proteins were only considered valid if they were identified in both replicates, to preserve high confidence. The putative functionality of the detected protein groups was assigned using the abovementioned InterProScan annotation of the protein sequences in the database as well as with the dbCAN2 meta server (Zhang et al 2018) (using CAZy-HMMs version 8) to detect putative carbohydrate-active enzymes.

To construct metaproteome-based metabolic maps (**Figure S12**), we scanned the detected proteins affiliated to each MAG (**Supplementary Data S2**) for enzymes involved in specific metabolic pathways (Frank et al 2015) In brief, to predict that a given population utilized monomeric sugars, we detected genes associated with the Embden-Meyerhof-Parnas pathway (glycolysis), including phosphofructokinases. Gluconeogenesis was predicted in a given population if a representative unidirectional fructose diphosphatase gene was detected in the proteome. The detection of both a phosphate acetyl/butyryl transferase-enzyme (contains phosphotransacetylase) and an acetokinase, or Acetyl-CoA hydrolase/transferase, was used to predict acetate metabolism. For predicting the ability of given populations to oxidize fatty acids, we detected key proteins encoded on a methylmalonyl-CoA (MMC) gene cluster and all four enzymes inferred in beta-oxidation (acyl-CoA dehydrogenase, enoyl-CoA hydratase, hydroxy acyl-CoA dehydrogenase, and ketoacyl-CoA thiolase). The prediction of an active Wood-Ljungdahl pathway was assessed as follows: the combination of a highly expressed CO dehydrogenase/acetyl-CoA synthase cluster, electron transfer complex, aldehyde ferredoxin oxidoreductase for potential acetate activation, and enzymes for beta-oxidation of fatty acids. The methanogen-affiliated proteomes were scanned for the detection of Coenzyme M methyl-transferase, a key enzyme in the methanogenesis. Nos (EC:1.7.2.4) levels were visualized using ggplot2 in RStudio. The proteome size of individual MAGs was estimated in two different manner, either by the number of proteins detected per MAG or as the sum of LFQ-values for all proteins belonging to one MAG normalized to the total LFQ for the sample.

6. Isolation of N_2O reducing bacteria

Three types of media were used for incubation of cultures in liquid medium or on agar plates (1.5 w. % agar). Unless otherwise stated, the media were brought to desired strength by diluting stock solutions or dry powders in milliQ H_2O, pH adjusted by addition of KOH/HCl to pH = 7.0 and autoclaved at 121 °C for 20 minutes. Sistrom's succinate medium (**SS**), contained (L^{-1}) 3.48 g K_2HPO_4, 0.195 g NH_4Cl, 4 g succinic acid, 0.10 g glutamic acid, 0.04 g aspartic acid, 0.5 g NaCl, 0.2 g nitrolotriacetic acid, 0.3 g $MgSO_4 \cdot 7H_2O$, 0.015 g $CaCl_2 \cdot 7H_2O$, 0.002 g $FeSO_2 \cdot 7H_2O$, 0.1 mL trace element solution and 0.1 mL vitamin solution. The trace element solution contained (g L^{-1}): 17.65 g EDTA (triplex 3), 109.5 g $ZnSO_4 \cdot 7H_2O$, 50 g $FeSO_4 \cdot 7H_2O$, 15.4 g $MnSO_4 \cdot H_2O$, 3.92 g $CuSO_4 \cdot 5H_2O$, 2.48 g $Co(NO_3)_2 \cdot 6H_2O$ and 1.14 g H_3BO_3; H_2SO_4 was added until the solution cleared. The vitamin solution contained (g L^{-1}) 10.0 g nicotinic acid, 5.0 g thiamine HCl and 0.10 g Biotin. Digestate medium (**D**) was prepared by centrifuging digestate from the VEAS WWTP at 8000 × g for 30 minutes, after which the supernatant was pH adjusted to ~6.5 and autoclaved (121 °C for 20 minutes). The heat treatment led to loss of dissolved CO_2 and a pH increase, giving a final pH of 7.5. Anaerobe basal medium (**AB**; OXOID CM0957, Thermo Scientific) contained (L^{-1}) 1.6 g peptone, 0.7 g yeast extract, 0.5 g sodium chloride, 0.1 g starch, 0.1 g arginine, 0.05 g sodium succinate, 0.05 g L-cysteine hydrochloride, 0.04 g sodium bicarbonate, 0.05 g ferric pyrophosphate, 0.01 g dithiothreitol, 0.05 g sodium thioglycolate, 0.0005 g haemin and 0.00004 g vitamin K.

Dilution series of dispersed N_2O enriched mesophilic digestate were prepared and spread on agar plates (50 µL diluted suspension per plate) on all media (SS, D and AB) shortly after ending the enrichment culturing. In order to select for N_2O reducing strains the agar plates were incubated anoxically in 8.6 L anaerobe boxes which were first sparged with N_2, followed by injecting ~8 vol % N_2O. To secure anoxic conditions anaerobic boxes were equipped with two oxygen scavenger bags (3.5 L AnaeroGen™, OXOID). The plates incubated at 20 °C and inspected after ~2 weeks, and a selection of visible colonies were picked and re-streaked on daughter plates with corresponding media and incubated anaerobically with N_2O as described. Growing colonies were picked and re-streaked on corresponding plates and incubated under aerobic conditions to avoid continuation of growth of obligate fermentative bacteria. The 16S gene of single colonies growing on aerobic plates was amplified by PCR using the DreamTaq™ Green PCR Master Mix (Thermo Scientific) using the bacteria specific primer 27F (3'-AGAGTTTGATCMTGGCTCAG-5') (Lane 1991, Invitrogen) and the universal primer 1492R (5'-GGTTACCTTGTTACGACTT-3') (Stackerbrandt and Liesack 1993, Invitrogen) in a 2720 Thermal Cycler (Applied Biosystems) with 2 °C s^{-1} ramp rate and a lid temperature of 105 °C. The temperature parameters of the 30 amplification cycles were 98 °C for 10 seconds, 55 °C for 30 seconds and 72 °C for 1 minute. The last cycle was followed by a 1-minute final elongation at 72 °C and a 4 °C hold step. The presence of contaminants was evaluated based on inspection of Sanger sequencing chromatograms of the 16S PCR amplicons (LightRUN™ sequencing services, Eurofins Genomics, Germany) and by inspection/microscopy of colony- and cell morphology. The 16S analyses showed that a large majority of the SS-, D- and AB agar plates had growing colonies related to *Azonexus* sp..

One colony of *Azonexus* sp., growing on SS agar, was selected for further work and was given the working name "**AN**". Another culture, related to *Pseudomonas sp*., growing on SS-agar, was obtained and given the working name "**PS**". Continuation of aerobic growth of AN on new SS agar plates revealed a minor contamination (contaminant was not visible in Sanger sequencing chromatograms of 16S amplicons obtained of the mother colony). Re-streaking and purification of the contaminated culture revealed that the contaminant had almost identical morphological features as **AN** when growing as single colonies, and when inspected under the light microscope. The contaminant, related to *Azospira* sp. by 16S, was given the working name "**AS**".

The cultures of **AS** and **PS** where grown aerobically at 20 °C in stirred (700 rpm) SS liquid media to OD_{660nm} ~ 1 (UV-1280 UV-VIS spectrophotometer, Shimadzu), and aliquots were snap frozen as glycerol stocks (15 wt. %) in liquid nitrogen and stored as precultures at -80 °C. **AN** was not revivable after freezing, and was kept as N_2O raised colonies on SS agar slabs stored at 4 °C.

7. Genome sequencing of isolates and comparison average nucleotide identity (ANI) with metagenome-assembled genomes

The isolates were recovered from snap frozen glycerol (15 vol%) stocks of aerobically grown cultures in SS liquid medium (AS and PS), or from single colonies grown on N_2O on SS-agar slabs stored at 4 °C (AN), and grown aerobically (stirred at 700 rpm, air atmosphere) at 20 °C in SS medium to late exponential phase ($OD_{660} \approx 1.0$). The cell suspensions were centrifuged at 10000 × *g* for 10 minutes and DNA was extracted from the pellet using the PowerLyzer™ Soil DNA extraction kit (QIAGEN) following a modified kit protocol (bead beating for 45 s at 4.5 $m.s^{-1}$ in a FastPrep®-24 (M.P. Biomedicals) substituted the vortexing step in the manufacturers protocol). Paired end MiSeq sequencing on extracted DNA was performed at the Norwegian Sequencing Center on a MiSeq v2 nano 250 PE platform with Nextera™ DNA Flex Tagmentation sample preparation for the isolates AN and AS. PS was sequenced at Novogene Co., Ltd., Hongkong on a HiSeq4000 platform 150 PE. Raw reads were quality checked with FastQC v0.11.5 (Andrews, 2010). Removal of low-quality sequences and ambiguous reads was done using Trimmomatic (Bolger et al 2014) with the following settings: sliding window 4:15; adapter clipping options: enabled for adapters NexteraPE-PE (for AN and AP only); seed mismatches 2; palindrome clip threshold 30; simple clip threshold 10; head crop length 12 (AN and AP only). Contig assembly was done with SPAdes (Nurk et al 2013) using default parameters. Quality assessment of the assembled contigs was done in Quast (Gurevich et al 2014) with the following settings: unaligned part size 1000; extensive mix size 1000; min alignment 50; min identity 80. Prokka v1.12 (Seemann 2014) and RAST (Aziz et al 2008) were used for annotation of the assembled contigs with default parameters. The OrthoANIu tool (Yoon et al 2017) was used to compare and to calculate average nucleotide identities the sequenced genomes and the metagenome assembled genomes.

8. Phenotyping of isolates

The capacity of the isolates to utilize a variety of carbon substrates was tested using PM1 and PM2 BiOLOG Phenotype MicroArray™ plates (BiOLOG Inc. Hayward, CA). The BiOLOG test method is based on the irreversible reduction of tetrazolium violet to formazan as in indicator of active metabolism (Bochner et al 2001). The isolates were raised on Merck Nutrient broth agar plates (20 g agar L^{-1}) and transferred to the BiOLOG plates according to the instructions of the manufacturer. The plates were incubated at 30 °C and analyzed by spectrophotometry after 72 hours. The experiments included control plates without inoculum, and 3 replicate plates for each isolate.

The characteristic regulation of denitrification (regulatory phenotypes) by the isolated cultures was determined as in previous investigations (Bergaust et al 2011, Liu et al 2013, Lycus et al 2018, Mania et al 2016) by monitoring the kinetics of O_2, N_2, N_2O, NO and CO_2 throughout the cultures' depletion of O_2 and transition from aerobic to anaerobic respiration in stirred batch cultures with He + O_2 (+/- N_2O) in the headspace.

The cells to inoculate these vials were raised under strict aerobic conditions to avoid synthesis of denitrification enzymes prior to inoculation for testing the regulatory phenotypes: 1 mL frozen pre-culture of the isolates **AS** and **PS**, and cells from a single colony of **AN** (this culture did not survive freezing), were raised in 50 mL liquid SS medium (initial OD_{660nm} of ~0.02 for **AS** and **PS** and <0.01 for **AN**) under oxic conditions (air, the 120 mL serum vials covered with Al-foil) at 20 °C with rapid stirring (700 rpm). When OD_{660nm} reached ~0.2, 1 mL was transferred to new vials containing 50 mL SS medium for continuation of aerobic growth.

When the cultures reached OD_{660nm} 0.05 – 0.1, they were used to inoculate the phenotype test vials.

The phenotyping was conducted in triplicate or duplicate 120 mL capped vials containing 50 mL SS medium supplemented with either NO_2^- (1 mM, 50 µmol), NO_3^- (2 mM, 100 µmol) or both. The headspace (He) was supplemented either with 1 mL O_2, or 1 mL O_2 + 1 mL N_2O. The vials were inoculated with 0.1 – 0.5 mL (depending of the OD) of the aerobically raised cultures (added using a sterile syringe) and monitored for gas kinetics while incubated at 20 ^oC (stirred, 700 rpm).

Nitrite concentrations were measured at various timepoints throughout the incubations, by taking 10 µL liquid samples which were injected immediately into a purging device containing 1% w/v NaI in 50% acetic, which converts nitrite instantaneously to NO, which is transported (by N_2-flow) to a chemiluminescence NO analyzer (Sievers 280i, GE Analytical Instruments) (Cox 1980, MacArthur et al 2007.

9. Protein extraction and quantitative proteomics in *Azonexus* sp. AN.

A cell culture of *Azonexus* sp. AN was raised from a single colony incubated at aerobic conditions at 20 °C with rapid stirring (700 rpm) in 50 mL SS liquid medium. When the pre-culture reached an OD_{660nm} of 0.2, 1 mL cell suspension was transferred to a new vial containing 50 mL Sistrom medium for continuation of aerobic growth at the same conditions. To determine the relative expression of N_2O reductase and nitrate reductase in the isolate AN in response to the transition to anoxia, six sterile 120 mL vials containing 50 mL SS liquid medium supplemented with 2 mM NO_3^- (0.1 mL 1M KNO3) and 1 mL O_2 in helium atmosphere (headspace volume 70 mL), was incubated at 20 °C and inoculated with 1 mL cell culture of *Azonexus* sp. AN (OD_{660nm} = 0.150) using a sterile syringe. At intervals throughout the incubation, single vials were subjected to destructive sampling: the vial was removed from the incubation robot and immediately cooled down, with stirring, in ice-cold water. The entire culture volume was then transferred to a 50 mL sterile Falcon™ tube and centrifuged at 10 000 × *g* for 10 minutes at 4°C. The supernatant was gently poured of and the cell pellet immediately frozen (-80 °C). The frozen cell pellets were thawed on ice, resuspended in lysis buffer (20 mM Tris-HCl pH 8.0, 0.1 % v/v Triton X-100, 200 mM NaCl, 1 mM DTT, 4% SDS) and treated with 3 × 45 s bead beating with glass beads (particle size ≤106 µm, Sigma) at maximum power and cooling on ice between the cycles (MP Biomedicals™ FastPrep- 24™, Thermo Fischer Scientific Inc). Cell debris was removed by centrifugation (10 000 × *g*; 5 min) and the supernatant, containing water soluble proteins, was used for proteome analysis using the NanoLC- Orbitrap-MS, as described above. Data analysis was performed in MaxQuant 1.6.2.3 (Cox and Mann 2008). The raw data was matched against the proteome of the type strain *Azonexus hydrophilus* 418702 (Uniprot, https://www.uniprot.org/proteomes/UP000187526) supplemented with sequences obtained from the predicted proteins of periplasmic nitrate reductase (Nap), nitrite reductase (Nir), nitric oxide reductase (Nor) and nitrous oxide reductase (Nos) obtained from the genome sequence of *Azonexus sp*. AN. The denitrification reductases were quantified by expressing their LFQ values. Since Nos is a homo-dimer and Nap a monomer, the LFQ values for Nos were divided by two to obtain the correct number of putatively functional enzymes.

10. Incubations of soils for determining if digestates with N_2O-reducing bacteria can reduce the N_2O emission from soil denitrification.

Two agricultural clay loam soils (pH = 5.5 and 6.5) were used, taken from a long-term liming experiment at Ås, Norway (described by Nadeem et al 2020). Prior to incubations, the soils were sieved through a 3 mm metal mesh, air dried at room temperature, and stored in plastic containers at 4 °C for 4 months. The nitrate content of the two soils (when used for experiments) was 1.32 (± 0.01) and 1.13 (± 0.01) µmol g^{-1} dry weight (standard error in parenthesis, n=3). The nitrite content of the soil was <5 nmol g^{-1} (below detection limit).

The soils were inoculated with digestates that were pretreated in various ways to assess the effect of 1) the indigenous bacteria (in digestates as taken directly from the anaerobic digester), 2) indigenous N_2O-reducing bacteria enriched by anaerobic incubation with N_2O, and 3) isolated cultures grown aerobically in digestates. The digestates used were (working names in bold italics):

1) ***Live digestate*** = digestate directly from the anaerobic digester of the WWTP (sampled ~3 hours before inoculation of soils)

2) ***70 ºC dig*** = Live digestate heated to 70ºC for 2 h to kill most of the indigenous denitrifying bacteria in the live digestate

3) ***AN, AS*** and ***PS*** = autoclaved digestates in which isolated *Azonexus sp.*, *Azospira sp.* and *Pseudomonas sp.,* respectively, were grown by aerobic respiration.

4) **N_2O enr.** = digestates in which N_2O-reducing bacteria were enriched by anaerobic cultivation with N_2O (repeat of the enrichment culturing shown in Figure 2).

The procedure for aerobic cultivation of the isolated cultures in autoclaved digestate (point 3 above) was: freshly sampled digestate was autoclaved (121 °C, 20 min), which increased the pH to ~9.8 (due to removal of CO_2), and sparged with sterile filtered air for 24 hours. The air sparging was necessary because the WWTP adds ferric chloride as a precipitation chemical post anaerobic digestion, which is reduced to ferrous iron (Fe^{2+}) during AD (Cheng et al 2015): abiotic oxidation of Fe^{2+} obscured measurements of oxygen consumption by respiration, and the abiotic oxidation may inhibit aerobic respiration due to formation of reactive oxygen species (Winterbourn 1995). After sparging, pH was adjusted to 7.5 by addition of HCl. The isolates where raised from frozen stocks (AS and PS), or from a single N_2O-raised colony picked from SS agar slabs stored at 4 °C (AN), in 50 mL SS medium at 20 °C under oxic conditions (air) with rapid stirring (700 rpm). At OD_{660nm} ~0.2 the cultures where transferred to new vials containing 50 mL SS medium and growth continued under the same conditions, and when OD_{660} reached ~1, 1 mL of each culture was added to 120 mL vials containing 50 mL autoclaved and the pre-aerated digestate, which were then incubated (stirred, 700 rpm) at 20 °C in the robotized incubation system. O_2 was injected several times throughout the incubation to maintain >10 vol % O_2 in the headspace and ended after 160 hours. At this time point, ***AN, AS*** and ***PS*** had consumed 16.3, 22.9 and 22.4 µmol O_2 mL^{-1}, respectively, which implies cell densities of 2.5-3.5*10^9 mL^{-1}, or 0.7-1 mg cell dry-weight mL^{-1} , if assuming 300 fg dry weight $cell^{-1}$ and growth yield= 15*10^{13} cells mol^{-1} O_2, as determined for *Paracoccus denitrificans* (Bergaust et al 2010, 2012).

Digestate amendments of soils was set up as duplicate 120 mL vials with 10 g soil, amended with 3 mL digestate+ 0.1 mL 0.5 M KNO_3, which was spread as small droplets over the soil surface (~19 cm^2 surface area) using a syringe, resulting in ~61 % waterfilled pore space (bulk density = 1.1). The vials were then capped (butyl rubber septa), He-washed (repeated evacuation and He-filling), and 1 mL pure O_2 was injected with a syringe. The vials were then placed in the water-bath (20 ^{0}C) of the incubation robot and monitored by frequent sampling of the headspace.

The N_2O production index (I_{N_2O}) was calculated for each individual by

$$I_{N_2O} = \frac{\int_0^T \mathrm{N_2O{-}N(t)dt}}{\int_0^T [\mathrm{N_2O{-}N(t)} + \mathrm{N_2{-}N(t)} + \mathrm{NO(t)}]\mathrm{dt}} \qquad (1)$$

where $\int_0^T N_2O - N(t)dt$ is the area under the curve (trapezoidal rule) for measured N_2O-N (µ mol N $vial^{-1}$ h) and $\int_0^T [N_2O - N(t) + N_2 - N(t) + NO(t)]dt$ is the area under the curve for measured N_2+N_2O+NO-N (µ mol N $vial^{-1}$ h), both for the time period 0-T (h). I_{N_2O} was calculated for two time periods: $I_{N_2O\ 40\%}$ is the index for the period (0-T) until 40% of the available NO_3^-- N was recovered as N-gas (NO+N_2O+N_2), $I_{N_2O\ 100\%}$ is the index for the time period (0-T) until 100% was recovered. I_{N_2O} was used by Liu et al (2014) as a proxy for the relative propensity of a soil to emit N_2O from denitrification, and its predictive capacity verified by Russenes et al (2016). The experiments included control treatment where distilled water replaced digestates (duplicate vials for both soils).

References

Albertsen M, Hugenholtz P, Skarshewski A, Nielsen KL, Tyson GW, Nielsen PH (2013) Genome sequences of rare, uncultured bacteria obtained by differential coverage binning of multiple metagenomes. Nature Biotechnology 31:533-538. DOI:10.1038/nbt.2579

Andrews S (2010) FastQC: a quality control tool for high throughput sequence data. Available online at: http://www.bioinformatics.babraham.ac.uk/projects/fastqc

Aziz RK, Bartels D, Best AA, DeJongh M, Disz T, Edwards RA, Formsma K, Gerdes S, Glass EM, Kubal M, Meyer F (2008) The RAST Server: rapid annotations using subsystems technology. BMC Genomics 9:1-15. DOI:10.1186/1471-2164-9-75

Bakken LR (2021) Spreadsheet for gas kinetics in batch cultures: KINCALC. Researchgate. DOI: 10.13140/RG.2.2.19802.36809.

Bergaust L, Mao Y, Bakken LR (2010) Denitrification response patterns during the transition to anoxic respiration and posttranscriptional effects of suboptimal pH on nitrogen oxide reductase in *Paracoccus denitrificans*. Applied and Environmental Microbiology 76:6387-6396. DOI:10.1128/AEM.00608-10

Bergaust L, Bakken LR, Frostegård Å (2011) Denitrification regulatory phenotype, a new term for the characterization of denitrifying bacteria. Biochemical Society transactions 39:207-212. DOI:10.1042/BST0390207

Bergaust L, van Spanning RJM, Frostegård Å, Bakken LR (2012) Expression of nitrous oxide reductase in *Paracoccus denitrificans* is regulated by oxygen and nitric oxide through *FnrP* and NNR. Microbiology 158:826-834. DOI:10.1099/mic.0.054148-0

Bochner BR, Gadzinski P, Panomitros E (2001) Phenotype microarrays for high-throughput phenotypic testing and assay of gene function. Genome Research 11:1246-1255. DOI:10.1101/gr.186501

Bolger AM, Lohse M, Usadel B (2014) Trimmomatic: a flexible trimmer for Illumina sequence data. Bioinformatics 30:2114-2120. DOI:10.1093/bioinformatics/btu170

Castresana J (2000) Selection of conserved blocks from multiple alignments for their use in phylogenetic analysis. Molecular Biology and Evolution 17:540-552. DOI:10.1093/oxfordjournals.molbev.a026334

Chaumeil PA, Mussig AJ, Hugenholtz P, Parks DH (2019) GTDB-Tk: A toolkit to classify genomes with the Genome Taxonomy Database. Bioinformatics 36:1925-1927. DOI:10.1093/bioinformatics/btz848

Cheng X, Chen B, Cui Y, Sun D, Wang X (2015) Iron(III) reduction-induced phosphate precipitation during anaerobic digestion of waste activated sludge. Separation and Purification Technology 143:6-11. DOI:10.1016/j.seppur.2015.01.002

Cox RD (1980) Determination of nitrate and nitrite at the parts per billion level by chemiluminescence. Analytical Chemistry 52:332-335. DOI:10.1021/ac50052a028

Cox J, Mann M (2008) MaxQuant enables high peptide identification rates, individualized ppb-range mass accuracies and proteome-wide protein quantification. Nature Biotechnology 26:1367-1372. DOI:10.1038/nbt.1511

Cox J, Hein MY, Luber CA, Paron I, Nagaraj N, Mann M (2014) Accurate proteome-wide label-free quantification by delayed normalization and maximal peptide ratio extraction, termed MaxLFQ. Molecular Cell Proteomics 13:2513-2526. DOI:10.1074/mcp.M113.031591

Edgar RC (2004) MUSCLE: multiple sequence alignment with high accuracy and high throughput. Nucleic Acids Research 32:1792-1797. DOI:10.1093/nar/gkh340

Frank JA, Arntzen MØ, Hagen LH, McHardy AC, Horn SJ, Eijsink VGH, Schnürrer A, Pope PB (2016) Novel syntrophic populations dominate an ammonia-tolerant methanogenic microbiome. mSystems 1:e00092-16. DOI:10.1128/mSystems.00092-16

Greenberg AE, Jenkins D, Connors JJ (1980) Standard methods for the examination of water and wastewater. American Public Health Association.; American Water Works Association. Washington, D.C. : APHA-AWWA-WPCF. ISBN: 0875530915

Gurevich A, Saveliev V, Vyahhi N, Tesler G (2014) QUAST: quality assessment tool for genome assemblies. Bioinformatics 29:1072-1075. DOI:10.1093/bioinformatics/btt086

Hein S, Witt S, Simon J (2017) Clade II nitrous oxide respiration of *Wolinella succinogenes* depends on the *NosG*, -C1, -C2, -H electron transport module, *NosB* and a Rieske/cytochrome bc complex. Environmental Microbiology 19:4913-4925. DOI:10.1111/1462-2920.13935

Hyatt D, Chen GL, LoCascio PF, Land ML, Larimer FW, Hauser LJ (2010). Prodigal: prokaryotic gene recognition and translation initiation site identification. BMC Bioinformatics 11:119. DOI:10.1186/1471-2105-11-119

Jones P, Binns D, Chang HY, Fraser M, Li W, McAnulla C, McWilliam H, Maslen J, Mitchell A, Nuka G, Pesseat S (2014) InterProScan 5: genome-scale protein function classification. Bioinformatics 30:1236-1240. DOI:10.1093/bioinformatics/btu031

Lane DJ (1991) 16S/23S rRNA sequencing. In: Stackebrandt E, Goodfellow M (editors). Nucleic acid techniques in bacterial systematics (Wiley New York, NY, 115-175). DOI:10.1002/jobm.3620310616

Langmead B, Salzberg S (2012) Fast gapped-read alignment with Bowtie 2. Nature Methods 9:357-359. DOI:10.1038/nmeth.1923

Letunic I, Bork P (2019) Interactive Tree of Life (iTOL) v4: recent updates and new developments. Nucleic Acids Research 47:256-259. DOI:10.1093/nar/gkz239

Li H, Handsaker B, Wysoker A, Fennell T, Ruan J, Homer N, Marth G, Abecasis G, Durbin R (2009) The Sequence alignment/Map format and SAMtools. Bioinformatics 15:2078-9. DOI:10.1093/bioinformatics/btp352

Liu B, Mao Y, Bergaust L, Bakken LR, Frostegård Å (2013) Strains in the genus *Thauera* exhibit remarkably different denitrification regulatory phenotypes. Environmental Microbiology 15:2816-2828. DOI:10.1111/1462-2920.12142

Liu B, Frostegård Å, Bakken LR (2014) Impaired reduction of N_2O to N_2 in acid soils is due to a posttranscriptional interference with the expression of *nosZ*. mBio 5:e01383-14. DOI:10.1128/mBio.01383-14

Lycus P, Bøthun KL, Bergaust L, Shapleigh JP, Bakken LR, Frostegård Å (2018) Phenotypic and genotypic richness of denitrifiers revealed by a novel isolation strategy. The ISME Journal 11:2219-2232. DOI:10.1038/ismej.2017.82

Mania D, Heylen K, van Spanning JM, Frostegård Å (2016) Regulation of nitrogen metabolism in the nitrate ammonifying soil bacterium *Bacillus vireti* and evidence for its ability to grow using N_2O as electron acceptor. Environmental Microbiology 18:2937-2950. DOI:10.1111/1462-2920.13124

MacArthur PH, Shiva S, Gladwin MT (2007) Measurement of circulating nitrite and S-nitrosothiols by reductive chemiluminescence. Journal of Chromatography B 851:93-105. DOI:10.1016/j.jchromb.2006.12.012

Mikheenko A, Saveliev V, Gurevich A (2016) MetaQUAST: evaluation of metagenome assemblies. Bioinformatics 32:1088-1090. DOI:10.1093/bioinformatics/btv697

Molstad L, Dörsch P, Bakken LR (2007) Robotized incubation system for monitoring gases (O_2, NO, N_2O, N_2) in denitrifying cultures. Journal of Microbiological Methods 71:202-211. DOI:10.1016/j.mimet.2007.08.011

Molstad L, Dörsch P, Bakken LR (2016) Improved robotized incubation system for gas kinetics in batch cultures. Researchgate. DOI:10.13140/RG.2.2.30688.07680

Nadeem S, Bakken LR, Frostegård Å, Gaby JC, Dörsch P (2020) Contingent effects of liming on N_2O-emissions driven by autotrophic nitrification. Frontiers in Environmental Science 8:598513 DOI:10.3389/fenvs.2020.598513

Nurk S, Bankevich A, Antipov D, Gurevich A, Korobeynikov A, Lapidus A, Prjibelsky A, Pyshkin A, Sirotkin A, Sirotkin Y, Stepanauskas R (2013) Assembling Genomes and Mini-metagenomes from Highly Chimeric Reads. In: Deng M, Jiang R, Sun F, Zhang X (editors). Research in Computational Molecular Biology. RECOMB 2013. Lecture Notes in Computer Science, vol 7821. (Springer Berlin, Heidelberg). DOI:10.1007/978-3-642-37195-0_13

Nurk S, Meleshko D, Korobeynikov A, Pevzner PA (2017) metaSPAdes: a new versatile metagenomic assembler. Genome Research 27:824-834. DOI:10.1101/gr.213959.116

Parks DH, Imelfort M, Skennerton CT, Hugenholtz P, Tyson GW (2015) CheckM: assessing the quality of microbial genomes recovered from isolates, single cells, and metagenomes. Genome Research 25:1043-1055. DOI:10.1101/gr.186072.114

Russenes AL, Korsaeth A, Bakken LR, Dörsch P (2016) Spatial variation in soil pH controls off-season N_2O emission in an agricultural soil. Soil Biology and Biochemistry 99:36-46. DOI:10.1016/j.soilbio.2016.04.019

Seemann T (2014) Prokka: rapid prokaryotic genome annotation. Bioinformatics 30:2068-2069. DOI:10.1093/bioinformatics/btu153

Stackebrandt E, Liesack W (1993) Nucleic acids and classification. In Goodfellow M and O'Donnell AD (editors). Handbook of new bacterial systematics (Academic Press London, England, 152-189). ISBN-13:978-0122896729

Stamatakis A (2014) RAxML version 8: a tool for phylogenetic analysis and post-analysis of large phylogenies. Bioinformatics 30:1312-1313. DOI:10.1093/bioinformatics/btu033

Talavera G, Castresana J (2007) Improvement of phylogenies after removing divergent and ambiguously aligned blocks from protein sequence alignments. Systematic Biology 56:564-577. DOI:10.1080/10635150701472164

Tyanova S, Temu T, Sinitcyn P, Carlson A, Hein MY, Geiger T, Mann M, Cox J (2016) The Perseus computational platform for comprehensive analysis of (prote)omics data. Nature Methods 13:731-740. DOI:10.1038/nmeth.3901

Vizcaíno JA, Côté RG, Csordas A, Dianes JA, Fabregat A, Foster JM, Griss J, Alpi E, Birim M, Contell J, O'Kelly G (2013) The PRoteomics IDEntifications (PRIDE) database and associated tools: status in 2013. Nucleic Acids Research 41:1063-1069. DOI:10.1093/nar/gks1262

Winterbourn CC (1995) Toxicity of iron and hydrogen peroxide: the Fenton reaction. Toxicology Letters 82:969-974. DOI:10.1016/0378-4274(95)03532-X

Yoon S, Nissen S, Park D, Sanford RA, Löffler FE (2016) Nitrous oxide reduction kinetics distinguish bacteria harboring clade I *NosZ* from those harboring clade II *NosZ*. Applied and Environmental Microbiology 82:3793-3800. DOI:10.1128/AEM.00409-16

Yoon SH, Ha SM, Lim J, Kwon S, Chun J (2017) A large-scale evaluation of algorithms to calculate average nucleotide identity. Antonie Van Leeuwenhoek 110:1281-1286. DOI:10.1007/s10482-017-0844-4

Yu Y, Lee C, Kim J, Hwang S (2005) Group-specific primer and probe sets to detect methanogenic communities using quantitative real-time polymerase chain reaction. Biotechnology and Bioengineering 89:670-679. DOI:10.1002/bit.20347

Yu-Wei Wu, Blake A, Simmons S, Singer W (2016) MaxBin 2.0: an automated binning algorithm to recover genomes from multiple metagenomic datasets. Bioinformatics 32:605-607. DOI:10.1093/bioinformatics/btv638

Zhang H, Yohe T, Huang L, Entwistle S, Wu P, Yang Z, Busk PK, Xu Y, Yin Y (2018) dbCAN2: a meta server for automated carbohydrate-active enzyme annotation. Nucleic Acids Research 46:95-101. DOI:10.1093/nar/gky418

Supplementary Information

N_2O-respiring bacteria in biogas digestates for reduced agricultural emissions

Kjell Rune Jonassen, Live H Hagen, Silas HW Vick, Magnus Ø Arntzen, Vincent GH Eijsink, Åsa Frostegård, Pawel Lycus, Lars Molstad, Phillip B Pope, Lars R Bakken

Correspondence to: lars.bakken@nmbu.no

This Supplementary Online Material contains 7 sections:

A. Gas kinetics during enrichment culturing

This section provides details of the gas kinetics and modelled bacterial growth for anaerobic enrichment culturing with N_2O, as well as gas kinetics in additional (control) experiments with other electron acceptors and a different (thermophilic) digestate.

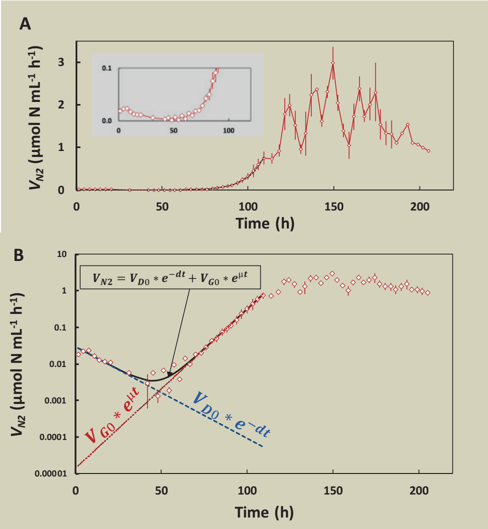

Figure S1: Modelling growth of N_2O reducing bacteria during enrichment by anaerobic incubation of a mesophilic digestate with N_2O, based on measured rates of N_2O reduction to N_2.

Panel A shows measured rates of N_2O reduction to N_2 (***V_{N2}***, µmol N mL^{-1} h^{-1}) in the second enrichment culture experiment (Figure 2BC). The values plotted are average of three replicate enrichment vials, with standard deviation as vertical lines. The insert is scaled to visualize the rates during the first 100 h. The fluctuations after 120 hours are due to episodes of N_2O depletion and subsequent injections of N_2O (see Figure 2B). Panel B shows the same data plotted on a log scale, illustrating that the rate declined exponentially during the first 30-40 h, and increased exponentially from 60 to 110 h. The kinetics suggested the presence of two groups of N_2O respiring organisms: One whose respiration died out gradually during the enrichment (**D**), and one which was growing by respiring N_2O (**G**). To assess the respiration kinetics of **D** and **G**, the following model was used:

$$V_{N2} = V_D + V_G = V_{D0} * e^{-dt} + V_{G0} * e^{\mu t}$$

where V_D is the rate of N_2O-reduction (µmol N mL^{-1} h^{-1}) by **D**, V_{D0} is their rate at time zero, and ***d*** is the first order rate of decline (h^{-1}); V_G is the rate of N_2O-reduction by **G,** and ***µ*** is the growth rate of **G** (h^{-1}). The parameters were estimated by fitting the modeled to the measured data for 0-110 h, using the Generalized Reduced Gradient Solver in Excel, yielding the following results: V_{D0}= 30 nmol N mL^{-1}h^{-1}, V_{G0} = 0.014 nmol N mL^{-1} h^{-1}, ***d***= 0.03 h^{-1}, ***µ***=0.1 h^{-1}. The modelled V_{N2} (black line in panel B) fits very well with the data (r^2 = 0.997). The rates of N_2O reduction by the growing and declining groups are shown as red and blue dotted lines.

The estimated growth rate of **G** (***µ***=0.1 h^{-1}) equals the maximum anaerobic growth rate of the model strain *Paracoccus denitrificans* at 20 ^{0}C, as measured by Bergaust et al (2010, 2012), who also determined the growth yield (***Y*** =1.9*10^{13} cells per mol electrons), and the cell specific electron flow rate at µ=0.1 h^{-1} ($V_{e\text{-}max}$= 5.26*10^{-15} mol e$^-$ cell^{-1} h^{-1}). These parameters were used to estimate the number of "*Paracoccus* equivalent" cells in the enrichment culture as shown in Figure 2C in the main paper. For the period 0-110 hours with exponential growth, the cell density was calculated as $N_G(t)$= $V_G(t)/V_{e\text{-}max}$ where $N_G(t)$ is the number of cells mL^{-1} at time t (h) after initiation of the enrichment culturing, $V_G(t)$ is the rate of N_2O-reduction (mol N mL^{-1} h^{-1}) at time t, and $V_{e\text{-max}}$ = 5.26*10^{-15} mol e$^-$ cell^{-1} h^{-1}. The estimated initial number of growing cells ($N_G(0)$) was 2.7*10^3 cells mL^{-1}, and the number after 110 hours ($N_G(110)$) was 1.6*10^8 cells mL^{-1} (numbers are given in Figure 2C in the main paper). After 110 h, the N_2O-reduction rate ceased to increase exponentially, presumably because the provision of electron donors was insufficient to sustain a growth rate of 0.1 h^{-1} for cell densities >1.6*10^8 cells mL^{-1}. Further growth was thus estimated by $N_G(t)$= $N_G(110)$ + **ΔN_2(t)*Y**, where $N_G(110)$ is the cell density reached at t=110 h (1.6*10^{8}mL^{-1}), **ΔN_2(t)** is the cumulated of N_2 produced from 110 h and onwards (mol N mL^{-1}), and **Y** is the growth yield = 1.9*10^{13} cells mol^{-1} N. The cell specific rate of electron flow (V_{e-}, mol e$^-$ cell^{-1} h^{-1}) throughout the enrichment culturing (Figure 2C of the main paper) was calculated by $V_{e-}(t)$= $V_{N2}(t)/N_G(t)$ where **V_{N2}(t)** is the measured rate of N_2 production (mol N mL^{-1} h^{-1}) and $N_G(t)$ is the estimated cell density, both at time t.

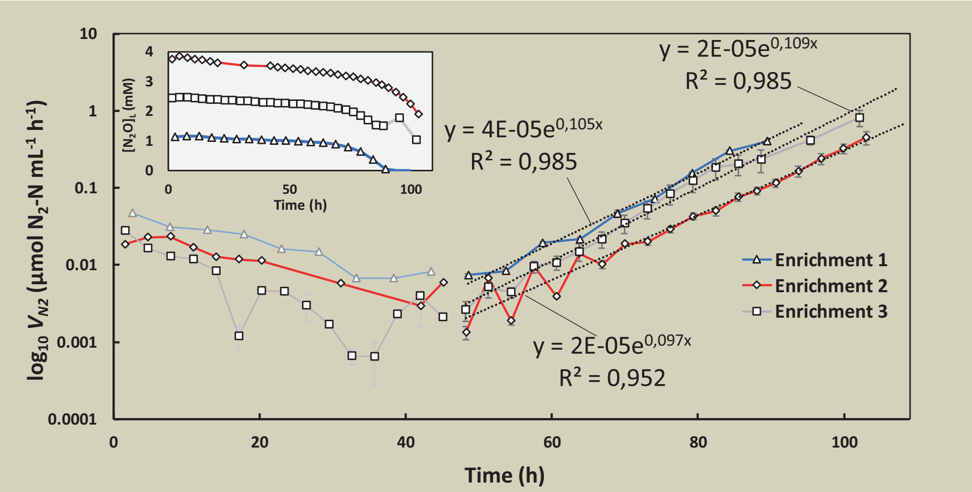

Figure S2: Reproducible N_2 production rates during anaerobic incubation of a mesophilic digestate with N_2O. Several enrichment experiments were run with mesophilic digestates, showing essentially identical N_2 production kinetics, i.e. declining rates during the first 50 hours, followed by exponential increase during the next 50 h. Enrichment 1 is the experiment used for metagenomics and metaproteomics (Figure 2A, main paper). Enrichment 2 is the experiment shown in Figure 2BC (main paper). All three enrichment experiments were equal except for the different initial concentrations of N_2O which were 4, 15 and 9 vol% N_2O in headspace for experiment 1, 2 and 3, respectively. The equilibrium concentrations in the digestate, given the temperature = 20 ^{0}C, are 1.1, 4.2 and 2.5 mM N_2O (Experiment 1, 2 and 3 respectively). In all enrichment experiments there were 3 replicates (vials), and the plotted values are average, with standard deviation as vertical lines. Different initial N_2O concentrations were used (ranging from 1-4 mM in the digestate; see inserted panel), without any significant effect on the N_2 kinetics. The insert shows the concentrations of N_2O in the digestate during the first 100 hours of each enrichment experiment.

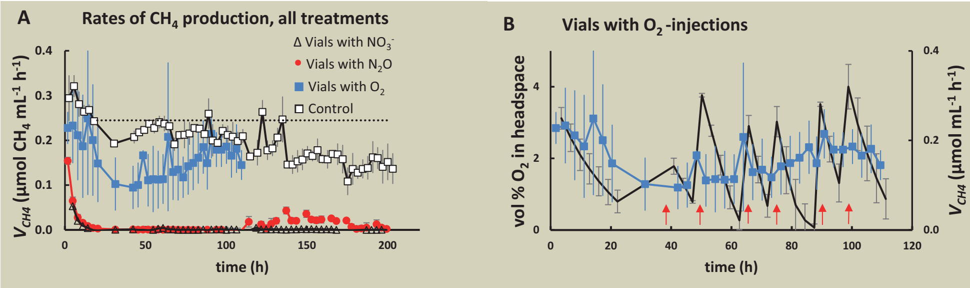

Figure S3: Effects of O_2, NO_3^- and N_2O on methane production. Freshly sampled digestate from the mesophilic anaerobic digester (37 °C) was incubated (20 °C) as stirred batches (50 mL in 120 mL vials, three replicates for each treatment), provided with either O_2, N_2O, NO_3^-, or without any electron acceptors added (=control). Oxygen and N_2O concentrations were sustained by repeated injections, while NO_3^- was supplied by peristaltic pumping of KNO_3 via a needle through the septum (1.57M KNO_3, flow rate 0.02 mL h^{-1} => 31.4 µmol NO_3^- h^{-1}). The vials were monitored for gas concentrations (N_2, NO, N_2O, O_2, CH_4, CO_2) in the headspace. Panel A shows the methane production rate (V_{CH4}) in all treatments (standard deviation shown as vertical lines). While CH_4 production was effectively suppressed by NO_3^- and N_2O, V_{CH4} in the vials with O_2 was 50-75% of that in the control vials (i.e. vials without any electron acceptors, basically resembling the anaerobic digester). The methane production in the mesophilic anaerobic digester was 1.48 µmol CH_4 mL^{-1} h^{-1} (Materials and Methods), which is an order of magnitude higher than the measured production rate in the control treatment. The temperature difference between the digester and the vials could account for this difference; indeed based on the apparent activation energy (Ea) for methane production in anaerobic digesters, determined by Elsgaard et al (2016) to be 80 kJ mol^{-1}, one would predict that the rate declines from 1.48 to 0.24 µmol CH_4 mL^{-1} h^{-1} by the downshift from 37°C (in the digester) to 20 °C (in the vials). This temperature-extrapolated rate of methane production is shown as a dashed line in Panel A. The similarity between the predicted and observed methane production rates in the control vials shows that a competent methanogenic consortium was maintained during culturing at 20 °C. Panel B shows the methane production together with the O_2 concentration in the headspace (vol % O_2) for the vials with oxygen in the headspace (standard deviation as vertical lines). The oxygen concentrations in the headspace fluctuated between 0 and 4 vol % (O_2 injection events marked by red arrows). The low rate of stirring in these experiments (300 rpm), implies relatively slow transport of O_2 from headspace to the liquid, and probably uneven distribution of O_2 within the liquid volume. Hence, there may have been anaerobic zones and microsites within the liquid, which could explain the sustained methanogenesis. The coexistence of aerobic and anaerobic metabolism, including methanogenesis is bioreactors has often been observed, and the inhibitory effect of low concentrations of oxygen on the methanogenesis in bioreactors may be marginal (Botheju and Bakke 2011).

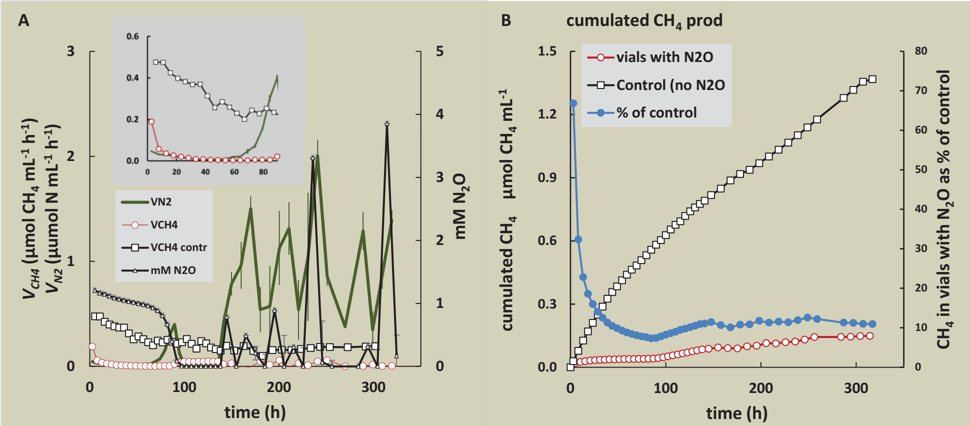

Figure S4: Methane production in the enrichment culture used for metagenomics and metaproteomics. In parallel with the enrichment culturing of N_2O reducers which was used for -omics analyses **(Figure 2A in the main paper),** we monitored control vials (n=3), i.e. vials without N_2O in headspace. Panel A shows the N_2O concentration in the digestate (mM N_2O), the rates of N_2 production (***V_{N2}***) and methane production (***V_{CH4}***) in the vials with N_2O in the headspace, as well as the rate of methane production in vials without N_2O (***$V_{CH4\ control}$***). Panel B shows cumulated CH_4 production in the control vials without N_2O (µmol CH_4 vial^{-1}) and in the vials with N_2O, as well as the latter expressed as % of CH_4 accumulation in the control. The data in panel B show that inhibition of methanogenesis by N_2O was incomplete, the total methane production in the N_2O enrichment vials being ~10 % of that in the control vials. The insert in panel A shows V_{CH4}, $V_{CH4control}$ and V_{N2} (symbols the same as in the main panel) for the first 90 hours. Hypothetically, the apparent N_2O inhibition of methanogenesis could be caused by N_2O-driven methanotrophy (N_2O replacing O_2 as co-substrate for methane monooxygenase), but if so, the oxidation of 1 mole CH_4 would reduce 2 mol of N_2O to N_2, i.e. **V_{N2}** =2*(**$V_{CH4control}$** -**V_{CH4}**). The inserted panel shows that the measured rates of N_2O-reduction was clearly insufficient, and the hypothesis must be rejected.

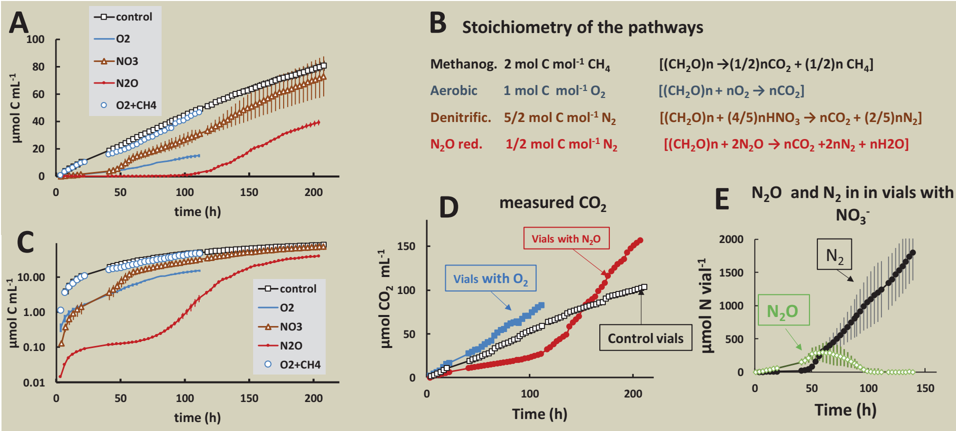

Figure S5: Estimated carbon mineralization with different terminal electron acceptors: O_2, N_2O, NO_3^- and CO_2. The Figure shows the effect of O_2, N_2O and NO_3^- on apparent C-mineralization rates for the experiment presented in Figure S3. Panels A and C show the estimated C-mineralization for the different pathways (linear and logarithmic scale, in A and C, respectively), based on measured gas consumption/production, and the stoichiometry of the pathways (Panel B). For the vials with NO_3^-, the stoichiometry was corrected for the transient accumulation of N_2O (Panel E), since $NO_3^- \rightarrow 1/2\ N_2$ consumes 5 electrons mol^{-1} N, while $NO_3^- \rightarrow 1/2\ N_2O$ consumes only 4. While N_2O and NO_3^- effectively inhibited methane production, this was not the case for O_2 (See Figure S3). For this treatment, two curves are shown (Panel A & C): one for the aerobic pathway alone (blue, marked O_2 in the legend), and one for the sum of aerobic respiration and methanogenesis (marked O_2+CH_4 in legend). This shows that aerobic respiration accounts for approximately 50% of the C mineralization.

Panel D: Estimated CO_2 production based on measure CO_2 in headspace. The values are uncertain, because the digestate contained large amounts of CO_2 and HCO_3^- when sampled (high partial pressure of CO_2 in the digester), and the pH in the digestate was high (7.6), which means that minor changes in pH throughout the incubation would affect the proportion of CO_2 present as HCO_3^- in the liquid. Nevertheless, the estimated of CO_2 production showed similar contrasts between treatments as the estimates based on stoichiometry (Panel A): both show a retarded mineralization in the N_2O treatment during the first 100 h compared to the control and the oxic treatment. No estimates could be made for the treatment with NO_3^- because denitrification raised the pH (measured only at the end), causing declining CO_2 concentrations in the headspace.

Panel E: Transient accumulation of N_2O during the incubation with NO_3^-. During the first 50 h, NO_3^- was reduced to N_2O exclusively, reflecting that in the original digestate, bacteria that reduce NO_3^- to N_2O outnumber those that are able to reduce N_2O to N_2. This is corroborated by the estimated C kinetics shown in Panel A-D (early onset of mineralization based on NO_3^- reduction while that based on N_2O reduction was initially very slow).

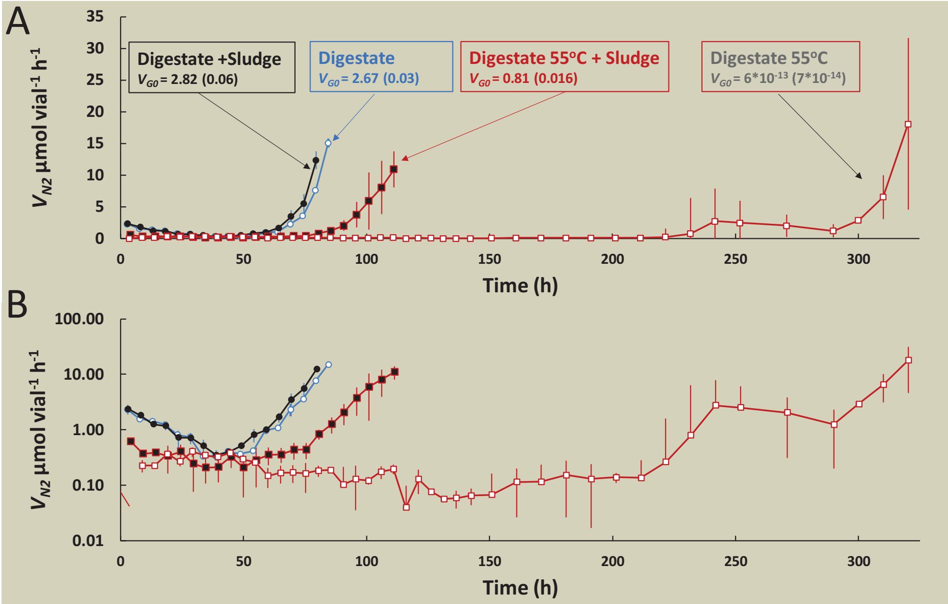

Figure S6: Comparison of N_2O reducing bacteria in raw sludge and the digestate. We hypothesized that only a fraction of the N_2O-reducing bacteria in the sludge would survive the passage through the anaerobic digester, and checked this by investigating the N_2O reduction kinetics in enrichment cultures with digestate, and digestate which had been heated to 55 ^{0}C, with and without the addition of raw sludge (50 mL digestate +/- 1 mL raw sludge in each vial). The panel shows the measured rate of N_2 production (with standard deviation, n=3) for the four treatments. As in Figure S1, we estimated the initial rate of N_2O reduction as a proxy for the density of N_2O-reducing bacteria, using the same model:

$$V_{N2} = V_D + V_G = V_{D0} * e^{-dt} + V_{G0} * e^{\mu t}$$

The model was fitted to the data for each single vial, using the Generalized Reduced Gradient Solver in Excel, resulting in three independent estimates of V_{G0} for each treatment (one for each replicate vial). Panel A shows measured V_{N2} for all treatments plotted against time (average values, standard deviation as vertical lines, n=3). The boxes show the average estimated initial rates V_{G0} as µmol N vial^{-1} h^{-1}, with standard deviations in parenthesis (n=3). Panel B shows the same data with a log scaled Y-axis.

V_{G0} in the 1 mL sludge added can be estimated by the increase in V_{G0} by adding 1 mL sludge to the digestates:

Unheated digestate: $V_{G0\_sludge} = V_{G0\_digestate+sludge} - V_{G0\text{-}digestate}$ = 0.15 µmol N mL^{-1} sludge h^{-1}

Heated digestate: $V_{G0\_sludge} = V_{G0\_digestate55+sludge} - V_{G0\text{-}digestate55}$ = 0.81 µmol N mL^{-1} sludge h^{-1}

The two V_{G0_sludge} estimates are very different, but they are both much higher than $V_{G0\text{-}digestate}$, which was 2.67 µmol N vial^{-1} h^{-1} (panel A) = 0.05 µmol N mL^{-1} digestate h^{-1}. The fraction of N_2O reducers which survives the passage of the anaerobic digester is estimated by **F=** $V_{G0\text{-}digestate}/V_{G0\_sludge}$, and F= 0.33 and 0.06 (based on the two widely different estimates of V_{G0_sludge}. A reasonable conclusion is that ≤1/3 of the viable N_2O-reducing organisms in the sludge survived the anaerobic digestion.

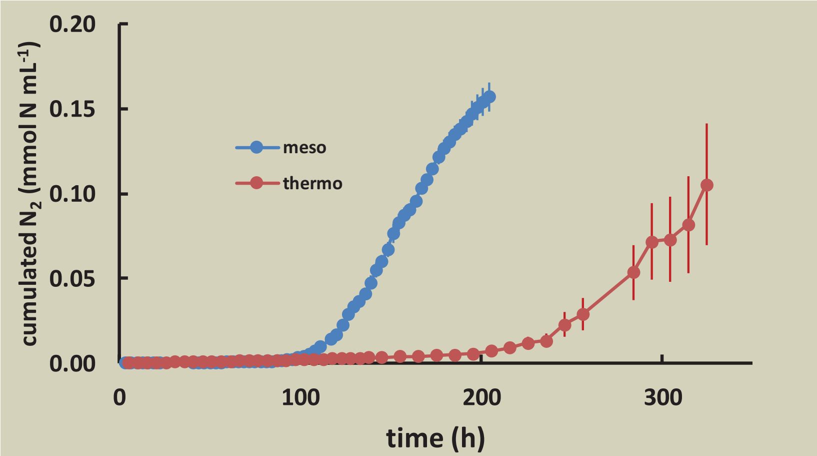

Figure S7: Comparison of digestates from a mesophilic and a thermophilic digester. We sampled digestates from the mesophilic and thermophilic digesters (37 °C and 52 °C respectively, both fed with the same sewage sludge), and incubated them anaerobically with N_2O at 20 ºC as in previously presented experiments (**Figure 2** main paper, **Figures S1-5**). Measurements of N_2 production (this Figure) showed that the thermophilic digestate contained orders of magnitude lower number of N_2O-respiring organisms than the mesophilic digestate.

B. Growth and decline of members of the microbial consortium

This section provides data regarding the growth or decline of different members of the microbial consortium of the digestate based on the abundance of individual MAGs in the metagenomes (**Supplementary Data S2)** and metaproteomes (**Supplementary Data S1)** at three timepoints during the enrichment (0, 115 and 325 hours; see Figure 2 and 3 in main paper).

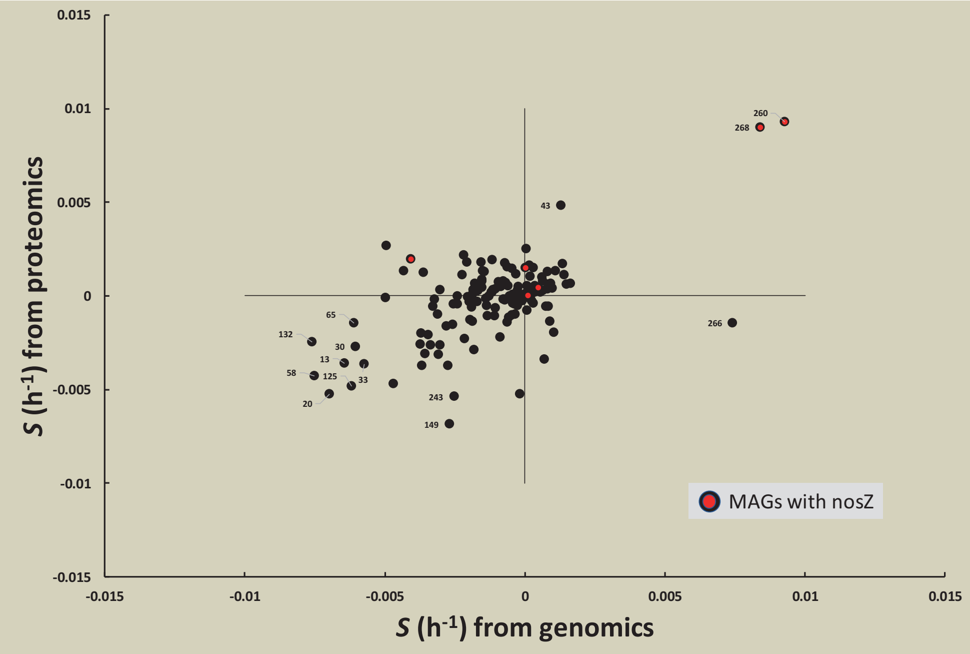

Figure S8: Abundance of MAGs during enrichment culturing. To assess how enrichment culturing with N_2O affected the abundance of members of the microbial consortium, we used the metagenomic and metagenomic data to calculate the relative increase of each MAG: $S = \frac{q}{\overline{x}}$, where q is the regression coefficient for x (x=coverage for genomics, sum of LFQ for proteomics) against time and $\overline{x}$ is the average for the MAG (all three time points), thus the unit for S is h^{-1}. The plot shows S from proteomics against S based on genomics for each MAG. MAGs with *nosZ* are marked with red circles. For the majority of MAGs, S ranged from -0.005 to +0.005 h^{-1}, regardless of the assessment method. The identity of the MAGs is shown for MAGS with at least one S-value outside this range. Only two of the MAGs with *nosZ* had S > 0.005 h^{-1} (MAG260 & MAG268). For the organisms without *nosZ*, the average S was -0.0013 h^{-1} for metagenomics data and -0.00045 h^{-1} for metaproteomics data.

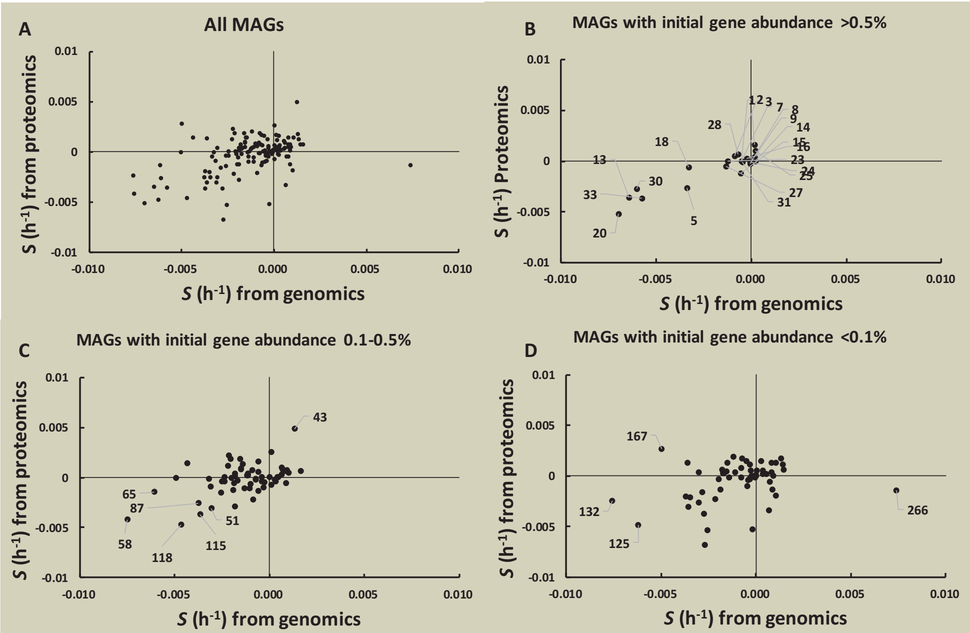

Figure S9: Evaluation of growth/decline of MAGs without *nosZ*, stratified according to relative abundance. To inspect if the growth/decline differed depending on the initial population size, we stratified the MAGs into three groups, i.e. MAGs with initial genomic abundance > 0.5 %, 0.1-0.5 % and < 0.1 %, and plotted the relative increase, *S* (as calculated for Figure S8) as calculated from proteomics against that from genomics. Panel A shows the plot of for all MAGS, and Panels C-D shows the plots for the three strata. The stratification demonstrated no clear relationship between initial abundance and the apparent ability to survive during the enrichment culturing: within each group, the majority of MAGs clustered around zero, while a minority showed a declining trend, both for the genomics and the proteomics.

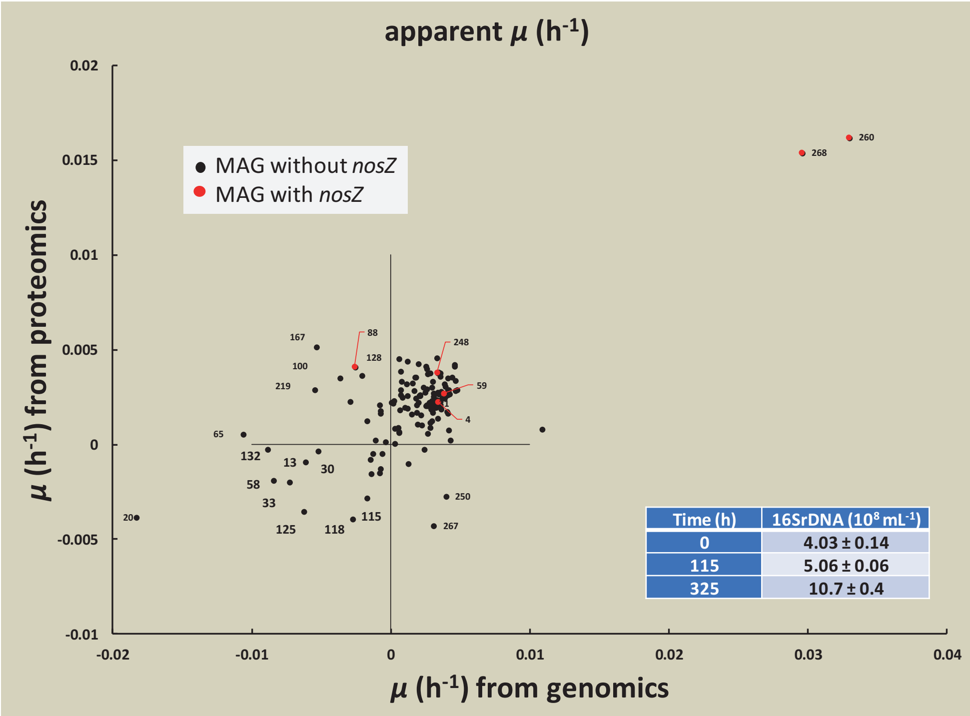

Figure S10: Apparent rate of growth/decline of MAGs by combining -omics and measured abundance of 16SrDNA. As a final approach to evaluate growth and decline of specific populations during the enrichment culturing, we combined omics data with 16SrDNA abundance (16S copies mL^{-1} digestate measured by digital droplet PCR, using universal primers), to assess the abundance of individual MAGs and to calculate the apparent growth rates (or decline) during enrichment culturing. Average total 16S rDNA abundance at each time point is shown in the inserted in panel, with standard error (n=3). For each time point (t= 0, 115 and 325 h), the cell density of each MAG was assessed by $\boldsymbol{N_{it}=S_t*C_{it}/\sum C_t}$ where $\boldsymbol{S_t}$ is the measured 16SrDNA abundance at time ***t***, and $\boldsymbol{C_{it}/\sum C_t}$ is the MAG's relative abundance at time t. For genomics, $\boldsymbol{C_{it}}$ = the MAG's coverage at time t, $\boldsymbol{\sum C_t}$ = the total read coverage of all 149 MAGS at time. For proteomics, $\boldsymbol{C_{it}}$ = the pooled LFQ value for the MAG at time t, $\boldsymbol{\sum C_t}$ = the sum of pooled LFQ for all MAGS at time t. The apparent growth/death rate was estimated by the slope of $\mathbf{ln(N_{it})}$ against time (linear regression). The results indicate slight growth (0-0.005 h^{-1}) for the majority of organisms (upper right quadrant), consistent strong growth for *nosZ* encoding MAG260 and MAG268, and consistent decline for 9 MAGs (lower left quadrant). The genomics- and proteomics-based μ were inconsistent for 8 MAGs (upper left and lower right quadrant). The relative abundance of the 9 declining MAGs is listed in **Table S1**). We did not find any convincing common traits between the MAGs that could explain their decline. One possible reason for their declining abundance could be inability to adapt to the lower temperature (20°C in the enrichment culture versus 37°C in the digester).

Table S1: Relative abundance from % total read coverage and % LFQ for MAGs that declined during the enrichment. GTDB classifications were assigned at a phylum level. MAG relative abundance was calculated as % of total read coverage of the 149 MAGs and from relative LFQ%, which denotes the relative protein intensity calculated as % of LFQ assigned to an individual MAG relative to the summed LFQ for the 149 MAGs used to construct the metaproteome database.

MAG ID	GTDB classification (phylum)	Relative abundance (%)			Relative LFQ (%)		
		Time (h)			Time (h)		
		0	115	325	0	115	325
MAG20	Myxococcota	0.764	0.176	0.001	4.076	1.017	0.388
MAG13	Spirochaetota	1.105	0.248	0.052	0.915	0.213	0.209
MAG132	Spirochaetota	0.082	0.004	0.001	0.050	0.026	0.016
MAG30	Spirochaetota	0.511	0.144	0.033	2.895	1.155	0.872
MAG58	Spirochaetota	0.269	0.015	0.005	1.933	0.459	0.330
MAG33	Desulfobacterota	0.531	0.264	0.020	0.339	0.176	0.064
MAG125	Firmicutes	0.104	0.031	0.005	0.510	0.166	0.056
MAG115	Firmicutes	0.108	0.097	0.025	0.135	0.096	0.021
MAG118	Thermotogota	0.105	0.055	0.016	1.386	0.601	0.141

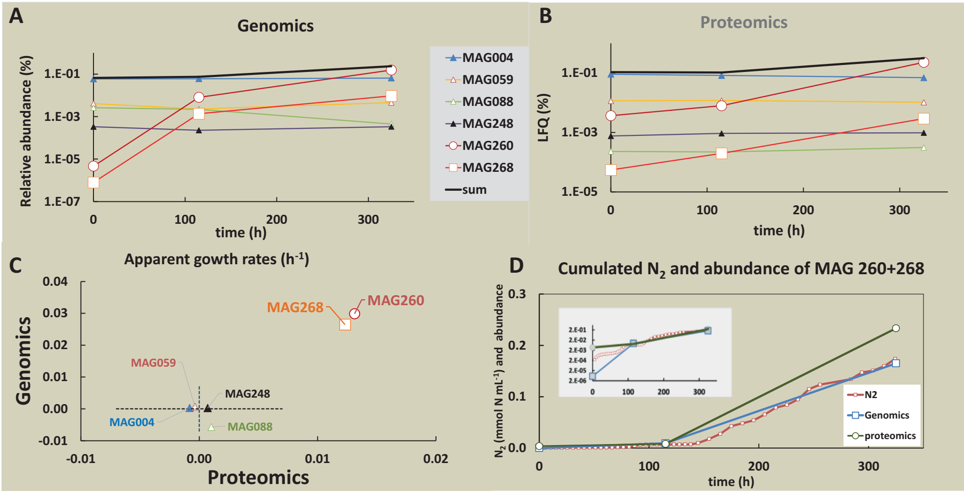

Figure S11: Abundance of MAGs with *nosZ*. Panel A shows the relative abundance of the *nosZ* containing MAGs based on genomics (reads as fraction of the sum of 149 MAGs). Panel B shows the relative abundance based on proteomics (LFQ as fraction of the sum of 149 MAGs). Panel C shows a crude estimate of apparent growth rates based on genomics and proteomics (= slope of ln(N) against time; N=relative abundance). These results demonstrate substantial growth for MAG260 and MAG268, but not for the other MAGs. In panel D, the sum of MAG260 and 268 is plotted against time, together with cumulated N_2 (derived from data shown in Figure 2, main paper). The inserted panel shows the same data on a log scale. This shows that the sum of the abundance of the two MAGs (based on proteomics of genomics) increased as cumulated N_2O-reduction to N_2 increased.

C. Metabolism of the methanogenic consortium

Here we present a metaproteome-centric metabolic map of possible substrate flows in the microbial consortium, and experimental evidence for the predicted effects of N_2O-inhibition of methanogenesis in this consortium: accumulation of volatile fatty acids and hydrogen.

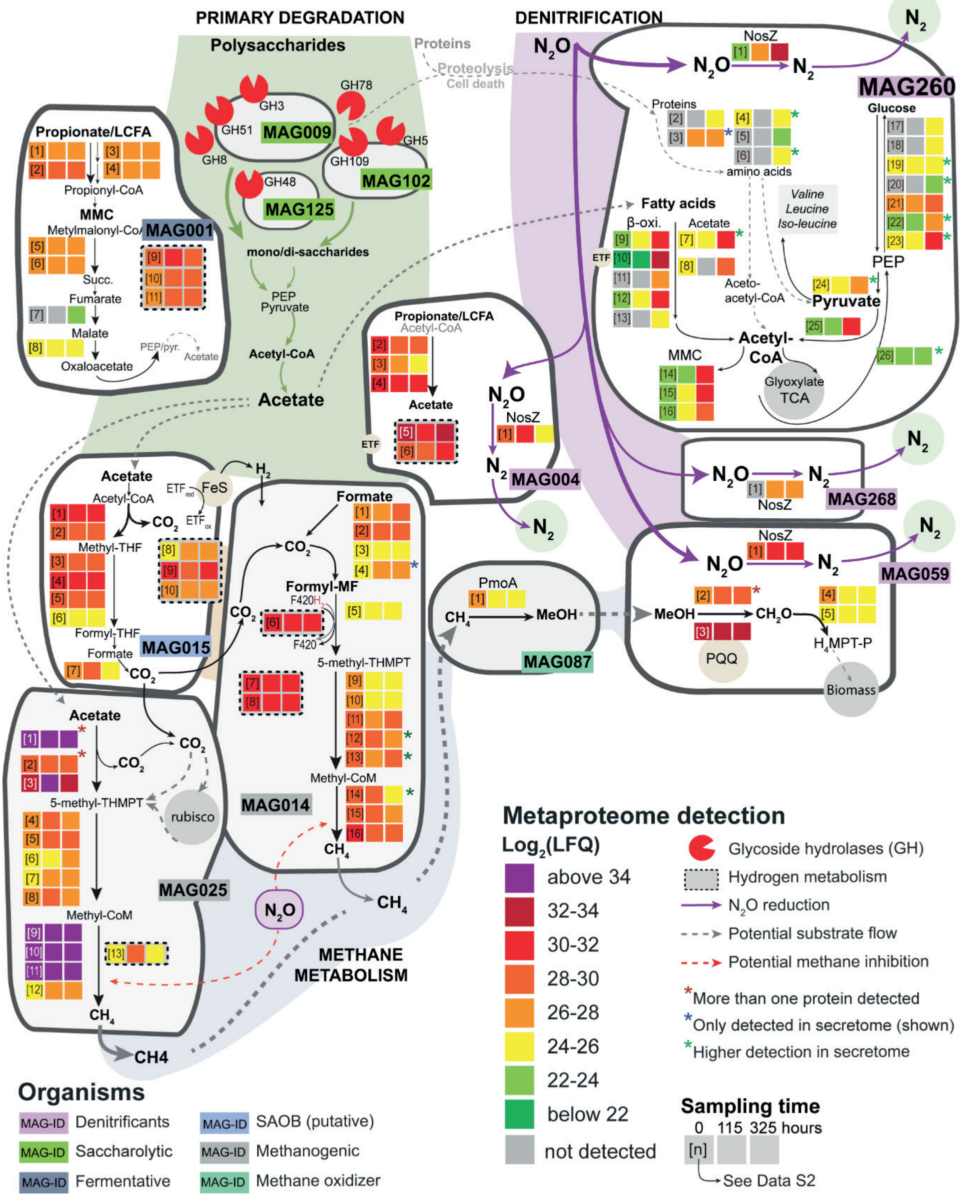

Figure S12: Metaproteome-centric metabolic map of the substrate flow in the microbial consortium. For metabolic reconstruction of the substrate flow, including primary degradation of carbon sources and N_2O reduction, we scanned the detected proteins affiliated to each MAG for enzymes involved in specific metabolic pathways. Detected protein levels (log_2(LFQ)) for the three sampling timepoints (after 0, 115 and 325 hours) are indicated by colored squares, where the number in the first square corresponds to the number in the first column in **Supplementary Data S2**. A variety of carbohydrate-active enzymes (CAZymes), including those active on cellulose (members of GH5, GH8 and GH48) were detected in the metaproteome. Only a selection is shown in the figure; a complete list of detected proteins annotated as CAZymes can also be found in **Supplementary Data S2**. Multiple MAGs also expressed proteins for fermentation processes and production of acetate and propionate. The metaproteome further supported the assumption that these fermentation products are metabolized by a population which included N_2O-reducers, represented by MAG004 and MAG260 in the figure. N_2O has been suggested to inhibit the enzymatic process of methanogenesis (Andalib et al 2011, Kengen et al 1988), which was supported by reduced methane-production rate in the microbial enrichment incubated with N_2O in the current study. Yet, the protein detection level of key enzymes involved in both hydrogenotrophic and acetoclastic methanogenesis (MAG014 and MAG025, respectively) were amongst the highest detected in the metaproteome, even after 115 and 325 hours of incubation. Another MAG with numerous highly detected proteins was affiliated to *Dethiobacteria*, a class recently suggested to encompass syntrophic acetate oxidizing bacteria (SAOBs) (Mosbæk et al 2016, Dyksma et al 2020). This MAG, MAG015, expressed proteins related to the Wood-Ljungdahl pathway (WLP), and combined with the detection of an electron transfer complex (gene cluster encompassing iron-sulfur ferredoxin, coenzyme F_{420} hydrogenase/dehydrogenase, electron transfer flavoprotein) and an aldehyde ferredoxin oxidoreductase for potential acetate activation (Swanson et al 2008, Keller et al 2019) we postulate that also this representative of *Dethiobacteria* might use WLP in a reverse direction to oxidize acetate. This was strengthened by the detection of enzymes central for β-oxidation of longer-chained fatty acids and the detection of the fructose diphosphatase used in anabolic metabolism (i.e., gluconeogenesis). Importantly, SAOBs are depending on an active hydrogen-scavenger population, often hydrogenotrophic methanogens (such as MAG014), to realize the oxidative direction of WLP, which reinforces our observations that the consortium is synergistically producing methane at some capacity. Finally, we detected predicted methane monooxygenase and methanol dehydrogenase proteins from MAG087 and MAG059 (respectively), which leaves tantalizing hypotheses as to the potential role of the methanotrophic community within this enrichment. Methanotrophic processes have recently been shown to be facilitated by the presence of N_2O as a terminal electron acceptor (Valenzuela et al 2020; Cheng et al 2019), but direct links, which may possibly exist within this enrichment, remain to be elucidated.

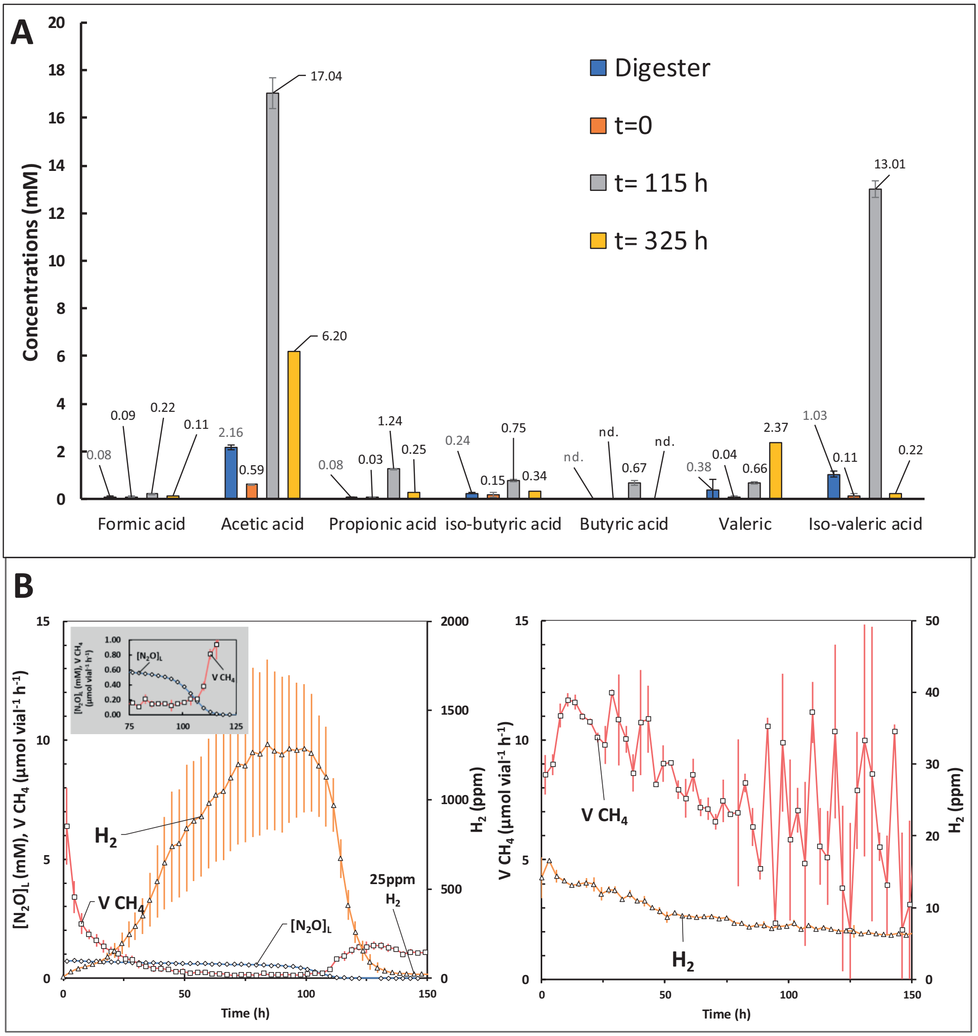

Figure S13: Quantification of volatile fatty acids (VFA) and H_2 during enrichment culturing. Inhibition of methanogenesis by N_2O could result in transient accumulation of intermediates such as VFA (**Figure S12**), which might last until the N_2O-respiring bacteria have become sufficiently numerous to effectively reap these intermediates. H_2 might also accumulate, until the partial pressure of H_2 reaches levels high enough to sustain hydrogenotrophic acetogenesis (Wood-Ljungdahl pathway).

Panel A shows the VFA concentrations (mmol L^{-1}) in samples of digestate directly from the digester (Digester, n=3 replicates, frozen immediately after sampling from the anaerobic digester), and at the three time points (0, 115 and 325 h) of the enrichment culturing experiment number 1, presented in **Figure 2A** in the main paper (n=2 for t=115 h, and 3 for the others). All samples were stored at -80 °C before being prepared for VFA analysis. The lower concentration at the onset of the enrichment culturing (t=0) compared to that in the digester could be due to oxygenation during transport from the WWTP to the laboratory, and to losses due to the He-washing (evacuation and He-filling) prior to enrichment culturing. The results clearly show the expected transient accumulation of VFAs.

Panel B shows the accumulation of H_2 in response to N_2O-mediated inhibition of methane production. This was measured in a repetition of the enrichment culturing shown in **Figure 2** of the main paper, using an improved version of the incubation robot system which measures H_2 by a Plasma Emission detector (PED) (©LDetek). The left panel shows the results for vials with N_2O in the headspace: concentration of N_2O in the liquid, concentration of H_2 in the headspace, and the rate of CH_4 production (V_{CH4}). The insert is scaled to show the onset of CH_4 production in response to N_2O depletion. The right panel shows H_2 and V_{CH4} in vials without N_2O. These results corroborate the hypothesis that H_2 accumulates in response to N_2O-inhibition of methanogenesis, reaching an apparent steady state concentration around 350 ppm in the headspace (P_{H2}=3.5*10^{-4} bar = 0.28 µM H_2 in the liquid).

D. Genetics of isolated organisms

Here, we present the results of genome sequencing of the three isolates, their phylogeny, their core denitrification reductase genes as well as genes coding for peripheral proteins which contributes to the denitrification pathway.

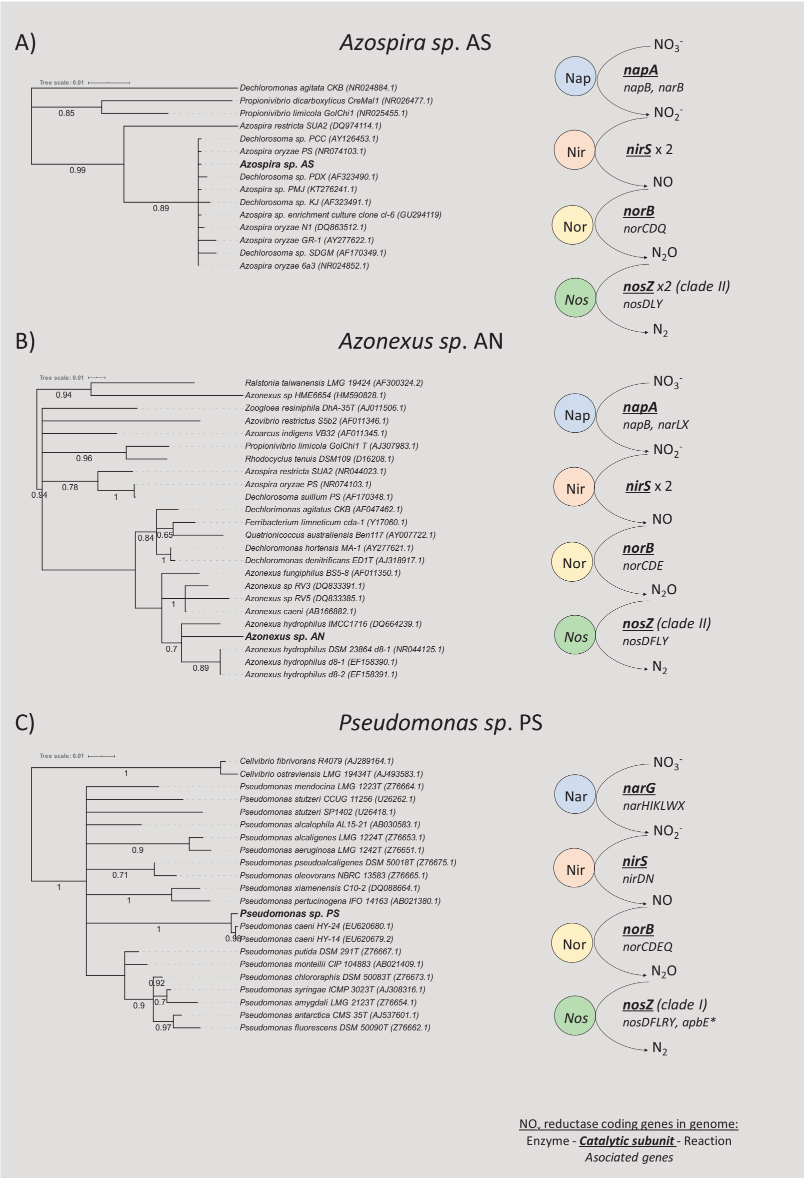

Fig S14: Phylogeny and denitrification genes annotated in draft genomes of isolated organisms. The panel shows the maximum likelihood phylogenetic trees of the three isolates, based on full length 16S rRNA DNA sequences (bootstrap values > 0.6 , 100 resamplings), their core denitrification genes coding for the four denitrification reductases (Nar/Nap, Nir, Nor and Nos), as well as a number of genes coding for peripheral proteins that contribute to a fully functional denitrification pathway (Vaccaro et al 2016). One of these is *nosR,* which was only found in *Pseudomonas sp.* PS. NosR is hypothesized to be involved in electron donation to Nos (Wunsch and Zumft 2005; Zhang et al 2017), but apparently only to Nos Clade I, because organisms with *nosZ clade II* often lack *nosR* (Hein et al 2017), which was the case for the two isolates with nosZ Clade II (AS and AN). *Pseudomonas sp.* PS lacked *nosX*, a flavin donor involved in maturation of norR, but insteadthe *apbE* (coding for flavin transferase, EC: 2.7.1.180) that has been suggested as a flavin donor candidate in maturation via covalent flavinylation of NosR in *Pseudomonas stutzeri* (Zhang et al 2017).

Table S2: QUAST quality parameters, PROKKA annotation summary, CheckM genome quality parameters and coverage of SPAdes assembled contigs of *Pseudomonas sp*. PS, *Azospira sp*. AS and *Azonexus sp*. AN.

	Pseudomonas sp. PS	*Azospira sp.* AS	*Azonexus sp.* AN
	QUAST quality parameters:		
Contigs total:	21	75	59
Largest contig (bp):	778 581	409 855	279 444
Contigs (>= 0 bp):	21	75	59
Contigs (>= 1000 bp)	18	68	48
Contigs (>= 10 000 bp)	13	44	26
Contigs (>= 100 000 bp)	9	11	13
Total length (bp):	3 378 613	3 810 942	2 882 318
N50:	440 975	133 847	176 807
L50:	3	9	7
Predicted genes (>= 300 bp):	2349	3019 + 11 partially	2364 + 6 partially.
GC (%):	47.89	65.42	60.82
Mismatches:			
# N's	195	199	109
# N's per 100 kbp	5.77	5.22	3.78
	SPAdes output		
Coverage (k-mer):	163.8x	59.72x	90.12x
	Prokka annotation summary:		
Number of genes predicted:	3153	3518	2766
Number of protein coding genes:	3104	3461	2713
Number of genes with non-hypothetical function:	2201	2404	1839
Number of genes with EC-number:	1223	1247	988
Number of genes with Seed Subsystem Ontology:	972	995	807
Average protein length:	323	327	319
	CheckM genome quality parameters:		
Marker Lineage	C_Gammaproteobacteria	C_Betaproteobacteria	C_Betaproteobacteria
#Genomes	263	223	233
#Markers	507	424	425
#Marker sets	232	211	211
0	6	0	4
1	498	422	421
2	3	2	0
3	0	0	0
4	0	0	0
5+	0	0	0
Completeness	97.7	100.0	98.1
Contamination	0.89	0.26	0.00

E. Carbon substrate utilization by isolated organisms

Here we show the results of the testing C substrate utilization by the three isolated organisms. The result show that PS (P*seudomonas sp*.) could utilize a wide specter of substrates, although it's capacity to utilize polymers was marginal. In contrast AN (*Azonexus sp.*) and AS (*Azospira sp.*) utilized very few C substrates, primarily intermediates of anaerobic fermentation of a methanogenic consortium.

Table S3: Screening the three isolates for C utilization using Biolog Phenotype MicroArray™ plates PM1 and PM2, which tests the isolates capacity to utilize various C substrates. Positive wells are marked with + (n=3 replicate plates)

PM1	PS	AS	AN	PM2	PS	AS	AN
A2 L-Arabinose				A2 Chondroitin Sulfate C			
A3 N-Acetyl-DGlucosamine	+++			A3 α-Cyclodextrin			
A4 D-Saccharic Acid				A4 ß-Cyclodextrin			
A5 Succinic Acid	+++	+++	+++	A5 γ-Cyclodextrin			
A6 D-Galactose				A6 Dextrin			
A7 L-Aspartic Acid	+++	+++		A7 Gelatin			
A8 L-Proline	+++			A8 Glycogen			
A9 D-Alanine	+++			A9 Inulin			
A10 D-Trehalose				A10 Laminarin	+++		
A11 D-Mannose	+++			A11 Mannan			
A12 Dulcitol				A12 Pectin			
B1 D-Serine				B1 N-Acetyl-DGalactosamine			
B2 D-Sorbitol				B2 N-AcetylNeuraminic Acid			
B3 Glycerol	+++			B3 ß-D-Allose			
B4 L-Fucose				B4 Amygdalin			
B5 D-Glucuronic Acid				B5 D-Arabinose			
B6 D-Gluconic Acid	+++			B6 D-Arabitol			
B7 D,L-α-GlycerolPhosphate	+++			B7 L-Arabitol	+++		
B8 D-Xylose				B8 Arbutin			
B9 L-Lactic Acid	+++	+++		B9 2-Deoxy-DRibose	+++		
B10 Formic Acid				B10 i-Erythritol			
B11 D-Mannitol				B11 D-Fucose			
B12 L-Glutamic Acid	+++	+++	+++	B12 3-0-ß-DGalactopyranosylD-Arabinose			
C1 D-Glucose-6-Phosphate	+++			C1 Gentiobiose			
C2 D-Galactonic Acid-γ-Lactone				C2 L-Glucose			
C3 D,L-Malic Acid	+++	+++	+++	C3 Lactitol			
C4 D-Ribose	+++			C4 D-Melezitose			
C5 Tween 20				C5 Maltitol			
C6 L-Rhamnose				C6 α-Methyl-DGlucoside			
C7 D-Fructose	+++			C7 ß-Methyl-DGalactoside			
C8 Acetic Acid	+++	+++	+++	C8 3-Methyl Glucose			
C9 α-D-Glucose	+++			C9 ß-Methyl-DGlucuronic Acid			
C10 Maltose				C10 α-Methyl-DMannoside			
C11 D-Melibiose				C11 ß-Methyl-DXyloside			
C12 Thymidine	+++			C12 Palatinose			
D1 L-Asparagine	+++			D1 D-Raffinose			
D2 D-Aspartic Acid				D2 Salicin			
D3 D-Glucosaminic Acid				D3 Sedoheptulosan			
D4 1,2-Propanediol				D4 L-Sorbose			
D5 Tween 40				D5 Stachyose			
D6 α-Keto-Glutaric Acid	+++	+++		D6 D-Tagatose			
D7 α-Keto-Butyric Acid				D7 Turanose			
D8 α-Methyl-DGalactoside				D8 Xylitol			
D9 α-D-Lactose				D9 N-Acetyl-DGlucosaminitol			
D10 Lactulose				D10 γ-Amino Butyric Acid			

D11 Sucrose				D11 δ-Amino Valeric Acid			
D12 Uridine	+++			D12 Butyric Acid		+++	+++
E1 L-Glutamine	+++			E1 Capric Acid	+++		
E2 m-Tartaric Acid				E2 Caproic Acid	+++	+++	
E3 D-Glucose-1-Phosphate	+++			E3 Citraconic Acid			
E4 D-Fructose-6-Phosphate	+++			E4 Citramalic Acid			
E5 Tween 80				E5 D-Glucosamine	+++		
E6 α-Hydroxy Glutaric Acid-γLactone				E6 2-Hydroxy Benzoic Acid			
E7 α-Hydroxy Butyric Acid	+++			E7 4-Hydroxy Benzoic Acid			
E8 ß-Methyl-DGlucoside				E8 ß-Hydroxy Butyric Acid		+++	+++
E9 Adonitol	+++			E9 Glycolic Acid			
E10 Maltotriose				E10 α-Keto-Valeric Acid			
E11 2-Deoxy Adenosine	+++			E11 Itaconic Acid			
E12 Adenosine	+++			E12 5-Keto-DGluconic Acid			
F1 Glycyl-L-Aspartic Acid	+++			F1 D-Lactic Acid Methyl Ester			
F2 Citric Acid	+++			F2 Malonic Acid			
F3 myo-Inositol				F3 Melibionic Acid			
F4 D-Threonine				F4 Oxalic Acid			
F5 Fumaric Acid	+++	+++	+++	F5 Oxalomalic Acid			
F6 Bromo Succinic Acid	+++	+++	+++	F6 Quinic Acid			
F7 Propionic Acid	+++	+++		F7 D-Ribono-1,4- Lactone			
F8 Mucic Acid				F8 Sebacic Acid			
F9 Glycolic Acid				F9 Sorbic Acid			
F10 Glyoxylic Acid				F10 Succinamic Acid			
F11 D-Cellobiose				F11 D-Tartaric Acid		+++	
F12 Inosine	+++			F12 L-Tartaric Acid			
G1 Glycyl-LGlutamic Acid	+++			G1 Acetamide			
G2 Tricarballylic Acid				G2 L-Alaninamide			
G3 L-Serine	+++			G3 N-Acetyl-LGlutamic Acid			
G4 L-Threonine	+++			G4 L-Arginine	+++		
G5 L-Alanine	+++			G5 Glycine			
G6 L-Alanyl-Glycine	+++			G6 L-Histidine	+++		
G7 Acetoacetic Acid	+++			G7 L-Homoserine			
G8 N-Acetyl-ß-DMannosamine				G8 Hydroxy-LProline	+++		
G9 Mono Methyl Succinate				G9 L-Isoleucine			
G10 Methyl Pyruvate	+++	+++		G10 L-Leucine	+++		
G11 D-Malic Acid	+++			G11 L-Lysine G			
G12 L-Malic Acid	+++	+++	+++	12 L-Methionine	+++		
H1 Glycyl-L-Proline	+++			H1 L-Ornithine			
H2 p-Hydroxy Phenyl Acetic Acid	+++			H2 L-Phenylalanine	+++		
H3 m-Hydroxy Phenyl Acetic Acid	+++			H3 L-Pyroglutamic Acid	+++		
H4 Tyramine	+++			H4 L-Valine			
H5 D-Psicose				H5 D,L-Carnitine			
H6 L-Lyxose				H6 Sec-Butylamine			
H7 Glucuronamide				H7 D,L-Octopamine			
H8 Pyruvic Acid	+++	+++		H8 Putrescine			
H9 L-Galactonic Acid-γ-Lactone				H9 Dihydroxy Acetone			
H10 D-Galacturonic Acid				H10 2,3-Butanediol			
H11 Phenylethylamine				H11 2,3-Butanedione			
H12 2-Aminoethanol				H12 3-Hydroxy-2- Butanone			

F. Denitrification phenotypes of isolated organisms

Here we present a series of experiments with each of the three isolated organisms, designed to characterize their denitrification regulatory phenotype, with emphasis on regulatory traits that could determine their capacity to function as sinks for N_2O in soil. The section starts with a synopsis of the results, with references to the subsequent figures showing the results of individual experiments.

In these experiments, cells were raised under strict aerobic conditions to secure negligible amounts of denitrification reductases in the cells. They were then inoculated to 120 mL vials with He + ~1vol% O_2 (with or without N_2O) in the headspace, containing 50 mL of Sistrom's succinate medium, either with NO_3^- or NO_2^- (1 mM), and with a Teflon-coated magnetic bars). The vials were placed in the thermostatic water bath (20 ^oC) of the incubation robot, stirred continuously at high speed (700 rpm), and monitored for gas kinetics (O_2, NO, N_2O and N_2) by frequent sampling of the headspace as the culture grows by aerobic respiration, depletes the oxygen and is forced to switch to denitrification. For each gas sample withdrawn, an equal volume of He is returned, and this dilution by sampling is taken into account when estimating the rates of gas production/consumption. Miniscule leakage of N_2 during sampling (40 -100 nmol) is also taken into account. In addition to the automatized gas sampling, small liquid volumes 20-100 µL were withdrawn manually (syringe) for determining the concentration of NO_2^-. The measured concentration of each gas in the headspace is used to calculate its concentration in the liquid, and the molar amount per vial (see Molstad et al 2007).

Each experiment is normally continued until metabolism comes to a halt due to depletion of all electron acceptors, i.e. that the only N-gas present is N_2, and that the production of N_2 comes to a halt (cumulative N_2 reach a stable plateau). NB: cumulative N_2 is total amount of N_2 produced at any time t is $N_t = N_t - N_0 + SN_t - LN_t$, where N_t is measured amount of N_2 (vial^{-1}) at time t, N_0 is the measured initial N_2 in the vial, SN_t is the amount of N_2 removed by all samplings prior to t and LN_t is the amount of N_2 leaked into the vial prior to sampling at time t.

Since the initial concentration of NO_3^-, NO_2^- and N_2O in each vial is known, <u>and</u> that all N-gases (NO, N_2O and N_2) are quantified, N-mass balance can be calculated throughout each experiment. For such mass balance, the sampling loss of N_2O and NO is also taken into account). This is useful for two purposes: 1: to check if the initial amounts of N_2O+NO_3^-+NO_2-N is recovered as N_2-N at the end, i.e. when cumulated N_2 reach a plateau, 2: to estimate the concentration of NO_3^- (or NO_2^-) throughout the incubation by mass balance calculation. For obvious reasons 2) can only be done with confidence if 100 % conversion to N_2 is confirmed, which was the case for all experiments (+/- 5%, ascribed to experimental error).

The convention when reporting the results is to express the amounts of each N-species as molar amounts if N per vial (2 mol N per mol N_2O and N_2!), to make the presentations more transparent with respect to N mass balance (1 mol NO_3^- is converted to 0.5 mol N_2, but 2 mol N_2-N). The concentrations in the liquid are reported conventionally however (ex: 1 nM N_2O is 1 nmol N_2O L^{-1}).

The elaborated routines for calculating rates of production/consumption of each gas has been explained in detail by Molstad et al (2007), and the excel program is freely available (Bakken 2020)

Synopsis of the results

***Azonexus sp*. (AN) Fig S15-17. AN** reduced NO_3^- quantitatively to N_2, with miniscule transient accumulation of N_2O (**Fig S15).** When provided with both N_2O and NO_3^-, all electrons were directed to N_2O reductase until the external N_2O was depleted (**Fig S15ABD**). This was expected since the nitrate reductase in **AN** is periplasmic (Nap), and the study of other organisms with Nap has demonstrated that the electron flow to N_2O reductase (Nos) outcompetes that to Nap when N_2O is available in excess (Mania et al 2020). **AN** was also apparently *bet hedging*: The electron flow rate declined as the culture switched from oxic to anoxic respiration, and increased exponentially therafter (**Fig S15C**), which is the typical pattern for a denitrifying organism that performs *bet hedging*. Such organisms express one (or several) of the denitrification enzymes only in a minority of the cells, as demonstrated for *Paracoccus denitrificans* (Lycus et al 2018). The denitrification kinetics indicate that **AN** is *bet hedging* with respect to nitrate reductase (Nap) (**Fig S15, 16**), i.e. that a minority of cells express Nap, while all cells express Nos and Nir, which was corroborated by proteomic analyses which showed very high Nos/Nap protein abundance ratio after transition to anoxic respiration (**Fig S17**). As a consequence, the majority of cells can only reduce (not produce) N_2O The *bet hedging* with respect to Nap and the strong competitive edge of Nos versus Nap for electrons explains the cultures capacity to keep N_2O extremely low when respiring NO_3^- (**Fig S15**), while producing >3 orders of magnitude more N_2O when provided with NO_2^- (**Fig S16**).

***Azospira* sp. (AS) Fig S18-21.** The phenotype of **AN** was similar to that of **AS**: marginal transient N_2O accumulation when provided with NO_3^- (**Fig S18**), preferential electron flow to Nos versus Nap (**Fig S20**), but not versus Nir (**Fig S21**), and hence higher N_2O accumulation, by 2 – 3orders of magnitude, when provided with NO_2^- compared to NO_3^- (**Fig S19**). The electron flow rate during the transition from oxic to anoxic respiration of NO_3^- showed a modest decline in response to oxygen depletion, suggesting that at least 50% of the cells expressed nitrate reductase (**Fig S18**). In contrast, the transition from oxic to anoxic respiration of NO_2^- was “seamless” (i.e. no depression, **Fig S19**), suggesting that all cells expressed nitrite reductase.

***Pseudomonas sp*. (PS) Fig S22-24.** The electron flow rates in **PS** during the transition from oxic to anoxic respiration suggested *bet hedging* with respect to the expression of nitrite reductase (**Fig S22 panel B2**), but not nitrate reductase (**Fig S22 panel A2**), and the isolate demonstrated fast depletion of externally provided N_2O both in the presence of NO_3^- (**Fig S23**) and NO_2^- (**Fig S24**). The gas kinetics indicate that N_2O reductase in this organism is a very strong sink for electrons, outcompeting both nitrite and nitrate reductase. The steady state N_2O concentration during anaerobic respiration was low: 50 nM whe respiring NO_3^- and 200 nM when respiring NO_2^- (**Fig S24**).

Based on the above phenotypes, **PS** stands out as the most robust N_2O sink in a complex environment like soil, where NO_2^- inevitably will be produced by other organisms, in response to oxygen depletion.

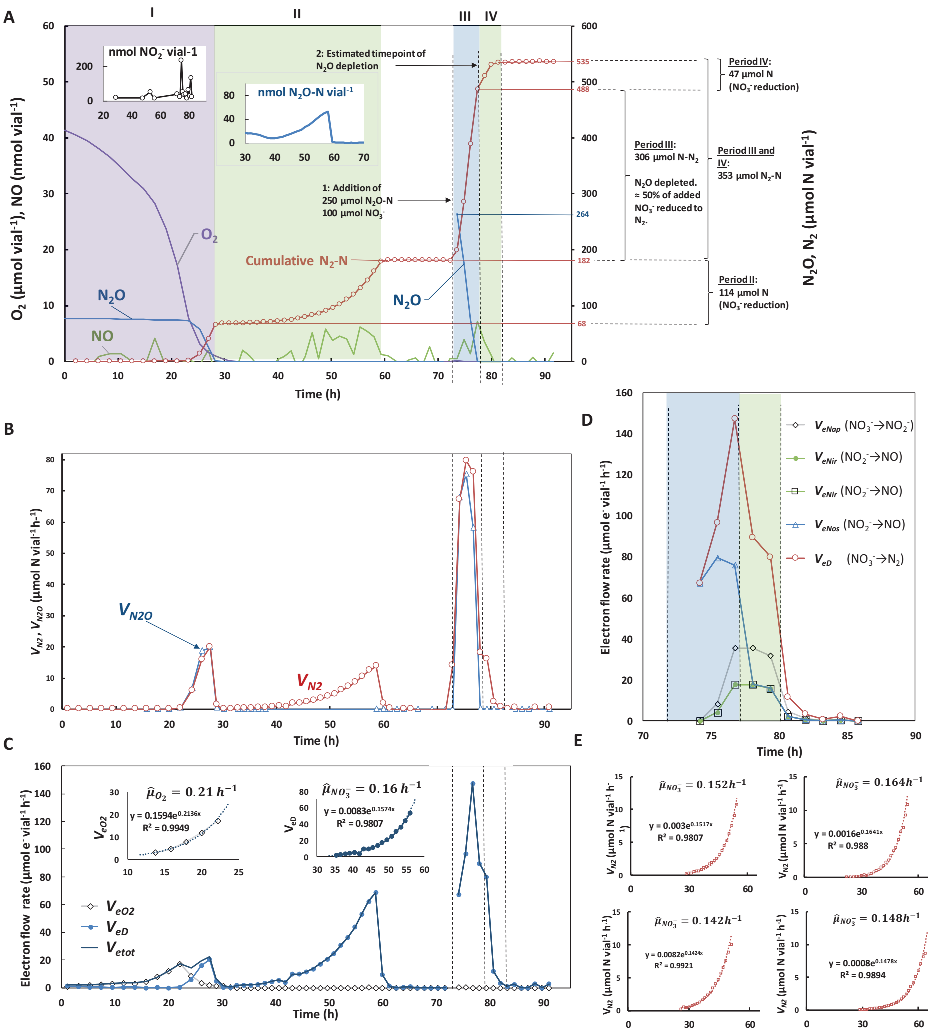

Figure S15: Denitrification phenotype of *Azonexus sp.* (AN) when provided with N_2O and NO_3^-. The panels A-D show kinetics of gases and NO_2^-, calculated electron flow rates and estimation of growth parameters for **AN** grown in gas tight 120 mL vials, initially supplemented with 1 mL O_2, 1 mL N_2O and 2mM NO_3^- in 50 mL Sistrom's succinate medium (headspace volume = 70 mL). The vails were incubated at constant temperature and stirring (20 °C, 700 rpm), and given a dose of 250 µmol N_2O-N, and 100 µmol NO_3^- after 72 hours. All gases are reported in molar amounts per vial.

Panels A-D show results for a single vial (2 replicate vials gave very similar results, except for a time frameshift with respect to NO_3^- reduction). Panel A: measured O_2, NO and N_2O and cumulative N_2 throughout the incubation (cumulative N_2 is the measured N_2 corrected for leakage and loss of N_2 by sampling, see materials and methods). Inserted panels show measured NO_2^- (nmol vial^{-1}) and N_2O (nmol N vial^{-1}). The panel highlights four periods: I, reduction of initial O_2 and N_2O; II, reduction of initial NO_3^-; III, reduction of the injected 250 µmol N_2O-N ; IV, subsequent reduction of the remaining NO_3^- (100 µmol NO_3^- was injected together with N_2O at the beginning of period III). Panel B: N_2 production rate (***V_{N2}***) and N_2O-reduction rate (***V_{N2O}***; this is the rate at which the externally provided N_2O was reduced). Panel C: Electron flow rates: ***V_{eO2}*** is the electron flow rate to terminal oxidases (electron acceptor = O_2), $\boldsymbol{V_{eD}}$ is the electron flow rate to denitrification reductases (electron acceptors= NO_3^-, NO_2^-, NO, and N_2O), $\boldsymbol{V_{etot}}$ = $\boldsymbol{V_{eO2}}$ + $\boldsymbol{V_{eD}}$. The inserted panels show exponential regression of $\boldsymbol{V_{eO2}}$ and $\boldsymbol{V_{eD}}$ against time, thus estimating the aerobic and anaerobic growth rates ($\widehat{\mu}_{O2}$ =0.21 h^{-1}, $\widehat{\mu}_{NO3}$ =0.16 h^{-1}). Panel D: Electron flow rates to individual N-reductases (and the sum of all) during the periods III and IV, illustrating the preferential electron flow to Nos ($N_2O \rightarrow N_2$).

Panel E shows the result of a separate experiment; four replicate vials supplemented with 2 mM NO_3^- and 1 mL O_2 (no external N_2O supplied), and initial OD_{660nm} = 0.0064 (inoculum 1 mL, OD_{660nm}= 0.32). The panels show exponential regression of N_2 production rates for each individual vial. The kinetics of O_2-reduction (not shown) and N_2-production were used to estimate the fraction of cells expressing Nap (F_{den}), using the model of Hassan et al (2016). The F_{den} estimates for the individual vials were 0.12 (vial 1), 0.04 (vial 2), 0.14 (vial 3), and 0.02 (vial 4). The values indicate that **AN** is *bet hedging* with respect to expression of Nap, but that the fraction of cells that express Nap (F_{den}) varied grossly between vials. Estimated F_{den} for 9 individual vials (same type of experiment, results not shown) were done, and the F_{den} estimates ranged from 0.006 to 0.24, average=0.07, stdev=0.08 (result not shown). The NO concentrations during denitrification were invariably low: 0-7 nmol $vial^{-1}$, which is equivalent to 0-5 nM NO in the liquid (1 nmol vial = 0.71 nM in the liquid at the given temperature (20 °C). Likewise, the concentration of N_2O was extremely low during denitrification: in the vials with NO_3^- only (panel E), the N_2O-level was 2-4 nmol N_2O $vial^{-1}$ (=6.4-12.8 nM N_2O in the liquid, 1 nmol N_2O-N vial = 3.27 nM N_2O in the liquid) during the early phase of NO_3^- reduction, increasing gradually to 5-9 nmol N_2O $vial^{-1}$ during the period with exponentially increasing rates of NO_3^- reduction (results not shown). Such gradual increase in N_2O concentration is expected for a *bet hedging* organism which expresses N_2O reductase in all cells and nitrate reductase only in a minority (see Hassan et al 2016).

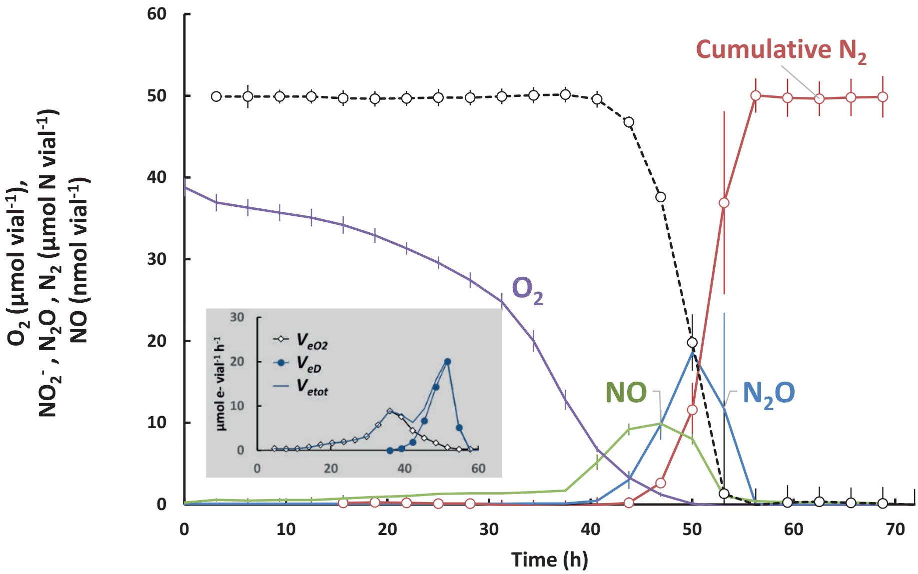

Fig S16: **Denitrification phenotype of *Azonexus sp*. (AN) when provided with NO_2^-.** The experimental conditions were as for **Fig S15**, but with 1 mM NO_2^- = 50 µmol NO_2^- $vial^{-1}$ (no NO_3^-) in the medium. The panel shows measured O_2, NO and N_2O and cumulative N_2 throughout the incubation (cumulative N_2 is the measured N_2 corrected for leakage and loss of N_2 by sampling, see materials and methods), and NO_2^- calculated by N-mass balance (initial NO_2^--N minus N recovered as NO+N_2O + N_2-N), all with standard deviation shown as vertical lines (n=2). Peak NO concentrations were ~10 nmol $vial^{-1}$ (~7 nM in the liquid), which is slightly higher than that in the NO_3^--fed cultures (**Fig S15A**), while the peak N_2O (20 µmol N_2O-N $vial^{-1}$) is >3 orders of magnitude higher than during denitrification of NO_3^- (**Fig S15A**). The inserted panel shows the electron flow rates; $\boldsymbol{V_{eO2}}$ is the electron flow rate to terminal oxidases (electron acceptor = O_2), $\boldsymbol{V_{eD}}$ is the electron flow rate to denitrification reductases (electron acceptors= NO_2^-, NO, and N_2O), $\boldsymbol{V_{etot}}$ = $\boldsymbol{V_{eO2}}$ + $\boldsymbol{V_{eD}}$. The relatively seamless transition to anoxic respiration (indicated by the only marginal depression in $\boldsymbol{V_{etot}}$ at oxygen depletion) suggests that the majority of cells expressed nitrite reductase.

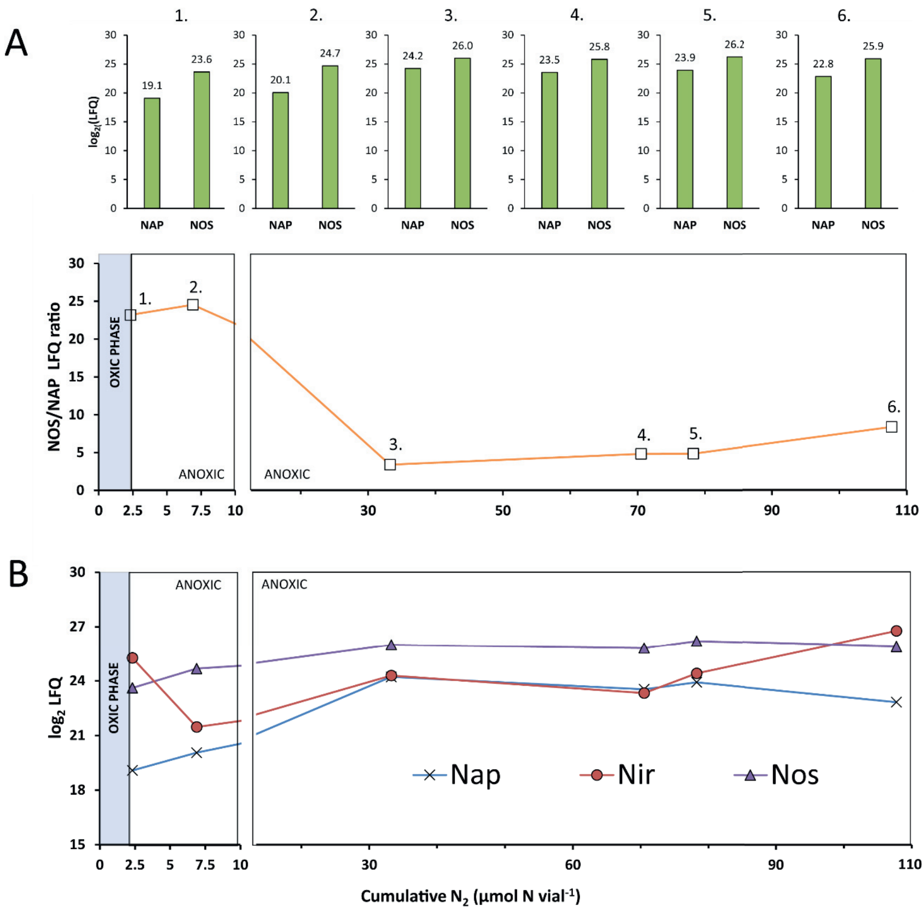

Figure S17: **Quantification of denitrification reductases for *Azonexus* sp. (AN) by proteomics.** Aerobically grown **AN**- cells were inoculated in replicate vials with 50 mL Sistrom succinate medium supplemented with 2 mM NO_3^- and 1 mL O_2 (Initial OD_{660} = 0.003 vial^{-1}), as for the experiment shown in **Figure S15.** Single vials where periodically subjected to destructive sampling and proteomic analysis throughout the incubation (six vials in total, numbered 1- 6). Vial 1 was analyzed at the oxic/anoxic transition (0.7 µM O_2 in the liquid). Relative LFQ values were corrected for nitrogen reductases with multiple identical subunits (NOS and NIR). Panel A: log_2(LFQ) values for Nap and Nos (bars) and their ratio, for each sample plotted against the vial-specific cumulative N_2-N (µmol vial^{-1}) at the time of destructive sampling. Panel B: log_2(LFQ) assigned Nap, Nir and Nos plotted against the cumulative N_2. Nor was only detected in the final sample. Each figure so split in two parts, with different scales for X-axis to improve visibility of the initial changes.

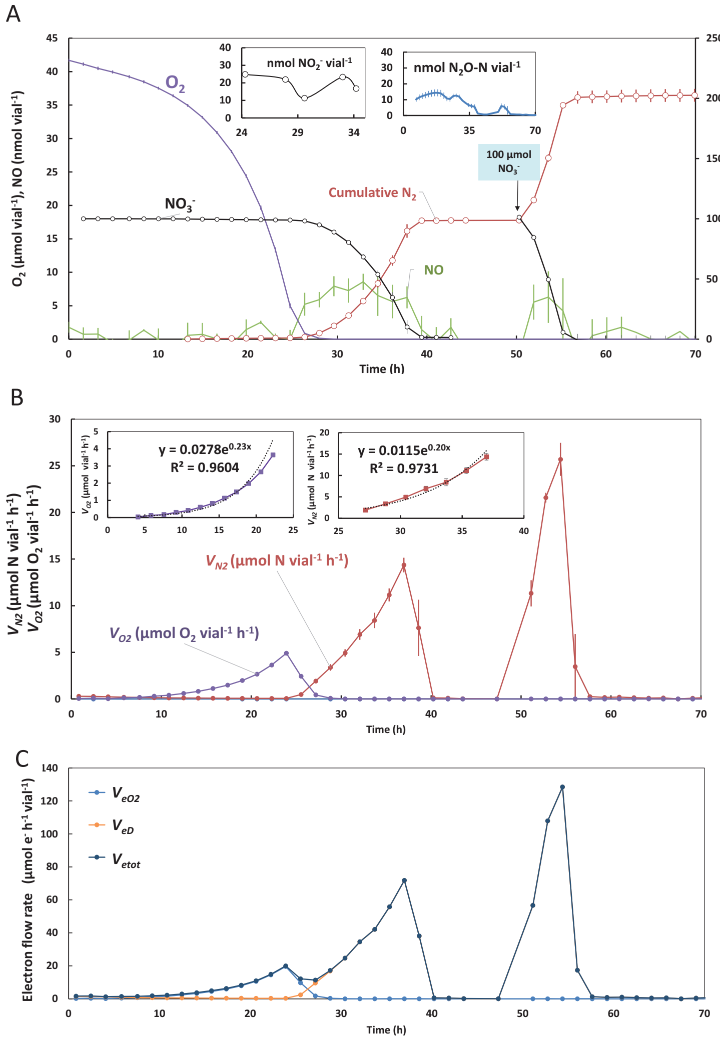

Figure S18: **Denitrification phenotype of *Azospira sp.* (AS), provided with NO_3^-**. The experimental conditions were as for **Fig S15** but without N_2O in the headspace. After 50 h, 100 µmol NO_3^- (to a final concentration of 2 mM) was injected. The initial inoculum had OD_{660} = 0.030 (1 mL added to the 50 mL medium in the vials). Error bars indicate standard deviations (n = 3). Panel A: measured O_2, NO, N_2O, cumulative N_2 and NO_3^- calculated by N-mass balance (initial NO_3^--N minus N recovered as NO+N_2O+N_2-N). Inserted panels show measured NO_2^- (nmol vial^{-1}) and N_2O (nmol N vial^{-1}). All the denitrification intermediates (NO_2^-, NO and N_2O) were extremely low during denitrification. Panel B: Rates of O_2-consumption (***V_{O2}***) and N_2- production (***V_{N2}***). The inserted panels show exponential regression of ***V_{O2}*** (oxic phase) and ***V_{N2}***, estimating aerobic and anaerobic growth rates (0.23 and 0.20 h^{-1}, respectively). Panel C: Calculated electron flow rates: ***V_{eO2}*** is the electron flow rate to terminal oxidases (electron acceptor = O_2), ***V_{eD}*** is the electron flow rate to denitrification reductases (electron acceptors= NO_3^-, NO_2^-, NO, and N_2O), ***V_{etot}*** = ***V_{eO2}*** + ***V_{eD}***. The dip in electron flow in response to oxygen depletion suggests some *bet hedging* with respect to expression of nitrate reductase (i.e. that ~50% of the cells express nitrate reductase). In contrast, a transition to anoxic respiration with NO_2^- showed no depression in electron flow (**Fig S19, panel C**).

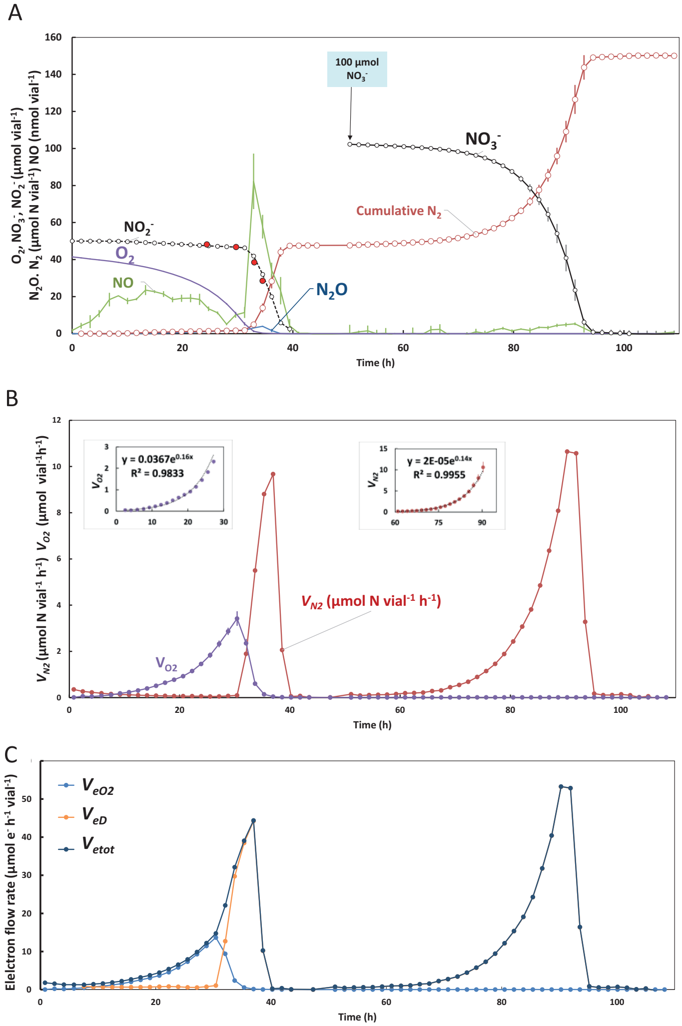

Figure S19: **Denitrification phenotype, *Azospira sp.* (AS), provided with NO_2^-.** The experimental conditions were as for **Fig S15**, but with 1 mM NO_2^- (no NO_3^-). A dose of NO_3^- (100 µmol NO_3^- vial^{-1}) was injected after 50 hours. Error bars indicate standard deviations (n = 3). Panel A: measured O_2, NO, N_2O, cumulative N_2, NO_2^- and NO_3^-. NO_2^- and NO_3^- were calculated by N-mass balance (initial amounts minus N recovered as $NO+N_2O+N_2$). Measured NO_2^- is shown as red dots, which are in good agreement with the values based on mass balance. NO was present throughout the entire oxic phase (~20 nmol vial^{-1} = 15 nM NO in the liquid) and peaked to 80 nmol NO vial^{-1} in response to oxygen depletion. The transient N_2O accumulation during NO_2^- reduction reached 4 µmol N_2O-N vial^{-1} (12 µM in the liquid), which is 3 order of magnitude higher than N_2O during denitrification with NO_3^- (**Fig S18**). The onset of NO_3^- reduction after NO_3^- injection was remarkably slow. Panel B: Rates of O_2-consumption (***V_{O2}***), N_2-production (***V_{N2}***). The inserted panels show exponential regression of ***V_{O2}*** (oxic phase) and ***V_{N2}*** (anoxic phase) estimating aerobic and anaerobic growth rates (0.16 and 0.14 h^{-1}, respectively). Panel C: Calculated electron flow rates: ***V_{eO2}*** is the electron flow rate to terminal oxidases (electron acceptor = O_2), ***V_{eD}*** is the electron flow rate to denitrification reductases (electron acceptors= NO_2^-, NO, and N_2O), ***V_{etot}*** = ***V_{eO2}*** + ***V_{eD}***. The seamless transition from oxygen- to nitrite-based respiration (no depression in ***V_{etot}***) indicate that all cells express nitrite reductase (no *bet hedging*). The response to the subsequent addition of NO_3^- suggests that only a minority of the cells had expressed nitrate reductase, hence, the majority of the cells were unable to utilize nitrate for anaerobic respiration. These cells (without Nap) were likely entrapped in anoxia, without energy to synthesize Nap.

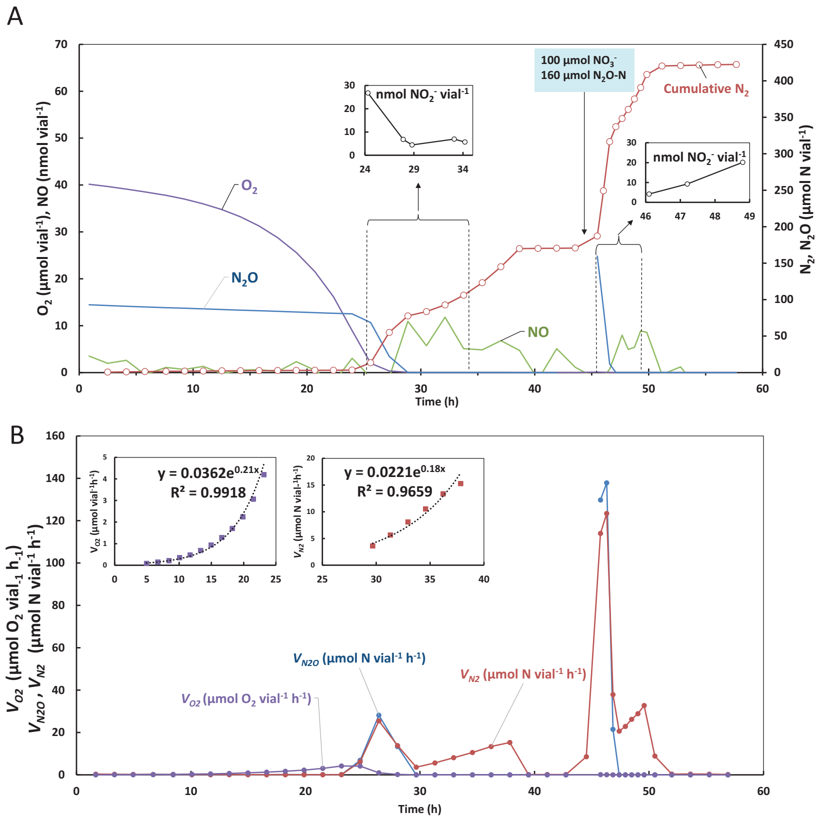

Figure S20: **Denitrification phenotype, *Azospira sp.* (AS), provided with NO_3^- and N_2O**. The experimental conditions were as for **Fig S15** (2 mM NO_3^- and 1 mL N_2O in headspace). 0.3 mL aerobically raised pre culture (OD_{660} = 0.096) was added to 50 mL medium. After 45 hours, a dose of 100 µmol NO_3^- + 160 µmol N_2O-N (per vial) was injected. The initial inoculum had. The panels show results for a single vial. The replicate vial showed very similar gas kinetics, but with a slight time frameshift. Panel A: measured O_2, NO and N_2O and cumulative N_2 production throughout the incubation. Inserted panels show measured NO_2^- (nmol vial^{-1}). Nitrite accumulation was miniscule (inserted panels). Panel B: Rates of O_2-consumption (***V_{O2}***), N_2-production (***V_{N2}***) and N_2O-reduction (***V_{N2O}***). NB: ***V_{N2O}*** is the rate of consumption of externally provided N_2O (positive for N_2O consumption). The rates of N_2 production (***V_{N2}***) equaled the rates of N_2O-consumption (***V_{N2O}***) during depletion of exogenous N_2O. This shows that during the transition from oxic to anoxic conditions, N_2O was converted stoichiometrically to N_2, while nitrate was only reduced after depletion of N_2O. The inserted panels show exponential regression of ***V_{O2}*** (oxic phase) and ***V_{N2}*** (anoxic phase) estimating aerobic and anaerobic growth rates (0.21 and 0.20 h^{-1}, respectively).

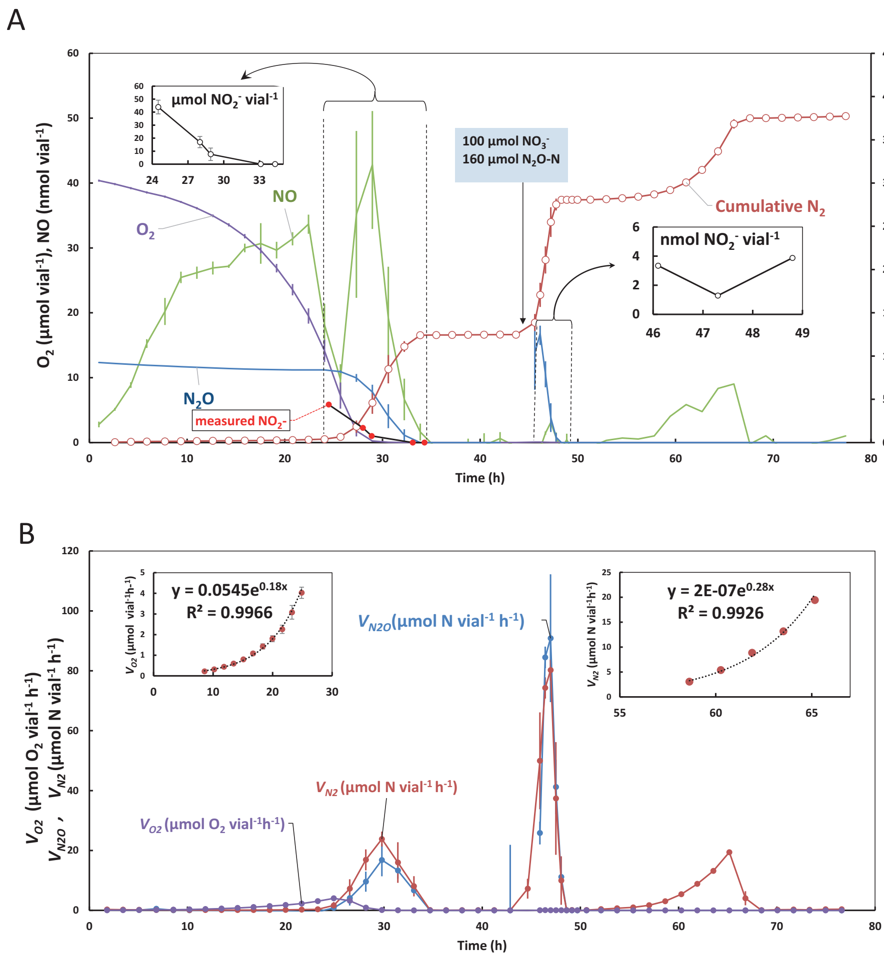

Figure S21: **Denitrification phenotype, *Azospira sp*. (AS) provided with NO_2^- and N_2O.** Experimental condition as for **Fig S15**, but with 1 mL N_2O and 1 mM NO_2^-. After 45 h, a dose of 100 µmol NO_3^- + 160 µmol N_2O-N (per vial) was injected. The panels show the average of two replicate vials. Panel A: measured O_2, NO, N_2O, N_2 (cumulative) and NO_2^-. Measured NO_2^- during the depletion of externally supplied N_2O is shown in the main panel, while the miniscule NO_2^- measured after injection of NO_3^- is shown in the inserted panel. During the transition from oxic to anoxic conditions NO_2^- - and N_2O- was reduced concomitantly. Following addition of 100 µmol NO_3^- and 160 µmol N_2O-N *Azospira* sp. AS quickly reduced exogenous supplied N_2O, but the immediate NO_3^- reduction rates was miniscule and gradually increasing. Panel B: rates of O_2- and N_2O-reduction, and N_2 production. During the depletion of exogenous N_2O with NO_2^- present (time span 22-30h), N_2 production rates clearly exceeded the rates of N_2 production, reflecting concomitant reduction of NO_2^- and the exogenous N_2O. During the depletion of exogenous N_2O in the presence of NO_3^- (time span 42-47 h), the rate of N_2 production did not exceed the rate of N_2O reduction, hence no NO_3-reduction took place. Inserted panels: exponential regression (against time) of the rates of O_2-reduction (oxic phase) and N_2-production.

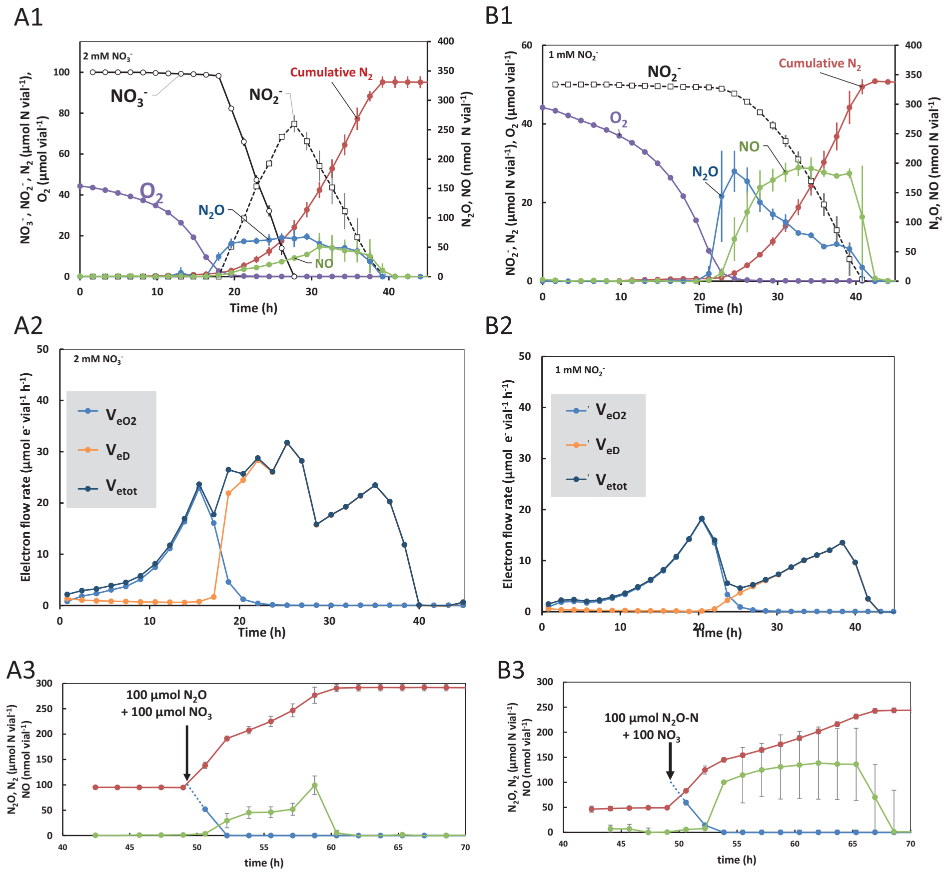

Figure S22: **Denitrification phenotype of *Pseudomonas sp*. (PS), provided with NO_3^- or NO_2^-**. The experimental conditions were as for **Fig S15**; vials, with 50 mL medium were supplemented with 1 mL O_2 and 2mM NO_3^- (=100 µmol NO_3^- vial^{-1} (panels A1&2, n = 3 replicate vials) or 1 mM NO_2^- (Panel B1&2, n = 2 replicate vials). The vials were inoculated with 1 mL of a culture with OD_{660nm} = 0.06. Panel A1: measured gases and nitrogen NO_2^- in vials with 2 mM NO_3^-. The panel also shows NO_3^- calculated by N mass balance (initial amount of NO_3^-- N minus N recovered as (NO_2^-+NO+N_2O+N_2)-N). The figure shows transient nitrite accumulation to 75 µmol vial^{-1}, while the NO and N_2O remained very low (50 nmol NO vial^{-1} ~35 nM in the liquid, 70 nmol N_2O-N vial^{-1} ~ 230 nM N_2O in the liquid). Panel A2 shows the calculated electron flow rates to O_2 (***V_{eO2}***) and to denitrification reductases (***V_{eD}***), and the total electron flow rate (***V_{etot}=V_{eO2}+V_{eD}***). The seamless transition from aerobic respiration to respiration by NO_3^- -reduction (marginal reduction of **V_{etot}**) suggests that all cells express nitrate reductase. The reduction of **V_{etot}** in response to NO_3^- depletion suggest that only a fraction of the cells express nitrite reductase. Panel A3: the vials (Panel A1&2) were given a dose of 100 µmol NO_3^- and 100 µmol N_2O after 49 hours. The kinetics reveal a strong preference for N_2O over NO_3^-.

Panel B1: Measured gases in vials with 1 mM NO_2^-. The panel also shows NO_2^- calculated by N mass balance (initial NO_2^- minus N recovered as (NO+N_2O+N_2)-N minus that. The figure shows that transient accumulation of intermediates reached 200 nmol NO vial (~140 nM in the liquid) and 190 nmol N_2O-N vial^{-1} (~620 nM in the liquid). Panel B2: calculated electron flow rates to O_2 (***V_{eO2}***), to denitrification reductases (***V_{eD}***), and the total electron flow (***V_{etot}***). The dip in the electron flow after the transition from aerobic to anaerobic respiration suggests that only a fraction of cells express nitrite reductase. Panel B3: the vials (B1&2) were given a dose of NO_3 and N_2O after 49 hours.

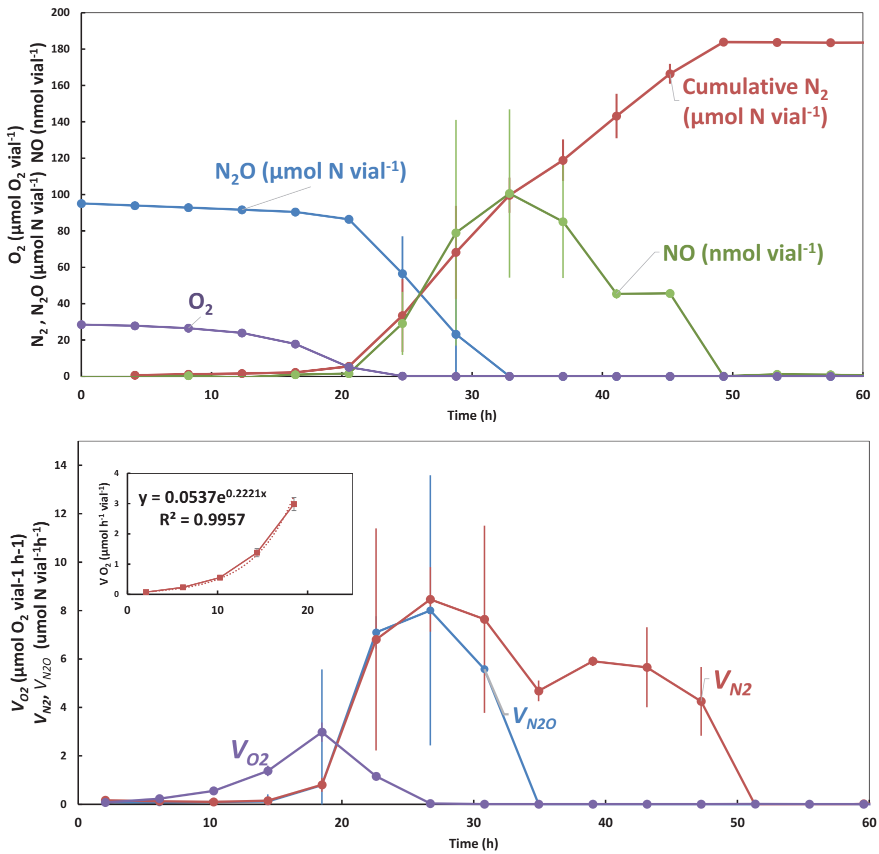

Figure S23: Denitrification phenotype of *Pseudomonas sp.* (PS), provided with NO_3^- and N_2O. Experimental conditions as in **Figure 15** (N_2O in headspace, 2 mM NO_3^- in the medium). Panel A shows measured O_2, NO, N_2O, N_2. Panel B shows rates of O_2-consumption (***V_{O2}***), N_2O consumption (***V_{N2O}***) and N_2-production (***V_{N2}***). Error bars: standard deviation, n = 2. The inserted panel shows estimated aerobic growth rate (exponential regression of O_2 reduction rate against time). The electron flow rates to the individual steps could not be calculated in this experiment because NO_2^- was not measured.

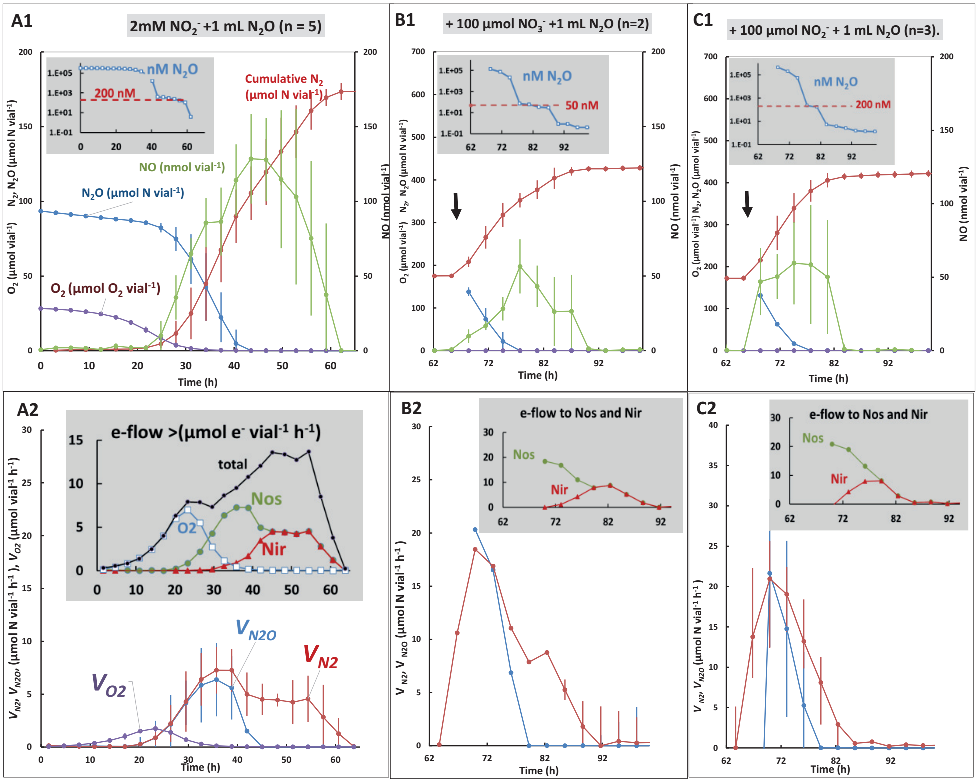

Figure S24: ***Pseudomonas sp*****. PS, elucidating the preference for N_2O versus NO_2^- and NO_3^-.** To assess the preferential reduction of N_2O versus NO_2^- and NO_3^-, we set up an experiment with 5 vials with 2mM NO_2^- and 1 mL N_2O (as **Fig S15**) and monitored the gas kinetics. After depletion of all electron acceptors (N_2O-N + NO_2-N recovered as N_2, Panel A1 and A2), the experiment was continued by injecting more electron acceptors: two of the vials received 100 µmol NO_3^- (2 mM NO_3^-) + 1 mL N_2O (Panels B1 and B2), while three vials received 100 µmol NO_2^- + 1 mL N_2O (Panel C1 and C2). The time of injections are indicated by black arrows (panel B1&C1). Top panels (A1-C1) show measured gases (molar amounts per vial), with inserted panels showing the N_2O concentration in the liquid (nM, log scale), illustrating steady state N_2O concentrations during respiration based on nitrogen oxyanion-reduction alone, i.e. after depletion of the externally provided N_2O (these steady state concentrations are indicated by dashed red lines). These steady state concentrations were ~200 nM when respiring NO_2^- (panel A1 and C1), and ~50 nM when respiring NO_3^- (panel B1), and again 200 nM when respiring NO_2^-. The lower panels (A2-C2) show calculated rates of O_2-consumption (V_{O2}), N_2O-depletion (V_{N2O} = the rate at which exogenous N_2O was depleted), and N_2-production (V_{N2}). Calculated electron flow rates are shown in the inserted panels. The insert in panel A2 shows the electron flow to terminal oxidases (marked O_2), and to the denitrification reductases Nir and Nos and the total (the electron flow to Nor is practically identical with that to Nir since only nanomolar amounts of NO accumulated). The inserts in panel B2 and C2 show electron flow to Nos and Nir only (no oxygen was present in these vials). The electron flow to Nar could not be estimated for (Panel B2) because NO_2^- was not measured.

The initial incubation (Panels A1&A2) demonstrates a strong preference for external N_2O versus NO_2^-, although the electron flow to Nir increased gradually as the concentration of exogenous N_2O declined. In response to a second dose of N_2O + NO_2 (panel C1 and C2), we see the same preference for N_2O versus NO_2^-.

G. Aerobic growth in sterilized digestate, and the effect of the enriched digestate on N_2O emissions

The cultures where grown in pre-aerated digestate and supplied with O_2 as the terminal electron acceptor prior to inoculation in soil (Soil incubations shown in Figure 5 (main paper) and Figure S27 and S28). The pre-aeration, done before inoculation of isolated cultures by blowing air through the sterile digestate suspension for 72 hours, was necessary to secure near-complete abiotic oxidation of the Fe^{2+} in the digestate before inoculation of the cultures ($FeCl_3$ is used at a precipitation chemical at the WWTP, se materials and methods). Fe^{2+} would otherwise obscure the measurements of O_2 consumption, and possibly inhibit aerobic respiration due to formation of reactive oxygen species (Winterbourn 1995).

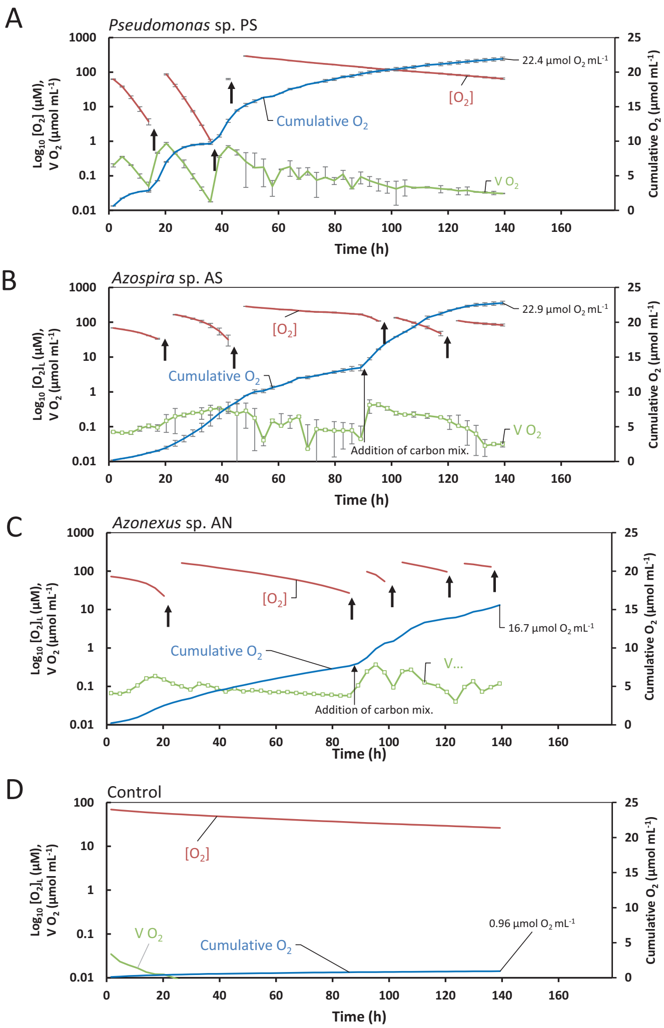

Figure S25: **Aerobic growth in autoclaved digestate.** 1 mL cultures of PS, AS and AN, grown oxicly (air) in stirred (700 rpm) Sistrom medium at 20 °C, were inoculated at 20 °C in closed 120 mL stirred vials (600 rpm) containing

50 mL autoclaved, pre-aerated and pH-adjusted (pH=7.5) digestate and monitored for gas concentrations of O_2 in the headspace. Inoculum OD_{660nm} in digestate was 0.26, 0.12 and 0.30 for cultures PS, AS and AN, respectively. The vials were helium flushed and 5 mL O_2 was added to the headspace before inoculation of the sioaltes. Panels A to D shows calculated liquid concentration of O_2 (µM) and rate of oxygen consumption on the primary y-axis (log_{10} scaled), and cumulative O_2 consumed (µmol mL^{-1}) throughout the incubation for the cultures PS (two replicates), AS (two replicates), AN (single vial) and a control vial containing digestate only (one vial), respectively. Error bars = standard deviation. Fat arrows represent replenishing of oxygen using a syringe piercing the rubber septum of the vials. Liquid concentration of oxygen was not calculable for the timepoint following O_2 addition and is therefore removed. Culture PS (Panel A) consumed significantly more O_2 in digestate compared to cultures AS (Panel B) and AN (Panel C). We therefore added a 1 mL of a carbon mix to vials of AN and PS (point of addition is indicated in panel B and C). The carbon mix contained 0.5 mM glutamate, 0.5 acetate, 0.5 mM puryvate and 0.5 mM ethanol dissolved in sterile water and pH adjusted to 7. The cumulative end point O_2 consumption per mL of digestate suspension is shown in Panel A – D. Assuming growth yields on oxygen to 1.5E14 cells mol^{-1} O_2, as determined for *Paracoccus denitrificans* (Bergaust et al 2010, 2012), and correcting for abiotic oxygen consumption in the control (Panel D) a cell density of 3.2E09, 3.3E09 and 2.4E09 mL^{-1} for *Pseudomonas sp*. PS, *Azospira sp*. AS and *Azonexus sp*. AN, respectively, was estimated.

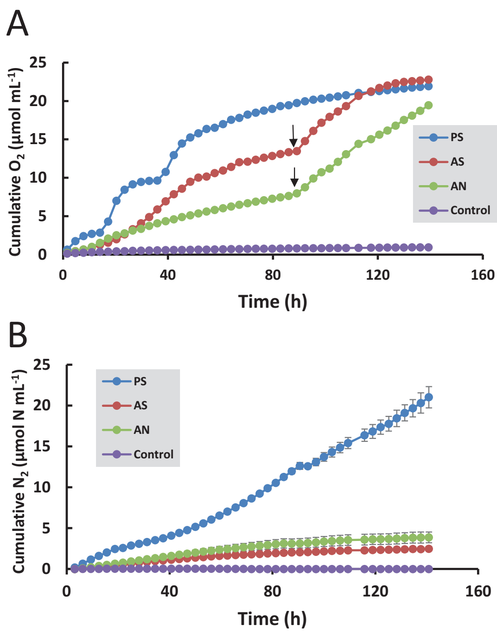

Figure S26. Aerobic and anaerobic growth of isolatess in autoclaved digestates. Panel A shows a compilation of the cumulated O_2 consumption during aerobic incubations, as shown in more detail in Fig S25. The timepoint of adding a carbon substrate cocktail to AS and AN (see Fig. S25) is indicated by arrows. (standard deviation is not included). Panel B shows the cumulated N_2 production in identical corresponding vials, but with a He + N_2O atmosphere. No carbon substrates were added to these vials. Error bars = standard deviation (n = 3).

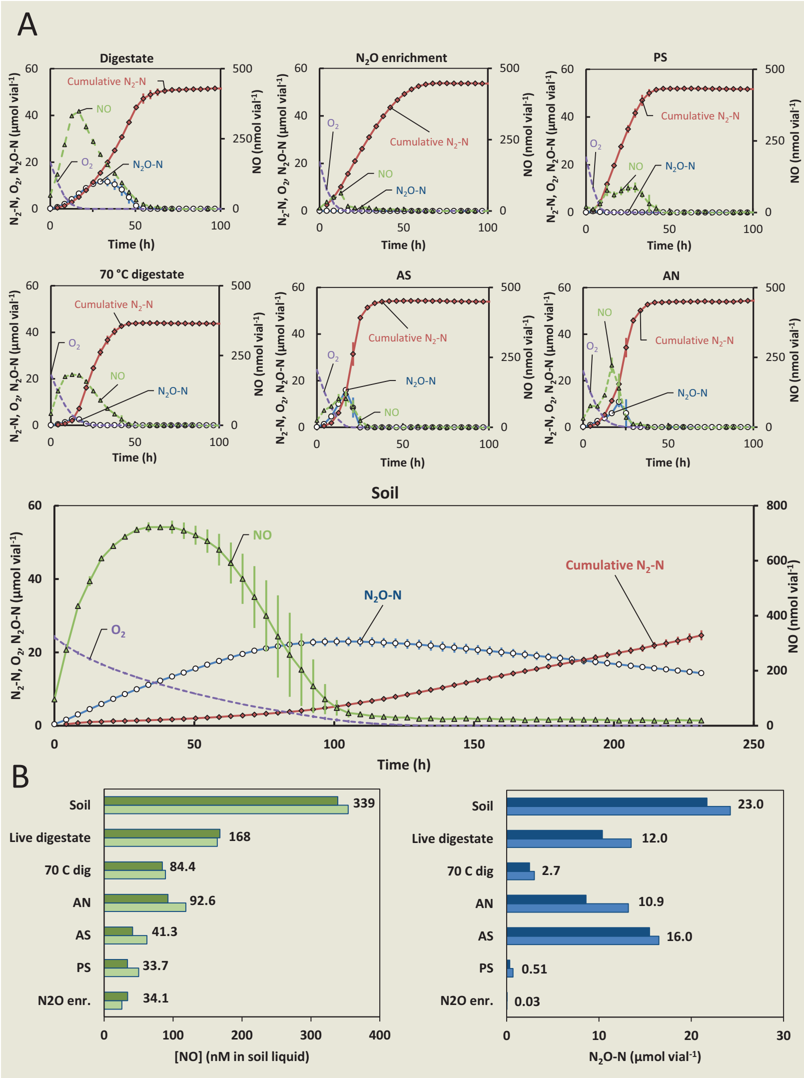

Figure S27: Incubation of digestates treated in various ways with soil with pH=5.5. Panel A: kinetics of O_2, NO, N_2O and N_2 throughout the incubation of soils amended with the various materials (one panel for each amendment) given as molar amounts per vial. The panels show average values (n=2). The initial oxygen (~20 µmol vial^{-1} corresponding to ~0.5 vol% in the headspace) was depleted within the first 20 hours for soils amended with digestates, while soil alone (lower panel) took around 100 hours to deplete O_2. This is due to the boost in respiration that occurs when the carbon-rich digestate is added to the soil. The amounts of O_2, NO and N_2O are as measured, while "Cumulative N_2" denotes the measured N_2 that is corrected for leakage and losses by sampling (see Molstad et al 2007). The N_2 and N_2O kinetics were used to calculate the N_2O index (***I_{N2O}***), which is the area under the N_2O-curve divided by the sum of the areas under the N_2O and N_2-curves for a specific time span. ***I_{N2O}*** values are shown in **Fig 5** (main paper) and provide a proxy for the propensity of the system to emit N_2O. Panel B: peak (maximum) amounts of NO and N_2O (results for single vials, 2 vials per condition; average value indicated). NO is shown as nM in the liquid phase (equilibrium concentrations with measured NO in headspace), while N_2O is shown as µmol N_2O-N vial^{-1}.

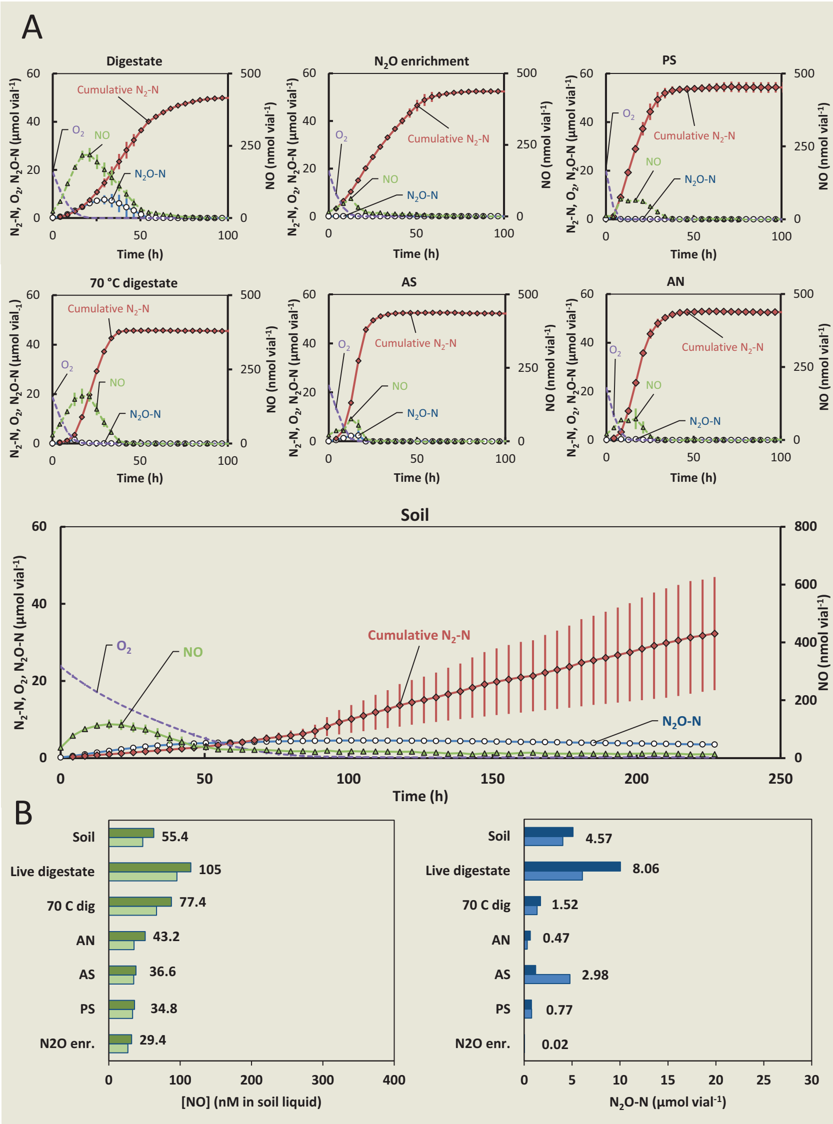

Figure S28: Incubation of isolates and N_2O enriched digestate in soil with pH=6.6. Panel A: kinetics of O_2, NO, N_2O and N_2 throughout the incubation of soils amended with the various materials (one panel for each amendment). Average values shown (n=2). The initial oxygen (~20 µmol vial^{-1}, ~0.5 vol% in the headspace) was depleted within the first 20 hours for soils amended with digestates, while soil alone (lower panel) took around 100 hours to deplete O_2. The amounts of O_2, NO and N_2O are as measured, while "Cumulative N_2" denotes the measured N_2 that is corrected for leakage and losses by sampling (see Molstad et al 2007). The N_2 and N_2O kinetics were used to calculate the N_2O index (I_{N2O}), which is the area under the N_2O- curve divided by the area under the N_2O+N_2 -curve for a specific time span. I_{N2O} values are shown in **Fig 5** (main paper) and is a proxy for the propensity of denitrification to emit N_2O. Panel B: peak (maximum) amounts of NO and N_2O (results for single vials). NO is shown as nM in the liquid phase (equilibrium concentrations with measured NO in headspace), while N_2O is shown as µmol N_2O- N vial^{-1}.

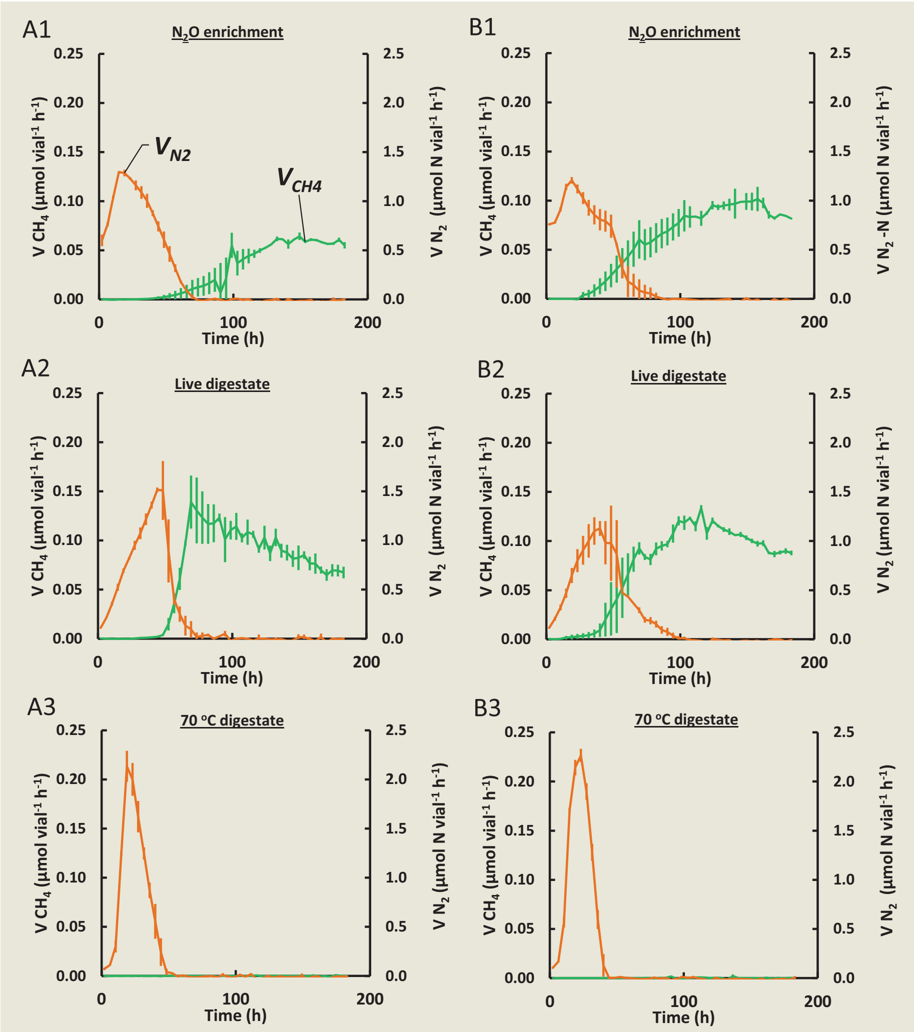

Figure S29: Potential methanogenesis in soil amended with digestates. The panels show the rate of N_2-production (***V_{N2}***) and rate of methane production (**V_{CH4}**) during incubations of soils amended with digestates (see **Figures S27 & S28**). Panels A1-A3 show results for soil with pH 5.5, and panels B1-B3 show results for soil with pH 6.6. The three panels for each soil show the results for 1) soils amended with digestate enriched with N_2O-reducing bacteria "N_2O-enrichment" (Fig 2B, main paper) 2) soils amended with "live digestate" (i.e. digestate taken directly from the anaerobic digester and 3) soils amended with digestate that had been heated to 70 °C for 2 hours. The results demonstrate that the methanogenic consortium of the digestate is alive and active in soil, but evidently suppressed by denitrification: once the nitrogen containing electron acceptors are depleted (V_{N2} approaches zero), methanogenesis resumed. This did not happen in soils amended with the digestate that had been heated to 70 °C and thus likely did no longer contain live methanogenic bacteria.

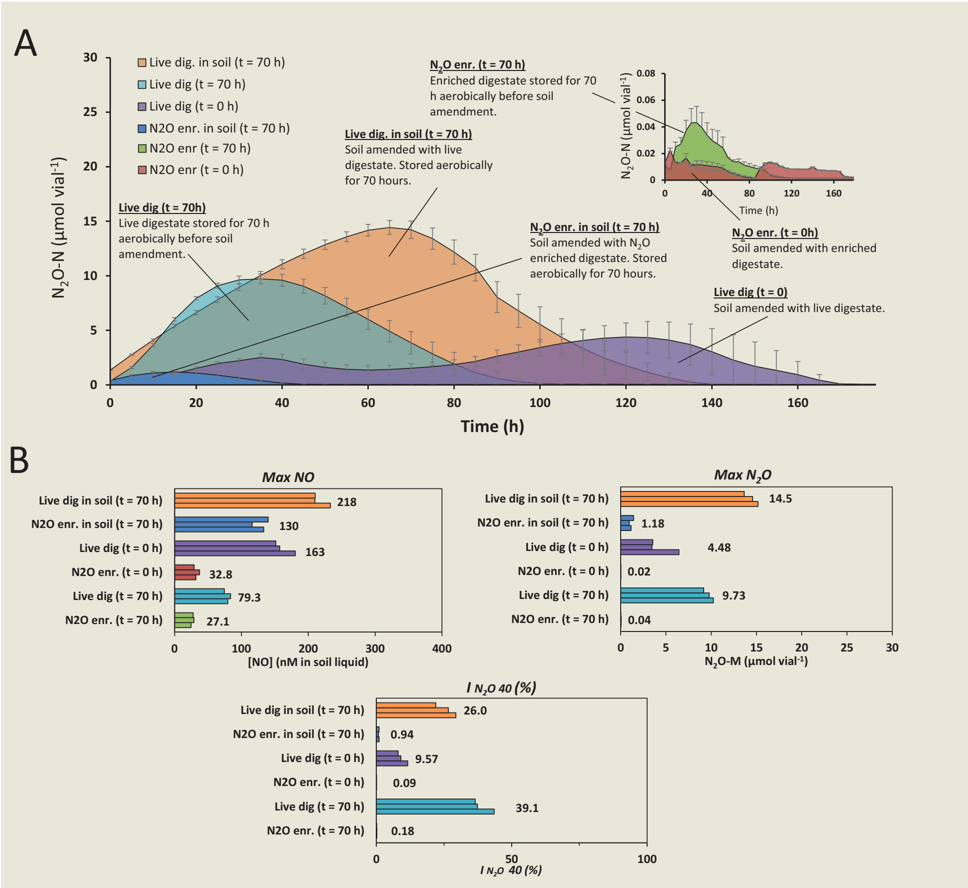

Figure S30: Storage experiment. To test the short term survival of the N_2O-scavenging capacity of N_2O reducers, we added 3 mL freshly sampled live digestate or 3 mL N_2O enriched digestate from the enrichment shown in Figure 2B in main paper to 10 g soil (pH 6.6) in 6 vials of which 3 were incubated anaerobically immediately for measurement of gas kinetics ("Live dig t = 0h" and "N2O enr. t = 0h"), and 3 were stored aerobically (open vials) for 70 hours in soil ("Live dig in soil t = 70h" and "N2O enr. in soil t = 70h") before being incubated anaerobically in the automated incubation and gas analysis system. In parallel, we also stored 50 mL of the freshly sampled digestate and 50 mL enrichment culture aerobically in open vials for 70 hours from which 3 mL digestate was then applied to 10 g soil (pH 6.6) ("N2O enr. t = 70 h" and "Live dig t = 70h"). Aerobic storage of digestates and digestate amended soil was conducted at 20 °C. Monitoring of gas kinetics was conducted at 20 °C. All treatments were supplemented with 50 µmol NO_3^- (50 µL 1 M KNO_3) just before gas analysis in.

Panel A shows the N_2O kinetics for all six soil treatments; the inserted panel shows the results for the two treatments with so low N_2O levels that they would be invisible in the main panel (n=3 for all treatments, standard deviations are shown as vertical bars). Panel B shows maximum NO, N_2O and the N_2O index for 40 % recovery of NO_3^- as N-gases (***$I_{N2O40\%}$***). NO is shown as nM in the liquid phase (equilibrium concentrations with measured NO in headspace), while N_2O is shown as µmol N_2O- N vial^{-1}. The results show that within a time frame of 70 h under aerobic conditions, be it as intact enrichment or after amendment to soil, the capacity to reduce the N_2O/N_2 product ratio of denitrification in soil is sustained.

References

Bakken LR (2021) Spreadsheet for gas kinetics in batch cultures: KINCALC. DOI:10.13140/RG.2.2.19802.36809

Bergaust L, Mao Y, Bakken LR, Frostegård Å (2010) Denitrification response patterns during the transition to anoxic respiration and posttranscriptional effects of suboptimal pH on nitrogen oxide reductase in *Paracoccus denitrificans*. Applied and Environmental Microbiology 76:6387-6396. DOI:10.1128/AEM.00608-10

Botheju D, Bakke R (2011) Oxygen Effects in Anaerobic Digestion – A Review. The Open Waste Management Journal 4:1-19. DOI:10.2174/1876400201104010001

Cheng C, Shen X, Xie H, Hu Z, Pavlostathis SG, Zhang J (2019) Coupled methane and nitrous oxide biotransformation in freshwater wetland sediment microcosms. Science of the Total Environment 648:916-922. DOI:10.1016/j.scitotenv.2018.08.185

Elsgaard L, Olsen AB, Petersen SO (2016) Temperature response of methane production in liquid manures and co-digestates. Science of the Total Environment 539:78-84. DOI:10.1016/j.scitotenv.2015.07.145

Dyksma S, Jansen L, Gallert C (2020) Syntrophic acetate oxidation replaces acetoclastic methanogenesis during thermophilic digestion of biowaste. Microbiome 8:1-14. DOI:10.1186/s40168-020-00862-5

Hassan J, Qu Z, Bergaust L, Bakken LR (2016) Transient accumulation of NO_2^- and N_2O during denitrification explained by assuming cell diversification by stochastic transcription of denitrification genes. PLoS Computational Biology 12:e1004621. DOI:10.1371/journal.pcbi.1004621

Hein S, Witt S, Simon J (2017) Clade II nitrous oxide respiration of *Wolinella succinogenes* depends on the NosG, -C1, -C2, -H electron transport module, NosB and a Rieske/cytochrome *bc* complex. Environmental Microbiology 19:4913-4925. DOI:10.1111/1462-2920.13935

Anja K, Schink B, Müller N (2019) Energy-conserving enzyme systems active during syntrophic acetate oxidation in the thermophilic bacterium *Thermacetogenium phaeum*. Frontiers in Microbiology 10:2785. DOI:10.3389/fmicb.2019.02785

Lycus P, Soriana-Laguna MJ, Kjos M, Richardson DJ, Gates AJ, Milligan DA, Frostegård Å, Bergaust L, Bakken LR (2018) A bet-hedging strategy for denitrifying bacteria curtails their release of N_2O. Proceedings of the National Academy of Sciences USA 115:11820-11825. DOI:10.1073/pnas.1805000115

Mania D, Wolily K, Degefu T, Frostegård Å (2020) A common mechanism for efficient N_2O reduction in diverse isolates of nodule-forming bradyrhizobia. Environmental Microbiology 22:17-31. DOI:10.1111/1462-2920.14731

Molstad L, Dörsch P, Bakken L (2007) Robotized incubation system for monitoring gases (O_2, NO, N_2O, N_2) in denitrifying cultures. Journal of Microbiological Methods 71:202-211. DOI:10.1016/j.mimet.2007.08.011

Mosbæk F, Kjeldal H, Mulat DG, Albertsen M, Ward AJ, Feilberg A, Nielsen JL (2016) Identification of syntrophic acetate-oxidizing bacteria in anaerobic digesters by combined protein-based stable isotope probing and metagenomics. The ISME Journal 10:2405-2418. DOI:10.1038/ismej.2016.39

Swanson MA, Usselman RJ, Frerman FE, Eaton GR, Eaton SS (2008) The iron− sulfur cluster of electron transfer flavoprotein−ubiquinone oxidoreductase is the electron acceptor for electron transfer flavoprotein. Biochemistry 47:8894-8901. DOI:10.1021/bi800507p

Vaccaro BJ, Thorgersen MP, Lancaster WA, Price MN, Wetmore KM, Poole FL, Deutschbauer A, Arkin AP, Adams MW (2016) Determining roles of accessory genes in denitrification by mutant fitness analyses. Applied and Environmental Microbiology 82:51-61. DOI:10.1128/AEM.02602-15

Valenzuela EI, Padilla-Loma C, Gómez-Hernández N, López-Lozano NE, Casas-Flores S, Cervantes FJ (2020) Humic substances mediate anaerobic methane oxidation linked to nitrous oxide reduction in wetland sediments. Frontiers in Microbiology 11:587. DOI:10.3389/fmicb.2020.00587

Wunsch P, Zumft WG (2005) Functional domains of NosR, a novel transmembrane iron-sulfur flavoprotein necessary for nitrous oxide respiration. Journal of Bacteriology 187:1992–2001. DOI:10.1128/JB.187.6.1992-2001.2005

Zhang L, Trncik C, Andrade SL, Einsle O (2017) The flavinyl transferase ApbE of *Pseudomonas stutzeri* matures the NosR protein required for nitrous oxide reduction. Biochimica et Biophysica Acta 1858:95–10. DOI:10.1016/j.bbabio.2016.11.008

Paper II

A novel dual enrichment strategy provides soil- and digestate-competent N_2O-respiring bacteria for mitigating climate forcing in agriculture

Kjell Rune Jonassen[1,2], Ida Ormaasen[1], Clara Duffner[3], Torgeir R Hvidsten[1], Åsa Frostegård[1], Lars R Bakken[1], Silas HW Vick[1*].

[1)] Faculty of Chemistry, Biotechnology and Food Science, Norwegian University of Life Sciences, Norway

[2)] VEAS WWTP, Bjerkåsholmen 125, 3470 Slemmestad, Norway.

[3)] Helmholtz Zentrum München, Deutsches Forschungszentrum für Gesundheit und Umwelt (GmbH), Germany.

* corresponding author

Journal: Water Science, or Environmental science and technology, or ISME

Graphical abstract

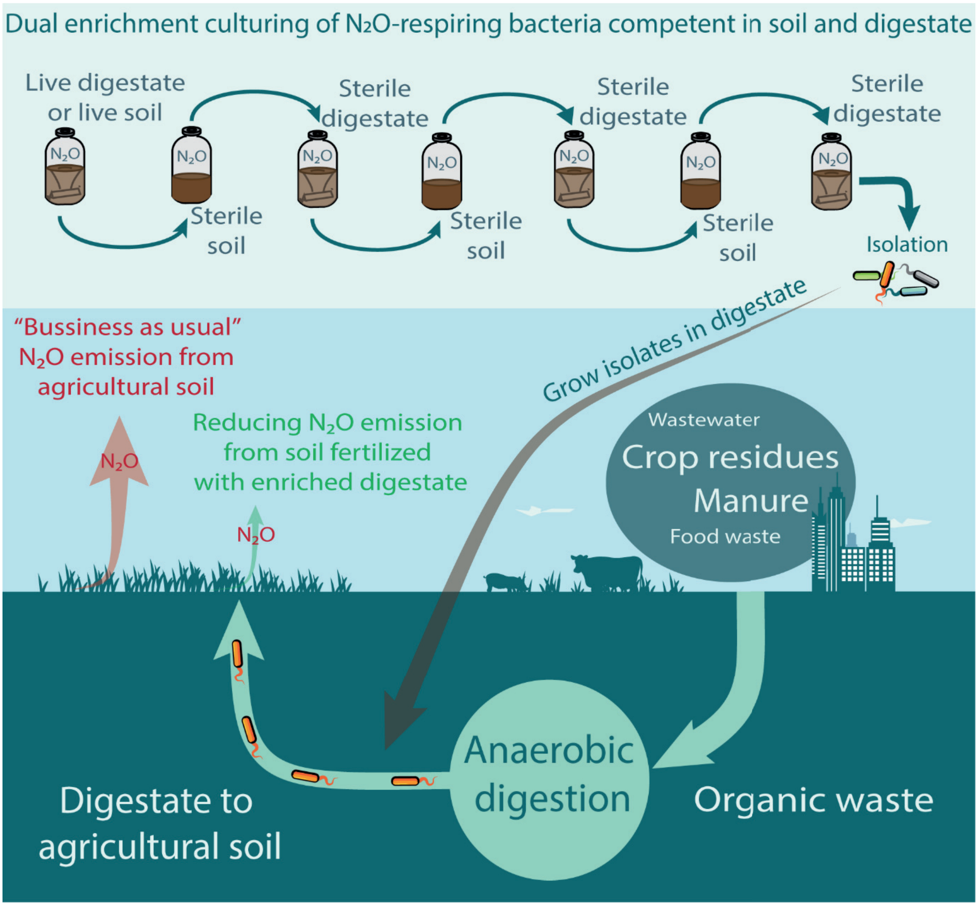

Abstract

Manipulating soil metabolism by heavy inoculation with microbes is deemed realistic if waste from anaerobic digestion (digestate) is utilized as substrate and vector, but requires organisms that can grow both in digestate and soil (=generalist). We designed a strategy to enrich and isolate such generalist N_2O-respiring bacteria (NRB) in soil and digestate, to provide inoculum for reducing N_2O-emissions from agricultural soil. Sequential anaerobic enrichment cultures were provided with a small dose of O_2 and unlimited N_2O, alternating between sterilized digestate and soil as substrates. The cultures were monitored for gas kinetics and community composition (16SrDNA), and cluster-analysis identified generalist-OTUs which became dominant, digestate/soil-specialists which did not, and a majority that were diluted out. Several NRBs circumscribed by generalist-OTU's were isolated, genome sequenced to screen for catabolic capacity, and phenotyped, to assess their capacity as N_2O-sinks in soil. The two isolates *Cloacibacterium* sp., carrying only N_2O-reductase (Clade-II) and *Pseudomonas sp.,* with full-fledged denitrification-pathway, were both very effective N_2O-sinks in soil, with *Pseudomonas* sp., showing a long-lasting sink effect, suggesting better survival in soil. This avenue for utilizing waste to bioengineer the soil microbiota holds promise to effectively combat N_2O-emissions but could also be utilized for enhancing other metabolic functions in soil.

Introduction

The N_2O-concentration in the atmosphere is increasing, largely driven by the input of reactive nitrogen species in agriculture (Davidson 2009, Thompson et al 2019). N_2O-emissions from farmed soils account for 52 % of the total anthropogenic emissions of N_2O (Tian et al 2020) and approximately 1/3 of the climate forcing from food production (Robertson 2014). Limiting the input of reactive nitrogen to soils would be an effective mitigation measure but at the expense of lowering crop yields. This dichotomy has proven difficult to bypass, and estimates indicate only modest N_2O mitigation potentials if currently available N_2O abatement options were to be implemented at large scale (Winiwarter et al 2018).

In agricultural soils nitrification and denitrification are the main sources of N_2O (Butterbach-Bahl et al 2013). Nitrous oxide reductase (Nos) is the only known enzyme catalyzing the reduction of N_2O. Nos is expressed as part of the denitrification pathway sustaining anaerobic respiration by stepwise reduction of $NO_3^- \rightarrow NO_2^- \rightarrow NO \rightarrow N_2O \rightarrow N_2$, catalyzed by the enzymes nitrate reductase (Nar), nitrite reductase (Nir), nitric oxide reductase (Nor) and nitrous oxide reductase (Nos) encoded by the genes *nar*/*nap*, *nir*, *nor* and *nosZ*, respectively (Zumft 2007). A significant share of denitrifying prokaryotes, however, are truncated, i.e. lacking genes encoding for 1 to 3 of the four enzymes (Shapleigh 2013; Graf et al 2014), and truncated denitrifying pathways may significantly affect the N_2O-emissions in soils under denitrifying conditions. Organisms that lack all denitrification genes other than *nosZ* are particularly interesting as they can act as net sinks for N_2O. The propensity of the soil community to emit N_2O can be reduced by increasing the relative abundance of such N_2O-respiring bacteria (NRB) (Philippot et al 2011, Domeignoz-Horta et al 2016). However, as a stand-alone operation, such modification of soil microflora by inoculation would be prohibitively expensive.

We have previously demonstrated that anaerobic digestion (AD) provides a promising industrial platform for low-cost large-scale introduction of N_2O-reducing bacteria to soil (Jonassen et al 2021): denitrifying bacteria with a strong preference for N_2O over NO_3 were isolated from an AD-digestate, which could be grown aerobically to high cell densities in a sterilized digestate, providing a cheap inoculum for reducing N_2O-emission from soil. The isolated organisms did not include NRB (bacteria with only *nosZ*), however, and it was evident that the organisms were not well adapted for activity and survival in soil. Here we present a new approach to obtain more ideal isolates by a deliberate attempt to enrich (and isolate) organisms that can grow both in digestate and soil. Conceptually the N_2O-reducing organisms within a community can be divided into three categories according to their ability to grow/survive in digestates and soil: *digestate specialists* (***D***) with a competitive advantage in digestate, *soil specialists* (***S***) with a competitive advantage in soil, and *generalists* (***G***) organisms capable of growth in both environments, but plausibly at lower growth rates in both substrates relative to the two specialists. We hypothesized that we could enrich ***G*** by sequential enrichment culturing, alternating between soil and digestate as substrate (coined *dual enrichment*), and explored this with a logistic growth model for the competition between three organisms, assigning hypothetical growth and death rates. The model revealed that the selective pressure could be modulated by the duration of each enrichment and the fraction of enriched material transferred from one enrichment to the next, and predicted that a reasonably competitive *generalist* would reach dominance after a limited number of repeated passages.

Using this theoretical framework, we designed an enrichment strategy whereby a microbial community, originating from digestate or soil, was passaged through a series of enrichment cultures alternating between gamma sterilized soil (ϒ-soil) and autoclave sterilized digestate (AC-digestate) (**Fig. 1**). We anticipated that *generalists* would gradually increase in abundance throughout the enrichment series and that organisms that are non-competitive in either substrates would be washed out due to the repeated dilution each transfer represented. Strong specialists would likely reappear when reintroduced in their preferred environment, and thus be easily identifiable. By means of this novel enrichment strategy along with targeted isolation of N_2O respiring isolates, genome sequencing and physiological experiments designed to unravel the isolates´ denitrifying regulatory phenotypes, we provide insight into the targeted enrichment of generalist type organisms and their performance as N_2O mitigating inoculants when vectored by digestate to agricultural soil.

Materials and methods

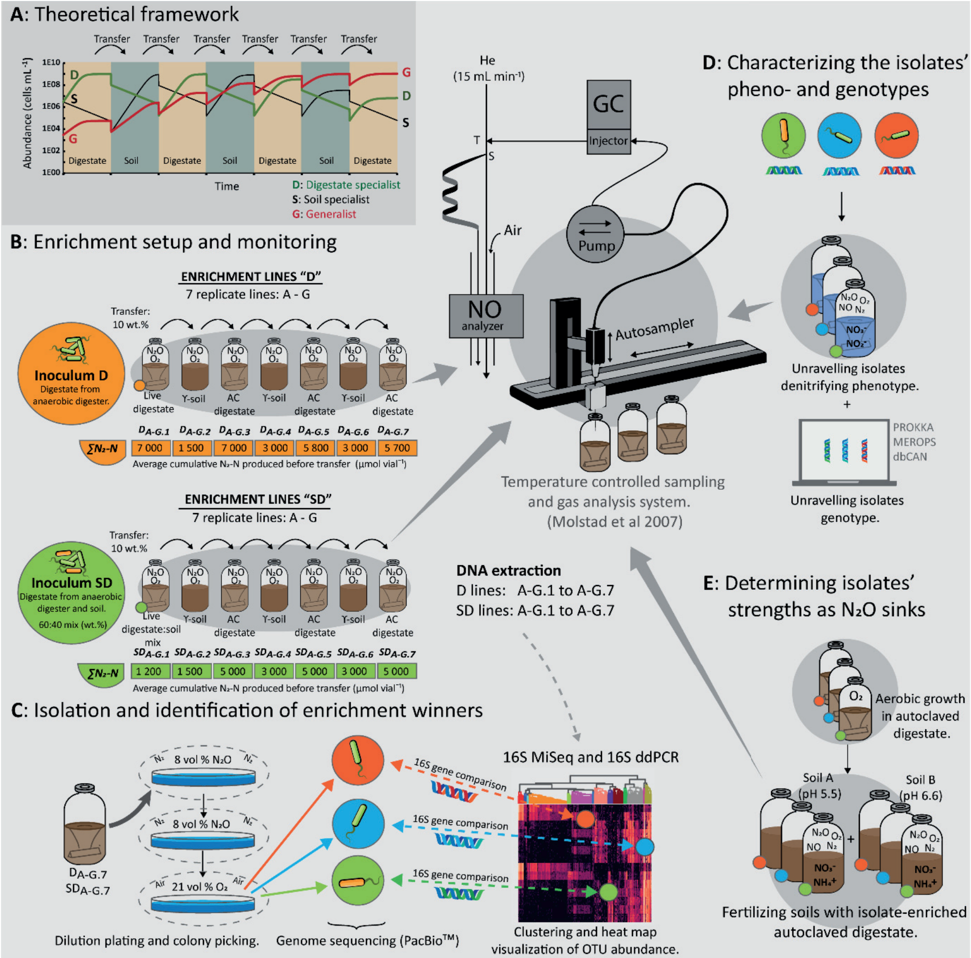

Figure 1: Graphical summary of materials and methods. **A:** The dual enrichment was modelled by a set of Lotka-Volterra logistic equations for three organisms; digestate specialist (D), soil specialist (S), and generalist (G), competing for a common substrate pool. The repeated transfer of enriched material from one enrichment to the next, alternating between soil and digestate, was predicted to enrich generalists by nature. The modelling is presented in detail in **Supplementary materials Section 1**: **Figs. S1** to **S6** and **Tab. S1**). **B**: Enrichment culturing experimental setup for the two enrichment lines "D" (digestate derived inoculum) and "SD" (soil and digestate derived mixed inoculum), each consisting of seven parallel replicate lines (A - G) over seven transfers. Each batch was supplemented with O_2 and N_2O (He background) in the headspace and monitored for O_2, N_2O, and N_2 kinetics by frequent sampling of the headspace. While O_2 was allowed to deplete by respiration, N_2O was sustained throughout by repeated injections. Average cumulative N_2 produced for each culture is indicated below vials ($\sum N_2$-N). DNA was extracted from every vial at the conclusion of each enrichment. **C**: Extracted DNA was subjected to 16S rDNA amplicon sequencing, OTU clustering, and taxonomic assignment. The abundance of organisms circumscribed by each OTU was calculated from their relative abundance and the abundance of 16S rDNA mL^{-1} as measured with digital droplet PCR (ddPCR). Relative abundance of the 500 most abundant OTUs throughout the enrichment was clustered using the Ward variance minimization algorithm. This allowed for identification of clades of OTUs with similar development throughout the dual enrichments. The OTUs 16S consensus sequences were aligned and matched with the 16S genes recovered from full genome sequencing of axenic N_2O-reducing isolates obtained from the final enrichments. **D**: The isolates' denitrifying phenotypes were assessed in pure culture incubations supplemented with either NO_3^- or NO_2^-, and O_2 or N_2O and O_2 and their phenotype matched against their denitrifying genotypes. Eco-physiological genome analysis by annotation of carbohydrate-active enzymes, peptidases, denitrification reductase genes, and other genes provided insight into the

suitability of these isolates as N_2O-reducing inoculants for soil inoculation. **E**: Each isolate was grown aerobically to high cell densities in autoclaved aerated digestate before amendment in two live soils (Soil A: pH 5.5 and Soil B: pH 6.6) supplemented O_2 and NO_3^- to assess performance as N_2O-reducing inoculants in soil.

Incubation- and gas measurement

All incubations were done in 120 mL serum vials sealed with butyl-rubber septa, using a robotized incubation system (Molstad et al 2007, 2016) which monitors gas kinetics (O_2, N_2, N_2O, NO, CO_2 and CH_4) by repeated sampling of the headspace, returning an equal volume of He each time. Elaborated calculus routines, accounting for dilution by sampling and leakage (Bakken 2021) secures accurate estimates of production/consumption rates of each gas, electron flow rates to the various electron acceptors (O_2, NO_3^-, NO_2^-, NO, N_2O), and N mass-balance. Digestates and liquid cultures of isolated strains were stirred continuously (600 rpm) with a 23 mm Teflon-coated triangular magnet. Prior to incubation, the headspace air was replaced with He by repeated evacuation and filling with He and supplemented with pure N_2O and/or O_2 (Molstad et al 2007).

Digestate and soils

The digestate was taken from the anaerobic digester of a municipal WWTP (Jonassen et al 2020), with chemical characteristics given in **Tab. S2**. Two clay loam soils were taken from a long-term liming experiment (Nadeem et al 2020), one with pH_{CaCl2}=6.6 (Soil A), and one with pH_{CaCl2}=5.5 (Soil B). Live digestate and live soil A were used in the initial enrichment cultures, while the substrates for subsequent enrichments (**Fig. 1B**) were autoclaved digestate (pH adjusted to 7.2 by titration with HCl), and ϒ-irradiated Soil A (25.9 kGy, 12 months prior to experiments). Digestate used for aerobic growth of the isolated N_2O-reducing bacteria before soil amendments (**Fig. 1E**) was autoclaved (121 °C, 20 min), then aerated by pumping sterile filtered air through a stirred suspension of digestate for 36 hours, and then pH adjusted to ~7.50-7.75 (**Tab. S2**) by titration with 4 M HCl. Aeration of the digestate was necessary in order to oxidize Fe^{2+} in the digestate to Fe^{3+}, as otherwise the abiotic reduction of O_2 by Fe^{2+} obscured measurements of oxygen consumption (Jonassen et al 2021).

Dual enrichment culturing

Enrichment series were started with two live materials: 50 mL digestate (**D-lines**) (pH 7.6±0.1) and 20 g Soil A + 30 mL digestate (**SD-lines**) (pH 7.2±0.1), each with 7 independent lines (A to G) (**Fig. 1A**). The nomenclature used throughout the text is: $D_{A\text{-}G,j}$ and $SD_{A\text{-}G,j}$, where D/SD denotes the initial live materials, *A-G* denotes the 7 independent replicates and *j* the enrichment number (1–7). D_0/SD_0 denotes live material before enrichment with N_2O. After replacing the headspace air with He, 3 mL N_2O, and 3 mL O_2 were injected into the vials, which were then incubated at 20 °C in the incubation system monitoring the O_2, N_2O and N_2. Additional N_2O was injected when needed to avoid N_2O depletion. Subsequent enrichment cultures (j=2-7), alternating between γ-sterilized soil (45 g soil dry weight vial^{-1}+ 16 mL sterile water) autoclaved digestate (45 mL), were inoculated with ~10 wt% of the previous enrichment, following the same experimental procedure and conditions as explained above for the live starting materials. At the completion of each enrichment, samples were taken for DNA extraction and analysis and for isolation in the final enrichment.

Community analysis

DNA was extracted from technical duplicates, sampled at the conclusion of each enrichment cycle, from all $D_{A\text{-}G,j}$ and $SD_{A\text{-}G,j}$ vials (j = 1-7), the live materials (D_0 and SD_0), autoclaved digestate and ϒ-soil. DNA was extracted from 1 mL digestate slurry or 0.25 g soil using the PowerLyzer™ Soil DNA extraction kit (QIAGEN) following a modified kit protocol where bead beating for 30s at 4.5 ms^{-1} in a MP Biomedicals™ FastPrep®-24 (Thermo Fischer Scientific Inc) replaced the vortexing step in the manufacturers protocol. Quantitative digital droplet PCR (ddPCR) was performed in technical triplicates on pooled samples of DNA extracts from biological and technical replicates from each enrichment cycle (j = 1-7), and pooled samples of technical replicate DNA extractions from D_0/SD_0, autoclaved digestate, and ϒ-soil, respectively. The ddPCR reaction mix (QX200 ddPCR EvaGreen® Supermix, BioRad) was prepared according to the manufacturer's instructions using the universal primers PRK341F (5'-CCTACGGGRBGCASCAG-3') and PRK806R (5'-GGACTACYVGGGTATCT-3') (Eurofins Genomic) targeting the V3-V4 region of the 16S rDNA gene (Yu et al 2005). The QX200 droplet generator (Bio-Rad) was used to generate oil droplet suspensions that were subjected to PCR with parameters given in **Tab. S3**. The PCR products were measured in a QX200 droplet reader (Bio-Rad), and the data analyzed in Quantasoft™ Analysis

Pro 1.0.596 software (Bio-Rad). Microbial community composition was determined through 16S rDNA amplicon sequencing (V3-V4 region) and taxonomic classification of 16S rRNA gene sequences. Library preparation and sequencing data processing were performed according to Nilsen et al (2020) except the library was quantified with the KAPA library quantification kit (universal; Roche) in a CFX96 Touch Real-Time PCR Detection System (Bio-Rad, USA). The amplicon library was diluted to 7 pM containing 20 % PhiX before sequencing on the MiSeq platform (Illumina, USA) using MiSeq reagent v3 kit to generate 300 bp paired-end reads. The sequencing produced 6139309 reads after quality filtering. The samples were rarefied at 9000 reads, resulting in the loss of 9 samples ($SD_{2.1}$-A, $SD_{7.6}$-B, $SD_{3.7}$-A, $SD_{7.7}$-A, $D_{1.1}$-A, $D_{1.3}$-B, $D_{2.3}$-A, $D_{2.4}$-A, $D_{3.6}$-A). The seaborn.clustermap in the Seaborn software suite (Waskom 2020) was used to generate hierarchically clustered heatmaps and was based on the Ward variance minimalization linkage algorithm (Ward 1963) for the 500 most abundant OTUs (sum abundance across all samples). Statistical analysis included principal component analysis (PCA) and similarity percentage (SIMPER) (Clarke 1996) using the PAST software (Hammer et al 2011). OTU absolute abundance was calculated as the product of its relative abundance and the abundance of 16S rDNA assessed by ddPCR for all OTUs (16S rDNA copies enrichment-vial^{-1}).

Isolation and characterization of N_2O-reducing organisms

Dilution series of the final enrichments ($D_{A\text{-}G,7}$ and $SD_{A\text{-}G,7}$) were spread on Sistrom's succinate medium (SS), R2-A, tryptic soy broth (TSB) and Nutrient broth (NB) agar plates (1.5 wt. %) (media composition is given in **Supplementary Materials Section 2**), incubated in N_2+ N_2O atmosphere as described in Jonassen et al (2021) (**Fig. 1C**). Colonies were transferred to 120 mL vials containing 50 mL of the corresponding liquid medium and incubated aerobically with stirring (700 rpm) at 20 °C. 16S gene analysis showed that several different isolates were obtained, six of which were selected for full genome sequencing (working names in **bold**): *Aeromonas* sp. **AM**, *Ochrobactrum* sp. **OB**, *Pseudomonas* sp. **PS-02** and *Brachymonas* sp. (**BM**), which were isolated on SS medium, and *Cloacibacterium* sp. (**CB-01** and **03**) isolated on NB medium. Cultures were grown aerobically at 20 °C in SS (**AM, OB, BM, PS-02**) or NB (**CB-01**, **CB-03**) medium to $OD_{660} \approx 1.0$. After centrifugation, DNA was extracted from the pellets using PowerLyzer™ Soil DNA extraction kit (QIAGEN) as described above. The genomic DNA was sheared to approximately 8-14 kb long fragments and a library was generated with the SMRTbell Express Template Prep Kit 2.0 (PacBio) without size selection. The library was sequenced on a PacBio™ SMRT cell with the PacBio™ Sequel System using 3.0 chemistry at the Helmholtz Centre, Munich. After data demultiplexing, the genomes **CB-01**, **CB-03, BM,** and **AM** were assembled with the 'HGAP4' pipeline (SMRT Link Software, PacBio) with a seed coverage of 30 for **CB-01**, **CB-03,** and **BM**, and a seed coverage of 22 for **AM. PS-02** and **OB** were assembled with the 'Microbial Assembly' pipeline (SMRT Link Software, PacBio) with a seed coverage of 20 and 15, respectively. Genome quality was assessed with CheckM v1.0.18 (Parks et al 2015). Annotation of coding genes was done with Prokka v1.14.5 (Seemann et al 2014) using default parameters. The draft genomes were functionally annotated for carbohydrate-active enzymes (dbCAN2 meta server, Zhang et al 2018) and peptidases (MEROPS database, release 12.3) (Rawlings et al 2010). Signal P 5.0 (Raut et al 2021) was used to identify genes containing putative signal peptides as defined for gram negative bacteria. The denitrification regulatory phenotypes of the isolated strains was investigated by monitoring the kinetics of O_2, NO, N_2O, NO_2^- and NO_3^- in stirred batch cultures as they depleted the oxygen and switched to anaerobic respiration as described by Jonassen et al (2021). 200 µL samples of liquid culture were taken for NH_4^+ measurements and immediately stored at -20 °C before colorimetric analysis in LCK303 cuvettes (Hach Lange) in a DR 3900 spectrophotometer (Hach Lange).

Evaluation of N_2O-reducing isolates as N_2O sinks in soil

The soils A and B were amended with five variations of digestate; **1:** live digestate (directly from the anaerobic digester), **2:** digestate heat treated to 70 °C for two hours, **3:** autoclaved pH-adjusted (7.75) digestate, **4:** autoclaved, aerated, and pH adjusted (7.75) digestate in which the isolates AM, BM, PS-02, CB-01 or OB had been grown by aerobic respiration, **5:** as 4, with CB-01, then heated to 70 ^{0}C (2 h). Each variation was tested in duplicate 120 mL vials containing 10 g soil (Soil A or Soil B) (**Fig. 1E**) amended with 0.6 mL digestate (1-5) and 50 µmol NO_3^- and 1 mL O_2 in a He atmosphere. Sterilized water was added to adjust the soil WFPS to 62 ± 1 % (Franzluebbers 1999). The vials were incubated at 20 ^{0}C, and monitored for O_2, NO, N_2O and N_2 (**Fig. 1D**). A follow-up experiment with the same experimental design was performed to test the dose dependence effect for three of the isolates. Finally, we tested the persistence of the strains in soil, by making an identical extra set of vials (**1-5** above) which were stored aerobically in moist chambers, then amended with 1 mg g^{-1} soil ground plant material (clover) to secure high metabolic activity, and incubated as described above.

To assess the effect of isolates on the potential N_2O emission from denitrification in soil, we used the N_2O- index, $\boldsymbol{I_{N2O}}$ (Liu et al 2014), which is the integral of the N_2O-curve divided by the integral of the total N-gas, for a given period (0-*T*):

$$I_{N_2O} = \frac{\int_0^T N_2O{-}N(t)dt}{\int_0^T [N_2O{-}N(t) + N_2{-}N(t) + NO(t)]dt} \qquad (1)$$

The time period (*T*) is not fixed but set as the time when a given percentage of the available nitrogen oxyanions (NO_3^-+NO_2^-) are reduced to N-gas (N_2+N_2O+NO). In our case, we calculated $\boldsymbol{I_{N2O}}$ for 40% and 100% recovery of nitrogen oxyanions as N_2+N_2O+NO (coined $\boldsymbol{I_{N2O40\%}}$ and $\boldsymbol{I_{N2O100\%}}$, respectively).

Data availability

The sequencing data for this study have been deposited in the European Nucleotide Archive (ENA) at EMBL-EBI under accession number PRJEB44171 (https://www.ebi.ac.uk/ena/browser/view/PRJEB44171).

Results and discussion

Dual enrichment culturing

To enrich and isolate N_2O-respiring organisms which can grow both in digestate and soil environments, we used a dual enrichment approach, i.e. sequential batch cultures, alternating between sterile digestate and sterile soil as substrates (**Fig. 1**). Each batch was provided with a small dose of O_2, to suppress obligate anaerobic organisms and select organisms capable of rapid transition from O_2- to N_2O-respiration. Subjecting the enrichments to recurrent changes (i.e. growth substrate, oxic/anoxic) selects for organisms with a capacity to adapt rapidly to changing environmental conditions (Brooks et al 2011), a desirable trait in an organism destined for soil amendment.

The kinetics of N_2O reduction to N_2 throughout the consecutive enrichments is shown in **Fig. 2A** (more detailed analyses of the gas kinetics are shown in **Figs. S7** and **S8**). In the line D enrichment, which started from live digestate only ($D_{A\text{-}G.1}$), the N_2-kinetics indicated the presence of two populations of N_2O-respiring organisms; one whose activity was gradually declining, indicated by declining N_2-rates (μ = -0.03 h^{-1}), and a second population growing from initially extremely low numbers until their N_2O respiration exceeded that of the declining population, increasing at a rate of 0.1 h^{-1} (modelled in **Fig. S8**, top right panel). In contrast, theline SD enrichment, which started with a mixture of live soil and live digestate ($SD_{A\text{-}G.1}$) showed exponentially increasing rates for N_2 production initially. Interestingly, the rates of N_2-production in $SD_{A\text{-}G.1}$ did not reach as high as $D_{A\text{-}G.1}$ (~10 vs ~120 µmol N_2-N h^{-1} $vial^{-1}$), which could be taken to suggest that a) the N_2O-reducing organisms originating from the soil quickly reached dominance due to the high initial numbers, b) these were less capable of scavenging electron donors in the digestate than the organisms originating from the digestate itself and/or c) the indigenous digestate bacteria were suppressed by the soil bacteria. Throughout the subsequent enrichments, the N_2-kinetics of the SD and D line became more similar, characterized by a short exponentially increasing rate, and subsequent more or less stable plateaus, probably reflecting an early depletion of the most easily available carbon substrates. The seven-replicate series within each line (D and SD) had remarkably similar kinetics, reflected in the marginal standard deviation (**Fig. 2A**).

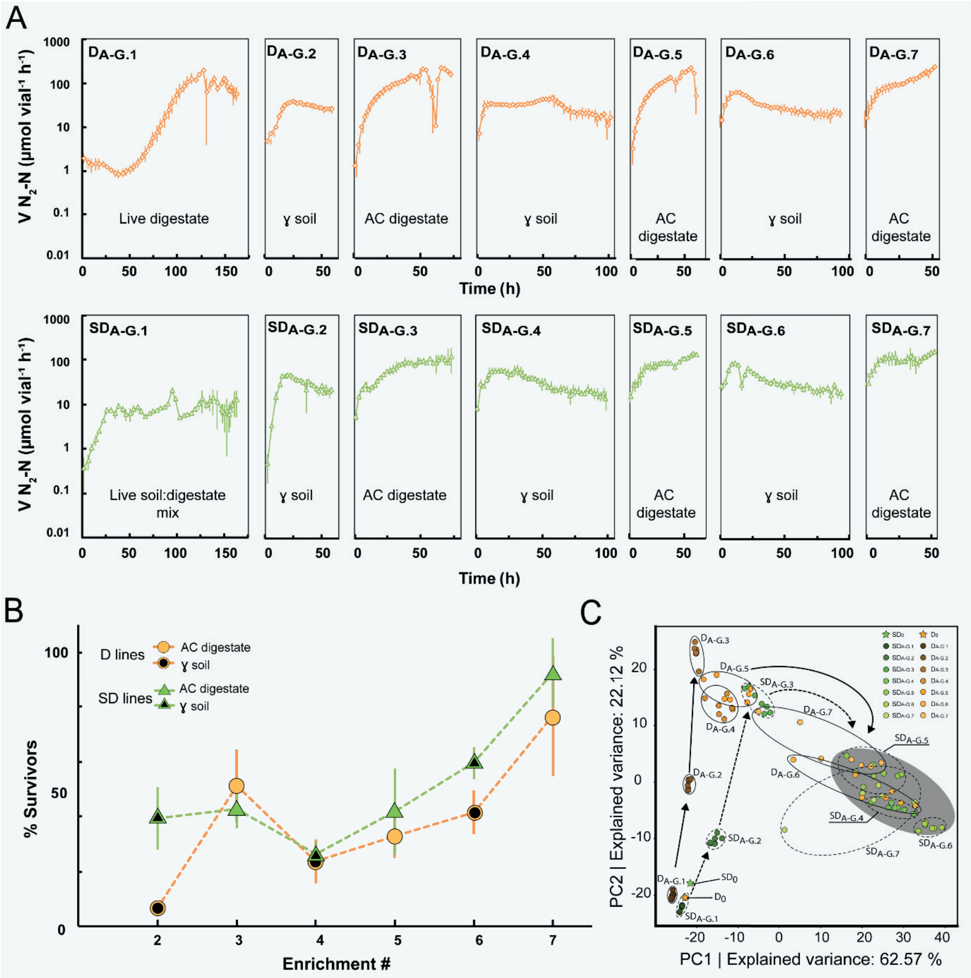

Figure 2: Gas kinetics and PCA of enrichment cultures. Panel A: Average rate of N_2-N production for the two lines of enrichment culturing. 10 weight % of enriched material was transferred from one replicate vial to the next ($D_{A\text{-}G.j}$ and $SD_{A\text{-}G.j}$ to $D_{A\text{-}G.j+1}$ and $SD_{A\text{-}G.j+1}$). AC digestate = autoclaved. ϒ soil = gamma sterilized. **Panel B**: Assessment of the fraction of the community surviving transfer to the next enrichment cycle (details in **Fig. S7). Panel C**: PCA of OTU relative abundances. Each dot represents an individual replicate (A-G). Standard deviation (n=7) is shown as vertical bars (panels A and B).

In theory (see supplementary **Figs. S1-S6**), the dual enrichment culturing should select for organisms that are able to grow both in soil and digestate (generalists **G**) over the organisms that can only grow in soil (soil specialists, **S**) and digestate (digestate specialists **D**), leading to a gradual increase in the G/(S+D) abundance ratio, which means that the percentage of N_2O-respiring cells that survive the transfer to a new substrate (from soil to digestate and *vice versa*) should increase. We achieved crude estimates of the % survivors for each transfer based on the cumulated N_2 in each enrichment and the initial rates in the next (explained in detail in **Fig. S9**), and the results (**Fig. 2B**) lend support to the hypothesis.

Microbial community development in enrichment cultures

The microbial community dynamics were analyzed based on 16S rRNA amplicon sequencing and OTU clustering. PCA of community profiles demonstrated close similarity between replicate vials (A-G) throughout the first three enrichments, and some divergence thereafter (**Fig. 2C)**. SIMPER analysis revealed that 10 OTUs accounted for 94.4 and 93.5 % of the explained variance in the D and SD line respectively, of which 8 OTUs were shared between the two lines (**Tabs. S4** and **S5**). The D and SD lines followed similar trajectories and clustered in proximity to each other from enrichment SD_4 and D_6 forward, indicating a convergence towards a similar community structure (grey circle in **Fig 2C**). The PCA clearly verified that the community underwent continuous dynamic succession and, surprisingly, that a high fraction of dominant OTUs were shared between the two lines.

By targeted isolation of N_2O-respiring bacteria from the final enrichment cycle in autoclaved digestate ($D_{A\text{-}G.7}$ and $SD_{A\text{-}G.7}$), we obtained seven axenic N_2O-respring cultures and sequenced the genomes of six, using the PacBio sequencing platform (**Tab. S6**). The isolates were named according to genera with which they clustered in the phylogenetic tree generated with the 16S rDNA gene sequences of the isolates and related strains (**Fig. S10**) and given working names (**bold**): *Pseudomonas* sp. **PS-02**, *Aeromonas* sp. **AM**, *Brachymonas* sp. **BM**, *Ochrobactrum* sp. **OB**, *Cloacibacterium* sp. **CB-01**, *Cloacibacterium* sp. **CB-03**, and *Azonexus* sp. **AN**. **AN** was not genome sequenced, as its 16S partial sequence (obtained from Sanger sequencing of 16S PCR amplicons using 27F/1492R primer pairs) matched the 16S gene (99.2 % sequence identity) of the dominating N_2O-reducing *Azonexus* sp. (ERR4842639) isolated and characterized in the aforementioned experiments of Jonassen et al (2021).

The 16S genes recovered from the annotated genomes were compared to 16S of the OTUs using usearch.global (Edgar 2010). This revealed high sequence identity (>97 %) in the overlapping region (404 -429 bp) of the 16S rDNA consensus sequence of some OTUs, hence these OTUs circumscribed the isolated species (**Tab. S7**). The isolates CB-01, CB-03, AN, BM and PS-02 were circumscribed by OTU1, OTU1, OTU2, OTU8 and OTU19, respectively. These OTUs represented four of the top six most abundant OTUs of the $D_{A\text{-}G.7}$ and $SD_{A\text{-}G.7}$ samples. Including OTU74, circumscribing the isolate **OB**, five of the top 15 OTUs circumscribed the isolates. Summed, the average abundances of these OTUs were 59.8 ± 1.2 % and 60.0 ± 1.1 % in the $D_{A\text{-}G.7}$ and $SD_{A\text{-}G.7}$ enrichments, of which the dominating OTU1 accounted for 33 ± 10 % and 39 ± 10 % of the total abundance.

The dynamic change in OTU abundance of the 500 most abundant OTUs (sum abundance across all samples) throughout the consecutive enrichments of the D and SD lines was hierarchically clustered based on Euclidian distance measures using the Ward´s linkage algorithm (Ward 1963) and visualized by heatmapping of OTU abundance (**Fig. 3A)**. The hierarchical clustering identified six clades, denoted A to E in **Fig. 3A**, that clustered OTUs according to their abundance patterns throughout the consecutive enrichments. To achieve a more quantitative assessment of the phenomena portrayed in the heatmap we combined the total 16S rDNA gene abundance (**Tab. S8**) with the relative abundance of each clade and individual OTUs (**Fig. 3BCD**). This analysis included an assessment of the relative increase of individual OTUs from the consecutive enrichment cultures calculated as $R_i = \ln(N_{(i)}/(N_{(i-1)} \cdot 0.1))$, where N_i is the estimated absolute abundance at the end of enrichment *i* and $N_{(i-1)}$ is the estimated absolute abundance at the end of the foregoing enrichment. The average R_i for soil (R_{soil}) and for digestate-enrichments ($R_{Digestate}$) for each OTU was used to judge whether the OTU is a soil specialist (high R_{Soil}, low/negative $R_{Digestate}$), a generalist (high R_{Soil} and $R_{Digestate}$) or a digestate specialist (high $R_{Digestate}$, low/negative R_{Soil}).

Most OTUs within Clade A were present initially in both enrichment lines (D_0 and SD_0), suggesting a primarily digestate origin of these OTUs, of which most were assigned to the phyla *Bacteriodetes*, *Cloacimonetes* and *Betaproteobacteria* (**Fig. 3A**). Clade A showed an increase in abundance throughout the enrichment in both enrichment lines (**Fig. 3B**) with an increase equivalent to ~5 cell divisions in the first 3-4 enrichment cultures (dashed line, **Fig. 3B**). Inspection of the growth of individual OTU's (R_i values) within Clade A showed that they were able to grow both in digestate and soil, but they span a range from soil specialists (R_{soil} close to zero) to generalists (R_{soil} and $R_{digestate}$ >2, **Fig. S11**). The OTUs circumscribing the isolated cultures **CB-01** (OTU1), **CB-03** (OTU1), **AN** (OTU2), **PS-02** (OTU8), **AM** (OTU19) and **BM** (OTU37) were all within Clade A (**Fig. 3EF**). OTU2, circumscribing *Azonexus sp*. **AN**, grew better in digestate than in soil ($R_{Digestate}$ 3.40 ± 0.35 and R_{Soil} 2.27 ± 0.35) and reached dominance in the first enrichment in live digestate ($D_{A\text{-}G.1}$ culture vials), which was also observed in the enrichments of Jonassen et al (2021).

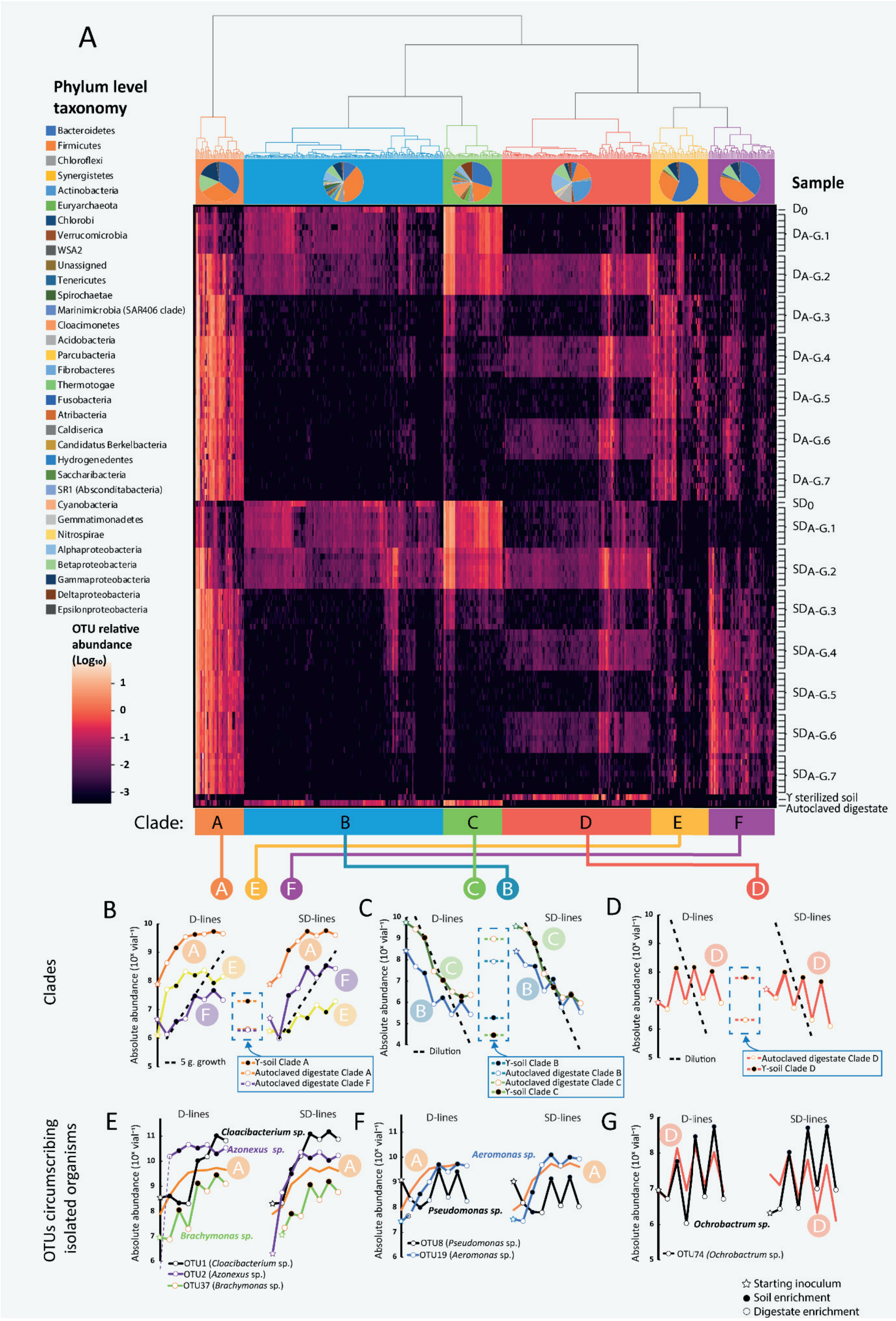

Figure 3: Abundance of clustered OTU's throughout the dual enrichment culturing. Panel A: Heatmapping and hierarchical clustering of the 500 most abundant OTUs from all biological replicates of the D line and SD lines of

the dual enrichment culturing, including starting inocula (D_0 and SD_0) and background samples of ϒ-soil and autoclaved digestate used as growth medium in the enrichments. OTUs are arranged in columns and samples in rows. The clustering has been delineated into six clades (A, B, C, D, E, F) with phylogenetic composition of OTUs in clades displayed below the cladogram. **Panels B-D** show the average absolute abundances (copies vial^{-1}=) for the OTU's within each clade throughout each enrichment; filled symbol= enrichment in soil, open symbol= enrichment in digestate, star = starting inoculum. The dashed lines in panels **C** and **D** represents the predicted decline by dilution, given a 10 % transfer rate, i.e. neither growth nor death. The dashed line in panel **B** represents a growth rate of 5 generations per enrichment. The OTU-abundancies in sterile materials are shown within dashed frames. **Panels E-G** shows the abundance of the OTU's which circumscribe the isolated strains, together with the averages of their resident clades.

Clade B and C plausibly harbored digestate derived OTUs, which were diluted out, rather than dying out, since their abundance declined with a rate largely as predicted by the dilution rate (**Fig. 3C** and **Figs. S12-13)**. In autoclaved digestate, the absolute abundance of OTUs clustered in clade B and C was ~10^8 and 10^9 vial^{-1} , respectively, while the abundance at the end of each enrichment was much lower, suggesting that their DNA is not destroyed by autoclaving, but that this relic DNA is degraded once the digestate is inoculated with live organisms. Thus, the high degree of clustering of samples by PCA (**Fig. 2C**) in the initial enrichments is probably not influenced by relic DNA as reported by others (Lennon et al 2018).

Clade D appeared to consist of soil specialist that sustained abundance in soil only, or alternatively, partly made up of relic DNA (DNA in the γ-sterilized soil) not metabolized during the enrichments in soil as mineral or humic substances may protect free DNA from rapid degradation (Nielsen et al 2007). However, some did appear to be true soil specialists due to their absence in the ϒ-sterilized soil (**Fig. 3A**). Our quantitative assessment confirmed that Clade D organisms grew in soil, while declining in digestate (**Fig. 3D**, and calculated *R* values **Fig. S14**). This clade harbored the soil specialist OTU74, circumscribing the isolated *Ochrobactrum* sp. **OB** (**Fig. 3G**), demonstrating the predicted characteristics of a soil specialist, reappearing at high abundance in soil enrichments.

Clade E showed an average increase in abundance throughout the enrichment in both enrichment lines but, interestingly, harbored organisms that were enriched to higher levels in the digestate derived line (D line) compared to the SD line (**Fig. 4B**), suggesting that they were suppressed by some organisms originating from the soil. Clade F appeared to contain organisms that were enriched in the SD line but remained at relatively low concentrations in the D line. OTUs of this clade were mostly soil derived organisms and their presence in the D line could be attributed to relic DNA (from the ϒ-soil) (Nielsen et al 2007) or an artifact of sequence OTU clustering.

Eco-physiological genome analysis of isolated organisms.

Throughout the enrichment series, the N_2O-respiring organisms were apparently growing under C-substrate limiting conditions most of the time (**Fig. 2A**), and tracing the OTUs circumscribing the isolated organisms throughout the enrichment cycles showed that many of these organisms grew to, and maintained, high abundance throughout the repeated transfers, i. e. growing in both materials (**Fig. 3EFG**). Acquisition of less accessible nutrients for growth and proliferation could therefore in part explain why the isolated organisms outperformed other species throughout the enrichments. To explore this metabolic versatility, we annotated carbohydrate-active enzymes (CAZymes) and peptidases/proteases in the isolate genomes using the dbCAN meta server (Zhang et al 2018) and the MEROPS database (Rawlings et al 2010), respectively, and further analyzed the predicted proteins for putative signal peptides using SignalP5.0 (Raut et al 2021).

A range of genes coding for CAZymes were identified in all isolates (**Tab. S9**), several of which are known to target complex carbohydrates also contained putative signal peptides, indicating that these proteins are transported to the cell exterior. Isolates **CB-01** and **CB-03** seemed to have CAZymes focused on the breakdown of plant materials, coding enzymes involved in degradation of cellulose, cellulose derivatives and starch (**Tabs. S9-10**). This was supported by the presence of the carbohydrate binding module (CBM) 48, that binds to various linear and cyclic α-glucans derived from starch and glycogen (Koay et al 2010, Chaen et al 2012). **AM** had a large repertoire of genes encoding CAZymes with multiple CMBs associated with binding to cellulose (CBM5, Kezuka et al 2006), starch/glycogen (CBM48), peptidoglycans and chitin (CBM50, Onaga and Taira 2008) (**Tabs. S9-10**). All isolates, except **BM,** had genes encoding cellulases, and genes encoding glycogen synthase (EC: 2.4.1.21 and 2.4.1.11) were recovered in **PS-02**, **AM**, **CB-01**, **CB-03** and **OB**. **AM** and **CB-01/CB-03** had genes encoding glycogen operon protein glgX homolog (EC: 3.2.1.-) and glycogen phosphorylase (EC: 2.4.1.1), both catalyzing breakdown of glycogen. This may be associated with a fitness advantage during the dual culture enrichment as glycogen metabolism has been shown to improve *E. coli* fitness when experiencing changing environments (Sekar et al 2020). Contrastingly to the other isolates, **BM** did not appear to be geared towards extracellular degradation of complex carbohydrates, nor contained genes involved in glycogen metabolism (**Tabs. S9-10**) and might be dependent on harvesting easily available carbohydrates in the sterilized growth media. Interestingly, the ability of the isolated strains to grow in sterilized digestate was strongly related to the number of genes coding for proteases and CAZymes (**Fig. S32H**)

All isolates encoded peptidases containing putative signal sequences, but the relative proportion of these varied between the isolates; with **CB-03** having the largest proportion of predicted peptidases containing putative signal sequences, followed by **AM** and **CB-01** (**Tab. S11**). Extracellular secreted peptidases may also reflect environmental adaptations; the isolates contained peptidases active at a more neutral pH range and known low-pH active peptidases (Nguyen et al 2019) were not recovered. This falls in line with the inherent pH of the environments from which the isolates were obtained – neutral/alkaline digestate and weak acidic soil. Interestingly, the genomes **CB-01** and **CB-03** had several characteristics similar to predatory bacteria, such as overrepresentation of genes for peptidases, genes for the complete mevalonate pathway for isoprenoid production, histidine kinase (EC: 2.7.13.3), serine protease (EC: 3.4.21.107), FMN NADH reductase (EC: 1.7.1.17, only recovered in CB-01) and Dipate enol-lactone hydrolase (EC: 3.1.1.24) (Pasternak et al 2013). In contrast, **AB**, **BM**, **OB** and **PS-02** encoded the complete MEP/DOXP pathway, common for non-predatory bacteria (Pasternak et al 2013). We speculate that these genomic features may have contributed to **CB-01** and **CB-03** achieving dominance throughout the enrichment, but, to the best of our knowledge predatory traits of *Cloacibacterium* sp. has not been reported, and further experimentation would be required to confirm this.

Species within the genus *Ochrobactrum* can fix nitrogen symbiotically in root-nodules (Trujillo et al 2005, Zurdo-Pineiro et al 2007, Imran et al 2014).Some genes coding for proteins involved nodule formation where recovered in *Ochrobacter* sp. **OB** genome (**Tab. S12**), but not for the catalytic subunits of nitrogenase.

Characterizing the isolates denitrifying regulatory phenotypes (DRP) and genotype

All isolates did encode the gene for Nos, *nosZ* (clade I or II, Hein and Simon 2019), as well as several other denitrification genes (**Fig. 4**). Although organisms with a full-fledged denitrification pathway can both produce and reduce N_2O, they may be strong sinks for N_2O in the environment, depending on their denitrification regulatory phenotype (**DRP**, Bergaust et al 2011), which is shaped by the regulatory network controlling their stepwise reactions of denitrification, both at the transcriptional (Spiro 2012) and metabolic (Mania et al 2020) level.

To characterize the DRP of our isolated strains, they were raised under strictly oxic conditions to secure absence of any denitrification proteins, and transferred to gas-tight vials with liquid medium containing 2 mM NO_3^-, and with He, O_2 and N_2O in the headspace. As these stirred cultures were allowed to deplete the oxygen and switch to anaerobic respiration, they were monitored for O_2, NO, N_2O and N_2 in the headspace and NO_3^-, NO_2^- and NH_4^+ in the liquid. Measured gases in incubations supplemented with 1 ml O_2, 1 mL N_2O and 2 mM NO_3^-, alongside with measured liquid concentrations of NO_2^- NO_3^- and NH_4^+ and genes coding for catalytic subunits, are shown for each isolate in **Fig. 4**.

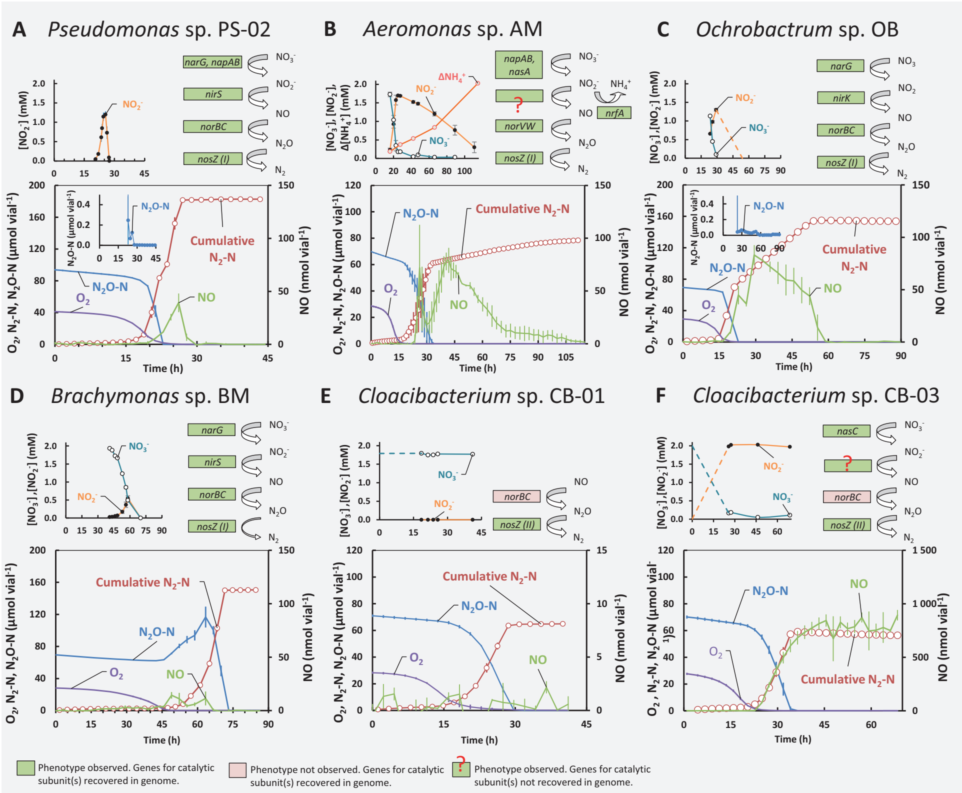

Figure 4: Denitrification genes and denitrification phenotypes of isolated organisms. Gas kinetics of O_2, N_2O-N, NO, and cumulative N_2-N (adjusted for leakage and sampling) in denitrifying phenotype experiments in 120 mL closed vials with He atmosphere containing 50 mL liquid growth medium supplemented with 1 mL O_2, 1 mL N_2O and 2 mM NO_3^-. Liquid concentrations of NO_2^-, NO_3^- and/or NH_4^+ (small panels, dashed lines = estimated by N-mass balance) and all genes coding for catalytic subunits of N-reductases recovered from the Prokka annotated genomes. **Panel A**: *Pseudomonas* sp. PS-01 (n = 2) grown in SS medium. PS-02 demonstrated strict control of gaseous denitrification intermediates throughout the incubation. **Panel B**: *Aeromonas sp.* AM (n = 3) grown in SS medium. AM demonstrated a DNRA+NOS phenotype, converting NO_3^- to NO_2^- and NH_4^+. Denitrification was ongoing throughout, but at a low and constant rate (0.4 µmol N_2-N h^{-1} $vial^{-1}$, **Fig. S22**). **Panel C**: *Ochrobactrum* sp. OB (n = 2) grown in SS medium. OB demonstrated strict control of gaseous intermediates throughout the incubation. **Panel D**: *Brachymonas sp.* BM (n = 2) grown in Sistrom's succinate medium. BM demonstrated a full-fledged denitrifying phenotype where N_2O was kept at high levels throughout the incubation. **Panel E**: *Cloacibacterium* sp. CB-01 (n = 3) grown in NB medium. CB-01 had a truncated denitrifying phenotype respiring primarily N_2O. **Panel F**: *Cloacibacterium* sp. CB-03 (n = 2) grown in NB medium. CB-03 had a truncated denitrifying phenotype converting N_2O to N_2, and nitrate to nitrite.

The genomes of *Pseudomonas* sp. **PS-02**, *Ochrobactrum* sp. **OB** and *Brachymonas* sp. **BM**, predicted a full-fledged dentification pathway, i.e. reduction of NO_3^- to dinitrogen gas, which was verified (**Fig. 4ACD**). However, theregulatory phenotypes were profoundly different: **PS-02** reduced available NO_3^- and N_2O concomitantly, before initiating NO_2^--reduction (**Fig. 4A**). Nos activity was higher relative to the other N-reductases at the oxic/anoxic transition as there was only miniscule, transient accumulation of N_2O during denitrification

($NO_2 \rightarrow NO \rightarrow N_2O \rightarrow N_2$), and the preferential reduction of N_2O was maintained if cultured with NO_2^-, with or without N_2O in the headspace (**Figs. S17** – **S20**). The phenotype of **OB** (**Fig. 4C**) was very similar to that of **PS-02** and was maintained under a variety of conditions (**Figs. S21** – **S24**). **BM**, however, reduced most of the available NO_3^- to N_2O at first (**Fig 4D**), and this trait was retained if cultured with NO_2^-, with or without N_2O in the headspace (**Figs. S25** – **S27**). This suggested that while **BM** would be a source of N_2O in the environment, **PS-02** and **OB** would be strong sinks.

DNRA organisms with *nosZ* could be attractive inoculants since they reduce NO_3^- to NH_4^+ rather than to N_2, thus retaining plant-available N in the soil (Rütting et al 2011), and at the same time scavenging N_2O produced by other organisms. The AM isolate simultaneously reduced the available NO_3^- to NO_2^- and N_2O to N_2 after O_2-depletion (**Fig. 4B,** analyzed in more detail in **Fig. S28**), and subsequently reduced NO_2^- to NH_4^+ and trace amounts of N_2. This indicated dissimilatory nitrate reduction to ammonium (DNRA), which was corroborated by the presence of *nrfA* in the genome, coding for a key enzyme of DNRA (Cytochrome c552 nitrite reductase, EC: 1.7.2.2) (Einsle, 2011). It also carried a *nasD* gene that showed high sequence similarity (protein blast) with NirB (NADH-dependent nitrite reductase) of a related *Aeromonas media* strain. Genes for the nitrite reductases NirS/K were not identified, and the source for the produced NO remains unresolved. The **AM** genome also apparently lacked genes for the nitrate reductase NarGHI, while genes coding for periplasmic nitrate reductase Nap (*napAB*) and N_2O reductase Nos (*nosZ*, clade I) were present. It also encoded the gene *nasA*, which showed high sequence similarity (protein blast) to a nitrate reductase of a related *Aeromonas media* strain. NasA is a constituent of the nitrate assimilatory system (Nas) and functions as a nitrate reductase in nitrate assimilation in a wide range of bacteria (Jiang et al 2015). The phenotypic analysis (**Fig. 4B**) showed that NO_3^- and N_2O were clearly reduced at the same time in incubations with the **AM** isolate. This contrasts earlier findings that Nos outcompetes Nap (for electrons) in denitrifying bacteria (Mania et al 2020), and it could be speculated that the gene annotated as NasA in **AM** may be responsible for the reduction of NO_3^- to NO_2^- that took place concomitantly with N_2O reduction. However, none of the other genes generally found in the *nas* operon of bacteria, such as *nasFEC* and *B*, were detected in the genome analysis.

The genotypes of *Cloacibacterium* sp. **CB-01** and **CB-03** predicted a truncated denitrification pathway ($NO \rightarrow N_2O \rightarrow N_2$), and one (CB-03) was also equipped with genes for assimilatory NO_3^- reductase (*NasC*, EC: 1.7.99.4) and a nitrite/nitrate transporter (*narK*). This was all verified by experiments showing stoichiometric conversion of N_2O to N_2 and reduction of NO_3^- to NO_2^- by **CB-03** (**Fig. 4EF**) and corroborated by experiments under a variety of conditions (**Figs. S29-S31**). The early onset of NO_3^- reduction, before depletion of oxygen, suggesting that NasC was active under oxic conditions in this isolate, which was also reported for *Paracoccus denitrificans* (Pinchbeck et al 2019). Of the two isolates, **CB-01** makes for a particularly promising N_2O-reducing soil inoculant. Both **CB-01** and **CB-03** were circumscribed by the dominating OTU1 of Clade A (**Fig. 3E**) which dominated in both D and SD enrichment lines.

Performance of isolated organisms as sinks for N_2O in soil

To produce inocula for testing isolates' capacity as N_2O sinks in soil, they were grown aerobically to high cell densities in autoclaved digestate (**Fig. S32**). The estimated the cell density at the end of the 45 h incubation was ranged from 0.5 to 1.4 mg dry-weight mL^{-1} (~3-7 · 10^{10} cells mL^{-1}) for the different isolates, the lowest value recorded for *Brachymonas* sp. **BM** (0.5) while Aeromonas sp. **AM** reached highest (1.4). Interestingly, the capacity of the isolates to grow was strongly correlated with the number of genes coding for CAZymes and proteases in their genomes (**Fig. S32H**).

To assess the N_2O sink capacity of these aerobically grown organisms, they were inoculated to soil in vials with He atmosphere (with traces of O_2), which were monitored for O_2, NO, N_2O and N_2. Since the effect of such inoculation confounds the effect of the isolates and the effect of the available carbon in the autoclaved digestate, we included a set of control treatments. Thus, the experiment included 5 different pre-amendments: 1) Autoclaved digestate enriched with isolate by aerobic growth, 2) live digestate sampled directly from the anaerobic digester, 3) live digestate heat-treated to 70 °C for two hours (70 °C digestate) to reduce the activity of native N_2O producers (Jonassen et al 2021) 4) digestate in which CB-01 was grown, subsequently heated to 70 °C for two hours (70 °C O_2 dig) to give comparable amounts of carbon added to the soil, and 5) soil without any amendments. The I_{N2O}-emissions ratio, which is the area under the N_2O-curve divided by the area under the N_2O+N_2-curve (Liu et al 2014; Russenes et al 2016) expressed as a percentage, was used as a proxy to assess the treatment effects in the amended soils (**Fig. 5**).

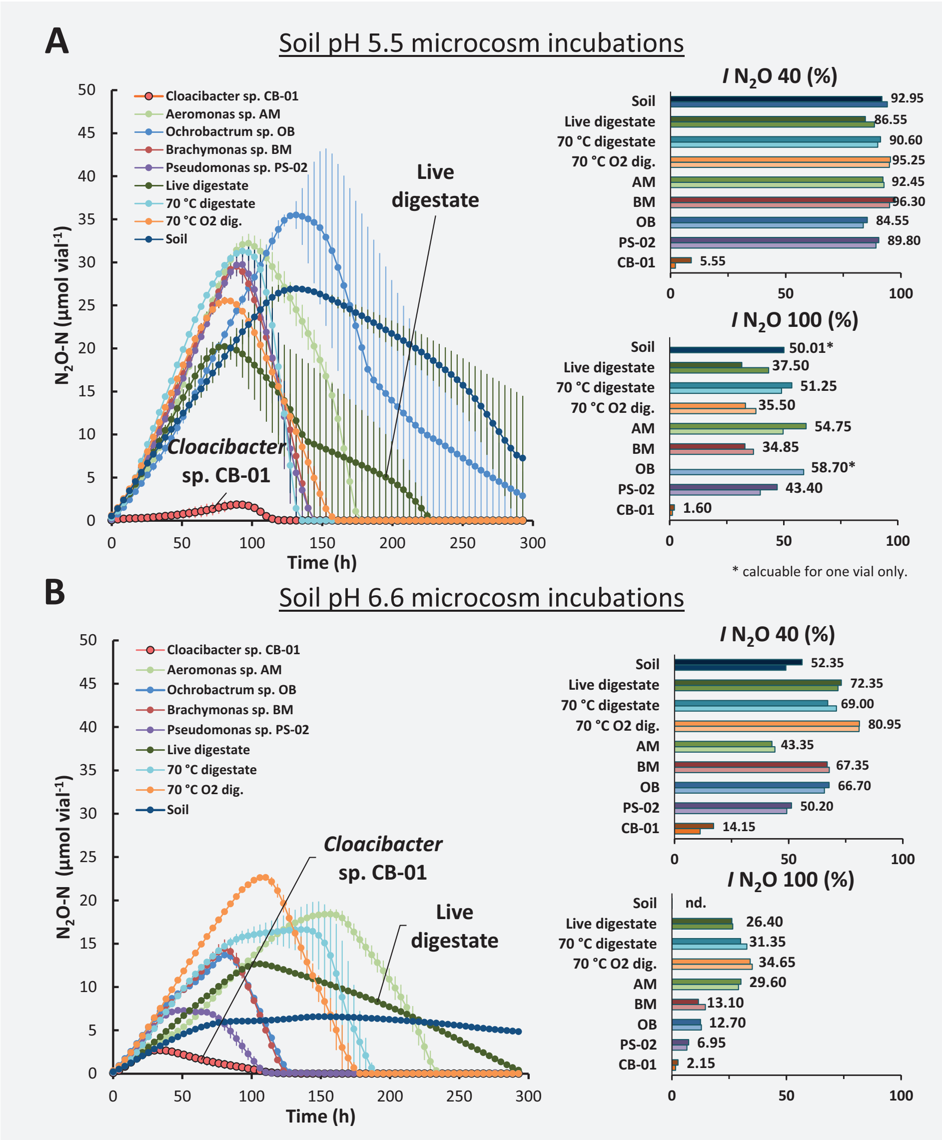

Figure 5: Gas kinetics during incubation of soils (**Panel A**: soil pH=5.5, **Panel B**: soil pH=6.6) amended with various pretreated digestates (0.06 mL g^{-1} soil): "Live digestate" = digestate directly from the anaerobic digester, "70 °C digestate" = live digestate heat treated to 70 °C for two hours, "70 °C O_2 dig." = autoclaved digestate used to grow strain CB aerobically, and then heat treated to 70 °C for two hours. **AM**, **BM**, **OB**, **PS-02** and **CB-01**: autoclaved digestate in which strains **AM, BM, OB, PS-02 and CB-01** had been grown aerobically.) to cell densities of 1.39, 0.51, 0.79, 0.81 and 0.72 mg cell dry-weight mL^{-1}, respectively (**Fig. S32**). The main graphs (panels A&B) show N_2O kinetics for each treatment (n = 2). The two bar graphs to the right show the N_2O indexes (***I*** $_{N2O}$, single vial values), which is the area under the N_2O-curve divided by the area under the N_2O+N_2-curve expressed as a percentage. Two ***I*** $_{N2O}$ values are shown: one for the timespan until 40% of the NO_3^--N is recovered as N_2+N_2O+NO-N (**I** $_{N2O\ 40\%}$), and one for 100% recovery (**I** $_{N2O\ 100\%}$). More details (including N_2 and NO kinetics) are shown in **Figs. S33 and S34.**

As expected, $\boldsymbol{I_{N2O}}$ values were generally higher in the pH 5.5 soil than in the pH 6.6 soil (**Fig. 5B**), and the isolates BM, OB, PS-02 lowered $\boldsymbol{I_{N2O}}$ only in the soils with pH 6.6. CB-01, however, resulted in extremely low $\boldsymbol{I_{N2O}}$ values in both soils, clearly outperforming any of the control treatments. We tested if the ability of **CB-01** to act as a strong N_2O sink in the pH 5.5 soil could be due to acid tolerance, by growing the organisms in stirred (600 rpm) liquid medium with pH ranging from 5.5 to 7, and found no evidence for acid tolerance, neither for growth nor for the synthesis of functional N_2O-reductase (**Fig. S31)**. An alternative explanation of the acid-tolerant N_2O-sink effect of **CB-01** could be that the cells were embedded in flocks/biofilms in the digestate, protected against low soil-pH by the buffer- capacity of the matrix. Strains of *Cloacibacterium* are known to secrete extracellular polymeric substances (Nohua et al 2015) and found in high abundance in biofilms of natural (Pang et al 2016), which lends support towards the hypothesis of matrix mediated shielding effects. This points towards the advantages of biofilm formation or other attachment strategies in generating favorable micro niches and so gaining advantage over competitors in a low pH environment.

Whilst our eco-physiological genome analysis revealed that several isolates had the genetic potential to utilize complex carbon sources and encoded several traits that might secure survival in a competitive situation, agricultural inoculants are most definitely invaders of the soil microbial community, and any longer-term establishment is dependent on the resistance by the residential community against alien species. The likelihood of a successful invasion is related to the resident community richness, referred to as the diversity-invasion effect (Mallon et al 2018), and reflects the key challenges of an invading organism; growth and establishment by utilizing resources not utilized by the resident community, or forcefully "overtake" a resident niche through competition or antagonism.

To assess the ability of our isolates to persist in soil and to retain their N_2O reduction capacity, a second experiment was set up with identical treatments to those in **Fig. 5**, but storing the amended soils for 1 month before testing the denitrification kinetics. A fertilization event was simulated by the addition of 50 µmol NO_3^-, 1 mg ground plant material g^{-1} soil, and 0.5 mL O_2 before sealing vials and monitoring denitrification kinetics throughout depletion of oxygen and the transition to anoxia. In this experiment the effect of the inoculated isolates on N_2O - emissions was evaluated based on maximum N_2O accumulation (no treatment reduced all available N-oxides, making it impossible to calculate I_{N2O} emission indexes) (**Figs. S35-36**). Whilst none of the inoculants significantly differed from the controls in pH 5.5 soil, PS-02 outperformed the other inoculants at pH 6.6. In fact, the soil treated with **PS-02** performed better after 30 days soil storage (maximum N_2O for PS-02 was ~1/10 of other treatments, **Fig. S36**) than immediately after amendment in the first soil experiment (**Fig. 5**). Likewise, maximum N_2O for **CB-01** treatment in pH 6.6 soil was approximately 2/3 of other amendments, but the difference was not statistically significant ($p > 0.05$).

A dose-response experiment with the isolates **CB-01**, **PS-02**, and **OB** was conducted to determine the minimum dose needed to obtain substantial reduction of N_2O production in soil. The isolates were grown aerobically in autoclaved digestate (pH adjusted to 7.5) as explained above, the cell density achieved was assessed by the cumulated oxygen consumption (explained in detail in **Fig. S37**), and the cell density was adjusted to 0.3 mg cell dry-weight mL^{-1} for all three strains, by dilution with autoclaved digestate. These enriched digestates were then used in an amendment experiment identical to that presented in **Fig. 5**, but with three different doses of enriched digestates (0.6, 0.3 or 0.15 mL; triplicates for each level), which is equivalent to an inoculation intensity of 18, 9 and 4.5 µg cell dry-weight g^{-1} soil, or 9, 4.5 and $2.3 \cdot 10^7$ cells g^{-1} soil, assuming the same dry-weight per cell as *Paracoccus denitrificans* ($2 \cdot 10^{-13}$ g dw $cell^{-1}$). The highest inoculation intensity in this experiment is approximately 50% of that used in the previous experiments (**Fig. 5**). The experiment included controls, amended with equivalent doses of sterile pre-aerated autoclaved digestate.

The results (summarized in **Fig. S38** and **Tab. S13)** showed a strong and dose-dependent effect of *Cloacibacterium* sp. **CB-01** on the N_2O accumulation, exemplified with the peak N_2O concentration (Max N_2O), which was reduced by 96, 64 and 20% (compared to the control without bacteria) by the inoculation levels 0.6, 0.3 and 0.15 mL digestate $vial^{-1}$, respectively ($p<0.05$ for all contrasts). *Pseudomonas* sp. **PS-02** and *Ochrobacter* sp. **OB** had weaker effects on Max N_2O, but statistically significant ($p<0.05$) at all inoculation levels. The $\boldsymbol{I_{N2O}}$ showed the same patterns, but several contrasts (bacteria versus control) lacked statistical significance for the lowest inoculation level.

Our inoculation levels were 2.7, 4.5 and $9 \cdot 10^7$ cells g^{-1} soil, which is within the upper range of inoculation levels used by Domeignoz-Horta et al (2016), who inoculated soils with 10^6 and 10^8 *Dyadobacter fermentans* - cells g^{-1} soil. *Dyadobacter fermentans* carry *nosZ* Clade II, but no other denitrification genes, which makes it comparable to our *Cloacibacterium* sp. CB-01, and a comparison of the performance of the two strains is interesting: inoculation with 10^8 *D. fermentans* – cells g^{-1} resulted in a reduction in the $N_2O/(N_2O+N_2)$ product ratio which is similar to what was achieved by the two highest inoculation levels with *Cloacibacterium*, i.e. $0.45\text{-}0.9 \cdot 10^8$ cells g^{-1}. Thus, the two strains appear to have similar capacities for acting as sinks for N_2O in soil. However, a closer inspection of the data reveals that *Dyadobacter* did not affect the N_2O-emission in soils with pH below 6.6, while *Cloacibacterium* performed well in our acid soil (pH 5.5, **Fig 5A**). This could indicate that *Cloacibacterium* sp. **CB-01** has a more robust N_2O sink capacity in low-pH soils. As suggested previously, this is probably not due to an inherent acid tolerance, but rather a combined effect of the organisms' tendency to aggregate and form biofilms, and the relatively high pH of the digestate (7.6). The matrix in which cells are embedded prior to inoculation to soils is probably a crucial issue.

Concluding remarks

The hierarchical clustering of 16S rRNA-based OTUs demonstrated that the dual enrichment effectively selected "generalist organisms" capable of growth by N_2O-respiration both sterilized digestate and soil, already after 3-4 transitions, as predicted by the model. (**Figs. S1** to **S5**).

Among the isolates, *Cloacibacterium* sp. **CB-01** stand out as particularly interesting because it grew well both in soil and digestates and was unable to denitrify *sensus stricto* (lacking the genes for dissimilatory NO_3^- and NO_2^- reduction). In addition, it proved a strong N_2O sink even in the acid soil (pH 5.5), where the other isolates appeared unable to synthesize functional N_2O reductase, as is the case for most organisms (Liu et al 2014, Lim et al 2021). Testing the pH-response of CB-01 in pure culture showed no particular tolerance to low pH (**Fig. S30**). We speculate that its ability to reduce N_2O in low pH soil is due to the ability of this organism to localize in alkaline microinches supplied by the digestate material, possibly through the production of a biofilm, a trait known to be common to members of this genus (Tiirola et al 2009, Revetta et al 2013, Biswas et al 2014, Pang et al 2016). The ability to retain activity in low pH soils is very desirable for agriculture due to the issue of soil acidification, driven by N-input and subsequent base cation depletion in agricultural soils (Tian et al 2015), and the uncertainty in net GHG-emission reduction of the few viable treatment options such as liming (Wang et al 2018, Hénault et al 2019) to mitigate N_2O derived from denitrification in these soils, but at a possible expense of increased emissions of carbonate-CO_2 (Wang et al 2021). The second isolate to show promise is **PS-02**. While **PS-02** can act as both a source and sink for N_2O, it showed the benefit of eliciting an N_2O-emissions reduction for an extended period after soil amendment. An interesting possibility and a future perspective is the option of combining **PS-02** and **CB-01**, to secure effective elimination immediately after fertilization (**CB-01**) as well as a more long-lasting effect (**PS-02**).

Not all the members of the generalist Clade A OTUs were obtained as pure cultures and extended isolation efforts may uncover yet more organisms with good qualities for an amended digestate material. Further, this enrichment technique could easily be expanded to new soils and new digestates to develop amendments suited to specific local materials and conditions. Future research investigating the performance of digestate amendments derived from these isolates would be valuable to accurately quantify the N_2O-emissions reduction effects under field conditions.

Acknowledgements

This work was financially supported by the Norwegian Research Council (project number: 260868). We wish to thank Elisabeth G. Hiis for indispensable assistance with the automated gas incubation and measurement system.

References:

Bakken LR (2021) Spreadsheet for gas kinetics in batch cultures. Researchgate DOI: 10.13140/RG.2.2.19802.36809

Bergaust L, Bakken L, Frostegård Å (2011) Denitrification regulatory phenotype, a new term for the characterization of denitrifying bacteria. Biochemical Society transactions. 39. 207-12. Doi: 10.1042/BST0390207.

Braman SR, Hendrix SA (1989) Nanogram nitrate and nitrite determination in environmental and biological materials by vanadium(III) reduction with chemiluminescense detection. Anal Chem 61: 2715-2718

Butterbach-Bahl K, Baggs EM, Dannenmann M, KieseR, Zechmeister-Boltenstern S (2013) Nitrous oxide emissions from soils: How well do we understand the processes and their controls? Philosophical Transactions of the Royal Society B: Biological Sciences, 368: 20130122.

Caporaso JG, Kuczynski J, Stombaugh J, Bittinger K, Bushman FD, Costello EK, Fierer N, Peña AG, Goodrich JK, Gordon JI, Huttley GA, Kelley ST, Knights D, Koenig JE, Ley RE, Lozupone CA, McDonald D, Muegge BD, Pirrung M, Reeder J, Sevinsky JR, Turnbaugh PJ, Walters WA, Widmann J, Yatsunenko T, Zaneveld J, and Knight R (2010) QIIME allows analysis of high-throughput community sequencing data, *Nature methods*, 7: 335-36.

Chaen K, Noguchi J, Omori T, Kakuta Y, Kimura M (2012) Crystal structure of the rice branching enzyme I (BEI) in complex with maltopentaose. Biochemical and biophysical research communications, 424(3), 508-511.

Cosentino S, Larsen MV, Aarestrup FM, Lund O (2013) PathogenFinder - distinguishing friend from foe using bacterial whole genome sequence data. Plos One 8. doi:10.1371/journal.pone.0077302

Cox RD (1980) Determination of nitrate and nitrite at the parts per billion level by chemiluminescence. Analytical Chemistry 52, 332–335. http://dx.doi.org/10.1021/ ac50052a028.

Davidson EA (2009) The contribution of manure and fertilizer nitrogen to atmospheric nitrous oxide since 1860. Nat. Geosci. **2**, 659–662

Domeignoz-Horta LA, Putz M, Spor A, Bru D, Breuil MC, Hallin S (2016) Non-denitrifying nitrous oxide reducing bacteria – an effective N2O sink in soil. Soil Biol Biochem 103:376-379.

Edgar RC (2010) Search and clustering orders of magnitude faster than BLAST, *Bioinformatics* 26(19), 2460-2461, doi: 10.1093/bioinformatics/btq461

Edgar RC (2013) UPARSE: highly accurate OTU sequences from microbial amplicon reads, *Nature methods*, 10: 996-8.

Einsle O (2011) Structure and function of formate-dependent cytochrome c nitrite reductase, NrfA. Methods in enzymology, 496, 399-422. https://doi.org/10.1016/B978-0-12-386489-5.00016-6

Forster P, Ramaswamy V, Artaxo P, Berntsen T, Betts R, Fahey DW, Haywood J., et al. Solomon S, Qin D, Manning M, Chen Z, Marquis M, Averyt KB, Tignor M, et al. (2007) Changes in atmospheric constituents and in radiative forcing, Climate Change 2007: the Physical Science Basis. Contribution of

Working Group I to the Fourth Assessment Report of the Intergovernmental Panel on Climate Change, Cambridge, Cambridge University Press (pg. 129-234).

Franzluebbers AJ (1999) Microbial activity in response to water-filled pore space of variably eroded southern Piedmont soils, Applied Soil Ecology, Volume 11, Issue 1, Pages 91-101, ISSN 0929-1393, https://doi.org/10.1016/S0929-1393(98)00128-0

Gardner AM, Gessner CR, Gardner PR (2003) Regulation of the nitric oxide reduction operon (norRVW) in Escherichia coli. Role of NorR and sigma54 in the nitric oxide stress response. The Journal of biological chemistry, 278(12), 10081–10086. https://doi.org/10.1074/jbc.M212462200

Graf DR, Jones CM, Hallin S (2014) Intergenomic comparisons highlight modularity of the denitrification pathway and underpin the importance of community structure for N 2 O emissions. PloS one, 9(12), e114118.

Hammer Ø, Harper DAT, Ryan PD (2001) PAST: Paleontological statistics software package for education and data analysis. *Palaeontologia electronica* 4.1: 9.

Hein S, Simon J (2019) Bacterial nitrous oxide respiration: electron transport chains and copper transfer reactions. *Advances in microbial physiology*, *75*, 137-175.

Hénault C, Bourennane H, Ayzac A et al (2019) Management of soil pH promotes nitrous oxide reduction and thus mitigates soil emissions of this greenhouse gas. Sci Rep **9,** 20182. https://doi.org/10.1038/s41598-019-56694-3

Imran A, Saadalla MJA, Khan SU, Mirza MS, Malik KA, Hafeez FY (2014) Ochrobactrum sp. Pv2Z2 exhibits multiple traits of plant growth promotion, biodegradation and N-acyl-homoserine-lactone quorum sensing. Annals of Microbiology, 64(4), 1797-1806.

Jiang X, Dang H, Jiao N (2015) Ubiquity and Diversity of Heterotrophic Bacterial nasA Genes in Diverse Marine Environments. PLoS ONE 10(2): e0117473. doi:10.1371/journal.pone.0117473

Jonassen KR, Hagen LH, Vick SHW, Arntzen MØ, Eijsink VGH, Frostegård Å, Lycus P, Molstad L, Phillip B. Pope PB, Bakken LR (2020) Bacteria in digestates for reduced climate forcing, bioRxiv.

Kezuka Y, Ohishi M, Itoh Y, Watanabe J, Mitsutomi M, Watanabe T, Nonaka T (2006) Structural studies of a two-domain chitinase from Streptomyces griseus HUT6037. Journal of molecular biology, 358(2), 472-484.

Koay A, Woodcroft B, Petrie EJ, Yue H, Emanuelle S, Bieri M, Bailey MF, Hargreaves M, Park JT, Park KH, Ralph S, Neumann D, Stapleton D, Gooley PR (2010) AMPK β subunits display isoform specific affinities for carbohydrates. FEBS letters, 584(15), 3499-3503.

Lennon JT, Muscarella ME, Placella SA, Lehmkuhl BK (2018) How, When, and Where Relic DNA Affects Microbial Diversity. mBio, 9(3), e00637-18. https://doi.org/10.1128/mBio.00637-18

Lim NY, Frostegard A, Vick SH, Bakken LR, Shapleigh JP (2020) Linking meta-omics to the kinetics of denitrification intermediates reveals pH-dependent causes of N2O emissions and nitrite accumulation in soil. *bioRxiv*.

Liu B, Frostegård Å, Bakken LR (2014) Impaired Reduction of N_2O to N_2 in acid soils Is due to a posttranscriptional interference with the expression of *nosZ.* mBio 5(3):e01383-14. doi:10.1128/mBio.01383-14.

MacArthur PH, Shiva S, Gladwin MT (2007) Measurement of circulating nitrite and S-nitrosothiols by reductive chemiluminescence. J Chromatography B 851:93-105. https://doi.org/10.1016/j.jchromb.2006.12.012

Mallon CA, Le Roux X, Van Doorn GS, Dini-Andreote F, Poly F, Salles JF (2018) The impact of failure: unsuccessful bacterial invasions steer the soil microbial community away from the invader's niche. The ISME journal, 12(3), 728-741.

Mania D, Wolily K, Degefu T, Frostegård Å (2020) A common mechanism for efficient N_2O reduction in diverse isolates of nodule-forming bradyrhizobia. Environmental Microbiology 22:17-31. https://doi.org/10.1111/1462-2920.14731

Molstad L, Dörsch P, Bakken LR (2007) Robotized incubation system for monitoring gases (O_2, NO, N_2O, N_2) in denitrifying cultures, Journal of microbiological methods 71:202-211

Molstad L, Dörsch P, Bakken LR (2016) Improved robotized incubation system for gas kinetics in batch cultures. Researchgate 2016, DOI: 10.13140/RG.2.2.30688.07680

Nadeem S, Bakken LR, Frostegård Å, Gaby JC, Dörsch P (2020) Contingent effects of liming on N_2O-emissions driven by autotrophic nitrification. Frontiers in Env Sci 598513 doi: 10.3389/fenvs.2020.598513

Nguyen TT, Myrold DD, Mueller RS (2019) Distributions of extracellular peptidases across prokaryotic genomes reflect phylogeny and habitat. Frontiers in microbiology, 10, 413.

Nielsen KM, Johnsen PJ, Bensasson D, Daffonchio D (2007) Release and persistence of extracellular DNA in the environment. *Environmental biosafety research*, *6*(1-2), 37-53.

Nilsen M, Madelen Saunders C, Angell IL, Arntzen MØ, Carlsen, KCL, Carlsen KH, ... Rudi K (2020) Butyrate levels in the transition from an infant-to an adult-like gut microbiota correlate with bacterial networks associated with eubacterium rectale and ruminococcus gnavus. *Genes*, *11*(11), 1245. https://doi.org/10.3390/genes11111245

Onaga S, Taira T (2008) A new type of plant chitinase containing LysM domains from a fern (Pteris ryukyuensis): Roles of LysM domains in chitin binding and antifungal activity, Glycobiology, Volume 18, Issue 5, Pages 414–423, https://doi.org/10.1093/glycob/cwn018

Parkin TB (1987) Soil microsites as a source of denitrification variability. Soil Sci Soc Am J 51:1194-1199

Parks DH, Imelfort M, Skennerton CT, Hugenholtz P, Tyson GW (2015) CheckM: assessing the quality of microbial genomes recovered from isolates, single cells, and metagenomes. Genome Res. 25: 1043 1055. doi:10.1101/gr.186072.114

Pasternak Z, Pietrokovski S, Rotem O, Gophna U, Lurie-Weinberger MN, Jurkevitch E (2013) By their genes ye shall know them: genomic signatures of predatory bacteria. *The ISME Journal*, *7*(4), 756-769.

Philippot L, Andert J, Jones CM, Bru D, Hallin S (2011) Importance of denitrifyers lacking the genes encoding the nitrous oxide reductase for N_2O emissions from soil, Global Change Biology 17, 1494 – 1504.

Pinchbeck BJ, Soriano-Laguna MJ, Sullivan MJ, Luque-Almagro VM, Rowley G, Ferguson SJ, Roldán MD, Richardson DJ, Gates AJ (2019) A dual functional redox enzyme maturation protein for respiratory and assimilatory nitrate reductases in bacteria. Molecular microbiology 111(6), 1592–1603. https://doi.org/10.1111/mmi.14239

Pruesse E, Quast C, Knittel K, Fuchs BM, Ludwig W, Peplies J, Glöckner FO (2007) SILVA: a comprehensive online resource for quality checked and aligned ribosomal RNA sequence data compatible with ARB, *Nucleic acids research*, 35: 7188-96.

Raut P, Glass JB, Lieberman RL (2021) Archaeal roots of intramembrane aspartyl protease siblings signal peptide peptidase and presenilin. *Proteins: Structure, Function, and Bioinformatics*, *89*(2), 232-241.

Rawlings ND, Barrett AJ, Bateman A (2010) MEROPS: the peptidase database. *Nucleic acids research*, *38*(suppl_1), D227-D233. https://doi.org/10.1093/nar/gkp971

Robertson GP (2014) Soil Greenhouse Gas Emissions and Their Mitigation. Encycl Agric Food Syst, 5:185–196.

Rogelj J, Shindell D, Jiang K, Fifita S, Forster P, Ginzburg V, Handa C, Kheshgi H, Kobayashi S, Kriegler E, Mundaca L, Séférian R, Vilariño MV (2018) Mitigation pathways compatible with 1.5°C in the context of sustainable development. In: Global warming of 1.5°C. An IPCC Special Report on the impacts of global warming of 1.5°C above pre-industrial levels and related global greenhouse gas emission pathways, in the context of strengthening the global response to the threat of climate change, sustainable development, and efforts to eradicate poverty [Masson-Delmotte V, Zhai P, Pörtner HO, Roberts D, Skea J, Shukla PR, Pirani A, Moufouma-Okia W, Péan C, Pidcock R, Connors S, Matthews JBR, Chen Y, Zhou X, Gomis MI, Lonnoy E, Maycock T, Tignor M, Waterfield T (eds.)].In Press.

Russenes AL, Korsæth A, Bakken LR, Dörsch P (2016) Spatial variation in soil pH controls off-season N_2O emission in an agricultural soil. Soil Biology and Biochemistry 99: 36-46

Rütting T, Boeckx P, Müller C, Klemedtsson L (2011) Assessment of the importance of dissimilatory nitrate reduction to ammonium for the terrestrial nitrogen cycle. Biogeosciences, 8(7), 1779-1791. https://doi.org/10.5194/bg-8-1779-2011

Schlüter S, Zawallich J, Vogel H-J, Dörsch P (2019) Physical constraints for respiration in microbial hotspots in soil and their importance for denitrification. Biogeosciences. 16. 3665-3678. 10.5194/bg-16-3665-2019.

Schulz-Bohm K, Martín-Sánchez L, Garbeva P (2017) Microbial Volatiles: Small Molecules with an Important Role in Intra- and Inter-Kingdom Interactions. Frontiers in microbiology, 8, 2484. https://doi.org/10.3389/fmicb.2017.02484

Sekar K, Linker SM, Nguyen J, Grünhagen A, Stocker R, Sauer U (2020) Bacterial glycogen provides short-term benefits in changing environments. Applied and environmental microbiology, 86(9).

Seemann T (2014) *Prokka: rapid prokaryotic genome annotation,* Bioinformatics 15;30(14):2068-9. PMID:24642063

Spiro S (2012) Nitrous oxide production and consumption: regulation of gene expression by gas-sensitive transcription factors. Philosophical Transactions of the Royal Society B: Biological Sciences, 367(1593), 1213-1225.

Thompson RL, Lassaletta L, Patra PK, Wilson C, Wells KC, Gressent A, Koffi EN, Chipperfield MP, Winiwarter W, Davidson EA, Canadell JG (2019) Acceleration of global N 2 O emissions seen from two decades of atmospheric inversion. *Nature Climate Change*, *9*(12), 993-998. Tian, H., Xu, R., Canadell, J.G. et al. (2020) A comprehensive quantification of global nitrous oxide sources and sinks. Nature **586,** 248–256. https://doi.org/10.1038/s41586-020-2780-0

Trujillo ME, Willems A, Abril A, Planchuelo AM, Rivas R, Ludena D, ... Velázquez E (2005) Nodulation of Lupinus albus by Strains of Ochrobactrum lupini sp. nov. Applied and Environmental Microbiology, 71(3), 1318-1327.

Wang Y, Guo J, Vogt RD, Mulder J, Wang J, Zhang X (2018) Soil pH as the chief modifier for regional nitrous oxide emissions: new evidence and implications for global estimates and mitigation. Global change biology, 24(2), e617-e626.Ward JH (1963) Hierarchical grouping to optimize an objective function, Journal of the American Statistical Association, 58, 236–244.

Waskom M et al (2020) Mvaskom/seaborn, Zendodo, DOI: 10.5281/zenodo.592845

Winiwarter W, Höglund-Isaksson L, Klimont Z, Schöpp W, Amann M (2018) Technical opportunities to reduce global anthropogenic emissions of nitrous oxide. Environ Res Lett, 13:014011.

Yu Y, Lee C, Kim J, Hwang S (2005) Group-specific primer and probe sets to detect methanogenic communities using quantitative real-time polymerase chain reaction. Biotechnol Bioeng 89(6), 670-679

Zhang H, Yohe, T, Huang, L, Entwistle S, Wu P, Yang, Z., Busk PK, Xu Y, Yin Y (2018) dbCAN2: a meta server for automated carbohydrate-active enzyme annotation. *Nucleic acids research*, *46*(W1), W95-W101. 10.1093/nar/gky418

Zumft WG (1997) Cell biology and molecular basis of denitrification. Microbiology Molecular Biology Review, 61, 553,536

Zurdo-Pineiro JL, Rivas R, Trujillo ME, Vizcaino N, Carrasco JA, Chamber M, ... Velazquez E (2007) Ochrobactrum cytisi sp. nov., isolated from nodules of Cytisus scoparius in Spain. International Journal of Systematic and Evolutionary Microbiology, 57(4), 784-788.

Supplementary material

A novel dual enrichment strategy provides soil- and digestate- competent N_2O-respiring bacteria for mitigating climate forcing in agriculture.

Kjell Rune Jonassen[1,2], Ida Ormaasen[1], Clara Duffner[3], Torgeir R Hvidsten[1], Åsa Frostegård[1], Lars R Bakken[1], Silas HW Vick[1*].

[1)] Faculty of Chemistry, Biotechnology and Food Science, Norwegian University of Life Sciences, Norway [2)] VEAS WWTP, Bjerkåsholmen 125, 3470 Slemmestad, Norway. [3)] Research Unit Comparative Microbiome Analysis, Helmholtz Center Munich, Neuherberg, Germany.

* Corresponding author

1 Dual enrichment, conceptual model

The idea was to enrich N_2O-reducing organisms that are able to grow both in soil and digestate by dual enrichment culturing, i.e. sequential anaerobic batch incubations (with N_2O) in the two substrates, starting with unsterilized digestate, with or without unsterilized soil. At the end of the batch incubation, a fraction is used to inoculate the next batch where the substratum is gamma-sterilized soil. At the end of this incubation, a fraction is then used to inoculate the next batch where the substratum is autoclaved digestate, and so on. Each batch incubation should be long enough to secure depletion of easily available carbon sources, to secure competition between the populations.

To visualize the selection of organisms depending on experimental conditions (length of incubation, fraction of one batch transferred to the next) and the properties of the organisms, we made a simple mathematical model with three conceptual types of organisms:

- ***D*** = digestate specialist: fast growth in digestate, gradual death in the soil
- ***S*** = soil specialist: fast growth in soil, gradual death in the digestate
- ***G*** = generalist: growth on both substrata, but slower than the specialists (in their preferred substrate)

All three were assumed to compete for the same pool of carbon substrates, and the competition was implemented by assuming logistic growth for each depending on the total increase in cell density (i.e. the sum of all three populations), and first-order death rates. The differential equations for the growth and death of the three population in a single batch are:

$$\frac{dN_D}{dt} = N_D * r_D\left(1 - \frac{N_t}{K}\right) - N_D * d_D \qquad (1)$$

$$\frac{dN_S}{dt} = N_S * r_S\left(1 - \frac{N_t}{K}\right) - N_S * d_S \qquad (2)$$

$$\frac{dN_G}{dt} = N_G * r_G\left(1 - \frac{N_t}{K}\right) - N_G * d_G \qquad (3)$$

Using ***D*** as an example to explain the model: $\boldsymbol{N_D}$ is the population size of D (cells mL^{-1}), $\boldsymbol{r_D}$ (h^{-1}) is its maximum growth rate (high for digestate, low/zero for soil), ***Nt*** is the summed growth of all three populations, ***K*** is the substratum's carrying capacity (i.e. the maximum cell number that can be produced in the substratum), d_D (h^{-1}) is the first order death rate. The growth and death rates are substrate-specific: for cultivation in digestate, D has high $\boldsymbol{r_D}$ and low (or zero) $\boldsymbol{d_D}$, while the opposite is the case for cultivation in soil: $\boldsymbol{r_D}$ is low (or zero), $\boldsymbol{d_D}$ is high.

Thus, in digestate, D will increase at a high rate as long as N_t<<K, the rate decline as N_t converge to K, reach zero when $N_t=K(1-d_D/r_D)$ and decline if $N_t>K(1-d_D/r_D)$, provided that $\boldsymbol{d_D}> 0$. In soil, the abundance is constant if $\boldsymbol{r_D}$ for soil is set to zero, and D will die out (first order) by a rate given by $\boldsymbol{d_D}$. The two other populations (equations 2 and 3) were simulated the same way, with the same ***K***-value as for D, but with individual substrate-specific growth- and death rates. The model calculates $\boldsymbol{N_t}$ by summing up the net increase of the three populations, while any decline is not affecting $\boldsymbol{N_t}$.

The model was implemented in excel, simulating the growth of each population by forward Euler. A simulation example is shown in **Fig. S1**, illustrating features of D, S and G type organisms.

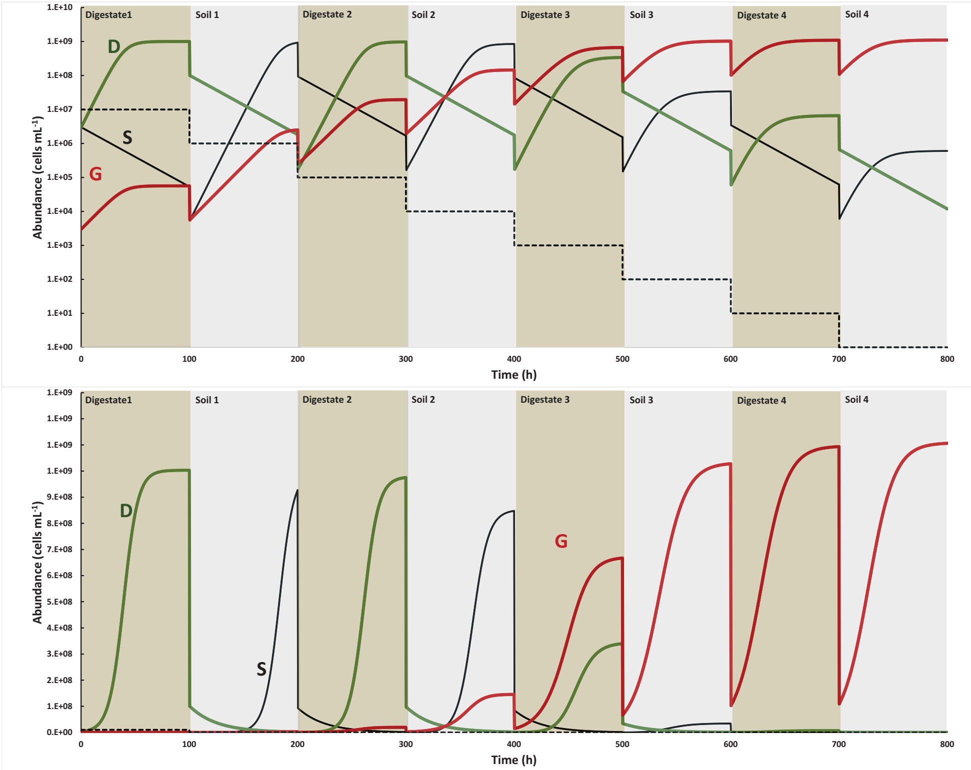

Figure S1: Simulation of the competition between three populations through a series of enrichment cultures. The three populations (S, D and G, see text for explanation) were simulated with the parameter values shown in **Table S1**, 100 hours incubation time for each batch and transfer of 10% of the culture volume to the next batch. Top panel shows abundance on log scale, bottom panel on a linear scale. D and S are sustained at stable levels (but fluctuating with substrates) only until G-abundance reaches significant levels. Thereafter they decline and approach extinction (< 1 cells mL^{-1}) if continuing the enrichment through 6-7 more batches (result not shown). The dashed line is the predicted dilution of a population which neither grows nor dies.

Table S1: Codes for substrate-specific rate constants (equation 1-3), and values used for simulation shown in Fig. S1, including the initial cell abundance for the soil specialist (S), the digestate specialist (D), and the generalist (G). K=10^{9} cells mL^{-1} both for soil and digestate.

Organism	**Initial abundance (cells mL^{-1})**	**Rate constants (h^{-1}) in:**			
		Digestate		**Soil**	
		r	***d***	***r***	***d***
D	3.E+06	r_{D_dig} = 0.15	d_{D_dig} = 0	r_{D_soil} = 0	d_{D_soil} = 0.04
S	3.E+06	r_{S_dig} = 0	d_{S_dig} = 0.04	r_{S_soil} = 0.15	d_{S_soil} = 0
G	3.E+03	r_{G_dig} = 0.075	d_{G_dig} = 0	r_{G_soil} = 0.075	d_{G_soil} = 0

In the following, the sensitivity of the model to parameter values was tested by changing one parameter at a time, using the parameter values and initial population densities in **Tab. S1** as default.

The fraction transferred from one batch to the next had a significant effect on the selective pressure as shown in **Fig. S2**.

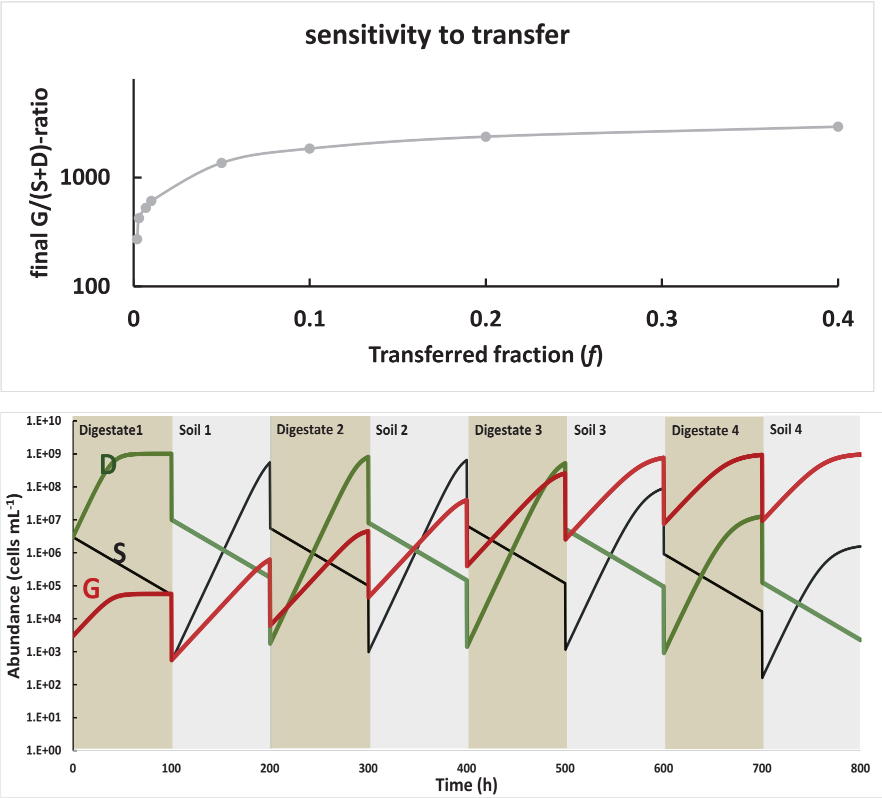

Figure S2: Selective pressure depends on the fraction (*f*) transferred from one batch to the next. The top panel shows the final G/(S+D) abundance ratio (i.e. in Soil 4, **Fig. S1**), for different values of ***f***, all other parameters were identical to that in **Fig. S1.** The G/(S+D) ratio is a measure of the selective pressure favoring G over S and D, and this shows drastic decline as ***f*** decrease below 0.1 (i.e. 10% transfer). The reason for this is that at very low ***f***, N_t remains << K throughout most of the time, hence growth is not limited by substrate availability, resulting in lower selection pressure. The phenomenon is illustrated in the bottom panel which shows a simulation for ***f***= 0.01. Selective pressure could be restored for ***f*** = 0.01 by increasing the time span for each batch cultivation (result not shown).

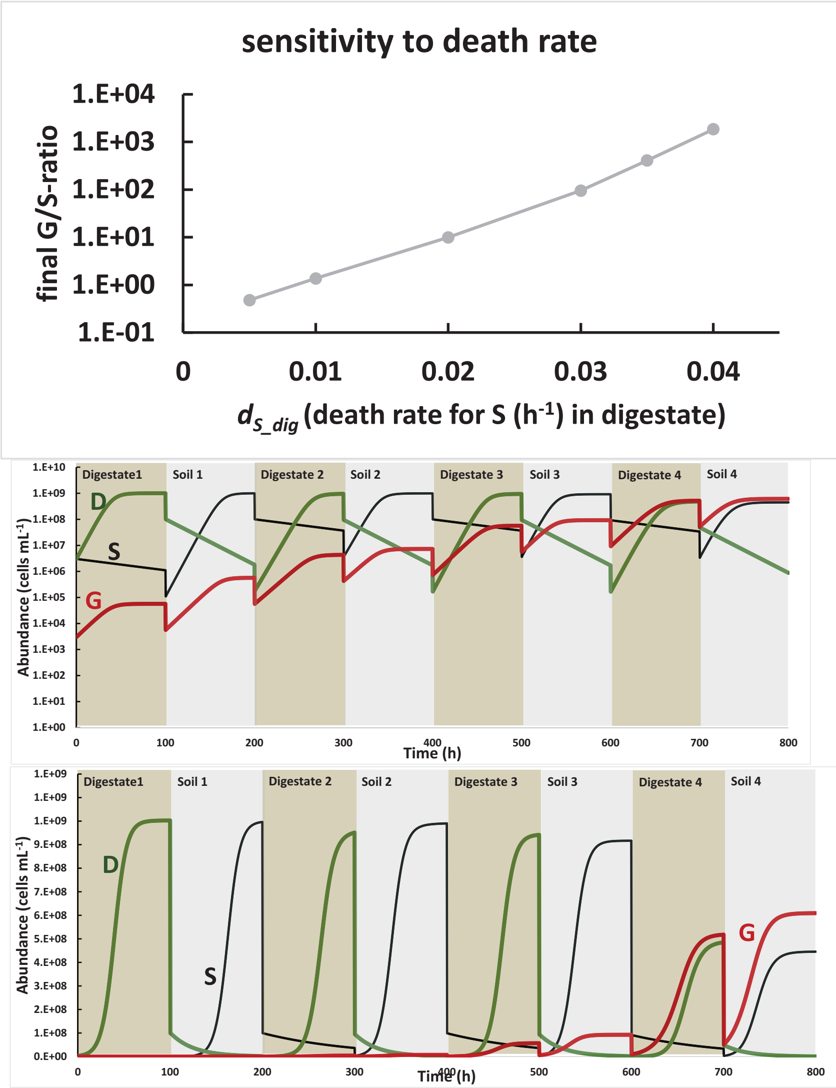

Figure S3: Sensitivity to death rate of S in digestate (*d_{S_Dig}*). To explore the sensitivity to death rate for S in digestate (*d_{S_Dig}*), simulations were run with different values (all other parameters as in **Tab. S1**). Top panel shows the final G/S ratio plotted against *d_{S_Dig}* (h^{-1}). Bottom panel shows simulation for *d_{S_Dig}* = 0.01 h^{-1} (Log scale in upper panel and linear scale in the lower). Although G will ultimately become dominant at any *d_{S_Dig}*>0, and ultimately exclude both S and D (NB: d_{D_soil} = 0.04 h^{-1} in these simulations), this would require a continuation of the dual enrichment (tested by simulation of a sequence of 24 batches, result not shown).

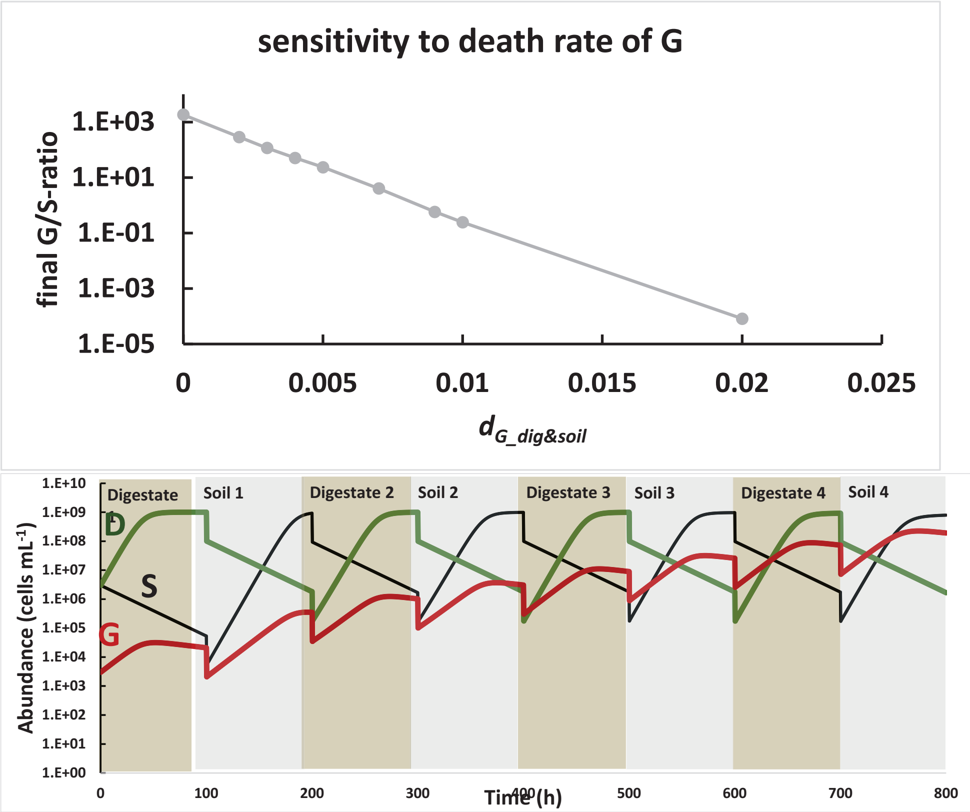

Figure S4: Sensitivity to death rate of G. The top panel explores the effect of cell death in G: Parameter values as in **Table S1,** except for the death rates of G in digestate ($d_{G\text{-}Dig}$) and soil ($d_{G\text{-}soil}$) which were both stepped up from 0 to 0.02 h^{-1} ($d_{G\text{-}Dig} = d_{G\text{-}soil}$ for each simulation), and the result is shown as the G/S abundance ratio after 800 h (i.e. at the end of the last enrichment in soil), plotted against $d_{G\text{-}Dig\&soil}$. The result suggests selection against G when $d_{G\text{-}Dig} = d_{G\text{-}soil} = 0.02$ h^{-1} but this is not the case: by simulating a continuation of the enrichment through 20*8=160 enrichments for $d_{G\text{-}Dig} = d_{G\text{-}soil} = 0.02$ h^{-1}, the G/S abundance ratio increased slowly but steadily, reaching 13 at the end (result not shown). This illustrates that although a competitive generalist can become dominant by dual enrichment culturing through 7-8 steps even at very low initial abundance (**Fig S1**), it would take very many batch cultivations for a less competitive organism to become dominant if it's initial abundance is low. The bottom panel shows the simulated population dynamics for $d_{G\text{-}Dig} = d_{G\text{-}soil} = 0.01$ h^{-1}: in this case, G almost reached dominance at the end of the first 8 batch cultivations. Extended simulation showed that G reached >10 times higher than S and G after 4 additional batches (result not shown).

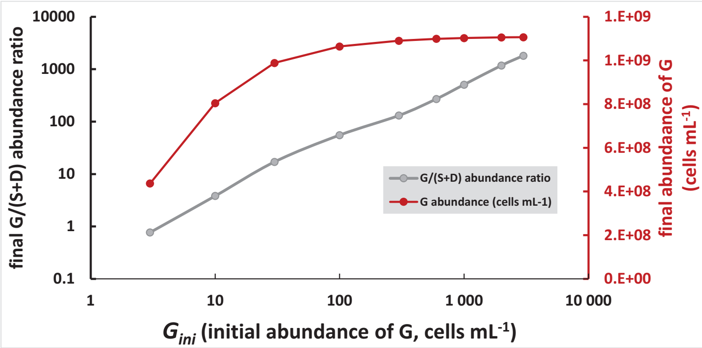

Figure S5: Minimum initial abundance of a competitive G to become dominant. To the explore the minimum initial abundance for competitive generalist (as modelled in **Fig. S1**) to become dominant through 8 cycles, simulations were run with different initial G-abundancies (***G_{ini}***) , and the result is shown as the final G/(S+D) abundance ratio (log scale) and the final abundance of G after 8 batches, plotted against ***G_{ini}*** (log scale). This illustrates that the final G abundance approach it's maximum (K=10^9 cells mL^{-1}) at ***G_{ini}*** around 100 cells mL^{-1}, while the G/(S+D) ratio continued to increase with increasing ***G_{ini}*** due to earlier onset of decline for D and S.

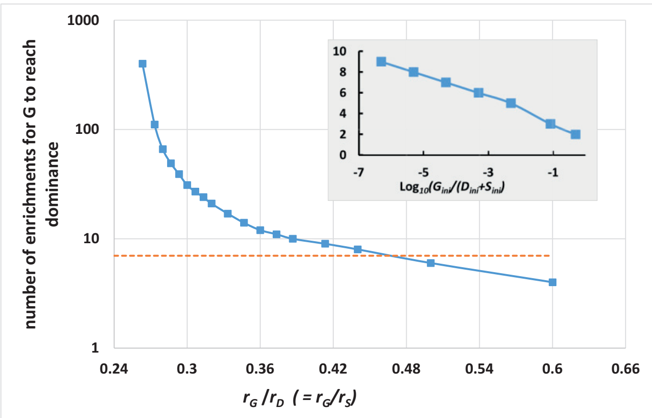

Figure S6: Number of enrichments needed for weakly and strongly competitive generalist to become dominant. To explore the minimum growth rate for G (r_G) to become dominant within 7-8 sequential enrichment cultures, and to explore the number of enrichment cultures that would be needed to reach dominance for weakly competitive generalists, simulations were run with a series of ***r_G*** values, but otherwise with the same parameters as in Table S1. The simulations were run until **G** reached dominance, arbitrarily defined as **G** > 10*(**D**+**S**). The panel shows the number of sequential enrichment cultures needed to reach G-dominance, plotted against r_G/r_S (which is equal to r_G/r_D because r_D=r_S=0.15 h^{-1} for all simulations). The dashed line mark 7 enrichment cultures. This shows the minimum ***r_G/r_D*** -ratio for **G** to be dominant in the 7th enrichment is ~0.47, i.e. the minimum rG= 0.07 h^{-1} (***r_G***=0.15*0.47= 0.07 h^{-1}). For a generalist with rG<0.07 h^{-1}, higher number of enrichment cultures are needed. NB. In the present simulations, the initial population ***G_{ini}*** is 1000 times lower than ***S_{ini}*** and ***D_{ini}***. For higher ***G_{ini}***, lower number of enrichments are needed. The minimum ***r_G/r_D*** ratio for G to be competitive is 0.26 (***r_G/r_D = r_G/r_S*** < 0.26 **results** in washout of G). The exercise shows that 7-8 enrichment cultures would be enough to enrich a competitive generalist, even at lower initial numbers than that used in previous simulations. The latter is illustrated in the inserted panel, showing the necessary number of enrichments for G to become dominant for ***r_G***= 0.075 h^{-1} (i.e. ***r_G/r_D=r_G/r_S***= 0.5), plotted against the $\log_{10}$ value of the relative initial abundance of G (***$G_{ini}/(S_{ini}+D_{ini})$***).

2 Supplementary materials and methods

Materials for inoculum and growth substrates

Table S2: Digestate characteristics at the time of sampling for enrichment culturing and soil incubations. The digestate was taken from an anaerobic digester of a municipal WWTP (same as that used by Jonassen et al 2021). Enrichment culturing and soil incubations were done with freshly sampled digestate (Sampling 1-4). Digestate characteristics were analyzed in the NS-EN ISO/IEC 17025 accredited laboratory belonging to the WWTP.

	Digestate characteristics						
	pH	% dry weight [a]	LOI [b] (% of DW)	TAK [c] (meq L^{-1})	VFA [c] (meq L^{-1})	VFA/TAK	NH_3+NH_4^+ (mg-N L^{-1})
Sample 1[d]	7.61	4.12	55.93	186	16.7	0.090	nd.
Sample 2[d]	7.73	3.97	55.45	199	17.3	0.087	nd.
Sample 3[d]	7.84	3.87	55.46	201	16.3	0.081	nd.
Sample 4[d]	7.60	3.73	54.87	189	15.2	0,080	1486 ± 7[e] (1883 ± 3)
Average[f]	**7.70**	**3.92**	**55.17**	**194**	**16.4**	**0.085**	**1824**

[a] Dry weight % expressed as percentage of wet weight (determined according to EN15934, given by WWTP). [b] Loss of ignition (volatile solids) as percentage of dry weight (determined according to EN15935, given by WWTP). [c] VFA = volatile fatty acids. TAK = total alkalinity (determined by titration described in EN12176:1998, given by WWTP). [d] Sample 1: sample used in enrichment experiment (live digestate inoculum, $D_{A\text{-}G.1}$ and $SD_{A\text{-}G.1}$, shown in **Fig. 2A** in main paper and Figs. **S8** and **S9**. Source of autoclaved digestate used as growth substrate in enrichment culturing. Sample 2 was used for aerobic growth of isolates, (**Fig. S32**). Sample 3 was used in soil incubations (live digestate) (**Fig. 5** in main paper and **S33-36**), Sample 4 was used in soil dose response experiment (**Figs. S38-38**). [e] Aeration of autoclaved digestate stripped off NH_4^+ (concentration in live digestate given in parenthesis). [f] Yearly average digestate characteristics given by the WWTP. Ammonium concentrations measured at the WWTP was measured as described by Greenberg et al (1980).

ddPCR

Table S3: PCR cycle settings for 16S ddPCR with primer pairs PRK341F/PRK806R.

Time:	Temperature (°C):	Description:	
5 min	95	Denaturation	
30 s	95	Denaturation	40 cycles
30s	55	Annealing	
45 s	72	Extension	
5 min	4	Signal stabilization	
5 min	90	Signal stabilization	
Indef.	4	Hold step	

Media composition

Sistrom's succinate medium (**SS**): contained (L^{-1}) 3.48 g K_2HPO_4, 0.195 g NH_4Cl, 4 g succinic acid, 0.10 g glutamic acid, 0.04 g aspartic acid, 0.5 g NaCl, 0.2 g nitrilotriacetic acid, 0.3 g $MgSO_4 \cdot 7H_2O$, 0.015 g $CaCl_2 \cdot 7H_2O$, 0.002 g $FeSO_2 \cdot 7H_2O$, 0.1 mL trace element solution and 0.1 mL vitamin solution. The trace element solution contained (g L^{-1}): 17.65 g EDTA (triplex 3), 109.5 g $ZnSO_4 \cdot 7H_2O$, 50 g $FeSO_4 \cdot 7H_2O$, 15.4 g $MnSO_4 \cdot H_2O$, 3.92 g $CuSO_4 \cdot 5H_2O$, 2.48 g $Co(NO_3)_2 \cdot 6H_2O$ and 1.14 g H_3BO_3. H_2SO_4 was added until the solution cleared. The vitamin solution contained (g L^{-1}) 10.0 g nicotinic acid, 5.0 g thiamine HCl and 0.10 g Biotin. Solid media agar plates were produced by addition of 1.5 wt.% agar. R-2A medium (**R-2A**): contained (L^{-1}) 0.5 g casein acid hydrolysate, 0.5 g dextrose, 0.3 g K_2HPO_4, 0.025 g $MgSO_4$, 0.5 g proteose peptone, 0.3 g sodium pyruvate 0.5 g starch (soluble), 0.5 g yeast extract. **R-2A** (Merck 17209) was used for preparing agar plates. Tryptic soy broth (**TSB**): containing (L^{-1}) 17 g casein peptone, 3 g soya peptone, 5 g NaCl, 2.5 g Na_2HPO_4 and 2.5 g dextrose (Sigma Aldrich 22092-500G). 1.5 wt. % agar plates were made with 0.1X strength TSB. Nutrient broth (**NB,** Merch): containing (L^{-1}) 15 g yeast extract, 3.0 g NaCl, 1 g dextrose. 1.5 wt.% agar plates were made with 0.2X strength NB.

3 Enrichment culturing

3.1 D-line

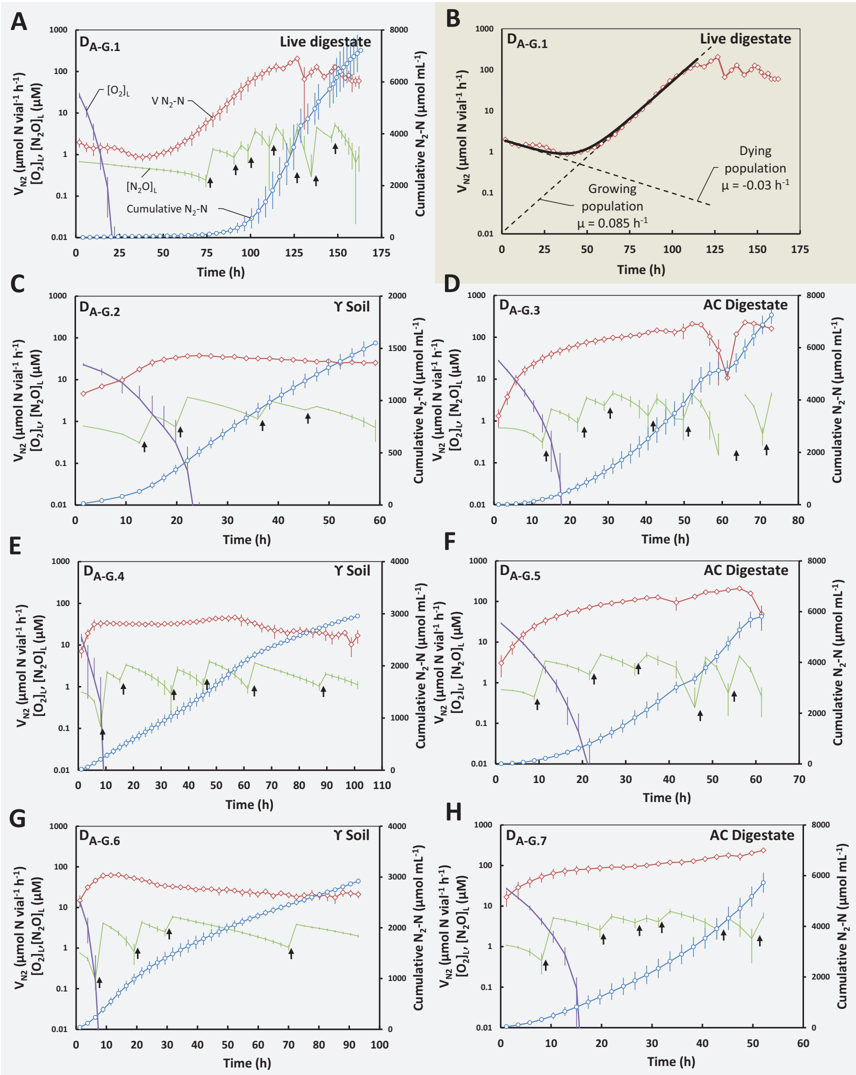

Figure S7: Enrichment culturing starting with live digestate – (D-line). Panel A&B shows the result for the initial enrichment culturing by anaerobic incubation of live digestate. Panel A shows N_2-N production rates, cumulative N_2-N produced, and liquid concentration of N_2O-N and O_2 throughout enrichment, while panel B shows the measured N_2 production rate on a log scale, together with a fitted model assuming a dying and a growing population as developed by Jonassen et al (2021). The panels C-H shows the same data as in panel A, for the subsequent enrichment cultures line $D_{A\text{-}G.2}$ to $D_{A\text{-}G.7}$. Each enrichment culture was started by transferring 10 weight % of material from the previous enriched culture ($D_{A\text{-}G.j}$ to $D_{A\text{-}G.j+1}$). Black arrows: exogenous addition of N_2O. Error bars is displayed as standard deviation (n = 7).

3.2 SD-line

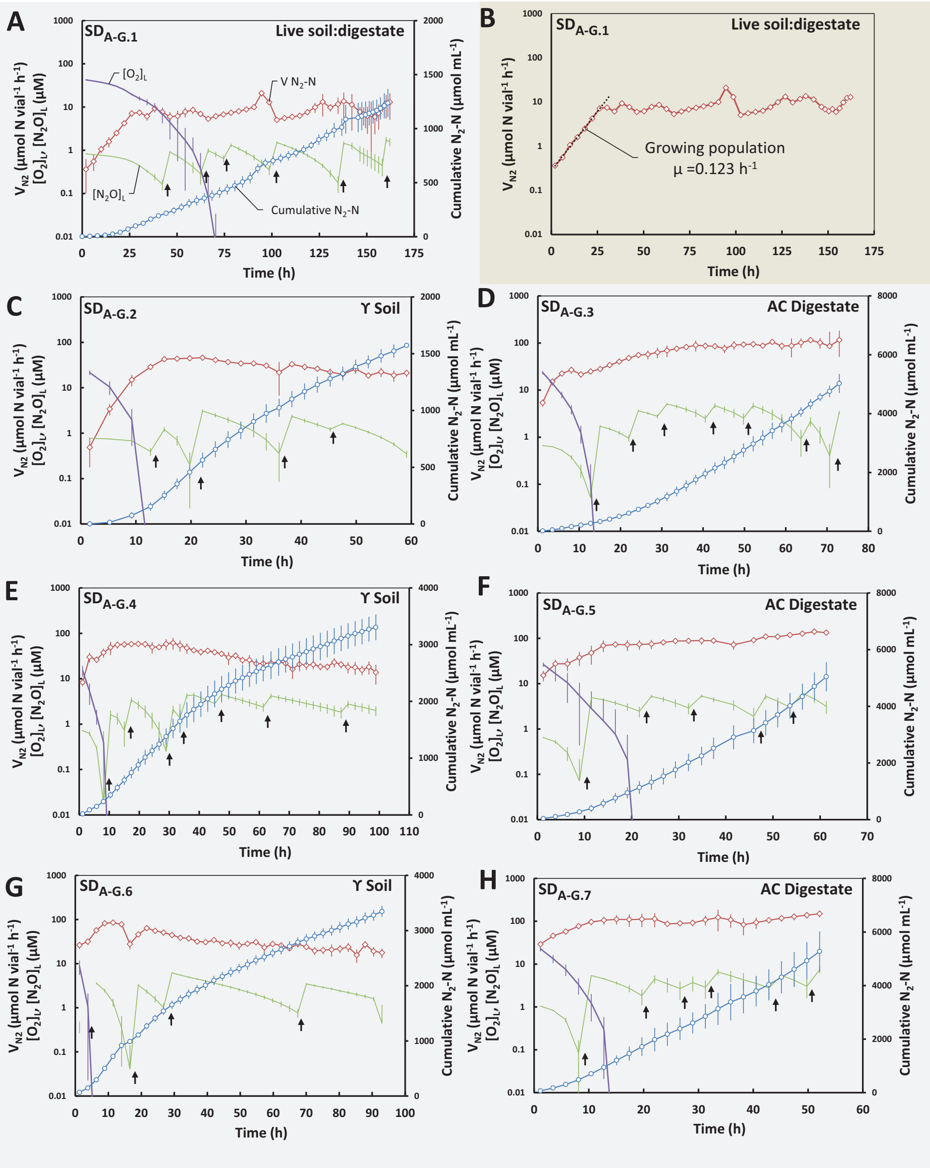

Figure S8: Enrichment culturing starting with live digestate + live soil (SD-line). Panel A&B shows the result for the initial enrichment culturing by anaerobic incubation of live digestate mixed with live soil. Panel A shows N_2-N production rates, cumulative N_2-N produced and liquid concentration of N_2O-N and O_2 throughout enrichment, while panel B shows the measured N_2 production rate on a log scale. In contrast to the D line (**Fig. S7**), the N_2 production increased exponentially from the very start. The panels C-H shows the same data as in panel A, for the subsequent enrichment cultures line $SD_{A\text{-}G.2}$ to $SD_{A\text{-}G.7}$. Each enrichment culture was started by transferring 10 weight % of material from previous enriched culture ($SD_{A\text{-}G.j}$ to $SD_{A\text{-}G.j+1}$). Black arrows: exogenous addition of N_2O. Error bars is displayed as standard deviation (n = 7).

Estimation of cells surviving the passage between digestate and soil

The N_2O reduction kinetics in the series of enrichment cultures were used to obtain crude estimates of the fraction of organisms surviving the transfer from one substrate to the next (from soil to digestate, and *vice versa*). The calculation was based on the assumption that all active organisms have equal growth yield (***Y*** = cells mol^{-1}electrons) and maximum growth rate (***μ_{max}***, h^{-1}), hence also cell-specific maximum respiration rate (***v_{max}***, mol electrons cell^{-1} h^{-1}).

The estimated number of N_2O-respiring respiring cells at the end of enrichment ***n***, $N_{n(end)}$ is:

$$N_{n(end)} = \frac{V_{e_{n(0)}}}{v_{max}} + E_{n-cum} \cdot Y \qquad (1)$$

where $V_{e_{n(0)}}$is the initial rate of electron transport to N_2O reductase for enrichment ***n*** , and E_{n-cum} is the cumulated electron flow to N_2O during enrichment ***n***.

The estimated number of N_2O-respiring respiring cells at the beginning of the next enrichment, ***n+1***, $N_{n+1(0)}$, is:

$$N_{n+1(0)} = V_{e_{n+1}(0)}/v_{max} \qquad (2)$$

where $V_{e_{n+1}(0)}$ is initial rate of electron transport to N_2O reductase for enrichment ***n+1***.

Since 10 % of the material in culture n was transferred to culture n+1, we have that the estimated fraction of N_2O-reducing organisms surviving this transfer, ***f***, is:

$$f = N_{n+1(0)}/(0.1 \cdot N_{n(end)}) \qquad (3)$$

Combining equation 1,2 and 3, and the fact that $Y \cdot v_{max} = \mu_{max}$, we have that

$$f = 10 \cdot V_{e_{n+1(0)}}/(V_{e_n(end)} + E_{n-cum} \cdot \mu_{max}) \qquad (4)$$

While E_{n-cum} was measured for each enrichment culture, while $V_{en(0)}$ and $V_{en+1(0)}$ were not, since each enrichment was initiated with ~1.4 vol% O_2 in the headspace, resulting in a mixture of aerobic and anaerobic respiration during the first 10-15 hours until O_2 was depleted (**Figure S9B**). To estimate $V_{en(0)}$ and $V_{en+1(0)}$ to be used to estimate ***f*** (equation 4), the measured rates of electron flow rate to N_2O immediately after oxygen depletion were extrapolated back to time 0, assuming exponential growth rate μ_{max}=0.1h^{-1}. The implicit assumption is the absence of any lag phase after transfer, thus $V_{e_{n+1(0)}}$, hence ***f*** should be considered minimum estimates.

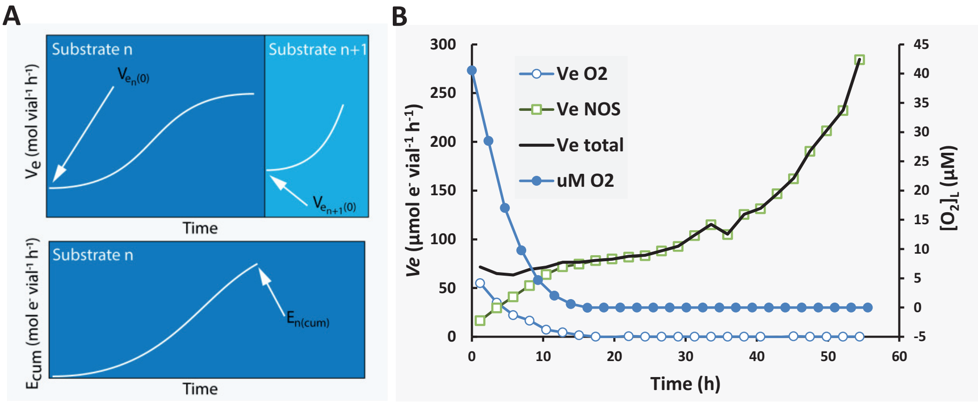

Figure S9 Panel A: Example kinetics of how the N_2O reduction kinetics in the series of enrichment cultures were used to estimate the % of active organisms surviving the transfer from one substrate to the next (from soil to digestate, and *vice versa*). The electron flow to N_2O reductase increased in *Substrate n* (soil or digestate) exponentially to begin with, leveling off gradually as growth becomes substrate limited. At the end of the enrichment culturing in *Substrate n*, 10 % is transferred to enrichment culturing in *Substrate n+1* (soil after digestate, or digestate after soil). The fraction of N_2O reducers in *Substrate n* which survives the transfer to *Substrate n+1* is to be calculated based on measured initial volumetric electron flow rate to N_2O ($\boldsymbol{V_{e\ n+1}}$) in *Substrate n+1*, and the *Substrate n*- data: initial volumetric electron flow rate to N_2O ($\boldsymbol{V_{e\ n}}$) and the cumulated electron flow ($\boldsymbol{E_{n\text{-}cum}}$) using equation 7 (see text preceding Fig S4). Panel B: The panel shows an example for enrichment culture vial $D_{A.1}$ (enrichment line A in digestate, enrichment number 1): The measured oxygen concentration declined rapidly during the first 10 hours. The estimated electron flow rate to oxygen (Ve O2) declined accordingly and was gradually replaced by the electron flow to N_2O (Ve NOS). Ve total is the sum of the electron flow to oxygen and N_2O.

3.3 SIMPER analysis on 16S amplicon data

Table S4: SIMPER analysis results output of the top 10 OTUs contribution to the explained variance in the D lines.

Taxon	Clade	Avgerage dissimil.	Contrib. (%)	Cumulat. (%)	Mean abundance (%)						
					$SD_{A\text{-}G.1}$	$SD_{A\text{-}G.2}$	$SD_{A\text{-}G.3}$	$SD_{A\text{-}G.4}$	$SD_{A\text{-}G.5}$	$SD_{A\text{-}G.6}$	$SD_{A\text{-}G.7}$
OTU1	A	0.0659	48.5	48.5	0.228	0.155	0.127	4.96	7.58	41.4	32.9
OTU3	C	0.0196	14.4	62.9	26.1	9.19	0.20	0.074	0.017	0.009	0.015
OTU6	A	0.0131	9.64	72.6	0.104	6.29	21.9	20.0	13.9	8.27	8.36
OTU2	A	0.0116	8.56	81.1	8.56	18.8	28.6	15.8	22.5	7.87	17.1
OTU4	C	0.0064	4.70	85.8	15.0	5.08	0.229	0.054	0.011	0.007	0.008
OTU5	A	0.0046	3.35	89.2	0.059	0.124	7.30	4.78	13.2	3.52	7.35
OTU8	A	0.0038	2.78	92.0	0.039	0.031	0.014	2.32	2.91	6.58	6.98
OTU14	A	0.0014	1.01	93.0	0.035	0.34	5.05	1.20	5.17	0.60	4.20
OTU7	C	0.0010	0.72	93.7	5.28	3.53	0.067	0.023	0.004	0.004	0.003
OTU29	A	0.0009	0.68	94.4	0.023	1.72	1.5	5.39	2.01	4.63	1.23

Table S5: SIMPER analysis results output of the top 10 OTUs contribution to the explained variance in the SD lines.

Taxon	Clade	Avgerage dissimil.	Contrib. (%)	Cumulat. (%)	Mean abundance (%)						
					$SD_{A\text{-}G.1}$	$SD_{A\text{-}G.2}$	$SD_{A\text{-}G.3}$	$SD_{A\text{-}G.4}$	$SD_{A\text{-}G.5}$	$SD_{A\text{-}G.6}$	$SD_{A\text{-}G.7}$
OTU1	A	0.1033	61.9	61.9	0.14	4.2	14.8	47.0	43.5	55.3	39.3
OTU11	A	0.0133	7.98	69.9	2.30	11.2	4.94	1.46	2.85	2.19	11.7
OTU2	A	0.0105	6.31	76.2	0.36	2.86	20.7	5.13	13.4	3.98	8.91
OTU6	A	0.0061	3.63	79.9	0.05	4.66	17.7	7.71	8.11	4.32	6.0
OTU3	C	0.0057	3.42	83.3	14.10	4.61	0.134	0.023	0.014	0.010	0.008
OTU4	C	0.0053	3.16	86.4	13.30	4.2	0.205	0.020	0.008	0.006	0.003
OTU17	A	0.0040	2.37	88.8	0.25	12.1	2.21	2.15	0.321	0.441	0.106
OTU7	C	0.0031	1.87	90.7	10.30	4.08	0.156	0.014	0.004	0.004	0.002
OTU5	A	0.0029	1.72	92.4	0.03	0.469	10.7	2.62	5.93	1.82	4.24
OTU8	A	0.0019	1.14	93.5	0.01	0.118	0.694	3.76	4.17	6.05	6.02

4 Genome sequencing, phylogeny and *eco-physiological genome analysis* of isolated organisms

Table S6: SMRT® link software (PacBio®) output (assembly parameters, alignment to draft assembly, polished assembly, coverage) and CheckM calculated completeness (presence of single copy marker genes) and contamination (multiple single copy marker genes) of isolated organisms.

Isolates:	CB-01	CB-03	BM	AM	PS-02	OB
Assembly Parameters						
Method	HGAP4	HGAP4	HGAP4	HGAP4	Microbial Assembly	Microbial Assembly
Seed Coverage	30	30	30	22	20	15
Expected Genome Length	2 740 000	2 740 000	2 710 000	4 630 000	4 340 000	4 830 000
Alignment to Draft Assembly						
Percent Aligned Bases	95.41%	92.53%	95.66%	84.55 %	93.60 %	76.39 %
Number of Subreads (aligned)	202 702	304 312	456 704	226 629	166 555	192 289
Number of Polymerase Reads (aligned)	13 088	20 485	43 392	18 713	14 278	14 180
Polymerase Read Length Mean (aligned) [bp]	50 243	50 040	37 734	38 599	38 419	42 567
Polymerase Read Length Max (aligned)	134 672	130 398	121 149	122 221	125 758	123 538
Polished Assembly						
Polished Contigs	1	1	2	1	5	54
Maximum Contig Length [bp]	2 979 886	2 718 917	2 711 532	4 571 002	4 016 625	297 087
Sum of Contig Lengths [bp]	2 979 886	2 718 917	2 754 828	4 571 002	4 494 782	4 640 821
Coverage						
Mean Coverage	207	354	552	146	113	120
Missing bases (%)	0.00 %	0.00 %	0.00 %	0.00 %	0.00 %	0.00 %
CheckM quality parameters						
Completeness	100 %	100 %	99.77 %	99.97 %	99.96 %	80.32 %
Contamination	0.74 %	0.25 %	0 %	0 %	1.16 %	0.43 %

Table S7: Isolates of N_2O reducing bacteria isolated from the final enrichment (samples D_7 and SD_7) in autoclaved digestate: The isolates were circumscribed by OTUs based on 16S identity (> 97 %). Average OTU abundance (7 biological replicates ± standard deviation) is shown for each OTU circumscribing isolated organisms for enrichment $D_{A\text{-}G.1}$/$SD_{A\text{-}G.1}$ (first enrichment in live material), $D_{A\text{-}G.1}$/$SD_{A\text{-}G.1}$ (last gamma sterilized soil enrichment) and $D_{A\text{-}G.1}$/$SD_{A\text{-}G.1}$ (final enrichment in autoclaved digestate).

Isolate:	Circumscribed by OTU	Clade	% 16S rDNA seq. ident. (Overlapping region: 404 - 429 bp)	Average OTU abundance (%) ± standard deviation (n = 7)					
				$D_{A\text{-}G.1}$	$D_{A\text{-}G.6}$	$D_{A\text{-}G.7}$	$SD_{A\text{-}G.1}$	$SD_{A\text{-}G.6}$	$SD_{A\text{-}G.7}$
Cloacibacterium sp. **CB-01**	1	A	99.8 %	0.23 ± 0.02	41.4 ± 9.6	32.9 ± 10.3	0.14 ± 0.04	55.3 ± 2.0	39.3 ± 9.6
Cloacibacterium sp. **CB-03**	1	A	99.8 %						
Azonexus sp. **AN***	2	A	98.2 %	8.56 ± 0.54	7.87 ± 1.82	17.1 ± 2.87	0.36 ± 0.16	17.1 ± 2.87	8.91 ± 3.12
Pseudomonas sp. **PS-02**	8	A	99.8 %	0.04 ± 0.05	6.58 ± 4.85	6.98 ± 5.52	0.011 ± 0.002	3,98 ± 0.55	6.02 ± 3.12
Aeromonas sp. **AM**	19	A	99.5 %	0.031 ± 0.026	2.15 ± 2.17	2.26 ± 2.27	0.017 ± 0.007	6.05 ± 1.74	4.49 ± 0.97
Brachymonas sp. **BM**	37	A	100 %	0.004 ± 0,003	1.125 ± 0.313	0.63 ± 0.12	0.0075 ± 0.0065	3.68 ± 0.96	0.308 ± 0.159
Ochrobactrum sp. **OB**	74	D	100 %	0.003 ±0,003	0.227 ± 0.055	0.003 ± 0.002	0.0017 ± 0.0013	0.57 ± 0.15	0.005 ± 0.003

* The genome of *Azonexus sp*. AN was not sequenced: 16S rDNA sequence identity with OTUs was determined by alignment of 16S OTU sequence and 16S from Sanger sequencing of PCR amplicons amplified using 27F and 1492R universal primer pairs (see main text).

Table S8: ddPCR quantification of 16S copy numbers on pooled samples (A to G) of DNA extracts from $D_{A\text{-}G.j}$ and $SD_{A\text{-}G.j}$ (j = 1-7), D0 and SD0, and sterile growth substrates used throughout the enrichment (AC-dig and ϒ-Soil) and standard error (n = 3).

Line	Material:	Sample:	16S/vial:	Stdev/sqrt(n)
D	Live digestate	D_0	3.50E+11	7.0E+09
	Live digestate	$D_{A\text{-}G.1}$	1.80E+11	4.7E+09
	ϒ Soil	$D_{A\text{-}G.2}$	1.40E+11	7.9E+09
	AC-Dig	$D_{A\text{-}G.3}$	1.60E+11	4.4E+09
	ϒ Soil	$D_{A\text{-}G.4}$	2.10E+11	1.4E+09
	AC-Dig	$D_{A\text{-}G.5}$	2.00E+11	7.1E+09
	ϒ Soil	$D_{A\text{-}G.6}$	2.50E+11	7.4E+09
	AC-Dig	$D_{A\text{-}G.7}$	2.00E+11	6.3E+09
SD	Live dig:soil mix	SD_0	2.60E+11	2.1E+09
	Soil:mix after enr.	$SD_{A\text{-}G.1}$	1.60E+11	9.9E+09
	ϒ Soil	$SD_{A\text{-}G.2}$	1.10E+11	6.9E+09
	AC-Dig	$SD_{A\text{-}G.3}$	1.10E+11	5.0E+09
	ϒ Soil	$SD_{A\text{-}G.4}$	2.60E+11	9.7E+09
	AC-Dig	$SD_{A\text{-}G.5}$	1.70E+11	7.3E+09
	ϒ Soil	$SD_{A\text{-}G.6}$	2.70E+11	3.0E+09
	AC-Dig	$SD_{A\text{-}G.7}$	1.90E+11	4.0E+09
Growth substrate	AC-Dig	Growth substrate	7.00E+10	6.8E+09
	ϒ Soil	Growth substrate	1.60E+10	1.8E+08

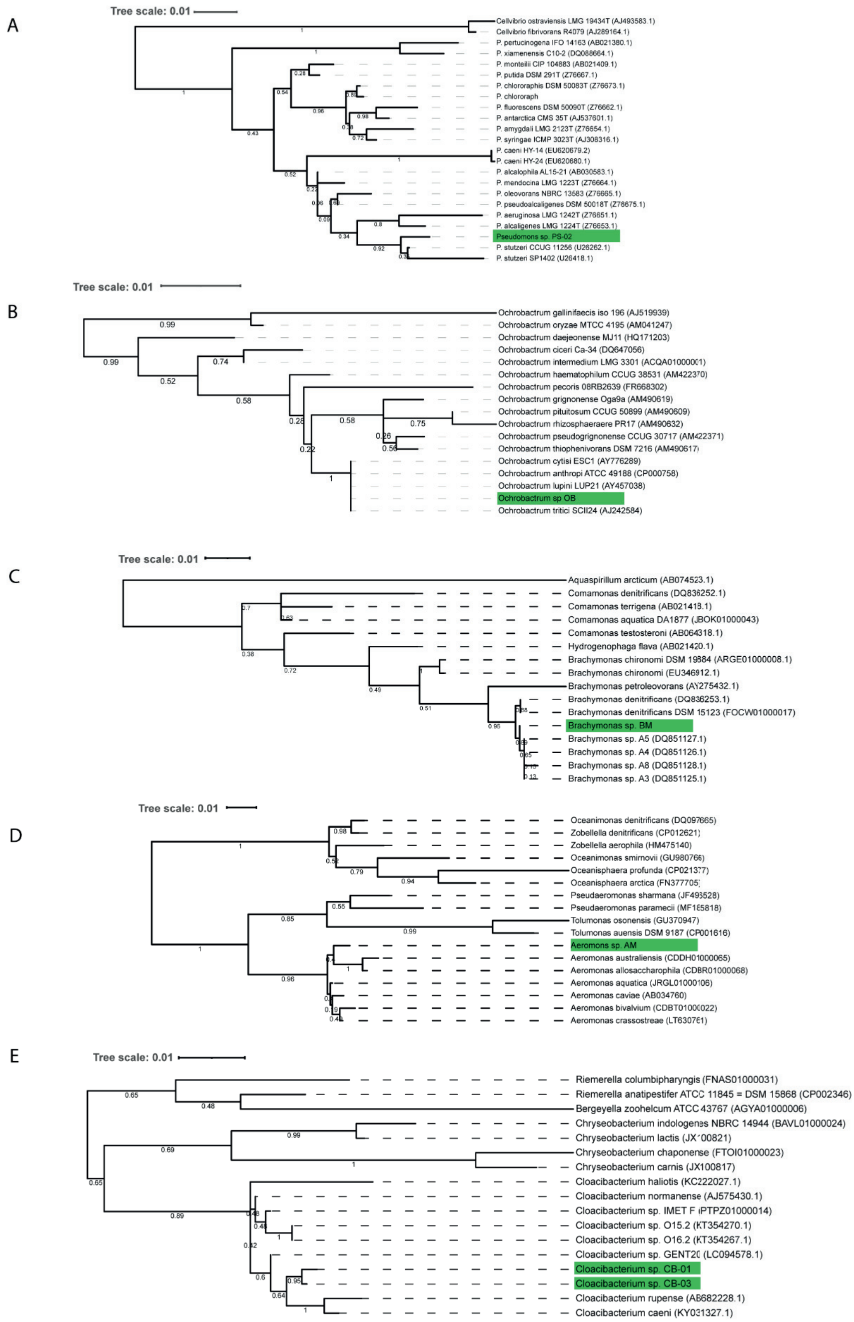

Figure S10: Representative characterized strains and close relatives of the isolated organisms were used to build a neighbor-joining tree (100 bootstrap samplings) from a ClustalW alignment of 16S rDNA sequences. Numbers represent the percentage of bootstrap samplings that generate at each node. Species names are followed by the accession numbers of their 16S rDNA sequences. Panel A: *Pseudomonas* sp. PS-02 (green box), Panel B: *Ochrobactrum* sp. OB (green box), Panel C: *Brachymonas* sp. BM (green box), Panel D: *Aeromonas* sp. AM (green box) and Panel E: *Cloacibacterium* sp. CB-01 and CB-03 (green boxes).

Table S9: The identified proteins predicted as carbohydrate-active enzymes (CAZymes) in the genomes of AM, BM, CB-01, CB-03, PS-02, and OB. The CAZymes were automatically annotated through the dbCAN meta server (Feb 2021), which integrates three tools/databases (i.e. HMMER, DIAMOND, Hotpep) and SignalP. The CAZymes assignment includes the enzyme classes Glycoside Hydrolysis (GHs), Glycosyl transferases (GTs), Polysaccharide lyases (PLs), Carbohydrate Esterases (CEs) and enzymes with Auxiliary Activity (AAs) in addition to Carbohydrate-Binding Modules (CBM). Identical annotation in ≥ 2 tools was required for a CAZY assignment to be considered robust. Prokka annotations of corresponding genes is given in **Supplementary Data S1**.

	PS-02		OB		BM		AM		CB-01		CB-03		
	#	Sign.p	#	Sign.p	#	Sign.p	#	Sign.p	#	Sign.p	#	Sign.p	
GH1			1				3						Glycoside hydrolases
GH2			1				3						
GH3	1	1	1		1		2		4	2	3	1	
GH5	2	2					2				1		
GH8							1	1					
GH9							1						
GH10													
GH13	7						7	3	5	3	6	4	
GH18							1	1					
GH19	2		1				1	1					
GH20							2	1					
GH23	6	5	9	8	6	3	9	9					
GH24			1										
GH25			2	2					1		1		
GH26			1	1									
GT28									1				
GH30									2	2	1	1	
GH31									1	1	1	1	
GH32							1						
GH36							1						
GH37	2												
GH39	1	1											
GH43							1	1					
GT51									1				
GH53									1	1	2	2	
GH63							1	1					
GH73	1		2				1		1	1	1	1	
GH77	1						1				1		
GH83					1								
GH84							1						
GH88	1												
GH89									1	1			
GH97									1	1	1	1	
GH102			1		1		1						
GH103	2	1	3	3	2	2	3	2					
GH104			1		1	0							
GH105							1						
GH108			2				1						
GH148			1	1									
GH166													
Sum	26	10	27	15	12	5	45	20	19	12	18	11	

	PS-02		OB		BM		AM		CB-01		CB-03		
	#	Sign.p	#	Sign.p	#	Sign.p	#	Sign.p	#	Sign.p	#	Sign.p	
CBM5							2	2					Carbohydrate-binding module families.
CBM20	1	1							1				
CBM48	2						1		1		1		
CBM50	2	2	2				4	2					
CBM73							1	1					
GT0	1		2				3						Glycoside transferases
GT1							1		1		1		
GT2	5		6		3		7		9		14		
GT4	5		10		4				7		15		
GT5									2		2		
GT9	2						4		1		1		
GT19	1		1		1		1		1				
GT20	2		1										
GT26	1												
GT25			4				1						
GT26			1										
GT28	1		1		1		1				1		
GT30	1		1		1		1		1		1		
GT32							1				1		
GT35	1						1		1		1		
GT41													
GT51	3	2	3		3		6		1				
GT83			1		1		1						
GT84			2		1								
GT102			1										
GT104	1				1		1						
GT107							1						
CE1					1						1	1	Carbohydrate esterases
CE4	1		2		1		1						
CE9			1				1						
CE11	1		1		1		1		1		1		
CE14									1		1		
AA3			3		2								Auxiliary acitivty
AA6	1		1										
AA10							1	1					

Table S10: A selection of identified enzymes predicted as carbohydrate-active enzymes (CAZymes) from the dbCAN meta-server and corresponding PROKKA annotations of enzymes targeting extracellular carbohydrates (indicated by identified signal sequence for membrane trans allocation (Signal P)) and genes encoding proteins involved in glycogen metabolism in the genomes of PS-02, OB, BM, AM, CB-01 and CB-03. BM did not contain annotated CAZymes of particular relevance. A complete list of dbCAN grouped genes is given together with corresponding Prokka annotations for each genome in **Supplementary Data S1**

	Enzyme	EC	Group (CAZy):	Target	Signal P
PS-02	Endoglucanase	3.2.1.4	GH5	Cellulose	Yes
	β-xylosidase	3.2.1.-	GH3	Xylose	Yes
	Glucan 1,4-α-maltotetraohydrolase	3.2.1.60	CBM20	Maltose	Yes
	Glycogen synthase	2.4.1.21	GT5	Glycogen	No
	Glycogen operon protein GlgX	3.2.1.-	CBM48	Glycogen	No
OB	Glycogen synthase	2.4.1.11	GT4	Glycogen	No
	β-glucosidase A	3.2.1.21	GH1	Cellulose	No
BM					
AM	Chitodextrinase	3.2.1.14	CBM73	Chitin	Yes
	α-glucosidase	3.2.1.-	GH63	Starch/Maltose	Yes
	N-diacetylchitobiase	3.2.1.52	GH20	Chitobiose/Glycoproteins	Yes
	α-amylase	3.2.1.1	GH13	Starch/Glycogen	Yes
	α-L-arabinofuranosidase	3.2.1.55	GH43	Arabinoxylan/arabinogalactan	Yes
	Metalloprotease (gene: *StcE*)	3.4.24.-	CBM5	Glycoproteins	Yes
	Endoglucanase	3.2.1.4	GH8	Cellulose	Yes
	Glycogen operon protein glgX homolog	3.2.1.-	GH13	Glycogen	No
	Glycogen syntase	2.4.1.21	GT5	Glycogen	No
CB-01	Arabinogalactan endo-β-1,4-galactanase	3.2.1.89	GH53	Arabinogalactan	Yes
	Cyclomaltodextrinase	3.2.1.54	GH13	Maltodextrin	Yes
	Glucan 1,4-α-glucosidase	3.2.1.3	GH97	Glycogen/starch	Yes
	Periplasmic alpha-amylase	3.2.1.1	GH13	Starch	Yes
	Beta-xylosidase	3.2.1.-	GH3	Xylobiose	Yes
	β-glucosidase	3.2.1.21	GH3	Cellulose	Yes
	Oligosaccharide 4-alpha-D-glucosyltransferase	2.4.1.161	GH31	(1->4)-α-D-glucans	Yes
	Glycogen phosphorylase	2.4.1.1	GT35	Glycogen	No
	Glycogen synthase	2.4.1.21	GT5	Glycogen	No
CB-03	Oligosaccharide 4-alpha-D-glucosyltransferase	2.4.1.161	GH31	(1->4)-α-D-glucans	Yes
	Alpha-amylase 2	3.2.1.1	GH13	Starch	Yes
	Cyclomaltodextrinase	3.2.1.54	GH13	Maltodextrin	Yes
	Glucan 1,4-α-glucosidase	3.2.1.3	GH97	Starch/Glycogen	Yes
	Arabinogalactan endo-β-1,4-galactanase	3.2.1.89	GH53	Arabinogalactan	Yes
	Arabinogalactan endo-β-1,4-galactanase	3.2.1.89	GH53	Arabinogalactan	Yes
	Periplasmic alpha-amylase	3.2.1.1	GH13	Glycogen/Starch	Yes
	β-glucosidase	3.2.1.21	GH31	Cellulose	Yes
	Glycogen phosphorylase	2.4.1.1	GT35	Glycogen	No
	Glycogen synthase	2.4.1.21	GT5	Glycogen	No

Table S11: MEROPS annotated peptidases in the genomes of PS-02, OB, BM, AM, CB-01 and CB-03. Every protein sequence was screened for presence of signal sequences in SignalP 5.0 and the MEROPS subfamilies were collapsed to families. Prokka annotations of corresponding genes is given in **Supplementary Data S1**

	PS-02		OB		BM		AM		CB-01		CB-03		
Group	#	Signal P	#	Signal P	#	Signal P	#	Signal P	#	Signal P	#	Signal P	
S1	3	2	4	4	3	2	4	2	2	1	2	1	Serine peptidases
S8	1				1		1						
S9	1		2				3	3	5	3	4	3	
S11	1		1	1	3	1	5	4	1		1		
S12	2		2						3	3	3	3	
S13							1	1	2	2	2	2	
S14			3		2		5		2		2		
S15									1	1	1	1	
S16	3		2		1		2		1		1		
S26	1		1		1		1						
S33	1		2		2		1						
S41	1	1					1	1	1	1	1	1	
S46									2	2	2	1	
S49	1						2		2	1	1		
S51			1				1		2	1	1		
S54	1						1		2		1		
S66					2	1			1		1		
M1	1		1		1		1						Metallo peptidases
M3	1				1		1		2		2	1	
M4	1						1	1					
M6							1	1					
M13							1	1	2	2	2	2	
M14							1	1					
M16	1	1	2	1			1						
M17	1		2		1		4				1		
M18	1												
M20							2		1		2		
M23	1	1					2	1					
M24	2		3		2		2		2		2	1	
M28	1	1	1				1	1	1	1	1	1	
M29			1										
M32							1						
M38							1						
M41	5		3		2		1		2		1		
M42	1	1	2	2					1		1		
M488	3	2			4	2	3	2	1		1		
M50	1		1		1				1		1	1	
M56											1		
M66							1	1					
M67	1												
M74							1	1					
M103	2		2		2	0	4						
C1					1								Cysteine peptidases
C14					1	1							
C15							1						
C40			1				1	1	1		1		
C76					1								
C82	2	2					2	2					
A8	1		2		1		1		1		1		Aspartic peptidases
A31							2		1				
A39					1								
T1	2		2		2		2						Threnonine peptidases
T2			2						3		1	1	
I8											1		Peptidase inhibitors
I32	1		1										
I87	2		3		1		2	1					
P1			3	1	1	0							Mixed catalytic type
U32	1				1	0	1	0					Unknown catalytic mechanism
Undef:	3	0	3	0	1	0	2	0	2	0	1	0	Mostly penicilin binding proteins.

Table S12: Prokka annotated genes coding for proteins involved nodule formation and nitrogenase activity in genome of *Ochrobacter* sp. OB*.

Gene:	Detected:	Onthology:	Reference:
nodN	Yes		Surin and Downing 1988, Baey et al 1992
nodM	Yes	Glutamine-fructose-6-phosphatase (EC: 2.6.1.16)	Surin and Downing 1988, Baey et al 1992
CC_0717	Yes	Nodulin related protein CC_0717. Unknown function.	
nifS	Yes	Cysteine desuluronase (EC: 2.8.1.7)	Kennedy and Dean 1992
nifU	Yes	NifU-like domain protein	Kennedy and Dean 1992
nifDKH	No	Catalytic subunits of nitrogenase	McGlynn et al 2013
anfG	No	Catalytic subunits of nitrogenase	McGlynn et al 2013
vnfDKGH	No	Catalytic subunits of nitrogenase	McGlynn et al 2013
fixK	Yes	Nitrogenase transcriptional regulator	Li et al 2010
fixN	Yes	ec:1.9.3.1- Cytochrome-c oxidase.	David et al 1988
fixL	Yes	Sensor protein fixL (EC 2.7.3.-)	Monson et al 1995.

* Quality checking the assembled genome of OB with CheckM did reveal that only 80 % of the single copy marker genes were recovered from the genome of OB (**Tab. S8**), and it is conceivable that potential missing parts of the genome could contain more nod- and nitrogen fixation related genes, as well as other genetic encoded traits as discussed in main text.

5 Assessment of growth or death of OTU's

To assess growth or decline of each OTU within the 6 clades, we calculated the relative increase for each consecutive enrichment culture as $R = \ln(N_{(i)}/(N_{(i-1)}*0.1)$ where N_i is the estimated copy number per vial at the end of enrichment i and $N_{(i-1)}$ is the estimated copy numbers at the end of the foregoing enrichment (both estimated by the relative abundance of the OTU in question and the total copy numbers of 16SrDNA quantified by digital PCR (**Tab. S10**). The multiplication with 0.1 is because 10% of the content of one enrichment culture was transferred to the next. *R* for the initial enrichment in live digestate (with and without live soil added is $\ln(N/N_0)$, where N is the abundance after enrichment and N_0 is the abundance measured at the onset of this enrichment). The result for the 6 clades is shown in **Figs. S11-S16.**

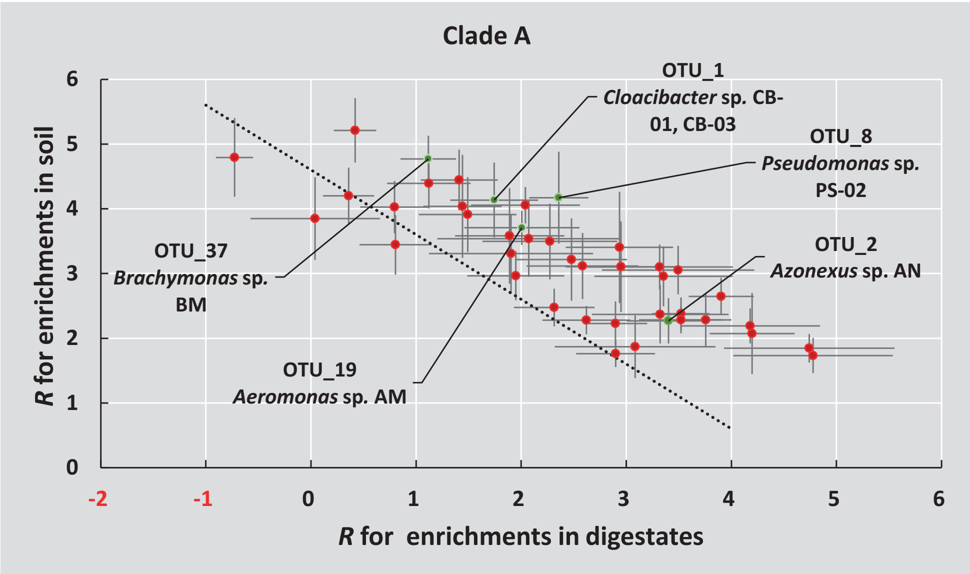

Figure S11 Assessment of growth/death (soil versus digestate) of OTU's within Clade A. For the 42 OTUs of Clade A the increase or decrease in copy numbers for each individual enrichment vial was estimated as $R = \ln(N_{(i)}/(N_{(i-1)} \cdot 0.1)$. For each OTU, the average *R* for the enrichments in autoclaved digestate ($R_{digestate}$) and γ-sterilized soil (R_{soil}) were calculated. The panel shows R_{soil} plotted against $R_{digestate}$, with standard error (n=8) marked by vertical and horizontal lines. The dashed line is the plotted equation $R_{soil}+R_{digestate}= 4.6$, which marks a division between OTU's that are sustained ($R_{soil}+R_{digestate} > 4.61$) or gradually washed out ($R_{soil}+R_{digestate} < 4.61$) throughout the dual enrichment cultures. The plotting of R_{soil} and $R_{digestate}$ for individual OTU's shows that the OTU's within Clade A span a continuum from "Soil specialists" (high R_{soil}, low/negative $R_{digestate}$ values) through "Generalists" (similar R_{soil} and $R_{digestate}$ values >2) and further on to "Digestate specialists" (low R_{soil}, high R_{dig}). Interestingly several of the isolates qualifies as Generalists, while *Azonexus* is more of a Digestate specialist, as suspected (Jonassen et al 2021). R_{soil} was negatively correlated with $D_{digestate}$ (regression function: $R_{soil}=4.7-0.6 \cdot R_{digestate}$, $r^2=0.7$, $p<0.01$).

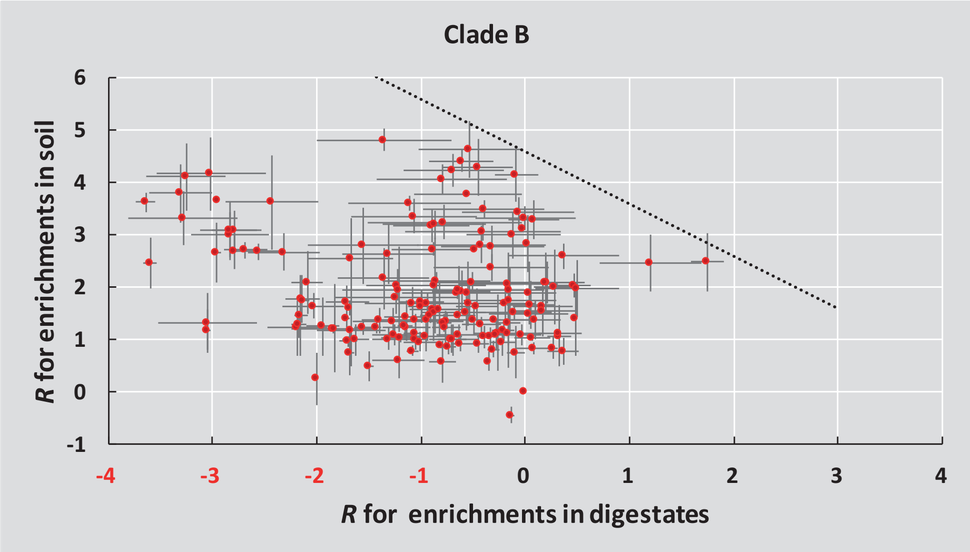

Figure S12: Assessment of growth/death (soil versus digestate) of OTU's within Clade B. For the 172 OTUs of Clade B the increase or decrease in copy numbers was estimated as R= ln($_{N(i)}$/($N_{(i-1)}$·0.1). For each OTU, the average R for the enrichments in autoclaved digestate and γ-sterilized soil were calculated. The panel shows R for Soil plotted against R for Digestate, with standard error (n=8) marked by vertical and horizontal lines. The dashed line marks the division between cells that are predicted to die out: R_{soil}+$R_{digestate}$ >4.61 for organisms that will increase throughout and <4.61 for organisms that will decline throughout. All OTU's within this clade are below the line. The distribution of R values suggests the majority dies out due to failure in the digestate, rather than in soil.

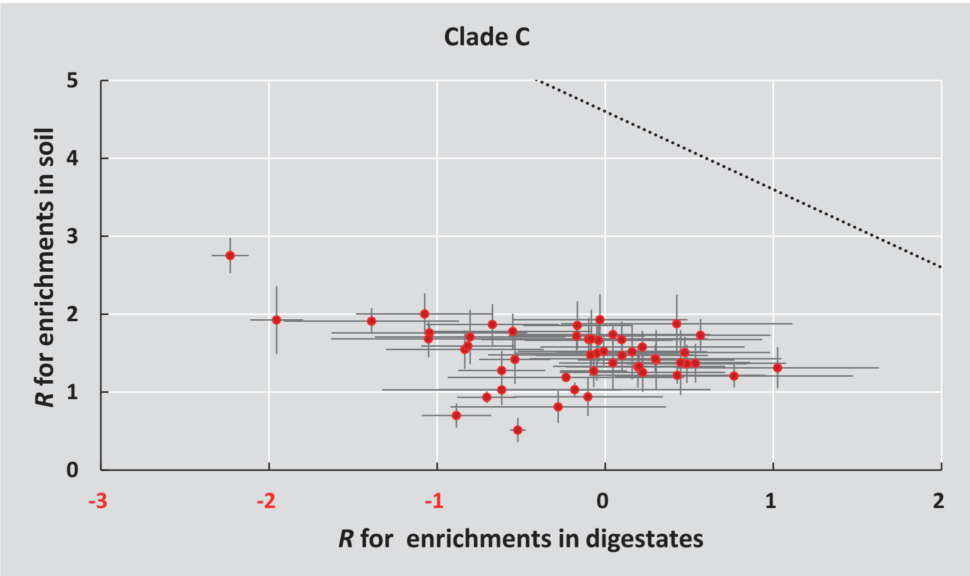

Figure S13: Assessment of growth/death (soil versus digestate) of OTU's within Clade C. For the 51 OTUs of Clade C the increase or decrease in copy numbers was estimated as R= ln($_{N(i)}$/($N_{(i-1)}$·0.1). For each OTU, the average R for the enrichments in autoclaved digestate and γ-sterilized soil were calculated. The panel shows R for Soil plotted against R for Digestate, with standard error (n=8) marked by vertical and horizontal lines. The dashed line marks the division between cells that are predicted to die out: $R_{soil}+R_{digestate}$ >4.61 for organisms that will increase throughout and <4.61 for organisms that will decline throughout. All OTU's within this clade are below the line.

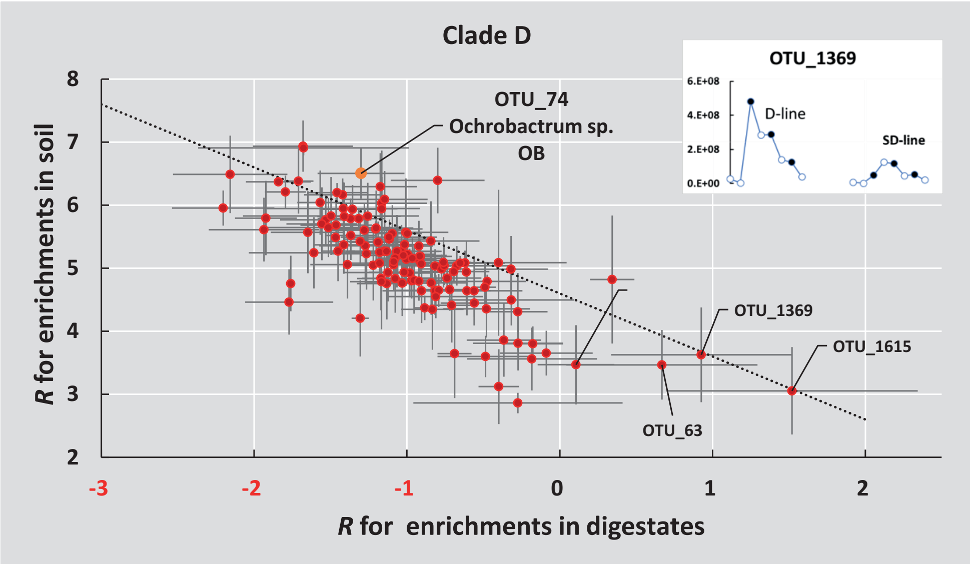

Figure S14: Assessment of growth/death (soil versus digestate) of OTU's within Clade D. For the 128 OTUs of Clade D the increase or decrease in copy numbers was estimated as R= $\ln(N_{(i)}/(N_{(i-1)}*0.1)$. For each OTU, the average R for the enrichments in autoclaved digestate and γ-sterilized soil were calculated. The panel shows R for Soil plotted against R for Digestate, with standard error (n=8) marked by vertical and horizontal lines. For digestate, the majority of OTU's had R between -2 and -1.5, which indicates a 80-85% decline during the enrichment in digestate. In contrast, R for enrichments in soil ranged from 3-7, indicating that the abundance increased by a factor of 150-1100 (=7-10 cell divisions) during the enrichment in soil. A clear negative correlation between R_{soil} and $R_{digestate}$ is observed (r^2=0.573, p<0.01). The outliers with apparent growth in digestate (R>0) showed somewhat erratic development of abundance throughout, as illustrated for OTU_1369 (inserted panel). The dashed line marks the division between cells that are predicted to die out ($R_{soil}+R_{digestate}$ >4.61 for organisms that will increase throughout and <4.61 for organisms that will decline throughout). The majority is below the line (= declining), while some are sustained or grow slightly, which was the case for the OTU 74 circumscribing the isolated *Ochrobactrum* sp. OB. The distribution of R values suggests that the majority dies out fast in the digestate but grow fast in soil.

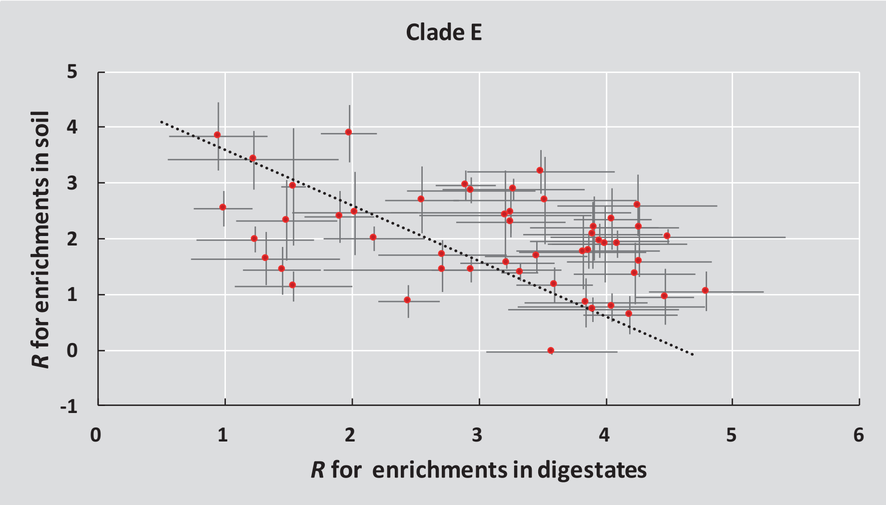

Figure S15: Assessment of growth and death of OTU's within Clade E. For the 50 OTUs of Clade E the increase or decrease in copy numbers was estimated as R= $\ln(N_{(i)}/(N_{(i-1)}*0.1)$. For each OTU, the average R for the enrichments in autoclaved digestate and γ-sterilized soil were calculated. The panel shows R for Soil plotted against R for Digestate, with standard error (n=8) marked by vertical and horizontal lines. The dashed line marks the division between cells that are predicted to die out: $R_{soil}+R_{digestate}$ >4.61 for organisms that will increase throughout and <4.61 for organisms that will decline throughout. 35 of the 50 OTU's within this clade are above the line.

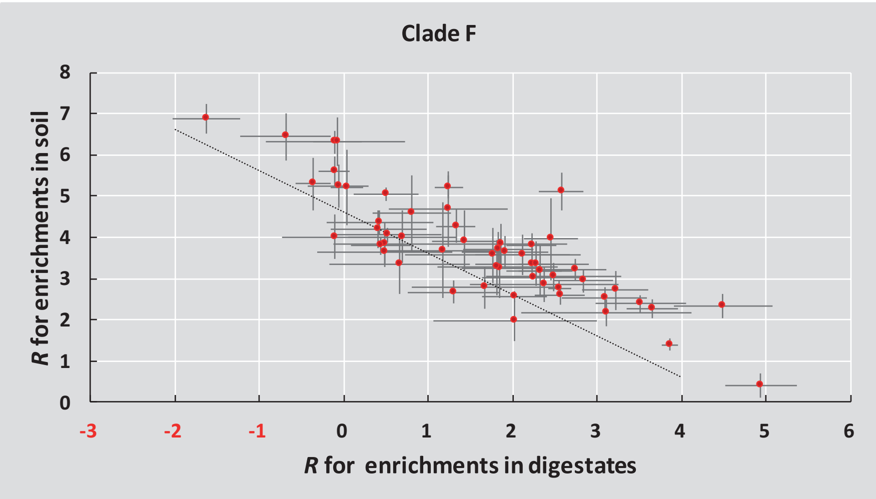

Figure S16: Assessment of growth and death of OTU's within Clade F. For the 57 OTUs of Clade F the increase or decrease in copy numbers was estimated as R= $\ln(N_{(i)}/(N_{(i-1)}\cdot 0.1)$. For each OTU, the average *R* for the enrichments in autoclaved digestate and γ-sterilized soil were calculated. The panel shows *R* for Soil (R_{soil}) plotted against *R* for Digestate ($R_{digestate}$), with standard error (n=8) marked by vertical and horizontal lines. The dashed line marks the division between cells that are predicted to die out: $R_{soil}+R_{digestate}$ >4.61 for organisms that will increase throughout and <4.61 for organisms that will decline throughout. 46 of the 57 OTU's within this clade are above the line. R_{soil} was negatively correlated with $D_{digestate}$ (regression function: $R_{soil}=5.0-0.8\cdot R_{digestate}$, $r^2=0.7$, $p<0.01$).

6 Denitrifying phenotype experiments

6.1 *Pseudomonas sp.* PS-02

The genome analysis of *Pseudomonas sp*. PS-02 (**Fig. 4A in the main paper**) revealed genes coding for all denitrification-related reductases involved in the sequential reduction of NO_3^- to N_2: cytoplasmic *nar*, *nirS*, *nor* and *nosZ* (clade I), thus predicting a full-fledged denitrifier. In liquid culture supplemented with NO_3^- or NO_2^- and O_2 cells transitioned seamlessly from oxic to anaerobic respiration on NO_3^- (**Fig. S17**) or NO_2^- (**Fig. S18**) whilst maintaining strict control of gaseous intermediates NO and N_2O. NO_2^- accumulated to mM levels when supplied with 2 mM NO_3^- (**Fig. S17**). Cells favored respiration of exogenously supplied N_2O over NO_3^- (**Fig. 4A main paper**, supplementing kinetics in **Fig. S19**) and NO_2^- (**Fig. S20**), which might indicate that the relative activity of Nos was higher than the other N-reductases at the oxic/anoxic transition, or a delay of Nar (and Nir) expression succeeding the oxic/anoxic transition relative to Nos, as competition for electrons between Nar and Nos was not expected. The strict control of N_2O under growth on NO_3^- and NO_2^-, and with an apparent over capacity for N_2O respiration over NO_3^- would deem PS-02 as a strong N_2O sink and an interesting candidate for inoculation of soils.

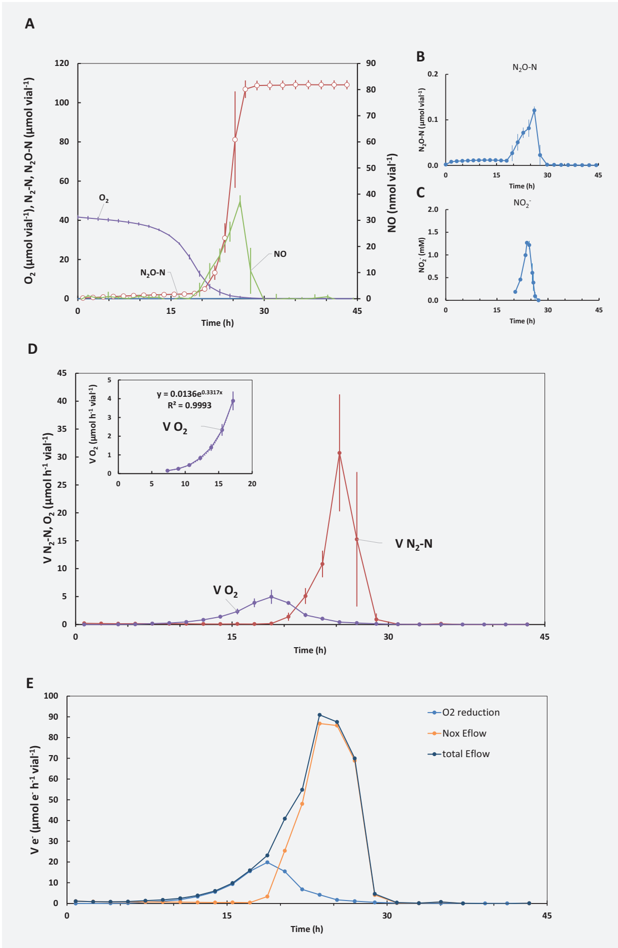

Figure S17 Denitrification phenotype of *Pseudomonas* sp. PS-02 when provided with O_2 and NO_3. PS-02 was grown in gas-tight 120 mL vials with 50 mL Sistrom's succinate medium initially supplemented with 1 mL O_2 and 2mM NO_3^- at constant temperature and stirring (20 °C, 600 rpm). Initial OD_{660} ≈ 0.001. Panel A**:** Measured gases (N_2O, NO, O_2) and calculated cumulative N_2 throughout the incubation. Panel B: Measured N_2O throughout the incubation. Panel C: Measured liquid concentration of NO_2^-. Panel D: Calculated O_2 consumption- and N_2 production rates. Inserted panels: exponential regression of initial rates of O_2-reduction (oxic phase). Panel E: Calculated the rates of electron flow channeled to O_2 (O2 reduction), and denitrification (Nox Eflow), and the sum (Total Eflow). The electron flow rate to denitrification was calculated from rates of NO_3^--reduction to NO_2^- (2 mol electrons per mol N), and the three subsequent reduction steps, $NO_2^- \rightarrow NO \rightarrow N_2O \rightarrow N_2$ (1 mol electron per mol N for each reaction), as derived from measurements. Error bars: standard deviation (n = 3).

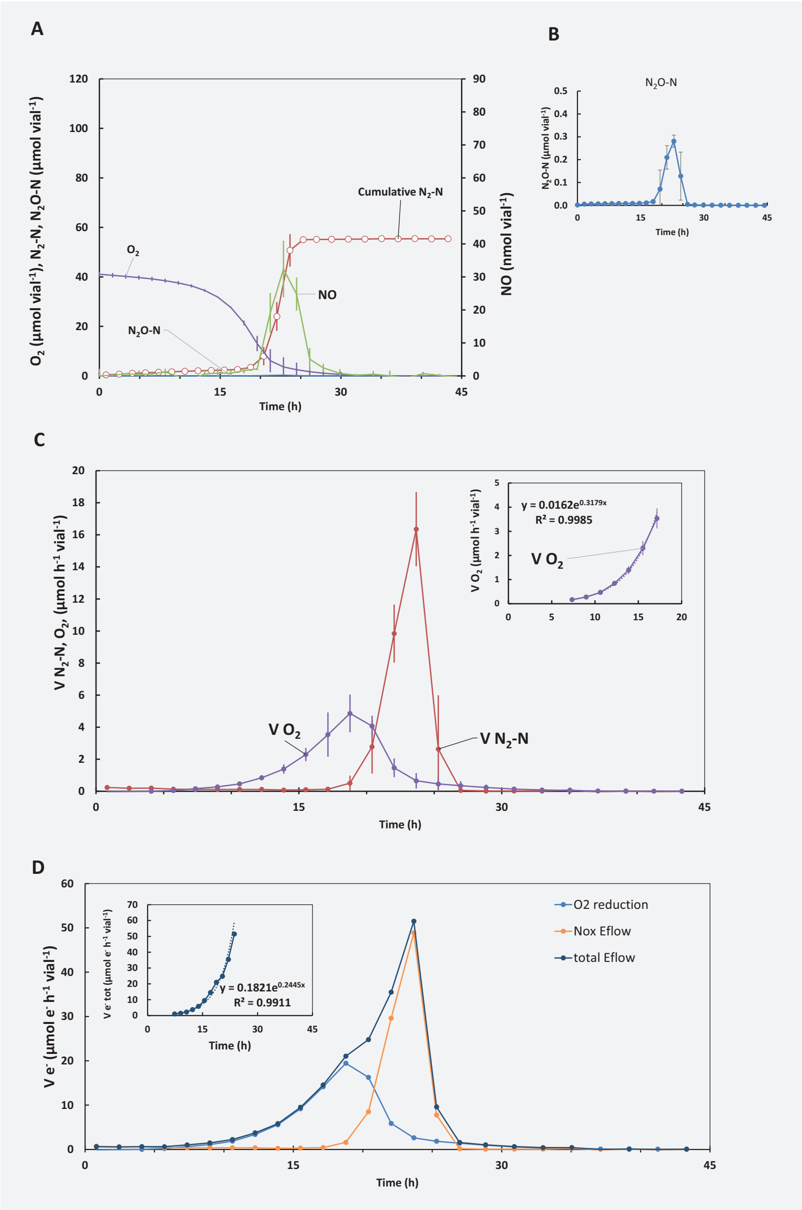

Figure S18: Denitrification phenotype of *Pseudomonas* sp. PS-02 when provided with O_2 and NO_2. PS-02 was grown in gas-tight 120 mL vials with 50 mL Sistrom's succinate medium initially supplemented with 1 mL O_2 and 1mM NO_2^- at constant temperature and stirring (20 °C, 600 rpm). Initial OD_{660} ≈ 0.001. Panel A**:** Measured gases (N_2O-N, NO, O_2) and calculated cumulative N_2-N throughout the incubation. Panel B: Measured N_2O-N throughout the incubation. Panel C: Calculated O_2 and N_2O-N consumption- and N_2-N production rates. Inserted panels: exponential regression of initial rates of O_2-reduction (oxic phase). Panel E: Calculated electron flow rates of total electrons channeled to O_2 (O2 reduction), the NO_x reductases (Nox Eflow), and the sum of the total electron flow to terminal oxidases (Total Eflow). Inserted panel: exponential regression of total electron flow from oxic to anoxic phase. Error bars displayed as standard deviation (n = 3).

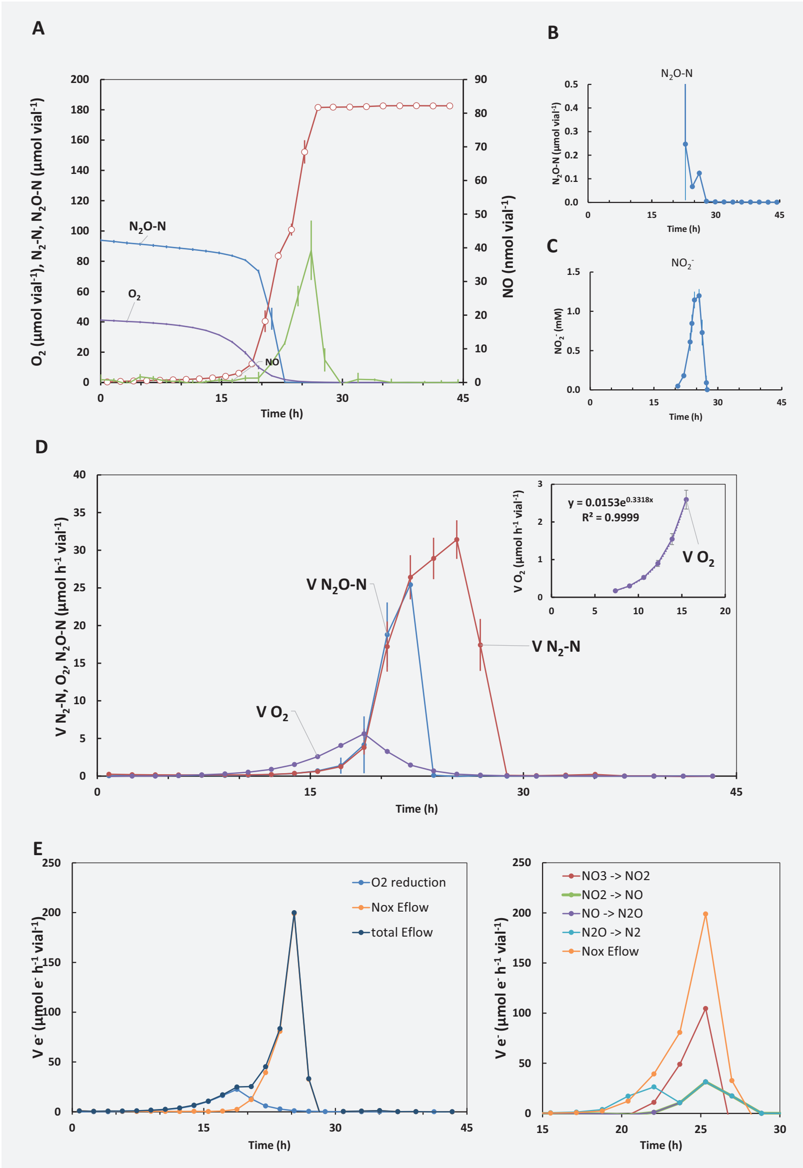

Figure S19: Denitrification phenotype of *Pseudomonas* sp. PS-02 when provided with O_2, N_2O and NO_3. PS-02 was grown in gas-tight 120 mL vials with 50 mL Sistrom's succinate medium initially supplemented with 1 mL O_2, 1 mL N_2O, and 2mM NO_3^- at constant temperature and stirring (20 °C, 600 rpm). Initial OD_{660} ≈ 0.001. Panel A: Measured gases (N_2O-N, NO, O_2) and calculated cumulative N_2-N throughout the incubation. Panel B: Measured N_2O-N throughout the incubation. Panel C: Measured liquid concentration of NO_2^-. Panel D: Calculated O_2 and N_2O-N consumption- and N_2-N production rates. Inserted panels: exponential regression of initial rates of O_2-reduction (oxic phase). Error bars displayed as standard deviation (n = 3). Panels E; Left panel: Calculated electron flow rates of total electrons channeled to O_2 (O2 reduction), the NO_x reductases (Nox Eflow), and the sum of the total electron flow to terminal oxidases (Total Eflow). Inserted panel: exponential regression of total electron flow from oxic to anoxic phase. Right panel: Calculated electron flow rates of total electrons channeled to Nar, Nir, Nor, and Nos and summed electron transfer to the NO_x reductases (Nox Eflow).

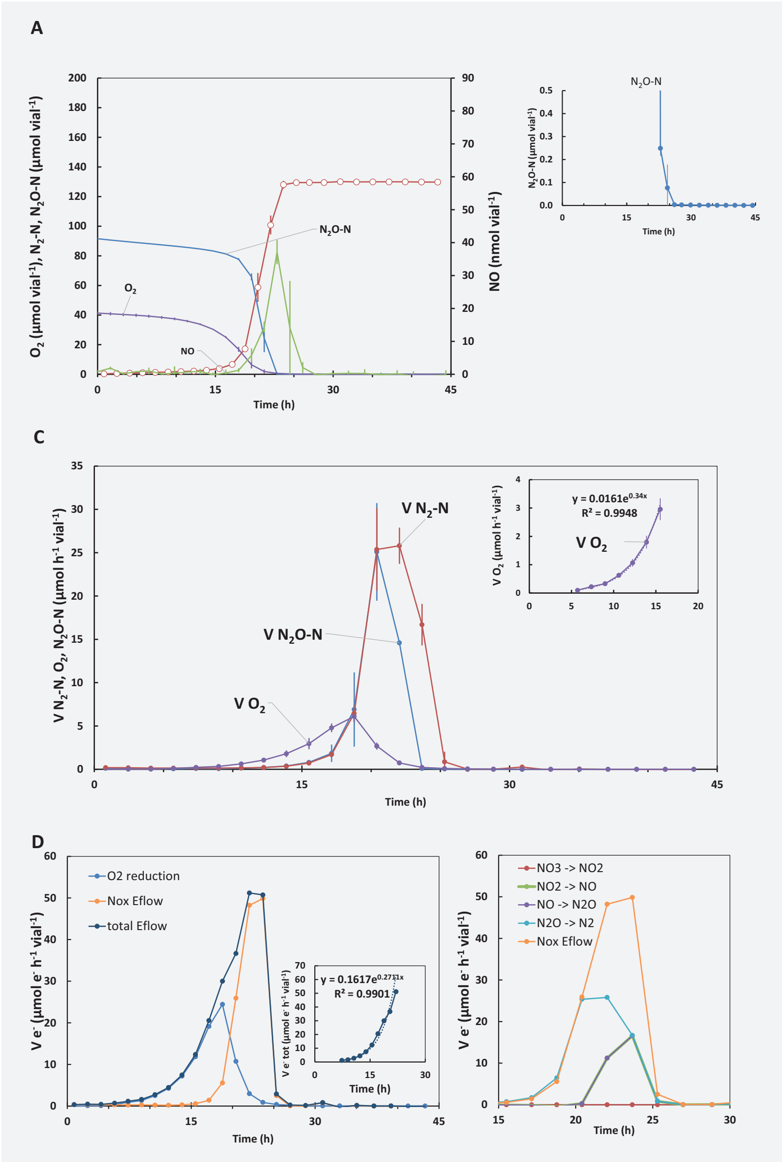

Figure S20: Denitrification phenotype of *Pseudomonas* sp. PS-02 when provided with O_2, N_2O and NO_2. PS-02 was grown in gas-tight 120 mL vials with 50 mL Sistrom's succinate medium initially supplemented with 1 mL O_2, and 1 mL N_2O and 1mM NO_2^- at constant temperature and stirring (20 °C, 600 rpm). Initial $OD_{660} \approx 0.001$. Panel A: Measured gases (N_2O-N, NO, O_2) and calculated cumulative N_2-N throughout the incubation. Panel B: Measured N_2O-N throughout the incubation. Panel C: Calculated O_2 and N_2O-N consumption- and N_2-N production rates. Inserted panels: exponential regression of initial rates of O_2-reduction (oxic phase). Error bars displayed as standard deviation (n = 3). Panels D; Left panel: Calculated electron flow rates of total electrons channeled to O_2 (O2 reduction), the NO_x reductases (Nox Eflow), and the sum of the total electron flow to terminal oxidases (Total Eflow). Inserted panel: exponential regression of total electron flow from oxic to anoxic phase. Right panel: Calculated electron flow rates of total electrons channeled to Nar, Nir, Nor, and Nos and summed electron transfer to the NO_x reductases (Nox Eflow).

6.2 *Ochrobactrum* sp. OB

Ochrobactrum sp. OB (**Fig. 4C** in main paper) had the genetic capacity of a full-fledged denitrifier carrying cytoplasmic *nar*, periplasmic *nap*, *nirK*, *nor* and *nosZ* (clade I), thus predicting a full-fledged denitrifier, which was also reflected by the isolate's denitrifying phenotype: it transiently accumulated nitrite, whilst keeping the gaseous intermediates NO and N_2O low throughout our incubations. A marginal dip in electron flow in the transition between oxic and anoxic respiration of NO_3^- (**Fig. S20**) or NO_2^- (**Fig. S21**) can be understood as a fraction of the respiring cells that did not fully commit to denitrification by not expressing Nir. However, the isolate also demonstrated non-exponential growth (linear increase in N_2 production rates) when respiring solely on NO_2^-, indicating restricted growth. In incubations supplemented with exogenous N_2O in addition to NO_3^- (**Fig. 4C** in main paper, additional gas kinetics in **Fig. S22**) or NO_2^- (**Fig. S23**) gas kinetics indicated that the reduction of N_2O was preferred over nitrate and nitrate. This sums up to make *Ochrobactrum* sp. OB a potential N_2O sink as N_2O reduction was favored over NO_3^- and NO_2^- while limiting the depletion of oxyanions at higher NO_2^- concentrations.

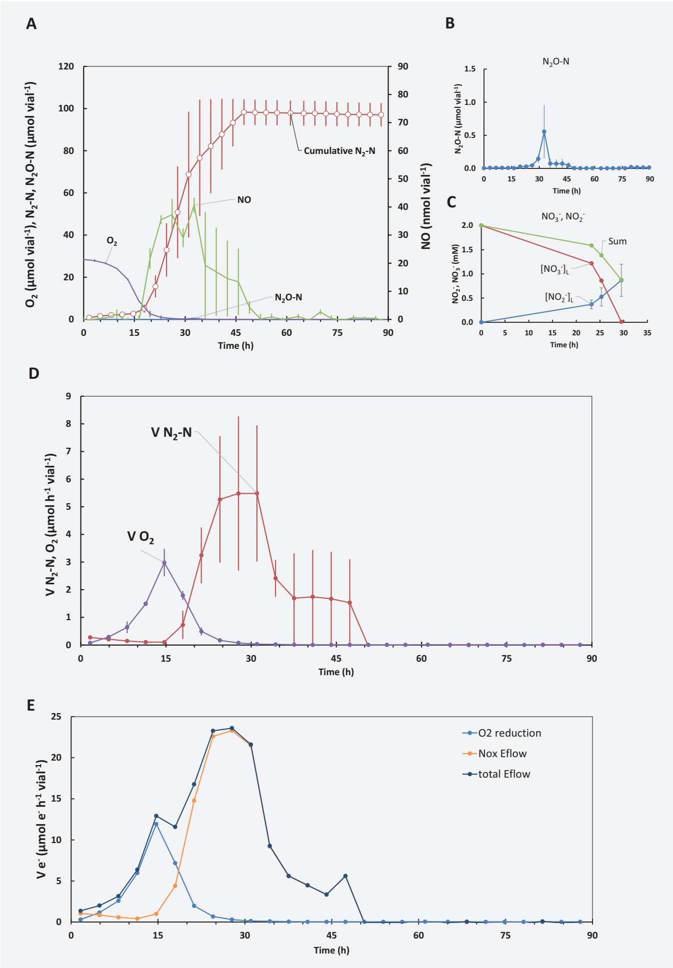

Figure S21 Denitrification phenotype of *Ochrobactrum* sp. OB when provided with O_2 and NO_3^-. OB was grown in gas-tight 120 mL vials with 50 mL Sistrom's succinate medium initially supplemented with 1 mL O_2 and 2mM NO_3^- at constant temperature and stirring (20 °C, 600 rpm). Initial $OD_{660} \approx 0.001$. Panel A**:** Measured gases (N_2O-N, NO, O_2) and calculated cumulative N_2-N throughout the incubation. Panel B: Measured N_2O-N throughout the incubation. Panel C: Measured liquid concentration of NO_3^- and NO_2^- and the sum of NO_3^- and NO_2^-. Panel D: Calculated O_2 and N_2O-N consumption- and N_2-N production rates. Inserted panels: exponential regression of initial rates of O_2-reduction (oxic phase). Panel E: Calculated electron flow rates of total electrons channeled to O_2 (O2 reduction), the NOx reductases (Nox Eflow), and the sum of the total electron flow to terminal oxidases (Total Eflow). Error bars displayed as standard deviation (n = 2).

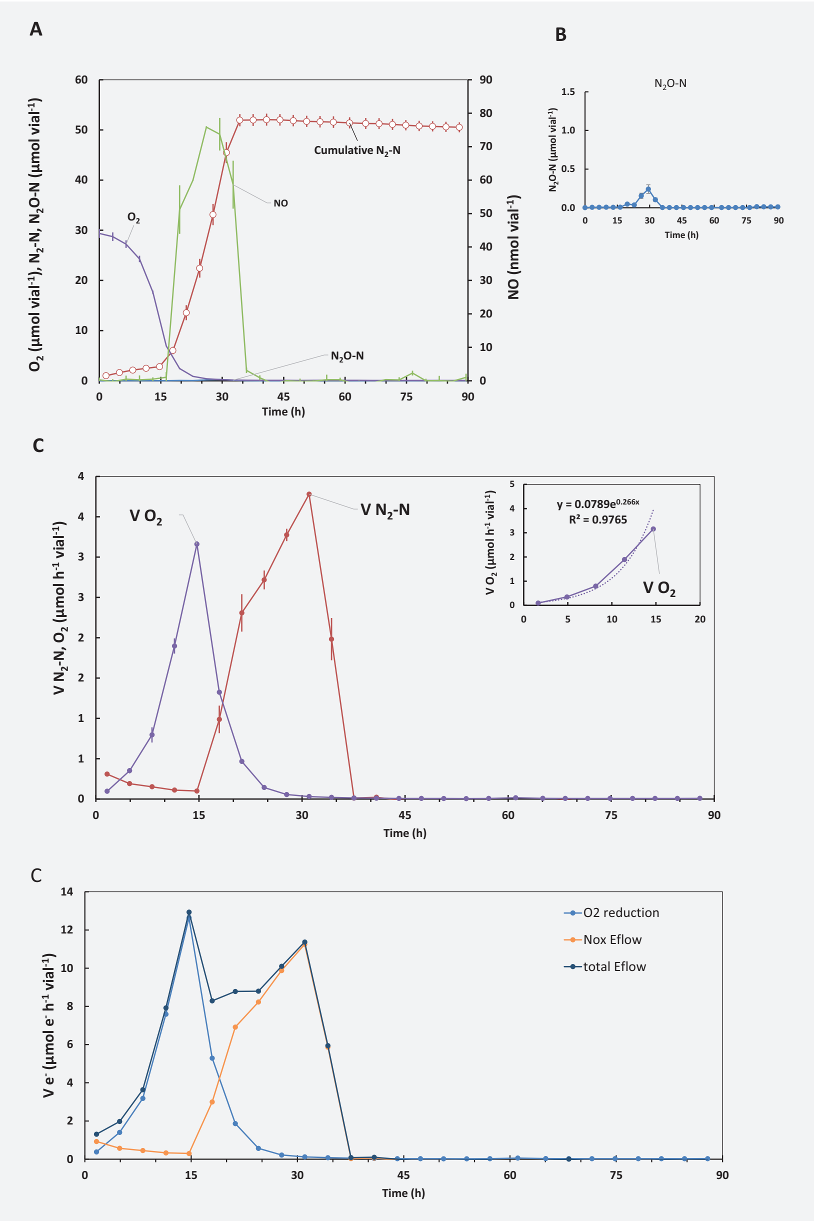

Figure S22: Denitrification phenotype of *Ochrobactrum* sp. OB when provided with O_2 and NO_2. OB was grown in gas-tight 120 mL vials with 50 mL Sistrom's succinate medium initially supplemented with 1 mL O_2 and 1mM NO_2^- at constant temperature and stirring (20 °C, 600 rpm). Initial OD_{660} ≈ 0.001. Panel A**:** Measured gases (N_2O-N, NO, O_2) and calculated cumulative N_2-N throughout the incubation. Panel B: Measured N_2O-N throughout the incubation. Panel C: Calculated O_2 and N_2O-N consumption- and N_2-N production rates. Inserted panels: exponential regression of initial rates of O_2-reduction (oxic phase) and N_2-N production rates. Panel E: Calculated electron flow rates of total electrons channeled to O_2 (O2 reduction), the NOx reductases (Nox Eflow), and the sum of the total electron flow to terminal oxidases (Total Eflow). Error bars displayed as standard deviation (n = 2).

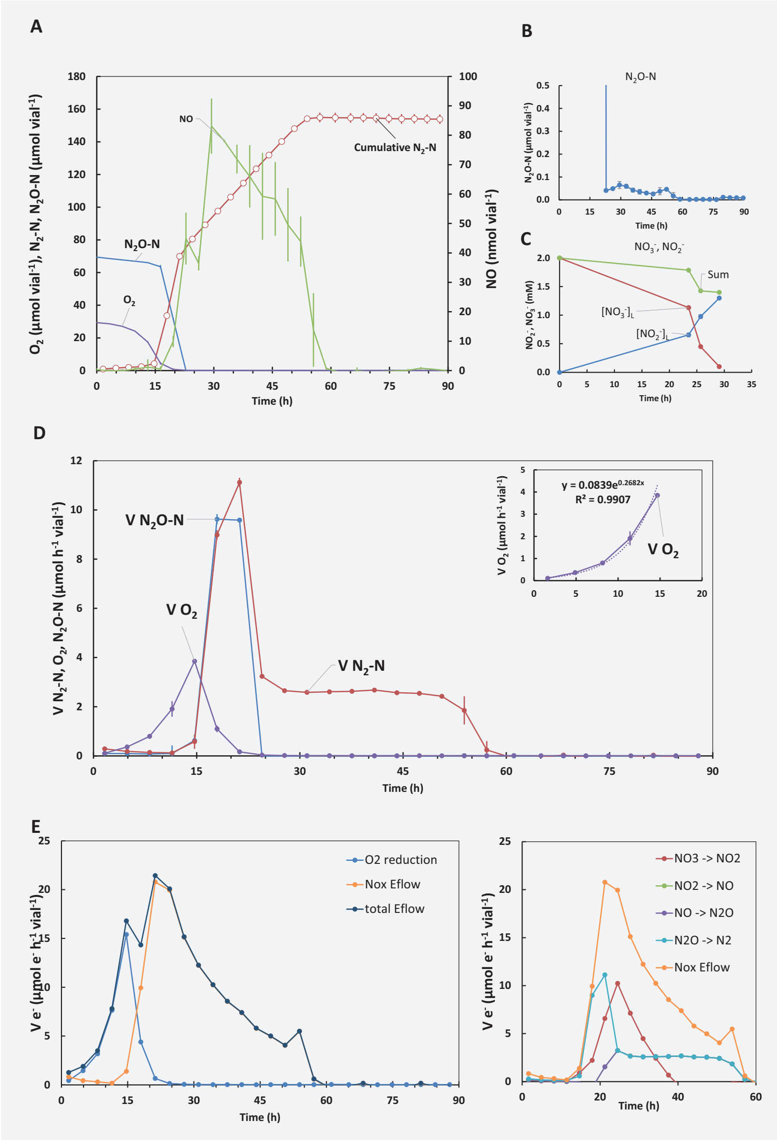

Figure S23: Denitrification phenotype of *Ochrobactrum* sp. OB when provided with O_2, N_2O and NO_3. OB was grown in gas-tight 120 mL vials with 50 mL Sistrom's succinate medium initially supplemented with 1 mL O_2, 1 mL N_2O and 2mM NO_3^- at constant temperature and stirring (20 °C, 600 rpm). Initial OD_{660} ≈ 0.001. Panel A: Measured gases (N_2O-N, NO, O_2) and calculated cumulative N_2-N throughout the incubation. Panel B: Measured N_2O-N throughout the incubation. Panel C: Measured liquid concentration of NO_3^- and NO_2^- and the sum of NO_3^- and NO_2^-. Panel D: Calculated O_2 and N_2O-N consumption- and N_2-N production rates. Inserted panels: exponential regression of initial rates of O_2-reduction (oxic phase). Error bars displayed as standard deviation (n = 2). Panel E: Left panel: Calculated electron flow rates of total electrons channeled to O_2 (O2 reduction), the NO_x reductases (Nox Eflow), and the sum of the total electron flow to terminal oxidases (Total Eflow). Inserted panel: exponential regression of total electron flow from oxic to anoxic phase. Right panel: Calculated electron flow rates of total electrons channeled to Nar, Nir, Nor and Nos and summed electron transfer to the NO_x reductases (Nox Eflow).

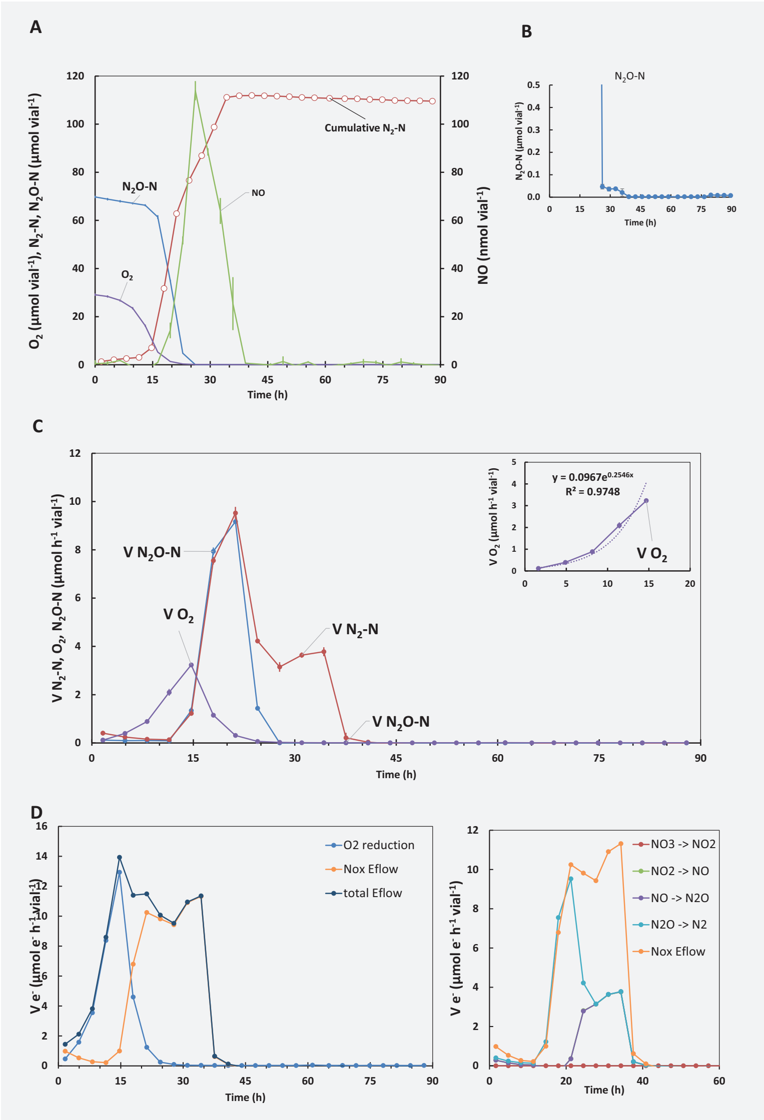

Figure S24: Denitrification phenotype of *Ochrobactrum* sp. OB when provided with O_2, N_2O and NO_2. OB was grown in gas-tight 120 mL vials with 50 mL Sistrom's succinate medium initially supplemented with 1 mL O_2, 1 mL N_2O and 1mM NO_2^- at constant temperature and stirring (20 °C, 600 rpm). Initial OD_{660} ≈ 0.001. Panel A: Measured gases (N_2O-N, NO, O_2) and calculated cumulative N_2-N throughout the incubation. Panel B: Zoom-in on measured N_2O-N throughout the incubation. Panel C: Calculated O_2 and N_2O-N consumption- and N_2-N production rates. Inserted panels: exponential regression of initial rates of O_2-reduction (oxic phase). Error bars displayed as standard deviation (n = 2). Panel E: Left panel: Calculated electron flow rates of total electrons channeled to O_2 (O2 reduction), the NO_x reductases (Nox Eflow), and the sum of the total electron flow to terminal oxidases (Total Eflow). Inserted panel: exponential regression of total electron flow from oxic to anoxic phase. Right panel: Calculated electron flow rates of total electrons channeled to Nar, Nir, Nor, and Nos and summed electron transfer to the NO_x reductases (Nox Eflow).

6.3 *Brachymonas sp.* BM

Brachymonas sp. BM demonstrated phenotypic characteristics of a full-fledged denitrifier, but, in contrast to PS-02, BM accumulated significant levels of N_2O as a response to transitioning from oxic to anoxic conditions. When respiring NO_3^- a continuous electron flow to the terminal oxidoreductases to terminal nitrogen reductases implied that most cells committed to denitrification when transitioning from oxic to anoxic conditions. NO_2^- accumulated to lower levels than the two other full-fledged denitrifying organisms that were isolated (PS-02 and OB) (**Fig. S25**). Parallel incubations supplemented with 1 mL O_2, 1 mL N_2O and 2 mM NO_3^- (**Fig. S26,** and **Fig. 4D** in main paper) or 1 mM NO_2^- (**Fig. S27**) demonstrated similar N_2O accumulation throughout the isolate's depletion of NO_x. Thus, BM did not prefer N_2O reduction over NO_3^- and could be predicted as a net N_2O source.

Figure S25: Denitrification phenotype of *Brachymonas* sp. BM when provided with O_2 and NO_3. BM was grown in gas-tight 120 mL vials with 50 mL Sistrom's succinate medium initially supplemented with 1 mL O_2 and 2mM NO_3^- at constant temperature and stirring (20 °C, 600 rpm). Initial OD_{660} ≈ 0.001. Panel A**:** Measured gases (N_2O-N, NO, O_2) and calculated cumulative N_2-N throughout the incubation. Panel B: Measured N_2O-N throughout the incubation. Panel C: Measured liquid concentration of NO_3^- and NO_2^- and the sum of NO_3^- and NO_2^-. Panel D: Calculated O_2 and N_2O-N consumption- and N_2-N production rates. Inserted panels: exponential regression of initial rates of O_2-reduction (oxic phase). Panel E: Calculated electron flow rates of total electrons channeled to O_2 (O2 reduction), the NOx reductases (Nox Eflow), and the sum of the total electron flow to terminal oxidases (Total Eflow). Inserted panel: exponential regression of total electron flow through transition from oxic to anoxic phase. Results from a single vial shown. Replicate vials showed similar gas kinetics.

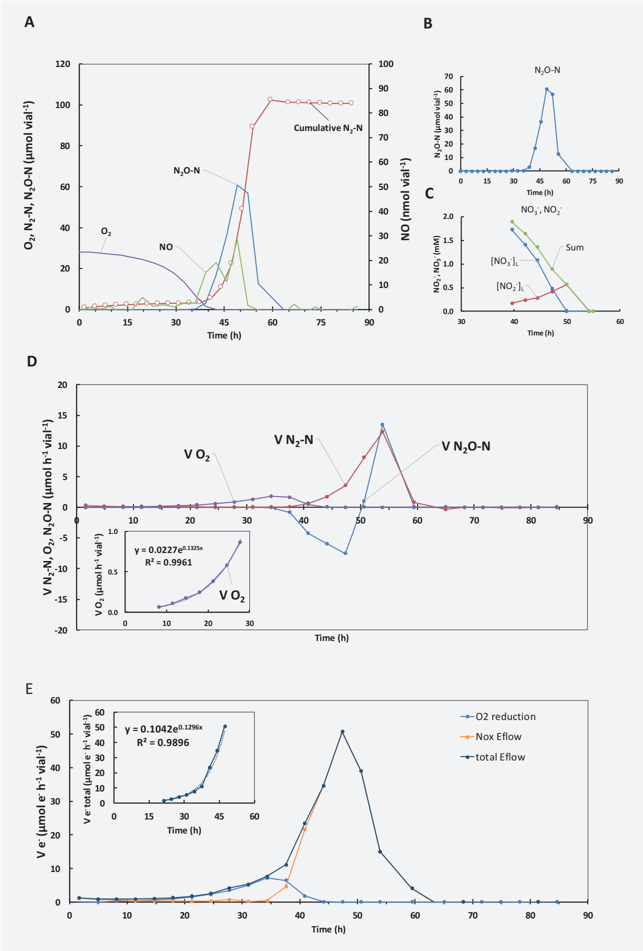

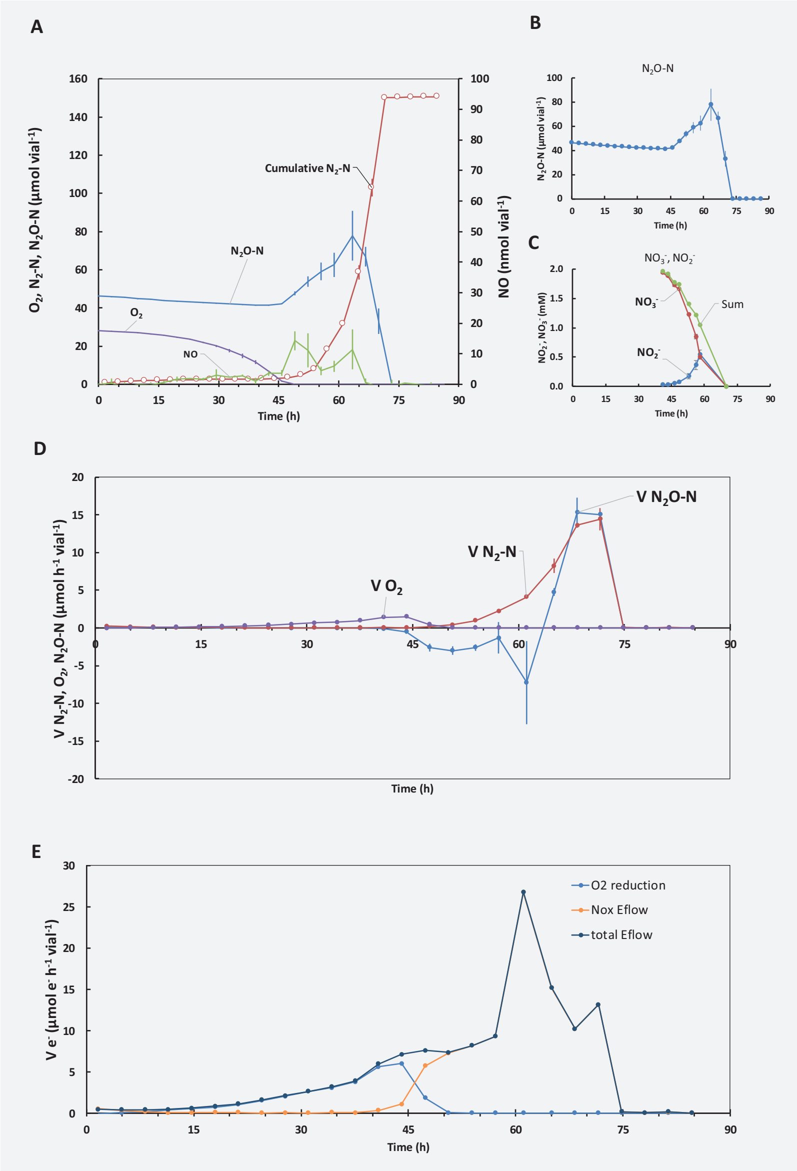

Figure S26: Denitrification phenotype of *Brachymonas* sp. BM when provided with O_2, N_2O and NO_3. BM was grown in gas-tight 120 mL vials with 50 mL Sistrom's succinate medium initially supplemented with 1 mL O_2, 1 mL N_2O and 2mM NO_3^- at constant temperature and stirring (20 °C, 600 rpm). Initial OD_{660} ≈ 0.001. Panel A: Measured gases (N_2O-N, NO, O_2) and calculated cumulative N_2-N throughout the incubation. Panel B: Measured N_2O-N throughout the incubation. Panel C: Measured liquid concentration of NO_3^- and NO_2^- and the sum of NO_3^- and NO_2^-. Panel D: Calculated O_2 and N_2O-N consumption- and N_2-N production rates. Inserted panels: exponential regression of initial rates of O_2-reduction (oxic phase) and N_2-N production. Panel E: Calculated electron flow rates of total electrons channeled to O2 (O2 reduction), the NOx reductases (Nox Eflow), and the sum of the total electron flow to terminal oxidases (Total Eflow). Error bars displayed as standard deviation (n = 2).

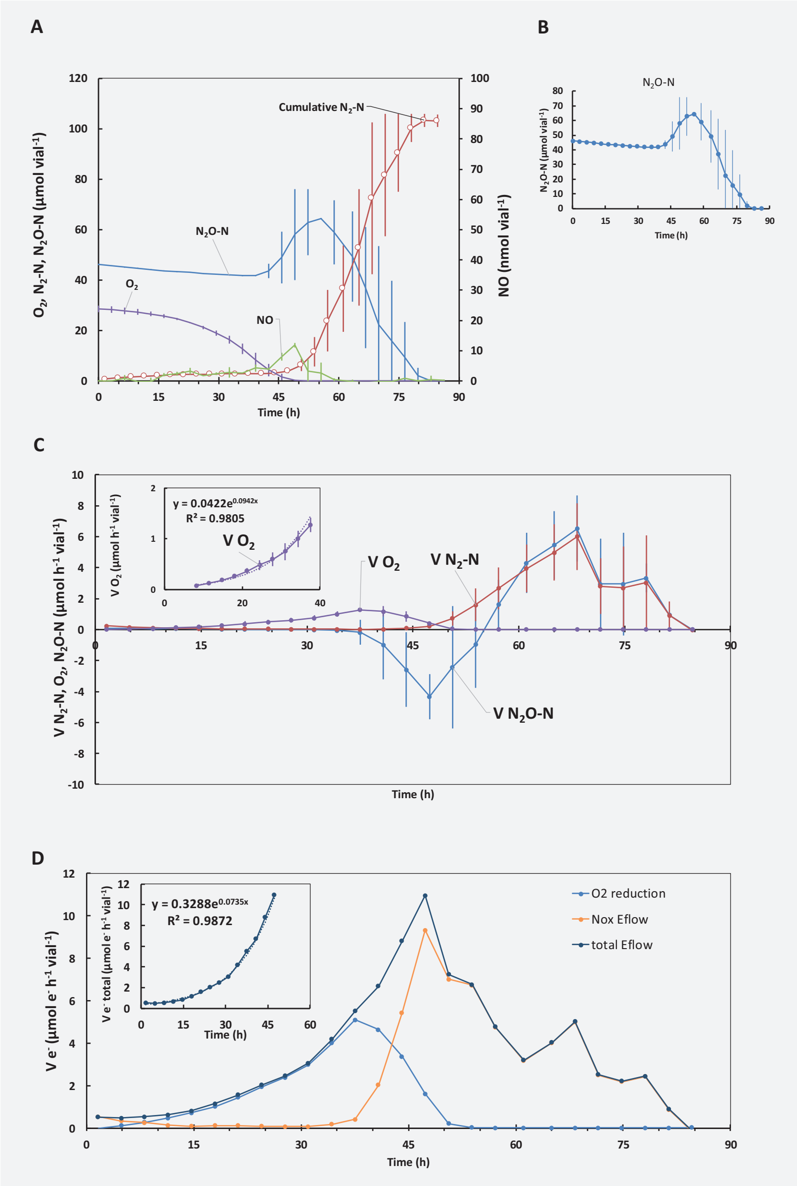

Figure S27: Denitrification phenotype of *Brachymonas* sp. BM when provided with O_2, N_2O and NO_2. BM was grown in gas-tight 120 mL vials with 50 mL Sistrom's succinate medium initially supplemented with 1 mL O_2, 1 mL N_2O and 1mM NO_2^- at constant temperature and stirring (20 °C, 600 rpm). Initial OD_{660} ≈ 0.001. Panel A: Measured gases (N_2O-N, NO, O_2) and calculated cumulative N_2-N throughout the incubation. Panel B: Measured N_2O-N throughout the incubation. Panel C: Calculated O_2 and N_2O-N consumption- and N_2-N production rates. Inserted panels: exponential regression of initial rates of O_2-reduction (oxic phase) and N_2-N production. Panel D: Calculated electron flow rates of total electrons channeled to O2 (O2 reduction), the NOx reductases (Nox Eflow), and the sum of the total electron flow to terminal oxidases (Total Eflow). Inserted panel: exponential regression of total electron flow through transition from oxic to anoxic phase Error bars displayed as standard deviation (n = 2).

6.4 *Aeromonas* sp. AM

In incubations supplemented with NO_3^- and N_2O *Aeromonas sp*. AM reduced the available NO_3^- to NO_2^- and N_2O to N_2 when transcending from oxic to anoxic conditions (**Fig. S28**, and **Fig. 4B** in main paper). The accumulated NO_2^- was slowly reduced to NH_4^+ throughout the incubation, indicative of dissimilatory nitrate reduction to ammonium (DNRA). Following N_2O depletion AM continued channeling electrons toward denitrification and N_2-N production indicating denitrification alongside DNRA activity. The phenotype was corroborated by annotation of the *nrfA* gene, coding for a key enzyme of DNRA (Cytochrome c552 nitrite reductase, EC: 1.7.2.2), and denitrification genes coding for periplasmic nitrate reductase (*napAB*) and N_2O reductase (*nosZ*, clade I) in AN's genome (**Fig. 4B** in main paper). N_2O was reduced alongside NO_3^-, which would contradict the hypothesis that Nos outcompetes Nap for electrons (Mania et al 2020), however, a nitrate reductase (NasA) was recovered in the genome. The genome also encoded the gene NasD, of which gene product shared high sequence identity (protein blast) with a NADH dependent nitrite reductase of Aeromonas media strain (see main text for details).

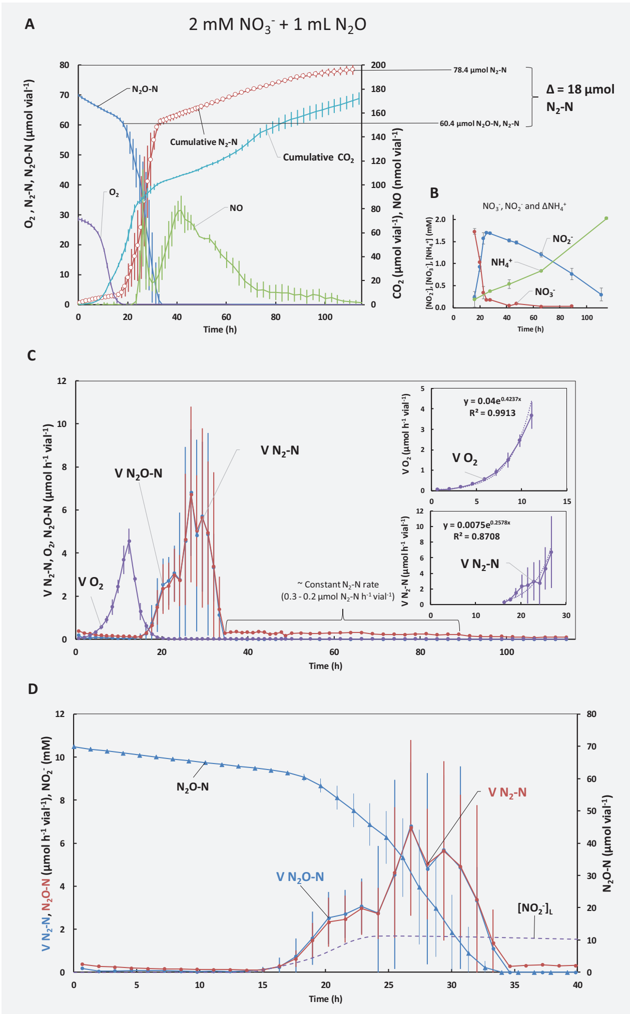

Figure S28: DNRA and denitrifying phenotype of *Aeromonas* sp. AM when provided with N_2O and NO_3. AM was grown in gas-tight 120 mL vials with 50 mL Sistrom's succinate medium initially supplemented with 1 mL O_2, 1 mL N_2O, and 2mM NO_3^- at constant temperature and stirring (20 °C, 700 rpm). Initial $OD_{660} \approx 0.001$. Panel A**:** Measured gases (N_2O-N, NO, O_2) and calculated cumulative N_2-N and CO_2 throughout the incubation. Panel B: Measured liquid concentration of NO_3^- NO_2^- and ΔNH_4^+. Panel C: Calculated O_2 and N_2O-N consumption- and N_2-N production rates. Inserted panels: exponential regression of initial rates of O_2-reduction (oxic phase) and N_2-N production rates. Panel D: N_2O-N consumption- and N_2-N production rates, measured N_2O-N, and estimated NO_2^- concentration (mM) (estimated based on measurements in Panel B with the Excel Spline function) throughout the first 40 hours of incubation. Error bars displayed as standard deviation (n = 3).

6.5 *Cloacibacterium sp.* CB-01 and CB-03

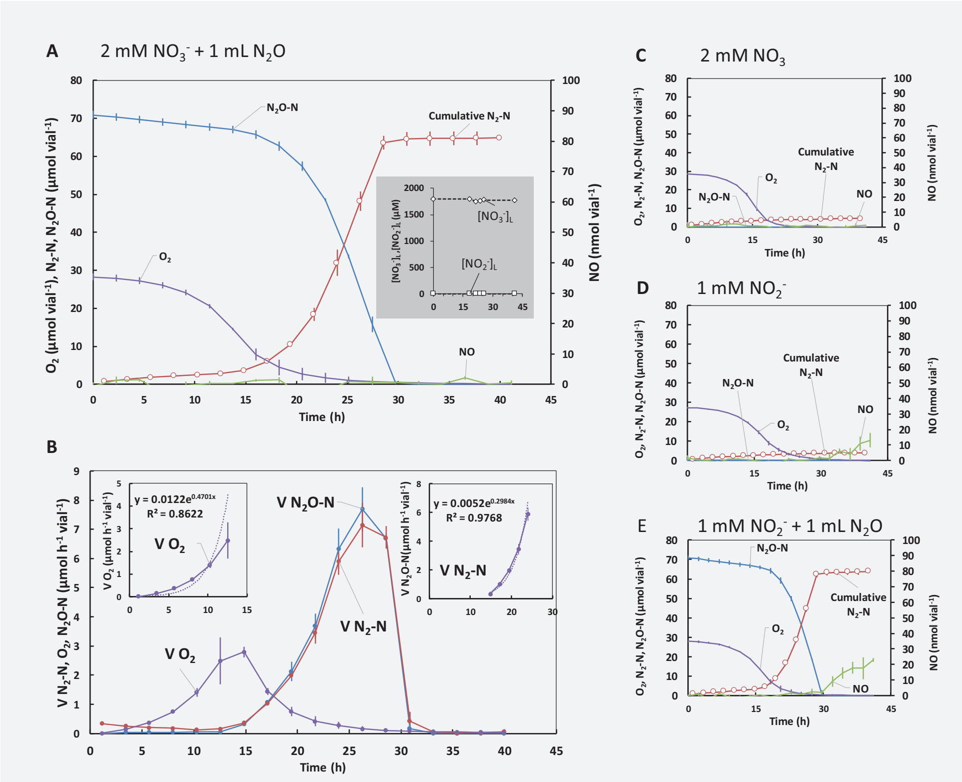

Figure S29: Denitrification phenotype of *Cloacibacterium sp*. CB-01 when provided with O_2 and combinations of NO_3, NO_2 and/or N_2O. CB-01 was grown in gas-tight 120 mL vials with 50 mL Nutrient Broth medium initially supplemented with 1 mL O_2 and combinations of 1 mL N_2O and/or 2mM NO_3^- and/or 1 mM NO_2^- at constant temperature and stirring (20 °C, 600 rpm). Initial OD_{660} ≈ 0.001. **Panel A:** Measured gases (N_2O-N, NO, O_2) and calculated cumulative N_2-N throughout an incubation initially supplemented with 1 mL O_2, 2 mM NO_3^- and 1 mL N_2O. Inserted panel shows measures liquid concentration of NO_3^- and NO_2^-. **Panel B**: Calculated O_2 and N_2O-N consumption- and N_2-N production rates. Inserted panels: exponential regression of initial rates of O_2-reduction (oxic phase) and N_2-N production rates. **Panel C, D and E**: Measured gases (N_2O-N, NO, O_2) and calculated cumulative N_2-N throughout incubations initially supplemented with 1 mL O_2 and 2 mM NO_3^-, 1 mL O_2 and 1 mM NO_2^- and 1 mL O_2, 1 mM NO_2^- and 1 mL N_2O, respectively. Error bars displayed as standard deviation (n = 2). Error bars for inserted panel in Panel A (measured NO_2^- and NO_3^-) displayed as standard deviation (n = 3).

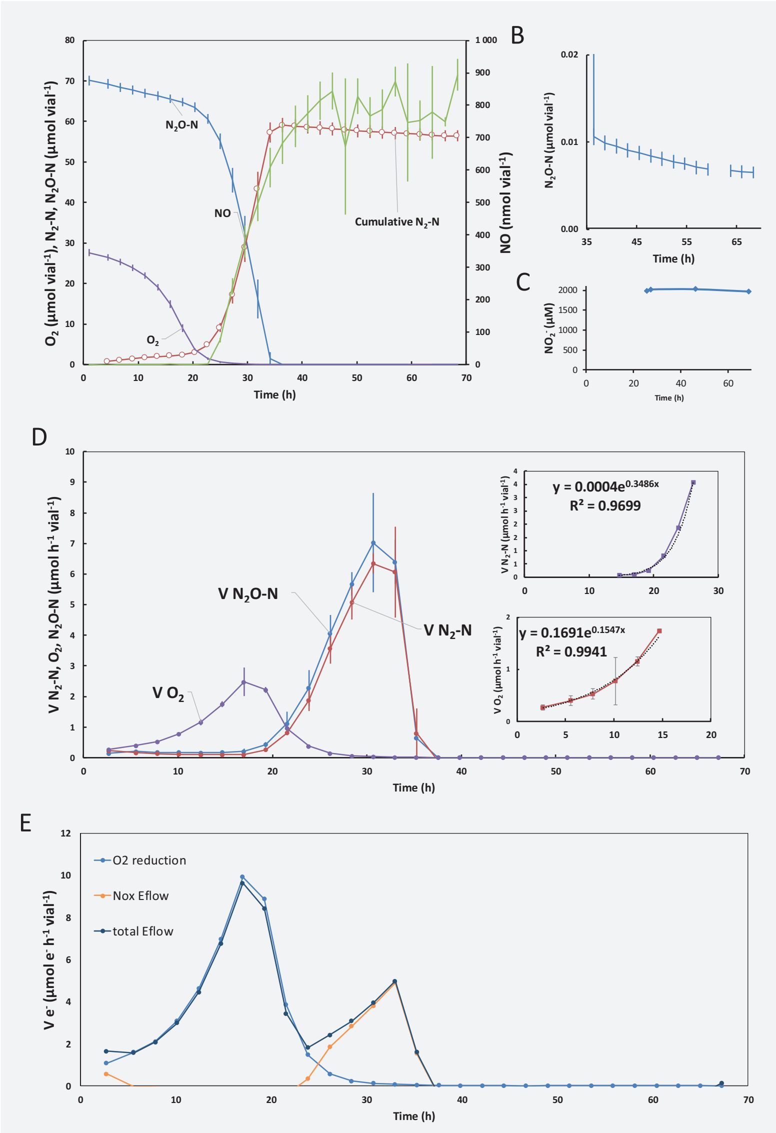

Figure S30: Denitrification phenotype of *Cloacibacterium* sp. CB-03 when provided with O_2, N_2O and NO_3. CB-03 was grown in gas-tight 120 mL vials with 50 mL NB medium initially supplemented with 1 mL O_2, 1 mL N_2O and 2mM NO_3^- at constant temperature and stirring (20 °C, 600 rpm). Initial $OD_{660} \approx 0.001$. Panel A**:** Measured gases (N_2O-N, NO, O_2) and calculated cumulative N_2-N throughout the incubation. Panel B: Zoom in on measured N_2O-N from t = 35 h and throughout. Panel C: Measured liquid concentration of NO_2^- (µM). Panel D: Calculated O_2 and N_2O-N consumption- and N_2-N production rates. Inserted panels: exponential regression of initial rates of O_2-reduction (oxic phase) and N_2-N production rates. Panel E: Calculated electron flow rates of total electrons channeled to O_2 (O_2 reduction), the NOx reductases (Nox Eflow) and the sum of the total electron flow to terminal oxidases (Total Eflow). Error bars displayed as standard deviation (n = 2).

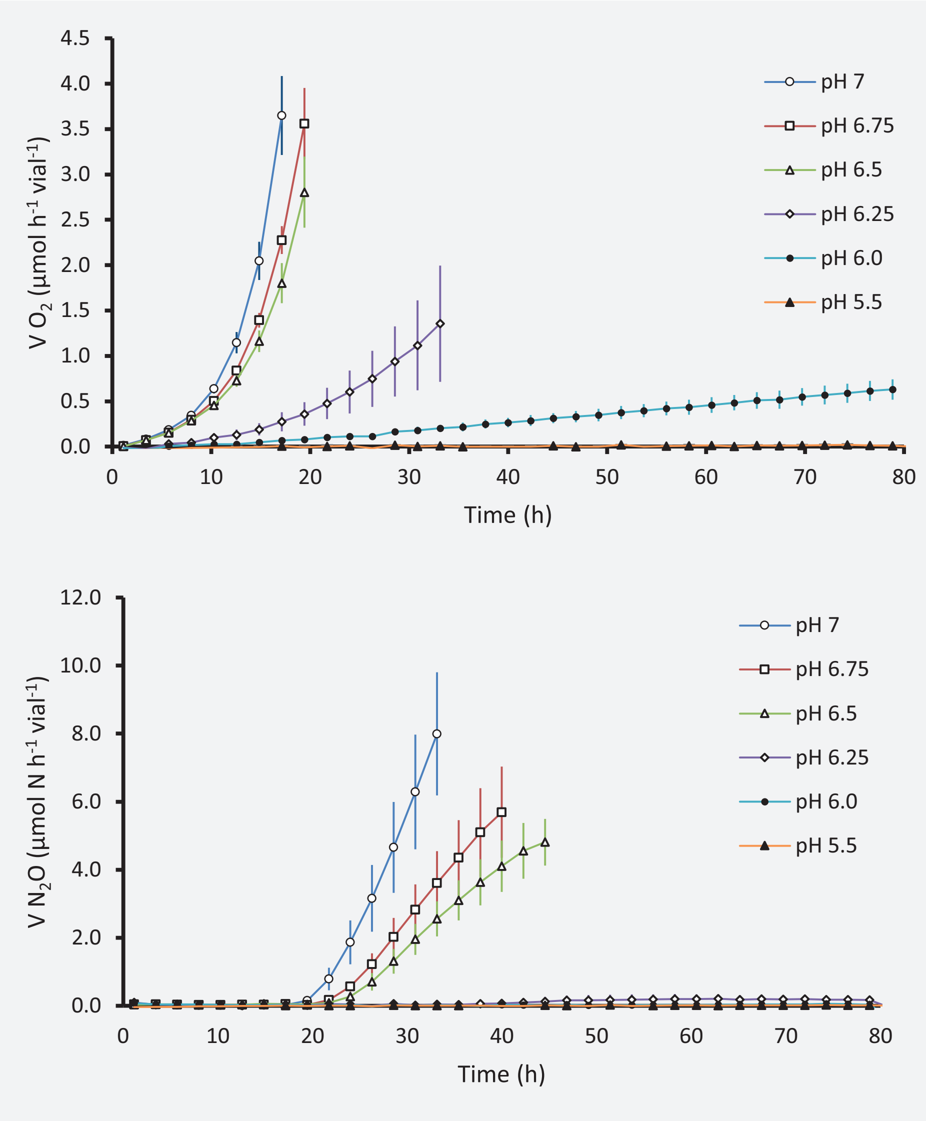

Figure S31: Denitrification phenotype of *Cloacibacterium* sp. CB-01 when provided with 1 mL O_2 and 1 mL N_2O at different pH levels. CB-01 was grown in gas,tight 120 mL vials with 50 mL NB medium initially supplemented with 1 mL O_2 and 1 mL N_2O at constant temperature and stirring (20 °C, 600 rpm). Initial OD_{660} ≈ 0.001. Top panel**:** First period of O_2 reduction (rate) during incubations with media adjusted to different pH levels. Bottom panel: Panel B: First period of N_2O reduction (rate) during incubations with media adjusted to different pH. Error bars displayed as standard deviation (n = 3).

7 Soil incubations

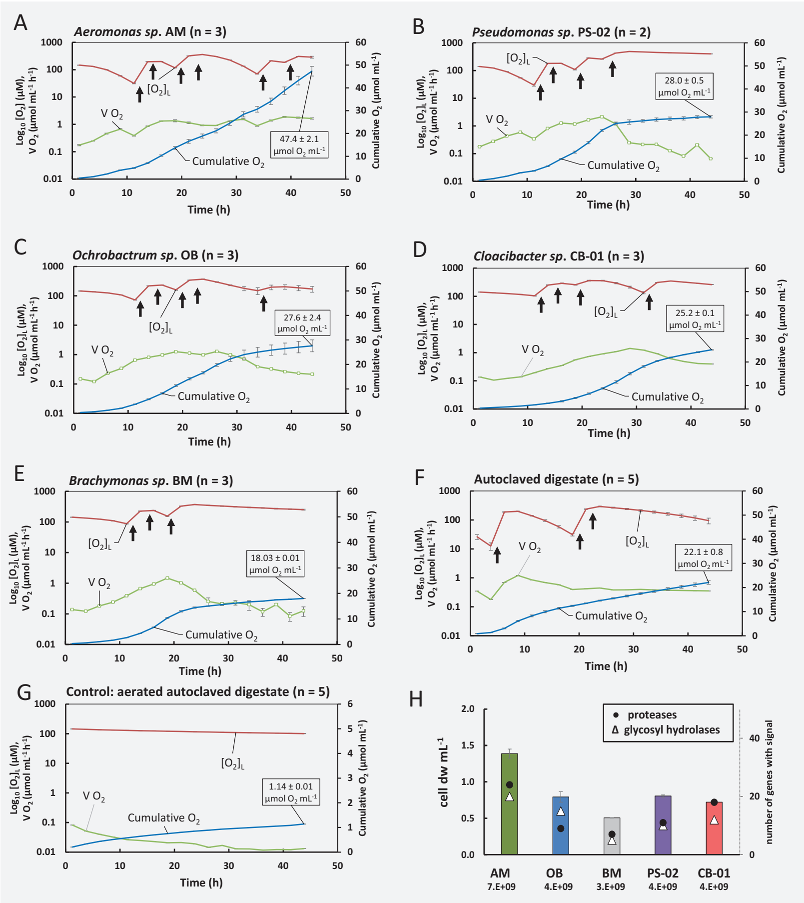

Figure S32: Aerobic growth in autoclaved digestate. AM, OB, BM, PS-02 and CB-01 were raised aerobically in 50 mL SS (AM, OB, BM and PS-02) or 50 mL NB (CB-01) to high cell densities (OD_{660nm} ~ 1), then transferred (1 mL) to vials with 50 mL stirred (600 rpm) autoclaved pH-adjusted (pH=7.75) and pre-aerated (aerated by pumping sterile filtered air through a stirred suspension for 36 hours) digestate at 20 °C. Oxygen concentration (red), arrows = exogenous O_2 addition. Cumulative O_2 reduced = blue. Rate of oxygen consumption = green. Aeration of the autoclaved digestate was necessary to secure near-complete abiotic oxidation of the Fe^{2+} in the digestate, which would otherwise obscure the measurements of O_2 consumption. **Panel A:** *Aeromonas sp*. AM (n=3). **Panel B:** Pseudomonas sp. PS-02 (n=2). **Panel C:** *Ochrobactrum sp*. OB (n=3). **Panel D:** *Cloacibacterium* sp. CB (n=3). **Panel E:** *Brachymonas sp*. BM (n=3), **Panel G:** Non-aerated, pH adjusted (pH = 7.65) autoclaved digestate (n = 5). **Panel F:** Control: Aerated, pH adjusted (pH = 7.75) autoclaved digestate (n = 5). **Panel H**: The cumulated oxygen consumption by each strain was used to estimate the amount of cells produced, assuming that the growth yield for all strains is the same as for *Paracocus denitrificans*, which is 30 g cell dry-weight mol^{-1} O_2 (based on Bergaust et al (2011): $2 \cdot 10^{-13}$ g dry-weight per cell, growth yield = $1.5 \cdot 10^{14}$ cells mol^{-1} O_2). The panel (H) shows estimated amount of cell dry-matter mL^{-1} for each strain as bars (left axis), the number of cells mL^{-1} (below labels). The number of genes coding for glycosyl hydrolases (**GH**) and proteases (**P**) in the genome of each strain (from Table S11 and S13) is shown (right axis, symbols explained in the pale). **P** and **GH** were correlated (r^2=0.93), and the cell dry-weight was correlated to both (r^2= 0.97 for both).

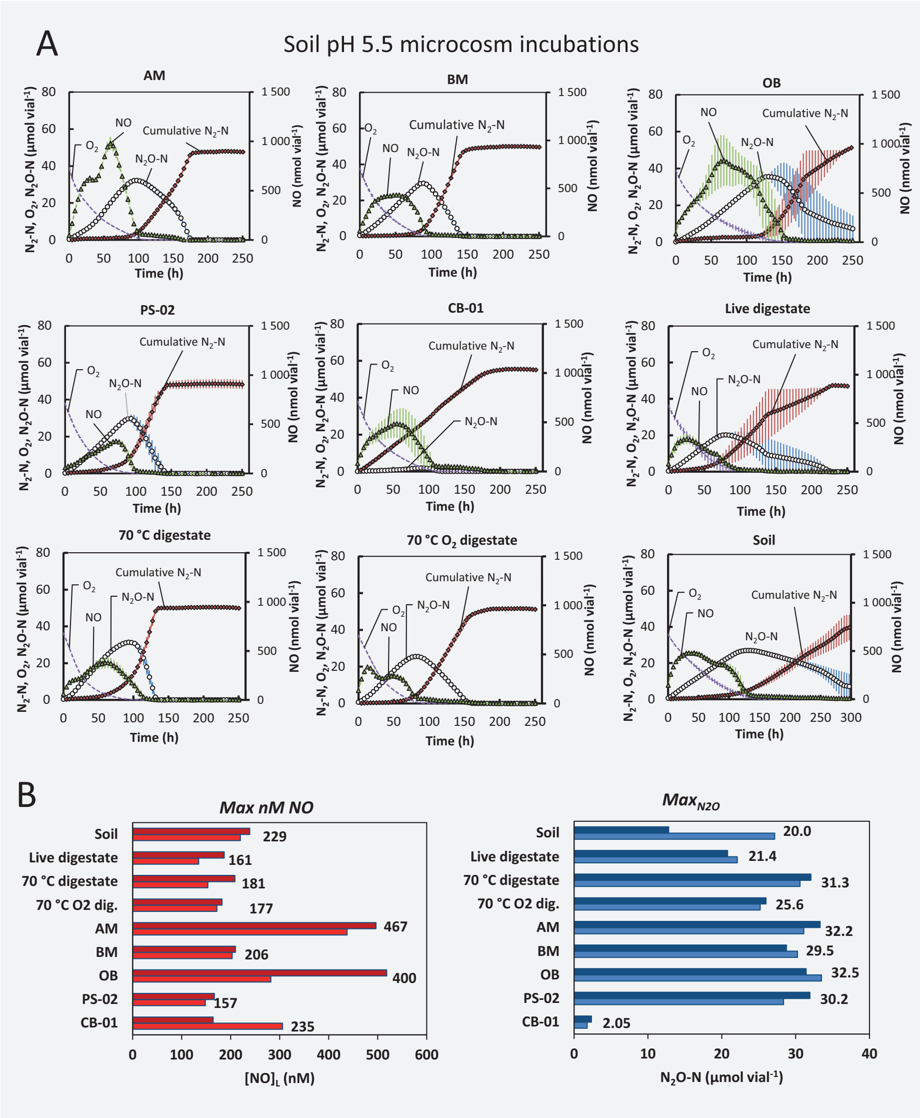

Figure S33: Incubation of digestate enriched with isolates (**Fig. S32**) (0.6 mL), live digestate (0.6 mL) and heat treated digestate (0.6 mL) in soil with pH=5.5 (10 g) at 20 °C**.** Panel A: kinetics of O_2, NO, N_2O and N_2 throughout the incubation of soils amended with the various materials (one panel for each amendment). Average values shown (n=2). Initial oxygen (~40 µmol vial^{-1}) corresponds to ~1.0 vol% in the headspace. The amounts of O_2, NO and N_2O are as measured, while "Cumulative N_2-N" denotes the measured N_2 that is corrected for leakage and losses by sampling (see Molstad et al 2007). The N_2 and N_2O kinetics were used to calculate the N_2O index (***I_{N2O}***), which is the area under the N_2O- curve divided by the area under the N_2O+N_2-curve for a specific time span. ***I_{N2O}*** values are shown in **Fig 5** (main paper) and is a proxy for the propensity of denitrification to emit N_2O. Panel B: peak (maximum) amounts of NO and N_2O (results for single vials). NO is shown as nM in the liquid phase (equilibrium concentrations with measured NO in headspace), while N_2O is shown as µmol N_2O- N vial^{-1}.

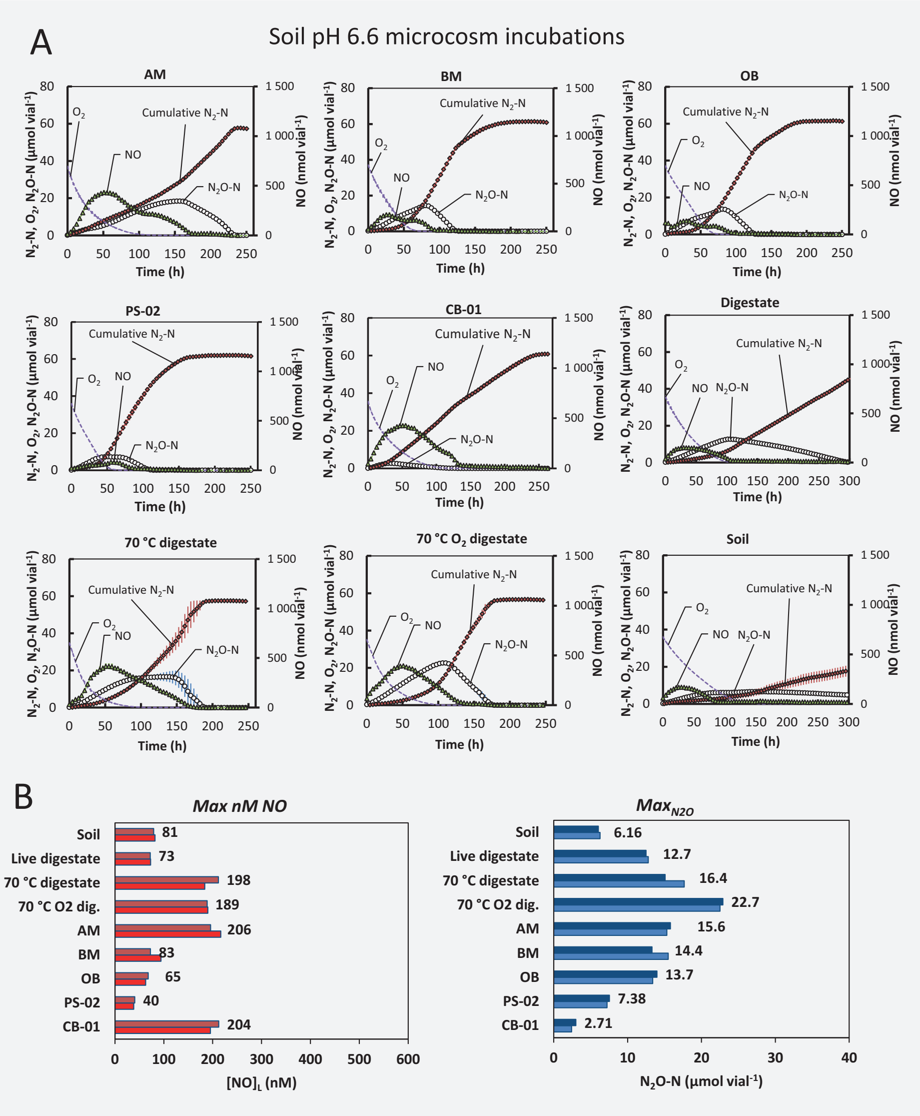

Figure S34: Incubation of digestate enriched with isolates (**Fig. S32**) (0.6 mL), live digestate (0.6 mL) and heat treated digestate (0.6 mL) in soil with pH=6.6 (10 g) at 20 °C**.** Panel A: kinetics of O_2, NO, N_2O and N_2 throughout the incubation of soils amended with the various materials (one panel for each amendment). Average values shown (n=2). Initial oxygen (~40 µmol vial^{-1}) corresponds to ~1.0 vol% in the headspace. The amounts of O_2, NO and N_2O are as measured, while “Cumulative N_2-N” denotes the measured N_2 that is corrected for leakage and losses by sampling (see Molstad et al 2007). The N_2 and N_2O kinetics were used to calculate the N_2O index (I_{N2O}), which is the area under the N_2O- curve divided by the area under the N_2O+N_2-curve for a specific time span. I_{N2O} values are shown in **Fig. 5** (main paper) and is a proxy for the propensity of denitrification to emit N_2O. Panel B: peak (maximum) amounts of NO and N_2O (results for single vials). NO is shown as nM in the liquid phase (equilibrium concentrations with measured NO in headspace), while N_2O is shown as µmol N_2O- N vial^{-1}.

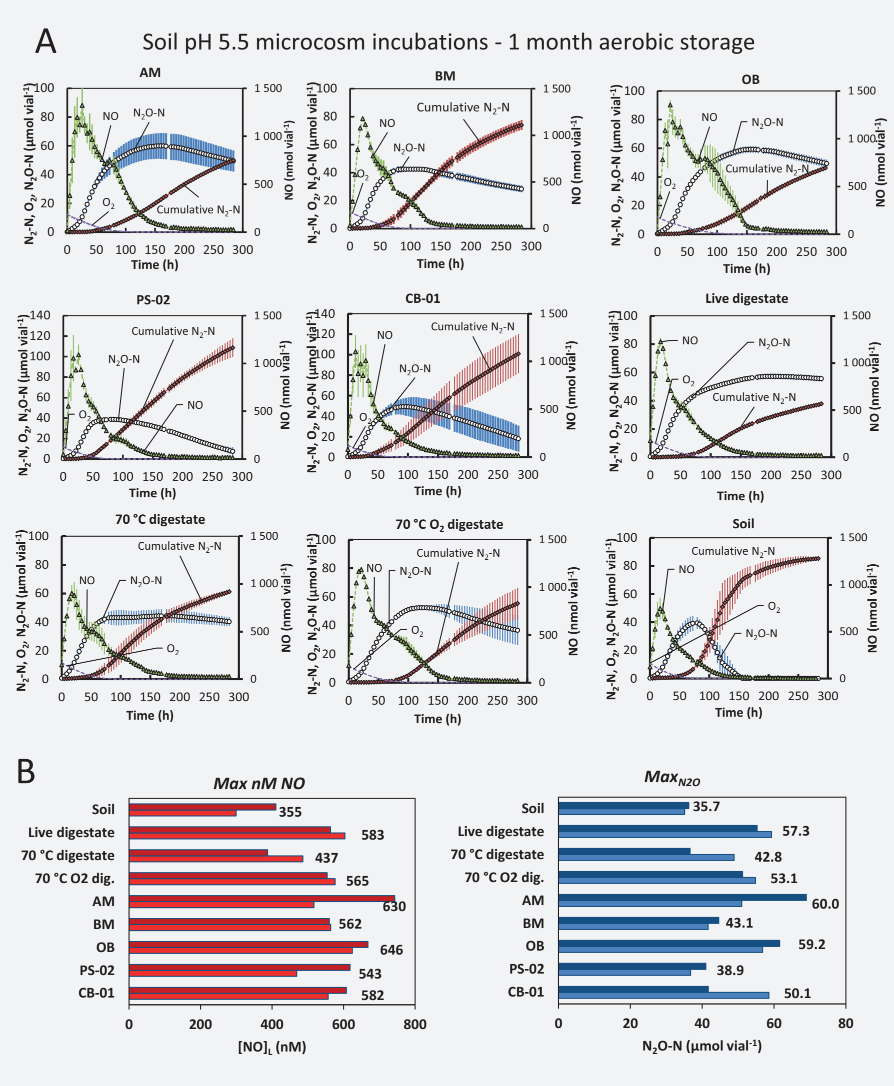

Figure S35: Incubation of digestate enriched with isolates (**Fig. S32**) (0.6 mL), live digestate (0.6 mL) and heat treated digestate (0.6 mL) in soil with pH=5.5 (10 g) at 20 °C after aerobic storage for 1 month (30 days) at oxic conditions (20 °C). Panel A: kinetics of O_2, NO, N_2O and N_2 throughout the incubation of soils amended with the various materials (one panel for each amendment). Average values shown (n=2). Initial oxygen (~40 µmol vial^{-1}) corresponds to ~1.0 vol% in the headspace. The amounts of O_2, NO and N_2O are as measured, while “Cumulative N_2-N” denotes the measured N_2 that is corrected for leakage and losses by sampling (see Molstad et al 2007). The N_2O index (***I_{N2O}***), which is the area under the N_2O- curve divided by the area under the N_2O+N_2 -curve for a specific time span, was not calculable for most treatments as the experiment was not run until all available oxyanions was reduced to N_2 or N_2O (increasing Cumulative N_2-N for most vials). Panel B: peak (maximum) amounts of NO and N_2O (results for single vials). NO is shown as nM in the liquid phase (equilibrium concentrations with measured NO in headspace), while N_2O is shown as µmol N_2O- N vial^{-1}.

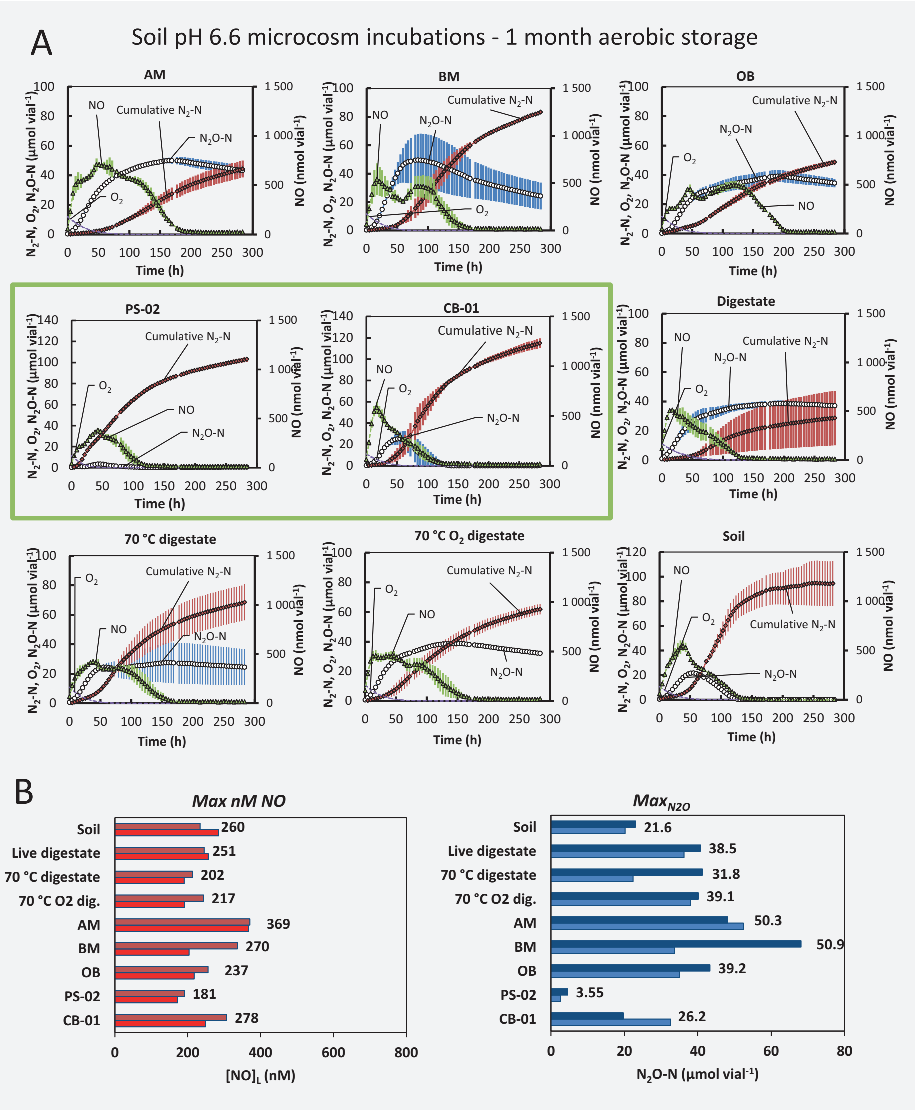

Figure S36: Incubation of digestate enriched with isolates (**Fig. S32**) (0.6 mL), live digestate (0.6 mL) and heat treated digestate (0.6 mL) in soil with pH=6.6 (10 g) at 20 °C were done after aerobic storage for 1 month (30 days) at oxic conditions (20°C) . Panel A: kinetics of O_2, NO, N_2O and N_2 throughout the incubation of soils amended with the various materials (one panel for each amendment). Average values shown (n=2). Initial oxygen (~40 µmol vial^{-1}) corresponds to ~1.0 vol% in the headspace. The amounts of O_2, NO and N_2O are as measured, while "Cumulative N_2-N" denotes the measured N_2 that is corrected for leakage and losses by sampling (see Molstad et al 2007). The N_2O index (***I_{N2O}***), which is the area under the N_2O- curve divided by the area under the N_2O+N_2-curve for a specific time span, was not calculable for most treatments as the experiment was not run until all available oxyanions was reduced to N_2 or N_2O (increasing Cumulative N_2-N for most vials). The green box indicates isolates PS-02 and CB-01. Panel B: peak (maximum) amounts of NO and N_2O (results for single vials). NO is shown as nM in the liquid phase (equilibrium concentrations with measured NO in headspace), while N_2O is shown as µmol N_2O- N vial^{-1}. While PS-02 had a statistically significant effect on maximum N_2O, the apparent effect of CB-01 was not statistically significant.

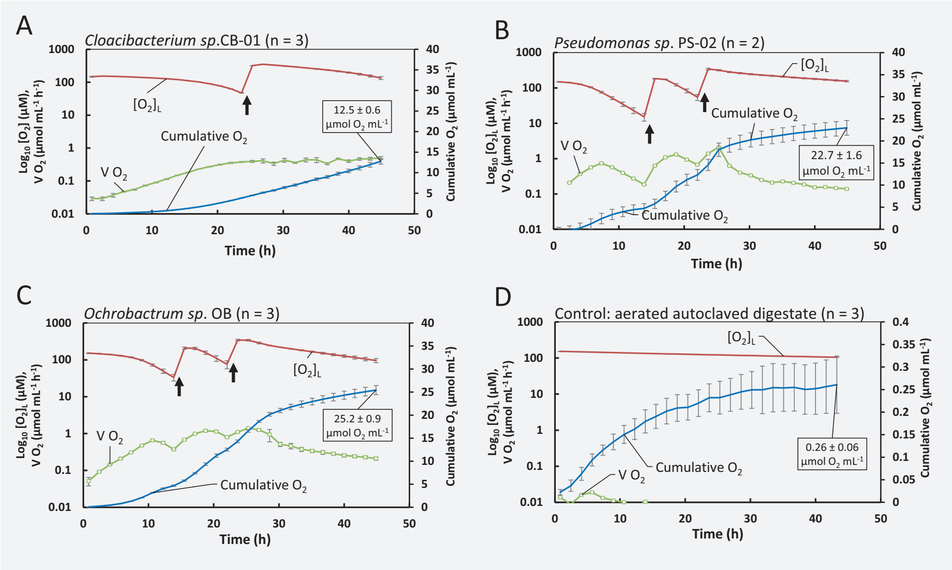

Figure S37: Aerobic growth of isolated organisms in autoclaved digestate for dose response experiment. The autoclaved digestate to be used for cultivation was pH- adjusted to 7.6 and vigorously aerated (sparging for 36 hours) before being used. The aeration was necessary because previous experiments had demonstrated substantial abiotic O_2-consumption by oxidation of Fe^{2+} in autoclaved digestate, which would obscure the measurement of aerobic respiration by the bacteria (see **Fig. S32**). Pre-cultures of CB-01, PS-02 and OB were grown aerobically in NB medium (CB-01) and SS medium (PS-02 and OB) to OD_{660nm} 0.798, 0.379 and 0.786, respectively, and used to inoculate 120 mL vials (1 mL per vial) containing 50 mL digestate (and a magnetic bar), which were capped (butyl rubber septa), incubated at 20°C with vigorous stirring (600 rpm), and monitored for O_2 concentration in the headspace. When needed, to secure oxic conditions, more O_2 was injected. **Panels A – D**: Oxygen concentration (red), arrows = O_2 injection. Cumulative O_2 reduction = blue. Rate of oxygen consumption = green. **A:** *Cloacibacterium sp*. CB-01 (n=3). **B:** *Pseudomonas* sp. PS-02 (n=3). **C:** *Ochrobactrum sp*. OB (n=3). **D:** Control: no bacteria (n = 3). The cumulated oxygen consumption by each strain was used to estimate the amount of cells produced, assuming that the growth yield for all strains is the same as for *Paracocus denitrificans*, which is 30 g cell dry-weight mol^{-1} O_2 (based on Bergaust et al (2011): $2{\cdot}10^{-13}$ g dry-weight per cell, growth yield= $1.5{\cdot}10^{14}$ cells mol^{-1} O_2). The estimated amount of cell dry-weight for the three strains were 0.36 (±0.01), 0.67 (±0.04) and 0.74 (± 0.02) mg cell dry-weight mL^{-1} for CB-01, PS-02 and OB, respectively. Assuming that the three strains has the same amount of dry-weight per cell as *Paracoccus* ($2{\cdot}10^{-13}$ g $cell^{-1}$) the estimated number of “Paracoccus equivalents” are 1.8, 3.4 and 1.9 $\cdot 10^9$ cells mL^{-1} for CB-01, PS-02 and OB, respectively.

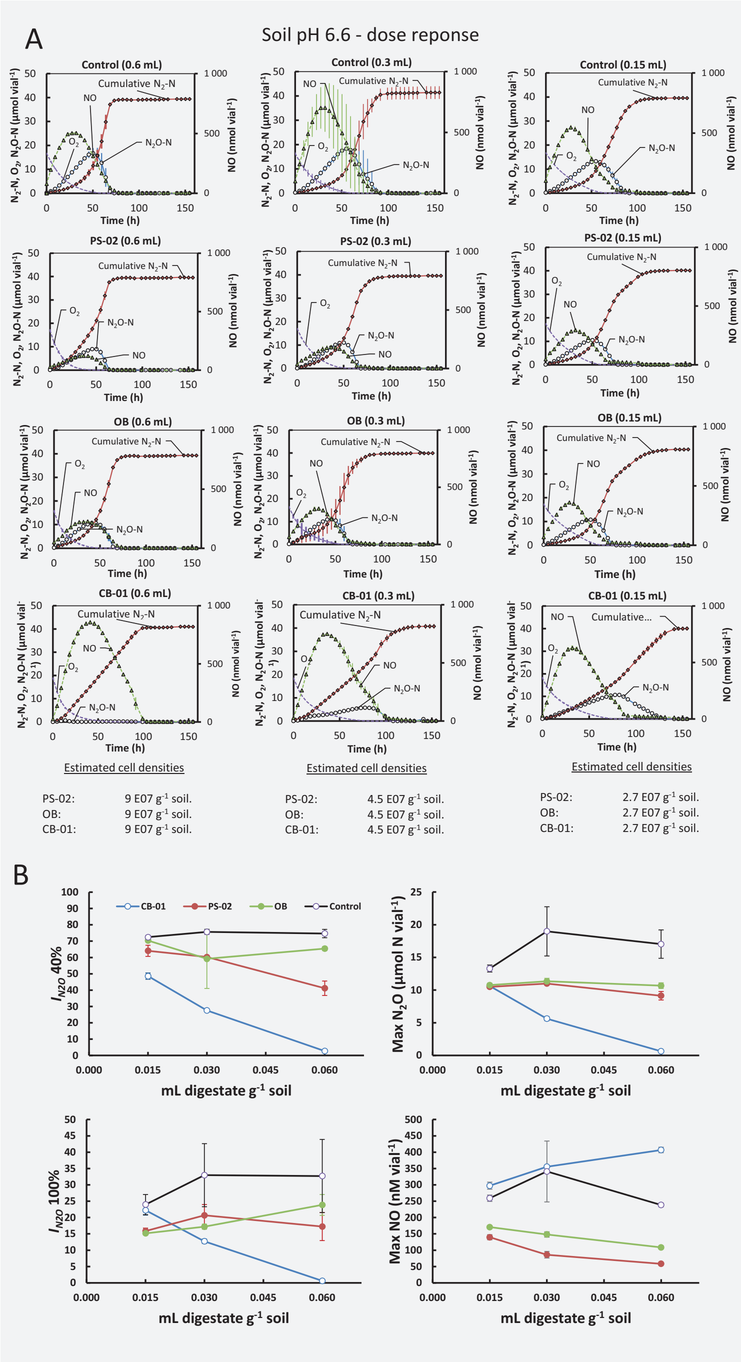

Figure S38: Incubation of digestate enriched with isolates OB, PS-02 and CB-01 and aerated pH adjusted autoclaved digestate (Control) in 10 g pH 6.6 soil supplemented with 25 µmol NO_3^- and 0.5 mL O_2. Panel A: kinetics of O_2, NO, N_2O and N_2 throughout the incubation of soils amended with the various materials (one panel for each amendment). Average values shown, with standard deviation (n=3). Initial oxygen (~20 µmol vial^{-1}) corresponds to ~0.5 vol% in the headspace. The amounts of O_2, NO and N_2O are as measured, while "Cumulative N_2-N" denotes the measured N_2 that is corrected for leakage and losses by sampling (see Molstad et al 2007). The digestate enriched with the isolates (**Fig. S37**) was diluted with sterile aerated digestate (as used in the controls) to give ~the same cell concentration per mL digestate (~$2 \cdot 10^8$ N_2O reducing cells mL^{-1} digestate). Error bars displayed as standard deviation (n = 3 for all treatments, besides PS-02 0.15 mL with n = 2). Panel B: average peak (maximum) amounts of NO and N_2O. NO is shown as nM in the liquid phase (equilibrium concentrations with measured NO in headspace), while N_2O is shown as µmol N_2O- N vial^{-1}. Two $\boldsymbol{I_{N2O}}$ values are shown: one for the timespan until 40% of the NO_3^- -N is recovered as N_2+N_2O+NO-N (**$I_{N2O\ 40\%}$**), and one for 100% recovery (**$I_{N2O\ 100\%}$**).

Table S13: Summary data for dose response experiment. The table shows the N_2O index values calculated for the period until 40 and 100% of NO_3 is converted to $NO+N_2O+N_2$ (I_{N2O} 40% and I_{N2O} 100%, respectively), and the maximum N_2O reached (Max N_2O) for the dose experiment (**Fig. S38**). Average values with standard deviation are given for each treatment (n=3 replicate vials). Treatments are digestate with bacteria (CB-01, PS-02 and OB), and digestate without bacteria (Control), and 3 levels of digestate: 0.6, 0.3 and 0.15 mL digestate vial^{-1} (containing 10 g soil). The digestates with bacteria contained 0.3 mg bacterial cell dry-weight mL^{-1}, hence the inoculation intensities the three levels were 18, 9 and 4.5 µg cell dry-weight g^{-1} soil. The third column for each variable shows the value expressed as % of the control value at the same inoculum intensity; significantly lower value for the bacterial treatment versus control is marked by * ($p>0.05$, t-test)

		I_{N2O} 40%			I_{N2O} 100%			Max N_2O (µmol N vial^{-1})		
Dose (mL vial-1)	**Strain**	**Avg**	**St.dev**	**% of contr**	**Avg**	**St.dev**	**% of contr**	**Average**	**Stdev**	**% of contr**
0.6	CB-01	0.027	0.005	**4 ***	0.006	0.001	**2 ***	0.64	0.16	**4 ***
0.6	PS-02	0.41	0.044	**55 ***	0.172	0.04	**53 ***	9.13	0.80	**54 ***
0.6	OB	0.65	0.012	**88 ***	0.239	0.03	**73 -**	10.68	0.53	**63 ***
0.6	Control	0.75	0.026		0.327	0.11		17.03	2.66	
0.3	CB-01	0.28	0.001	**36 ***	0.127	0.01	**39 ***	5.62	0.42	**30 ***
0.3	PS-02	0.60	0.006	**80 ***	0.207	0.03	**63 -**	11.00	0.21	**58 ***
0.3	OB	0.59	0.181	**78 -**	0.172	0.01	**52 ***	11.34	0.58	**60 ***
0.3	Control	0.76	0.015		0.330	0.10		18.99	4.61	
0.15	CB-01	0.49	0.019	**67 ***	0.222	0.01	**93 -**	10.62	0.36	**80 ***
0.15	PS-02	0.64	0.034	**88 -**	0.159	0.01	**66 ***	10.50	0.30	**79 ***
0.15	OB	0.70	0.010	**97 -**	0.152	0.00	**63 ***	10.75	0.35	**81 ***
0.15	Control	0.72	0.011		0.240	0.03		13.30	0.66	

8 References

Baev N, Schultze M, Barlier I, Ha DC, Virelizier H, Kondorosi E, Kondorosi A (1992) Rhizobium nodM and nodN genes are common nod genes: nodM encodes functions for efficiency of nod signal production and bacteroid maturation. Journal of bacteriology, 174(23), 7555-7565.

Bergaust et al 2011

David M, Daveran ML, Batut J, Dedieu A, Domergue O, Ghai J, Hertig C, Boistard P, Kahn D (1988) Cascade regulation of nif gene expression in Rhizobium meliloti, Cell, Volume 54, Issue 5, Pages 671-683

Greenberg AE, Jenkins D, Connors JJ (1980) Standard methods for the examination of water and wastewater. American Public Health Association.; American Water Works Association. Washington, D.C.: APHA-AWWA-WPCF. ISBN: 0875530915

Jonassen KR, Hagen LH, Vick SHW, Arntzen MØ, Eijsink VGH, Frostegård Å, Lycus P, Molstad L, Phillip B. Pope PB, Bakken LR (2020) Bacteria in digestates for reduced climate forcing, bioRxiv.

Kennedy C, Dean D (1992) The nifU, nifS and nifV gene products are required for activity of all three nitrogenases of Azotobacter vinelandii. Molec. Gen. Genet. **231,** 494–498.

Li, H., Xu, F., Ren, X. et al (2010) Functional analysis of the fixL/fixJ and fixK genes in Azospirillum brasilense Sp7. Ann Microbiol **60,** 469–480 (2010). https://doi.org/10.1007/s13213-010-0065-9

Mania D, Wolily K, Degefu T, Frostegård Å (2020) A common mechanism for efficient N_2O reduction in diverse isolates of nodule-forming bradyrhizobia. Environmental Microbiology 22:17-31.

McGlynn SE, Boyd ES, Peters JW, Orphan VJ (2013) Classifying the metal dependence of uncharacterized nitrogenases. Frontiers in microbiology, 3, 419.

Molstad L, Dörsch P, Bakken LR (2007) Robotized incubation system for monitoring gases (O_2, NO, N_2O, N_2) in denitrifying cultures, Journal of microbiological methods 71:202-211

Monson EK, Ditta GS, Helinski DR. The oxygen sensor protein, FixL, of Rhizobium meliloti. Role of histidine residues in heme binding, phosphorylation, and signal transduction. J Biol Chem. 1995 Mar 10;270(10):5243-50. doi: 10.1074/jbc.270.10.5243. PMID: 7890634.

Surin BP, Downie JA (1988) Characterization of the Rhizobium leguminosarum genes nodLMN involved in efficient host-specific nodulation. Molecular microbiology, 2(2), 173-183.

ISBN: 978-82-575-1824-0
ISSN: 1894-6402

Norwegian University
of Life Sciences

Postboks 5003
NO-1432 Ås, Norway
+47 67 23 00 00
www.nmbu.no

110570 / ANDVORDGRAFISK.NO